DEPARTAMENTO DE ASTROFISICA

Universidad de La Laguna

THE EARTH IN TIME AS A TEMPLATE FOR THE CHARACTERIZATION OF INHABITABLE EXOPLANETS

Memoria que presenta Doña Esther Sanromá Ramos
para optar al grado de
Doctor en Ciencias Físicas.

INSTITUTO Đ ASTROFÍSICA Đ CANARIAS
Diciembre de 2013

Director del Proyecto:

Dr. Enric Pallé Bagó

Resumen

La búsqueda de planetas extrasolares se ha convertido en uno de los campos de mayor interés de la Astrofísica en los últimos años. Desde el descubrimiento del primer planeta fuera del Sistema Solar orbitando una estrella de secuencia principal en 1995, el número de planetas detectados ha crecido exponencialmente. Aunque la mayoría de los exoplanetas encontrados hasta ahora son gigantes gaseosos, en los últimos años hemos sido capaces de detectar planetas cada vez más pequeños, siendo algunos de ellos supertierras que orbitan cerca o incluso dentro de la zona de habitabilidad de sus estrellas. Además, hemos llegado a detectar planetas tan pequeños como La Tierra, e incluso algunos de tamaños similares al de La Luna, por lo que la detección de planetas tipo Tierra parece ser una cuestión de tiempo.

El estudio de La Tierra es una herramienta fundamental tanto para entender e interpretar futuras observaciones de planetas similares al nuestro, como para la caracterización y la búsqueda de vida en otros planetas. En los últimos años, diversos estudios tanto teóricos como observacionales se han llevado a cabo con la finalidad de determinar cómo se verían las características de nuestro planeta si éste fuera visto por un observador extrasolar. En la presente tesis hemos querido ampliar dichos estudios a escalas temporales de millones de años, a lo largo de la evolución terrestre, estudiando cómo diferentes distribuciones continentales, niveles de nubosidad, composiciones atmosféricas y/o la evolución de distintas formas de vida, podrían haber afectado las características fotométricas y espectroscópicas de nuestro planeta.

Las nubes, uno de los parámetros más importantes en el balance energético de nuestro planeta, están asociadas a escalas globales a la orografía y a las corrientes marinas. Por ello, en la primera parte de la presente tesis hemos tratado de estudiar el comportamiento a gran escala de la nubosidad terrestre, con la finalidad de utilizar este conocimiento para reconstruir la posible distribución de la nubosidad en épocas pasadas de La Tierra. El albedo, que está intrínsecamente relacionado con la nubosidad, es otro de los parámetros más importantes en el balance energético del planeta ya que influye directamente en la temperatura superficial. En esta tesis hemos utilizado un modelo de albedo para estudiar la variabilidad fotométrica de nuestro planeta a lo largo de millones de años, cuando la distribución de los continentes era muy distinta a la que conocemos en la actualidad.

Con el objetivo de ampliar el estudio fotométrico llevado acabo en la primera parte de la tesis, en la segunda parte de la misma hemos estudiado las características espectroscópicas de nuestro planeta. Para ello, hemos utilizado un código de transporte radiativo con la finalidad de generar una base de datos de espectros unidimensionales que cubren un amplio rango de tipos de superficie, ángulos de incidencia y de observación, nubes, aerosoles y composición atmosférica, para luego poder calcular observaciones de La Tierra integradas en el disco para una gran variedad de geometrías.

Finalmente, esta base espectral de datos ha sido utilizada para poder estudiar el posible efecto que la aparición de vida en los oceanos y sobre la superficies continentales podría haber tenido en el espectro de nuestro planeta. A lo largo de la evolución terrestre, han tenido lugar diversos eventos tales como la colonización de las bacterias púrpuras –uno de los primeros seres fotosintéticos que poblaron nuestro planeta– o la evolución de los mantos microbianos y de las plantas sobre los continentes. En esta tesis se muestra como la presencia de distintos tipos de vida sobre la superficies continentales, podrían detectarse y caracterizarse mediante el estudio de la luz reflejada por nuestro planeta.

CÓDIGOS UNESCO: 2104.03, 2104.07

Abstract

The search for extrasolar planets has become one of the most exciting fields of astrophysics in the last years. Since the discovery of the first planet orbiting a main sequence star other than the Sun in 1995, the number of detected exoplanets has increased exponentially. Although most of the discovered planets are gas giants, in the last few years we have been able to detect smaller exoplanets, some of them being super-Earths that orbit near or even within the habitable zone of their stars. Moreover, the detection of some Earth-size and Moon-size planets has been recently announced. Therefore, it seems that the detection of an Earth-twin is just a matter of time.

The study of Earth will be essential for understanding future observations of planets similar to our own, and also for the characterization and the search for life elsewhere. In the last years, several studies both theoretical and observational have been carried out with the aim of determining how our planet would look like to an extrasolar observer. In this thesis we extend these studies to time scales of millions of years, throughout the Earth evolution, by studying how different continental distribution, cloudiness levels, atmospheric compositions and/or the evolution of different life forms, could have affected the photometric and spectroscopic characteristics of Earth.

Clouds, one of the most important parameters in the energy balance of our planet, are tied to ocean currents and orography. Thus, in the first part of this thesis we have attempted to study the Earth's large-scale cloudiness behavior with the goal of using these knowledge to reconstruct the possible cloud distribution in past epoch of our planet. Albedo, which is intrinsically related to cloudiness, is one of the most important parameters in the energy balance of our planet since it directly controls the temperature. In this thesis we have used a simple albedo model in order to study the photometric variability of our planet along its history, when the continental distribution was very different from that which we are familiar with today.

With the objective of extending the photometric study carried out in the first part of this thesis, in the second part we have studied the spectroscopic characteristics of our planet. To do that, we used a radiative transfer model with the aim of generating a 1-dimensional spectra database which covers a wide range of surface types, incident and observing angles, clouds, aerosols, and atmospheric compositions, in order to be able to calculate disk-integrated views of our planet for a variety of geometries.

Finally, this spectral database was used to study the possible effect that the appearance of life over continents and oceans could have had on the Earth's spectrum. Throughout the Earth's evolution, several events such as the colonization of purple bacteria – one of the first photosynthetic life forms that colonized our planet – or the evolution of microbial mats and land plants over continents. In this thesis we show

that the presence of different forms of life over continental surfaces, could be detected and characterized by studying the sunlight reflected by our planet.

UNESCO CODES: 2104.03, 2104.07

Contents

1 Introduction **1**
- 1.1 The road to exoplanets . . . 1
- 1.2 Exoplanet detection methods . . . 2
  - 1.2.1 Radial velocity . . . 2
  - 1.2.2 Transits . . . 5
  - 1.2.3 Astrometry . . . 6
  - 1.2.4 Timing . . . 6
  - 1.2.5 Microlensing . . . 7
- 1.3 Discovered exoplanets so far . . . 7
- 1.4 The Earth . . . 11
  - 1.4.1 Earth's energy budget . . . 11
  - 1.4.2 Earth's albedo . . . 12
  - 1.4.3 Clouds on Earth . . . 14
- 1.5 The search for life: What makes a planet habitable? . . . 16
  - 1.5.1 Habitability within the Solar System? . . . 17
  - 1.5.2 Current potentially habitable exoplanets . . . 19
  - 1.5.3 Biosignatures . . . 20
- 1.6 The Earth as an exoplanet . . . 23
- 1.7 The Earth through time . . . 27
  - 1.7.1 Plate tectonics . . . 28
  - 1.7.2 The origin of life . . . 29
  - 1.7.3 The faint young Sun problem . . . 31
  - 1.7.4 The Great Oxidation Event . . . 32
- 1.8 Objectives . . . 33

2 Model Inputs **35**
- 2.1 Atmospheric profiles . . . 35
- 2.2 Earth's continental distribution along time. . . . 37
- 2.3 Cloud distribution and properties . . . 39
  - 2.3.1 A semiempirical model for Earth's clouds . . . 39
  - 2.3.2 Cloud reconstruction . . . 45
- 2.4 Optical properties of aerosols and clouds . . . 47

2.5 Spectral albedo 47
2.5.1 Purple bacteria spectral albedo 49

3 Constructing a disk-integrated Earth spectrum model 53
3.1 A simple reflectance model 53
3.1.1 Example model outputs: Test planets 54
3.2 Spectral Earth model 57
3.2.1 Radiative transfer model 58
3.2.2 Disk-integrated spectrum of Earth 64

4 Reconstructing the Cloud Distribution and Light Curves of Earth Along its History 73

5 On the Effects of the Evolution of Microbial Mats and Land Plants on Earth 83

6 Characterizing the Purple Earth 93

7 Results and Conclusions 107

A Annex A 111

1

Introduction

1.1 The road to exoplanets

Interest in knowing if there exist other worlds like ours is not new. As far back as ancient Greeks, philosophers speculated that other solar systems might exist and that some would harbor life. At that time, Epicurus (c. 300 B.C.) stated *"There are infinite worlds both like and unlike this world of ours...We must believe that in all worlds there are living creatures and plants and other things we see in this world."* Several centuries later, in 1584, the philosopher and astronomer Giordano Bruno defended this idea affirming that there were *"countless suns and countless earths all rotating around their suns... The countless worlds in the universe are no worse and no less inhabited than our Earth"*. Nonetheless, his point of view was not accepted by the Catholic Church and he was accused of heresy. Meanwhile, Copernicus suggested that the Earth, along with the other known planets, orbits the Sun and not the other way around, as it had been thought long before, being this suggestion one of the most relevant events of the history of astronomy.

But evidence of the existence of other worlds had to wait until the 17th century when Galileo turned his telescope to the sky. This new instrument allowed him to observe the Universe in greater detail than ever before. Jupiter was found to have four moons and the appearance of the Moon was not smooth as it had been thought before. In fact, it showed hills and valleys that resembled those of our own planet, showing a similar nature to the Earth. Galileo Galilei's telescope paved the way for future discoveries of solar sytem's planets like Uranus (William Herschel, 1781) and Neptune (Johan Galle, 1846).

However, we had to wait until 1987 to witness the first steps from discovering planets to discover exoplanets. The first published scientific results of a possible exoplanet was made by the Canadian astronomers Bruce Campbell, Gordon Walker and Stephenson Yang (Campbell et al. 1988). Their radial-velocity data suggested the presence of a possible 1.7 M_J planet around the star γ Cep. Nevertheless, they

were extremely cautious about claiming the planetary detection and that planet was not confirmed until much later, in 2003 by the studies of Hatzes et al. (2003).

Two years later, Latham et al. (1989) also obtained radial-velocity observations which showed evidence of a possible companion to the solar-type star HD114762. However, as the mass of this exoplanet was thought to be considerably larger than 10 M_J, it lead to the suggestion that the companion was a brown dwarf. Shortly afterwards, Wolszczan & Frail (1992) used a very precise timing method to report that the pulsar PSR1257+12 was orbited by at least two planet-size bodies of about 2.8 and 3.4 Earth masses. Their work supposed the first confirmed discovery of planets beyond the Solar System, though orbiting a non-main sequence star. This led to the awareness that planets could exist even around stars in their final evolutionary stages.

The first discovery of a planet orbiting a star similar to the Sun came in 1995. By using the radial velocity method, Mayor & Queloz (1995) announced the discovery of a very-short-period 0.47 M_J planet orbiting the star 51 Peg. Alternative explanations for such discovery were promptly proposed, but the discovery was confirmed a short time later by Marcy & Butler (1996) who also reported two more new exoplanets. These discoveries of planetary-mass objects orbiting main sequence stars gave a boost to the search and study of planetary systems beyond our own, generating one of the most active and exciting fields of astrophysics.

1.2 Exoplanet detection methods

Detecting exoplanets is a very difficult and demanding task, since an exoplanet is small, of low mass and very faint compared with its host star. For these reasons, only few of the discovered extrasolar planets, less than 5%, have been observed directly. Then, the first exoplanet was not imaged until 2004 (Chauvin et al. 2004). Even then the imaged planets tend to be massive, young and orbit at a large distance from the parent star. Therefore, alternative detection methods, based on detecting the effect that exoplanets have on their stellar system, need to be used. Below is a brief summary of the most common indirect methods for finding exoplanets. For an extensive review of the used observational methods and the more relevant historical background see Perryman (2012) and Figure 1.1.

1.2.1 Radial velocity

The radial velocity method was one of the first techniques to be developed and was the first one to be successful in finding an exoplanet. This method is still the most productive technique used to search for exoplanets (about 58% of the discoveries have been made by this technique).

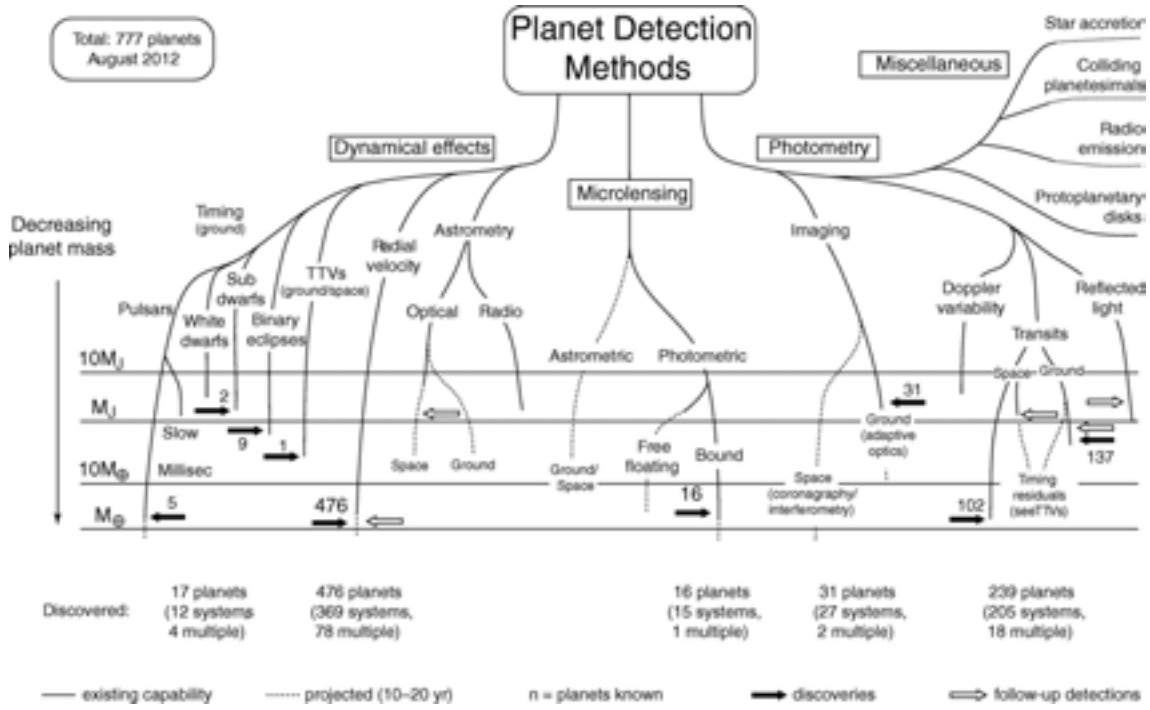

Figure 1.1: Detection methods for extrasolar planets. The lower limits of the lines indicate the detectable masses that are in principle within reach of present measurements (solid lines) and those that might be expected within the next 10-20 years (dashed). The (logarithmic) mass scale is shown on the left. The miscellaneous signatures to the upper right are less well quantified in mass terms. Solid arrows indicate detections according to approximate mass. Open arrows indicate that relevant measurements of previously detected systems have been made. The Figure presents the status as of August 2012. Adapted from Perryman (2012).

If a planet, or several planets, are orbiting a star, the radial velocity method try to detect slight changes in the star's velocity, caused by the presence of the planet, as the star and the planet move around their common center of mass. These variations are detected by analyzing the spectrum of the host star (Figure 1.2) and allow us to determine the orbital period of the planet, the orbital eccentricity and a minimum value of the planet's mass ($M_P \sin i$, where M_P is the mass of the planet and i is the orbital inclination).

Planets orbiting low-mass stars, with large masses and short orbital periods are more likely to be detectable with this method. The detection of exoplanets using the radial velocity technique needs a precision of at least 30 m/s and 1 m/s to detect giants planets and Neptune-mass planets, respectively. For an Earth-size planet, the precision required would be about 0.1 m/s (Seager 2011 and references therein).

Radial velocity measurement precision has continually improved. In the 1950s, the typical radial velocity precision was of about 750 m/s. In 1979, G. Walker and B. Campbell developed a method capable of measuring radial velocities with a precision of 15 m/s (Campbell & Walker 1979). Several years later, Butler et al.

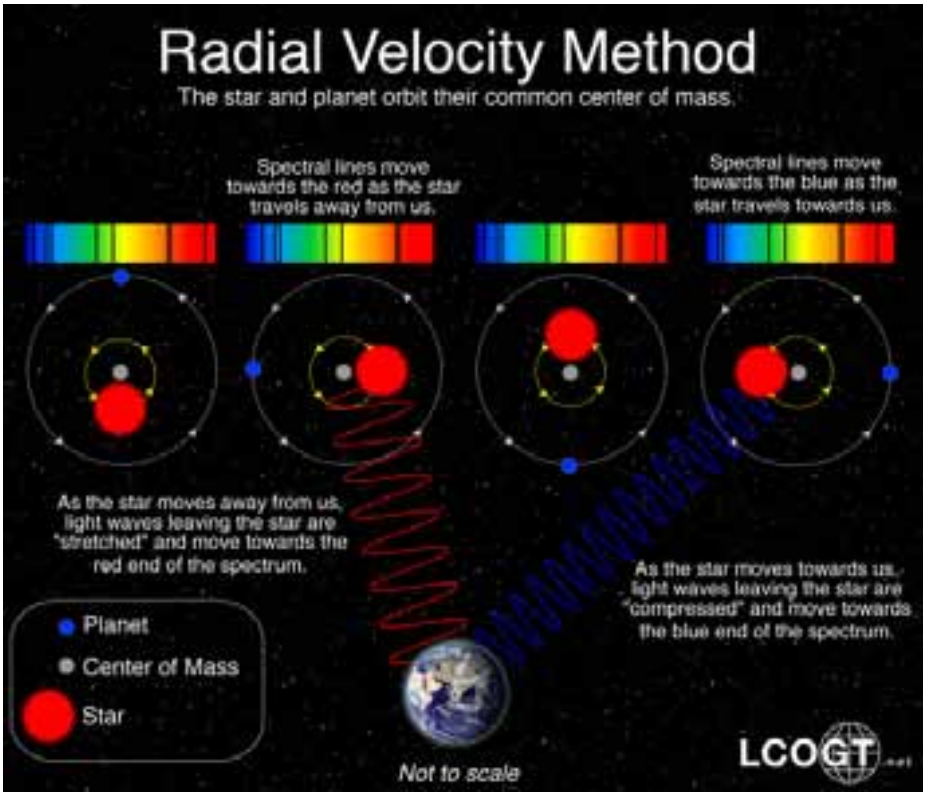

Figure 1.2: Illustration of the radial velocity method. This method tries to detect the small variations in the velocity of a central star, due to the changing direction of the gravitational pull from its exoplanet as it orbits the star.

(1996) proposed a technique which yields relative radial velocity errors of 3 m/s. More recently, in 2003, the installation of the High Accuracy Radial Velocity Planet Searcher (HARPS) on the ESO's 3.6 m telescope at La Silla Observatory, supposed a major improvement in radial velocity precision. HARPS was specifically designed to search for exoplanets in the southern hemisphere, and with the goal of achieving a precision of 1 m/s (Mayor et al. 2003). In fact, HARPS has been able to achieve a short-term (during one night) precision better than 0.2 m/s. More recently, HARPS-N, an instrument similar to HARPS installed on the Italian 3.6 m Telescopio Nazionale Galileo (TNG) at Roque de los Muchachos Observatory, has allowed to obtain measurements of radial velocities with the highest accuracy currently available in the north hemisphere. The main goals of HARPS-N are the follow-up of Kepler's planet candidates and the detection of nearby rocky planets. Moreover, CARMENES, (Calar Alto high-Resolution search for M dwarfs with Exoearths with Near-infrared and optical Echelle Spectrographs), is a next-generation instrument being built for the 3.5 m telescope at the Calar Alto Observatory, and has been designed to perform high-accuracy radial-velocity measurements (1 m/s). The aim of CARMENES is to carry out a survey of about 300 late-type main-sequence stars with the goal of detecting low-mass planets in their habitable zones (Quirrenbach et al. 2010).The first light of CARMENES is expected to take place in Autumn 2014.

1.2.2 Transits

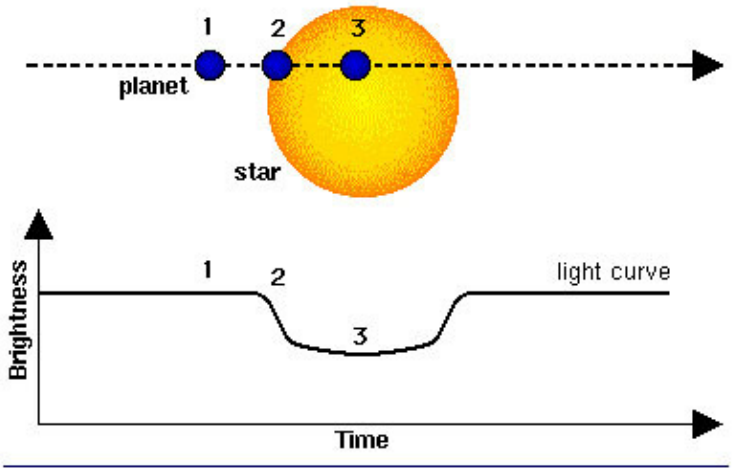

Figure 1.3: Transit method. If a planet happens to pass between its star and the observer, it blocks out part of the star's light, slightly reducing its apparent brightness.

The transit method is the second most successful technique in the search for exoplanets. The first exoplanet transit, HD 209458, was detected in 1999 by Henry et al. (1999, 2000), and simultaneously by Charbonneau et al. (2000). So far, this method is responsible for the discovery of almost 300 exoplanets, about 35% of the total exoplanet population.

Given a suitable alignment geometry, a small part of the light from the host star is blocked by the planet when it is traveling across the stellar disk once each orbital period (Figure 1.3). Sensitive instruments can detect this periodic dip in brightness. The probability of observing such a transit is small and so is its effects. The probability of transit of a Jupiter-like planet orbiting a Sun-like star is about 10%, while the transit depth is of $\sim$ 1%. Detecting an Earth analog orbiting a Sun-like star is much more challenging. In this case, the fractional transit depth is 10^{-4} and the transit probability is about 0.5%.

Ground based telescopes are only able to discover transits with depth up to about 1%, thus the requirements to observe a transiting Earth analog can not be met from the ground and space-based monitoring is needed. Surveys from space, such as Kepler have discovered planets with transits depths of a few times 10^{-4}, extending detectable exoplanet masses to below 1 M_E. The Kepler Mission is a space-based mission, launched in 2009, whose main goal is to detect Earth-size and smaller planets in and near the habitable zone of stars similar to our Sun. This mission monitors more than

150.000 stars looking for transiting planets and is designed to continuously observe a specific region of our galaxy (Borucki et al. 2010). In this way, if Earth-size planets are common then Kepler will detect hundreds of them. So far, Kepler mission has detected more than 2.700 planet candidates, of which only 5-10% are expected to be false positives, and more than 120 planets have already been confirmed. However, this prolific space mission is likely to be over. Last May the telescope went into safe mode as a result of a star tracker anomaly. One of the establishing wheels is broken, and hence, the telescope is not able to point precisely at its targets.

The detection of a transiting planet allows us to determine the size of the planet relative to the size of the star by using the transit depth. The orientation of the planet's orbit relative to the sky plane and relative to the stellar rotation axis can also be determined. When combined with radial velocity measurements, the planetary mass can be calculated, and as a result, the density of the object. Moreover, in some cases, it is also possible to determine the composition of the atmosphere, or at least to determine the presence of some atmospheric components.

1.2.3 Astrometry

Astrometry is the science of measuring the positions, and the changes in these positions, of objects in the sky. Astrometry is generally used to make the detection of a star's unseen companion. When applied to exoplanets, this method tries to measure the slight motion of a star attributed to an accompanying exoplanet.

Even though astrometry has a successful record in detecting unseen stellar companions, only one exoplanet, HD 176051 b (Muterspaugh et al. 2010), has been discovered with this technique so far. This situation might be changed with the future launch of ESA's astrometry mission Gaia (Lindegren & Perryman 1996). Gaia will conduct a census of a thousand million stars in our Galaxy, monitoring each of its target stars about 70 times over a five-year period. This mission is expected to discover hundreds of thousands of new celestial objects, including extrasolar planets and brown dwarfs.

1.2.4 Timing

A pulsar is a rapidly-spinning neutron star with a strong magnetic field. Pulsars emit radio waves extremely regularly as they rotate. Thus, as the rotation of the pulsar is so regular, slight anomalies in the timing of the pulses can be used to infer the presence of an exoplanet.

This method is really sensitive, it can detect planets with masses lower than other techniques can do. However, pulsars are relatively rare celestial objects and just 15 extrasolar planets have been discovered by using this method.

1.2.5 Microlensing

The gravitational microlensing method derives from one of the insights of Einstein's theory of general relativity. It occurs when a foreground star happens to pass very close to our line of sight to a more distant background star (the source). The foreground star acts as a lens, splitting the light rays from the source creating images of it which are distorted and possibly amplified. If the foreground star happens to host a planet, the planet's gravity will behave like a lens. Thus, the planet will further perturb the images, resulting in a characteristic, short-lived increase in brightness (Figure 1.4).

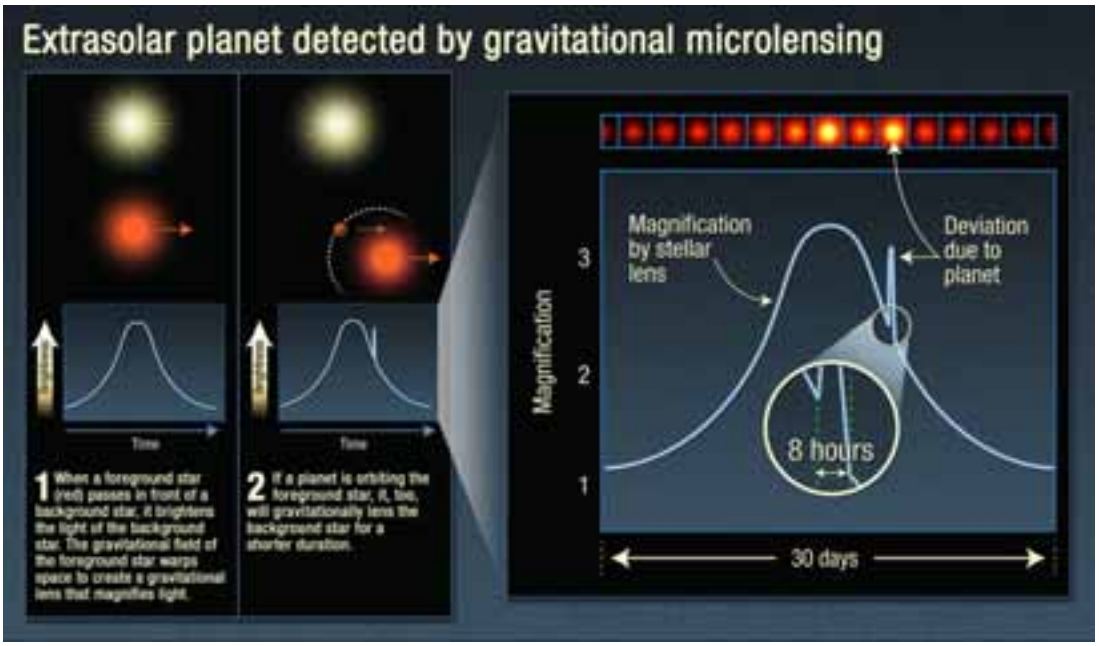

Figure 1.4: Illustration of planet detection through the microlensing method. Credit: NASA, ESA, and K. Sahu (STScI).

The microlensing technique is particularly well-suited for finding low-mass planets and planets around distant or very dim stars. Nevertheless, less than 20 extrasolar planets have been discovered through gravitational microlensing so far.

1.3 Discovered exoplanets so far

In the last decades, by using a variety of techniques (see subsection 1.2 and Figure 1.5), more than 990 exoplanets have been detected; as of October 2013 (see exoplanet.eu/catalog) while thousands of potential planet candidates from the NASA's Kepler mission are awaiting for confirmation by follow-up observations.

Most of the discovered exoplanets are gas giant, as larger planets are easier to

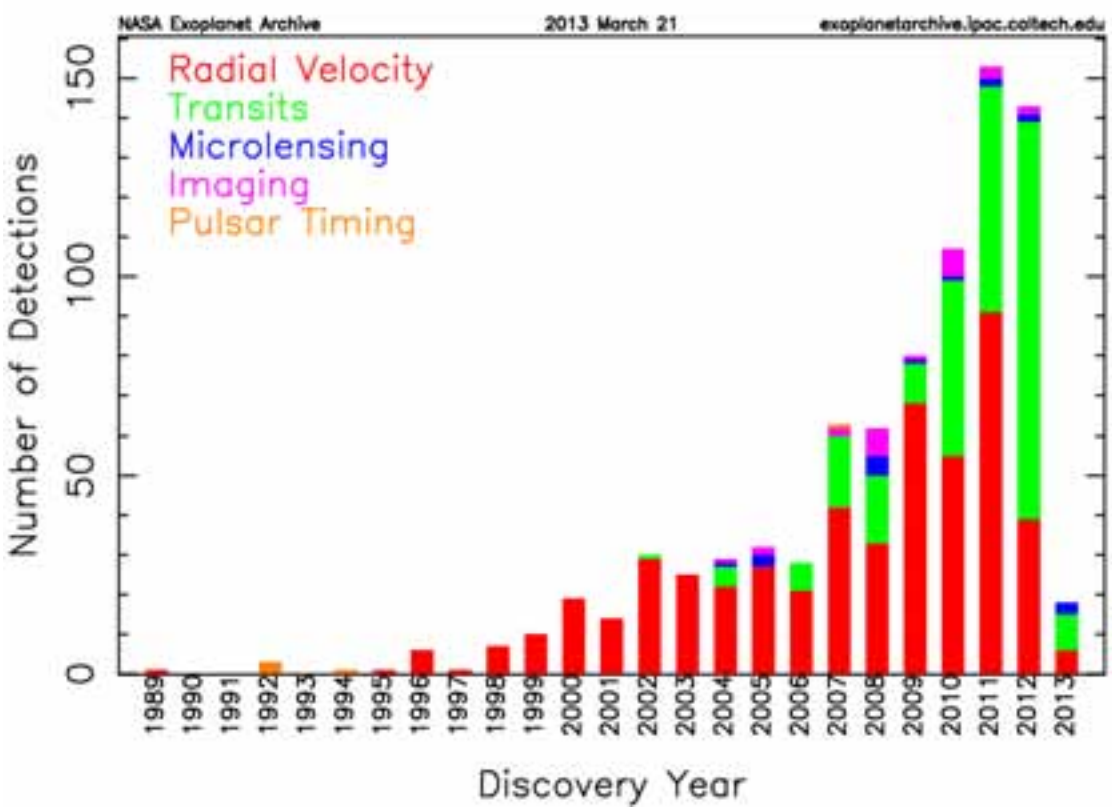

Figure 1.5: Number of extrasolar planets discovered by year and by detection method. Image credit: NASA exoplanet archive.

detect than smaller, rocky ones. Moreover, due to detection method effects, many of the first discovered exoplanets were giants and were found close to their host stars (e.g. Bouchy et al. 2004, 2005; Hellier et al. 2009; Street et al. 2010). These so called "Hot Jupiters" surprised astronomers since they called into question the theories about planetary formation. The general consensus was that giant planets should only form at large distances from their hot stars. Observations of F, G, and K stars have suggested that about 12% of these types of stars harbor at least one gas giant planet with orbital distance within 20 AU, while the occurrence of hot Jupiters within 0.1 AU is about 1.2% (Marcy et al. 2005).

Improvement in observational techniques have allowed us to discover tens of planets in the super-Earth mass range in the last few years (e.g. Udry et al. 2007b; Charbonneau et al. 2009; Pepe et al. 2011; Borucki et al. 2012) some of them probably lying within, or close to, the habitable zone of their host star (Udry et al. 2007a; Borucki et al. 2012; Barclay et al. 2013; Borucki et al. 2013). The habitable zone (HZ) is traditionally defined as the region around a star where a planet could maintain liquid water in its surface (see Section 1.5).

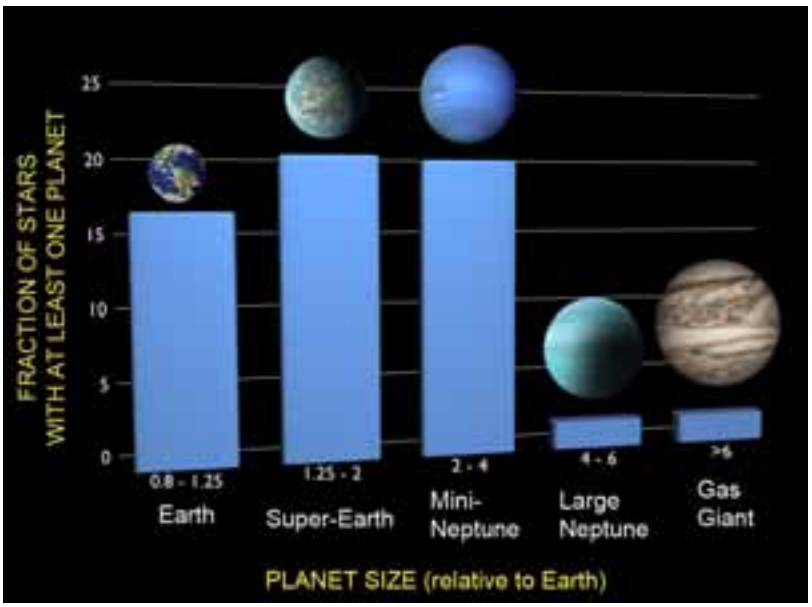

Figure 1.6: Fraction of Milky Way's stars with at least one planet as a function of planet size. Calculations based on NASA's Kepler findings. The results show that about 16.5% of stars have at least one Earth-size planet in a tight orbit, around 20% a super-Earth, and about the same percentage have a mini-Neptune. Credit: F. Fressin (CfA).

Furthermore, some Earth-size, and even smaller, extrasolar planets have recently been announced (Fressin et al. 2012; Muirhead et al. 2012; Gilliland et al. 2013; Borucki et al. 2013). In fact, early statistics indicate that about 62% of the Milky Way's stars may host a super-Earth (Cassan et al. 2012), while Fressin et al. (2013), based on findings from NASA's Kepler mission, have pointed out that around 16.5% of stars have at least one Earth-size planet with orbital periods up to 85 days (see also Figure 1.6). Other surveys, like the NASA-UC Eta-Earth, have shown that the planet mass distribution of close-in planets rises steeply towards low masses (Howard et al. 2010). Thus, we can expect that true Earth analogues will be found in large numbers in the near future.

In the last years, we have also learned that multiple planetary systems are common in our galaxy. In fact, 23% of the planet host stars observed by Kepler have at least two transiting planets (Burke et al. 2013). Holman et al. (2010) reported the first confirmation of multiple-transiting system. They detected two Saturn-size planets transiting a Sun-like star (Kepler-9) by using the transit timing variations method. Lissauer et al. (2011) also announced the discovery of six transiting planets orbiting a Sun-like star (Kepler-11). While Fressin et al. (2012) announced the discovery of two planets, one Earth-size ($1.03R_E$) and the other one smaller than the Earth ($0.87R_E$), orbiting the star Kepler-20. More recently, Borucki et al. (2013) have also reported the discovery of a five-planet system with some of them with radii close to that of the Earth, 1.4 and 1.6 R_E for Kepler-62 e and f, respectively, and even one planet smaller than the Earth, Kepler 62c (Figure 1.7).

Figure 1.7: Comparison between the planets of the inner Solar System and those around Kepler-62, a five-planet system in the constellation of Lyra. Similar to our solar system, Kepler-62 harbors two planets lying in its habitable zone, Kepler-62f and Kepler-62e. Kepler-62f orbits every 267 days and is only 40% larger than Earth, making it the smallest exoplanet known in the habitable zone of another star. Kepler-62e, orbits every 122 days and is roughly 60% larger than Earth .Image credit: NASA Ames/JPL-Caltech

Moreover, the field is shifting from finding planets to characterizing their properties. We have started to characterize the atmosphere of some discovered extrasolar planets, e.g., we have detected absorption lines of planetary atmospheric constituents by using primary and secondary eclipse measurements. For instance, Charbonneau et al. (2002) reported the detection of absorption from sodium in the planetary atmosphere of the HD 209458 planet. Furthermore, Tinetti et al. (2007) found absorption from water vapor in HD 189733 b, while Swain et al. (2009b) reported the detection of carbon dioxide, carbon monoxide, and also water in the same exoplanet. Swain et al. (2009a) also reported the presence of water, methane, and carbon dioxide in the dayside spectrum of the exoplanet HD 209458b. More recently, by using high-resolution ground-based spectroscopy, Rodler et al. (2012) and Brogi et al. (2012) were able to detect carbon monoxide absorption lines produced in the τ Boo b atmosphere, while de Kok et al. (2013) also detected it in the atmosphere of HD 189733 b.

At the light of all these results, and with the development of technology for exoplanet missions, it seems possible that, in the not too far future, we will be able to detect and characterize hundreds of potentially habitable worlds.

1.4 The Earth

When looking for extrasolar planets that could present the right conditions to harbor life, or planets that show signs of life in their atmosphere, the logical starting point is to study the Earth's atmosphere. Present day Earth's atmosphere is mainly made out of 78% nitrogen, 21% oxygen, 0.93% argon and 0.04% carbon dioxide, and shows several spectral signatures that are related to the existence of life or with habitability (for more details about biosignatures see section 1.5.3). Oxygen and ozone are Earth's two most robust biosignatures gases. Oxygen is highly reactive and consequently will remain in significant quantities in the atmosphere only if it is continually produced, and ozone is a photolytic product of oxygen. Nitrous oxide is a relatively minor constituent of the modern atmosphere and is primarily produced by life, albeit in small quantities, with no strong abiotic sources, although it shows no strong features in the Earth's spectrum. Methane is produced both biotically, by methanogens and termites, and abiotically, through hydrothermal vents systems. Another chemical species which indicate habitability and shows strong spectral features in Earth's atmosphere is water vapor, which is an important greenhouse gas. Other spectral signatures that not reveal direct information about life or habitability but present a strong signal in the Earth's spectrum include carbon dioxide.

1.4.1 Earth's energy budget

Earth's climate is driven by the net sunlight deposited in the terrestrial atmosphere, and so, is critically sensitive to the solar irradiance and the Earth's albedo -the amount of sunlight reflected back to space by the atmosphere and surface of the Earth (see subsection 1.4.2 for more details).

A significant portion of this solar energy is absorbed by the Earth (70%), where it drives terrestrial phenomena before being radiated back into space through the atmospheric window as infrared radiation. Globally, over the course of the year, the Earth (land surface, oceans and atmosphere) absorbs an average of about 240 watts of solar power per square meter. This power going into the Earth's climate system can be written as:

$$P_{in} \;=\; C\pi {R_E}^2(1-A)$$

where C is the solar constant (adjusted for the Sun-Earth distance), R_E is the Earth's radius and A is the short-wavelength Bond albedo.

The Sun does not heat the Earth evenly. Because the Earth is a sphere, the Sun heats equatorial regions more than polar regions. The atmosphere and ocean work non-stop to even out solar heating imbalances through evaporation of surface water, convection, rainfall, winds, and ocean circulation. This coupled atmosphere

and ocean circulation is known as the Earth's heat engine. The climate's heat engine must not only redistribute solar heat from the equator toward the poles, but also from the Earth's surface and lower atmosphere back to space. This outcoming power re-radiated back into space can be written as:

$$P_{out} = C\pi {R_E}^2 \sigma {T_E}^4$$

where σ is the Stefan-Boltzmann constant and T_E ($\sim$ 255 K) is the effective temperature of the Earth, a physical averaged long-wave emission temperature at about 5.5 km height in the atmosphere (depending on wavelength and cloud cover, altitudes from 0 to 30 km contribute to this emission). That temperature can be related to other more global parameter as the globally averaged surface temperature T_S. A greenhouse forcing parameter $G[W/m^2]$, which is defined as the difference between the emission at the top of the atmosphere and the surface, can be introduced. This forcing, G, increases with increasing concentration of greenhouse gases. Taking this parameter into account, we can define the normalized greenhouse effect g as $g = G/\sigma {T_S}^4$ (Raval & Ramanathan 1989). Then, the outgoing power can be written as:

$$P_{out} = 4\pi {R_E}^2 \sigma (1-g) {T_S}^4$$

The net flow of energy into and out of the Earth system is the Earth's energy budget. When the flow of incoming solar energy is balanced by an equal flow of heat to space, the Earth is in radiative equilibrium, i.e., $P_{in} = P_{out}$. And one obtains:

$${T_S}^4 = \frac{C}{4\sigma(1-g)}(1-A)$$

This means that the solar irradiance, together with the greenhouse effect and the Bond albedo, directly control the Earth's temperature. A change in any of these three parameters will lead to a global temperature rise or fall in response.

1.4.2 Earth's albedo

Albedo is a measure of the total radiation reflected from an object compared to the total incident radiation. In this way, an ideal white body has an albedo of 100% and an ideal black body, 0%. This term has its origins from a Latin word albus, meaning "white". There exist various types of albedo in the literature, the first one is the geometric albedo, which is defined as the amount of radiation relative to that from a flat lambertian surface which is an ideal reflector at all wavelengths. The Bond albedo is the fraction of all incident light, integrated over the entire stellar spectrum, which is scattered back to space by a planet. Care must be taken when distinguishing these albedos as they can differ greatly from one another. For Earth, the Bond albedo

is 0.29 while the geometric albedo is 0.37 (Goode et al. 2001).

The reflectance properties of Earth change due to seasonal changes in meteorological parameters, the seasonal variations in the extent of snow and ice cover (Randall et al. 1994), changes in the forest leaf coverage (Betts 2000) and is also affected by parameters such as volcanic eruptions and atmospheric constituents (aerosols, water vapor and clouds (Cess et al. 1996; Ramanathan et al. 1989; Charlson et al. 1992)).

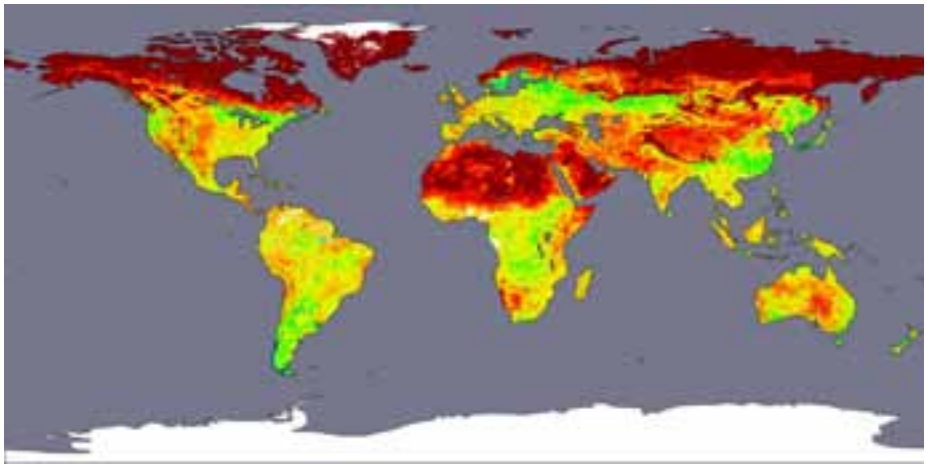

Figure 1.8: The colors in the image show the Earth's surface albedo, ranging from 0.0 to 0.4. Red areas show the brightest regions, yellows and greens are intermediate values, and blues and violets show the darkest surfaces. Albedo values over oceans are not provided and white indicates where no data were available, and no albedo data. This image was produced using MODIS data composited over a 16-day period, from April 7-22, 2002. Image courtesy: Crystal Schaaf, Boston University.

Figure 1.8 illustrates annual mean surface reflectance values of the Earth. One can see that these annual mean reflectance values exhibit large geographic variation. The local value of the albedo depends, among other things, on the nature of the surface (type of soil, vegetation cover, oceans, etc) but also on the reflection angle. Annual mean albedo values differ considerably between the equator and the poles, largely due to the presence of snow and ice-covered surfaces along with cloudy skies in high latitudes, which greatly increases albedo values in those areas.

In order to show how different surface types affect the Earth's albedo, Figure 1.9 shows the wavelength-dependent surface albedo corresponding to water, forest, grassland, shrubland, desert, and snow. Data is taken from the ASTER Spectral Library[1] and the USGS Digital Spectral Library[2].

A great unknown is how stable are the reflectance properties of the Earth over geological time scale. For instance, 2300 and some $700 - 800$ million years ago, the Earth underwent epochs of extreme glacial temperatures known as the "Snowball"

[1] http://speclib.jpl.nasa.gov
[2] http://speclab.cr.usgs.gov

events. At these times, the extent of the sea ice is believed to have reached as far as the tropics. As the albedo of ice and snow is high, the average albedo of Earth must have been much larger than the present day value. If Earth was covered in ice like a giant snowball, its surface albedo would be about 0.84, meaning that it would reflect most of the incident sunlight. On the other hand, if Earth were completely covered by a dark green forest canopy, its albedo would be about 0.14, meaning that most of the sunlight would be absorbed and our world would be far warmer than it is today (Vázquez et al. 2010).

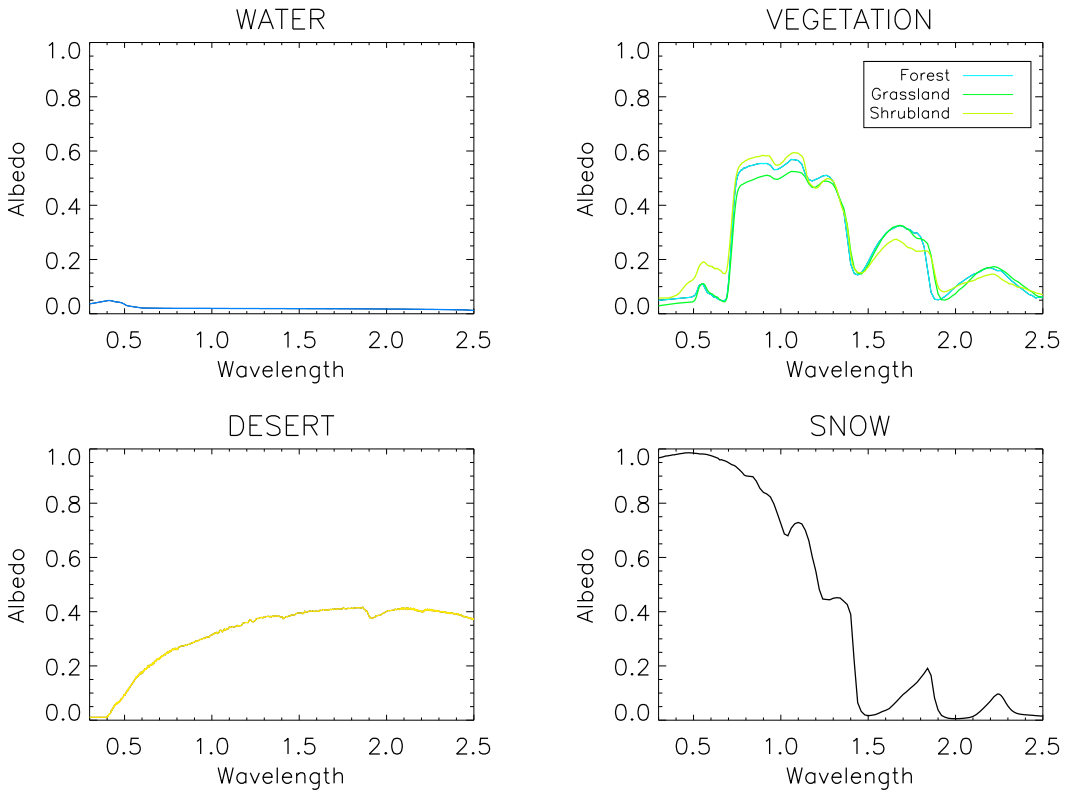

Figure 1.9: Spectral reflectance of water, forest, grassland, shrubland, desert, and snow. Data are taken from the ASTER Spectral Library and the USGS Digital Spectral Library.

1.4.3 Clouds on Earth

The patchy distribution of clouds over the Earth's surface is a unique feature in our solar system. Clouds are immensely complex three-dimensional entities that have profound interactions with weather and climate, play a very important role in the energy exchange, affect the spectra of scattered and emitted radiation, and the detectability by direct imaging of the planet. On Earth, clouds are perhaps one of the hardest parameters to infer in actual climate models, and are continuously forming

and disappearing, covering on average about 60% of the Earth's surface (Rossow et al. 1996). They have a geographical large-scale structures that are tied to continents and ocean currents, thus they are not just random noise added to the surface signal of reflected light (Pallé et al. (2004) and see Figure 1.10.

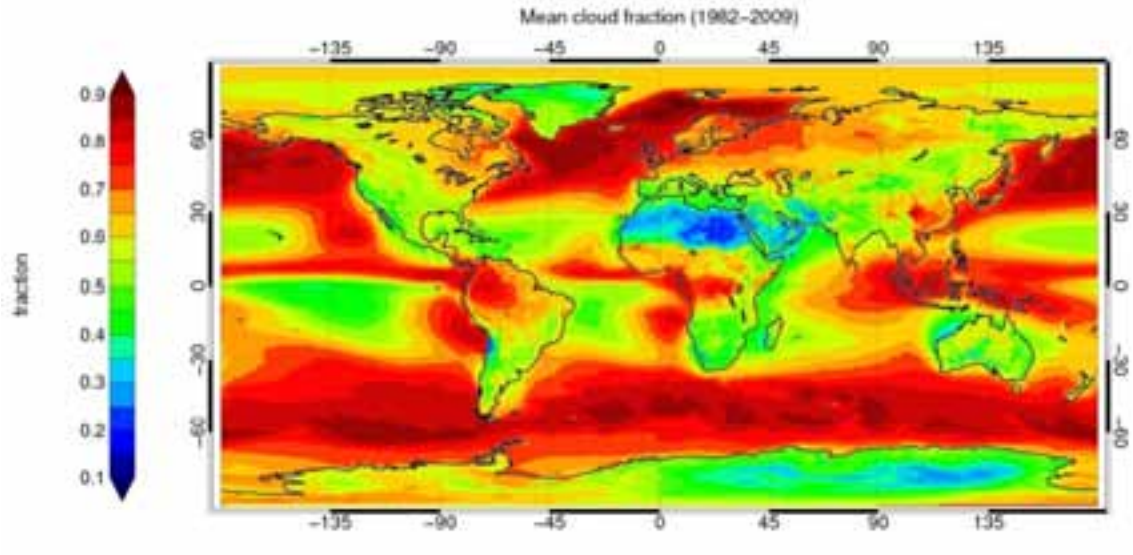

Figure 1.10: Distribution of 1984-2009 annual mean cloud amount. The average cloudiness is about 60%. At the same latitude, continents tend to be less cloudy than adjacent oceans. Moreover, the major fraction of clouds are found between 40-60°.

Cloud coverage increases the albedo, reducing the absorption of sunlight and promoting cooler conditions. However, as tropospheric temperatures regularly decrease with altitude, cloud tops are usually cooler than the ground and therefore radiate less infrared energy to space, promoting warmer conditions. These effects compete with each other. The effects of clouds on albedo depends on their depth, height, content of ice and water and their geometric shape.

Clouds also have a strong impact on the emitted infrared flux, dampening spectral features of molecules and decreasing thermal radiation flux. Moreover, thermal emission spectra are very sensitive to the types and fractional coverages of clouds present in the atmosphere (Kitzmann et al. 2011a; Rugheimer et al. 2013). Clouds can also cancel spectral signatures related to life on Earth like the one of surface vegetation, the red-edge, playing a crucial role for the detection of these signatures in the reflection spectra (e.g. Arnold et al. 2002; Hamdani et al. 2006; Montañés-Rodríguez et al. 2006; Tinetti et al. 2006c). Furthermore, Kitzmann et al. (2011b) studied the influence of water and ice clouds on low-resolution reflection spectra of Earth-like planets, finding that the high scattering efficiency of clouds causes both the amount of reflected light and the related depths of the absorption bands to be substantially larger than clear sky conditions. Moreover, low-level clouds have a

stronger impact on the spectra than high-level clouds because of their larger scattering optical depth. Hence, the presence of clouds is one of the most important factors determining reflection spectra. Regarding transmission spectra, Ehrenreich et al. (2006) included the effect of optically thick cloud layers in transmission spectral models of Earth-size transiting planets to show that transmission spectra only contain information about the atmosphere above the cloud layer and that clouds can effectively increase the apparent radius of the planet. Thus, the impact of clouds in the transmission spectrum of a planet is strongly dependent on the height of the clouds.

Clouds are found in solar sytem's planets others than Earth and are likely to be common in extrasolar planetary atmosphere as well. One of the most convincing evidence of clouds on extrasolar planets to date lies in the spectra of the planets of the star HR 8799 (Bowler et al. 2010; Madhusudhan et al. 2011; Marley et al. 2012). Planets b, c, and d are found to have near-infrared colors that can be explained by the presence of clouds. Another feasible evidence is the transiting planet HD 189733b whose spectrum lacks the deep absorption bands expected for a clear atmosphere (Sengupta 2008).

1.5 The search for life: What makes a planet habitable?

As observational techniques develop, astrophysicists become interested in a new concept named habitability. Habitability can be defined as the potential of an environment to develop and support life, even if life does not currently exist (Javaux & Dehant 2010). Thus, the question to ask is not only if a planet (or a moon) is habitable, but also if life could have originated and evolved there.

The metabolism and the structure of living organisms have at least three basic requirements: a dissolvent media, a source of energy, and a given amount of organic materials. It is generally believed that the most important requirement for a planet to be habitable is the presence of liquid water (e.g., Kasting et al. 1993). Moreover, it has been also pointed out that liquid water is the best solvent for life to emerge and evolve in. Water is an abundant compound in our galaxy, and is liquid at a wide range of temperatures and pressures. Due to this, the habitable zone of a star (HZ) has been defined as the circumstellar region in which a planet might maintain liquid water on his surface. Whether a planet is in the HZ of its star would depend on the stellar type of the star, the planet-star distance, and the atmospheric composition of the planet.

As said before, another requirement is the presence of a source of energy in order to allow life to carry out the corresponding biochemical functions. A variety of energy forms could be used by organisms (Sertorio & Tinetti 2001), but terrestrial

Table 1.1: Extreme forms of life found on Earth. Adapted from Gargaud et al. (2012).

Parameters	Organism	Defining Growth Condition	Example Habitat
Temperature (C)	Hyperthermophile	> 80	Submarine hydrothermal vents
Temperature (C)	Thermophile	$60-80$	Hot springs, solfataras
Temperature (C)	Psychrophile	< 5	Snow, high mountains
Acidity (pH)	Acidophile	$<$ 2-3	Mines, solfataras
Acidity (pH)	Alkaliphile	$>$ 9-10	Soda lakes
Salinity	Halophile	$2-5$ M NaCl	Marine brines, salt mines
Pressure	Barophile	High pressure	Deep oceans, deep subsurface
Radiation	Radioresistance	Resists high levels of ionization, or UV radiation	Deserts, radioactive mines

life only uses solar radiation and/or chemical energy. Sunlight is the fundamental energy source of life on Earth. On the early Earth, organism learned how to use this energy through the process of photosynthesis. The evolution of life would also require that this central star must be neither too massive, that will produce too lethal UV radiation and will have too short life-span to allow life to evolve, nor too small which will not produce enough radiation in order to sustain life.

It is also necessary the existence of a source of elements and other nutrients to support life. On Earth, life structures need complex organic molecules that are based on carbon. Carbon is a particularly versatile element because it can bond with up to four atoms at a time. However, life also needs other elements, like hydrogen, oxygen, and nitrogen, as these compounds are the basis to form carbon-biomolecules.

Finally, it would be also a requisite that the physical conditions of the planet, or the moon, are not too extreme for the development and persistence of life. It is not unlikely that life beyond Earth would be able to use a variety of chemistries and liquids different from that used on Earth (e.g., Bains 2004; Baross et al. 2007). From our experience on Earth, it seems that if life once originated, it will be able to adapt to a wide range of extreme environment conditions (e.g. Rothschild & Mancinelli 2001 and see table 1.1).

1.5.1 Habitability within the Solar System?

One possible way to investigate the habitability of exoplanets and their satellites may be through the study of the bodies in our own solar system. Several authors have suggested that it might be possible to find life within the Solar System (e.g., Seckbach & Libby 1970), in places other than Earth. In particular, there are two planets, Venus and Mars, and several moons, e.g., Europa and Enceladus, that are most likely candidates to harbor life.

Mars has always been a focus in the search for life. Early Mars is thought to have been similar to early Earth, and therefore, it is possible that life might have arisen on Mars as well. The first serious experiments sent to Mars took place in 1976 and were the Viking biological experiments. These experiments were part of the NASA's Viking mission in which, the main objectives were to obtain high resolution images of the Martian surface, characterize the structure and composition of the atmosphere and surface, and search for evidence of microbial life. Results from this first attempt to seek for life on Mars were found inconclusive regarding the presence of life.

The surface of Venus is the hottest in the Solar System, so there is no liquid water. This is thought to have been caused by a run-away greenhouse effect where the carbon dioxide-rich atmosphere (96% CO_2 and 3% N2) trapped incident sunlight making temperatures rise. Clouds of sulfuric acid are abundant and the atmospheric pressure is over 90 times that of Earth. All the information that we have about Venus comes from the Russian Venera landers (which survived on the venusian surface just about 60 minutes), the NASA's Magellan spacecraft, and the ESA's Venus Express mission. Although Venus has a extreme surface environment and is generally believed to be uninhabitable, some authors have suggested that there might exist some regions in its atmosphere which might be habitable (Morowitz 1967; Cockell 1999; Schulze-Makuch et al. 2004).

Some authors have examined the potential for sustaining life within the Galilean moons of Jupiter. There is strong evidence for the existence of a subsurface liquid water ocean on Europa (Anderson et al. 1998; Zimmer et al. 2000) and evidence for the existence of oceans buried in the deep interiors of Callisto and Ganymede (Spohn & Schubert 2003; Kivelson et al. 2002). Future missions have already been planned, e.g., Jupiter's icy moons Explorer (Sterken et al. 2012), to study Jupiter's moons. This mission will be mainly focus on studying Europa, Ganymede and Callisto as potential habitats for life.

Other potentially habitable environments in the Solar System include Enceladus' subsurface (Parkinson et al. 2008), which it is thought to have a salty subsurface ocean which could harbor life (Parkinson et al. 2008), and Titan's hydrocarbon lakes (McKay & Smith 2005). Titan gives rise to interesting speculations about possibility of life using a solvent other than water.

However, none of these possible forms of life would has colonized the whole planet/moon, as it is the case of our planet. On Earth, life has spread across the entire planet, colonizing every corner and changing the properties of the planet's surface and atmosphere, and only a case like this will be plausible to be detected on exoplanets in the future.

1.5.2 Current potentially habitable exoplanets

In the last few years, we have found some exoplanets that have been considered objects of interest for the search for life, some of them being potentially habitable worlds. Here we summarize the current potential habitable worlds that we know as of September 2013 (Figure 1.11).

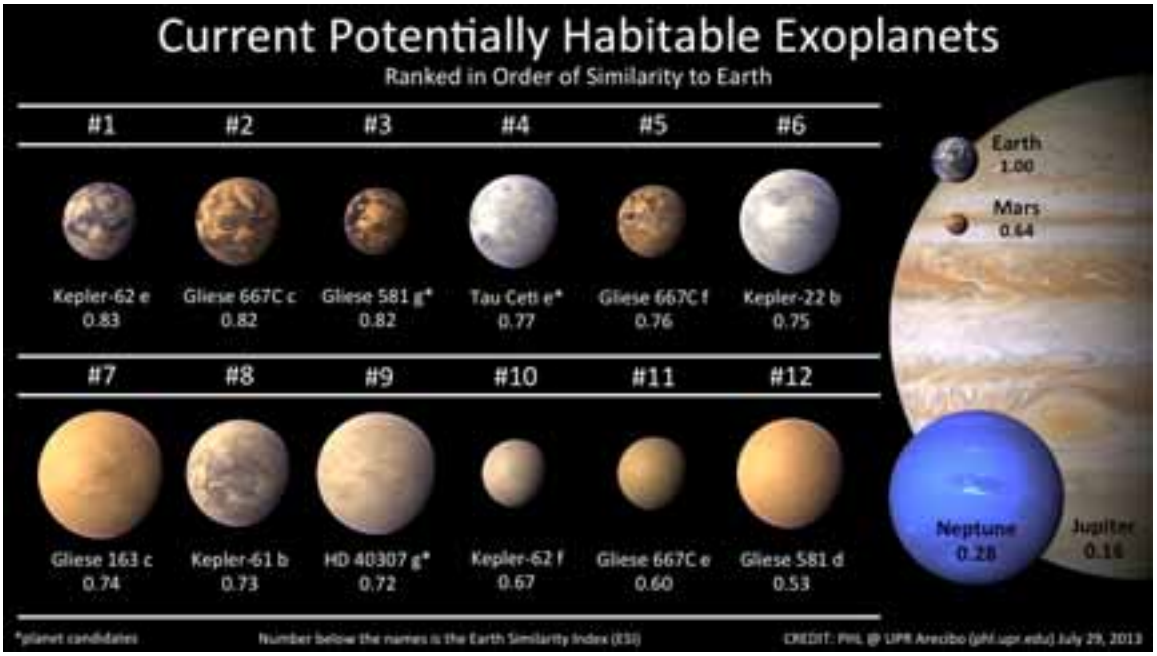

Figure 1.11: Artistic representation of the current potentially habitable exoplanets (July 29, 2013). Kepler-62e is now the best candidate for an Earth-like planet based on measured parameters. Image credit: PHL.

Gliese 581d is a super-Earth orbiting a M3 dwarf star, it has a mass of $7.7M_E$ and orbits close to its host star, at 0.25 AU (Udry et al. 2007a). Although being located in the outer edge of Gl 581's habitable zone, it is thought to be potentially habitable. Selsis et al. (2007) used radiative-convective atmospheric models to derive theoretical and empirical habitable distances for planets orbiting F, G, K, and M stars. Their conclusion was that Gl 581 d could potentially host surface liquid water because of a possible greenhouse effect due to the presence of CO_2-ice clouds. A mixture of several greenhouse gases could also maintain habitable conditions on this planet.

Kepler-22b was the first potentially habitable planet (it is located within the habitable zone of its star) detected by NASA's Kepler mission. Kepler-22 b is a super-Earth which orbits a solar type star (a G5 spectral type), and its radius is just about 2.4 times the Earth's radius. Borucki et al. (2012) found that the surface temperature would be appropriate for liquid water to exist on the Kepler-22b's surface.

Gliese 667C c was discovered in 2011 by Anglada-Escudé et al. (2012) using the radial velocity method. Gliese 667C c is a super-Earth, it is at least 4.5 times as massive as our planet, orbits a M1.5 dwarf, and completes an orbit every 28 days. What is interesting about this exoplanet is that it is located in the center of the habitable zone of its host star, and receives just 10% less stellar energy than the Earth receives from the Sun (Delfosse et al. 2013).

Kepler-62 e and f are two super-Earth-size planets, with radii of 1.61 and 1.41 R_E, that have been recently reported by the Kepler's team. They orbit a K2V star at periods of 122.4 (Kepler-62e) and 267.3 days (Kepler-62f) and lie in the habitability zone of their star. Theoretical models suggest that both planet could be solid, either with a rocky composition or composed of mostly solid water in their bulk (Borucki et al. 2013).

Gliese 163 c was discovered in 2012 by the European HARPS team. It is found orbiting the habitable zone of a red dwarf star in the Dorado constellation. Gliese 163 c is a super-Earth which has a minimum mass of 6.9 M_E and a orbital period of 26 days.

Kepler 61 b is a 2.15 R_E exoplanet that was discovered by using the transit method. Ballard et al. (2013) reported that this planet orbits near the inner edge of the habitable zone of a low-mass star (a K7V spectral type) with a rotational period of approximately 60 days.

Gliese 667C e and f were discovered in 2013 by Anglada-Escudé et al. (2013) by using the radial velocity method. Gliese 667C e and f are two Earth-mass planets with orbital periods of 62 and 39 days, respectively, and are part of a system with six, perhaps seven, planets. Both planets lie within the habitable zone of the star system.

The other three planets in Figure 1.11, Gliese 581 g, Tau Ceti e, and HD 40307 g, are still awaiting for confirmation.

1.5.3 Biosignatures

As exoplanet characterization is progressing rapidly and some Earth-like planets have been already discovered, the question that we should ask is: How will we look for the presence of life on a extrasolar planet?. The approach that astrophysicist have taken is to look for biosignatures, i.e., to identify the fingerprints of life. The concept of biosignature was introduced for the first time by Lovelock. Lovelock (1965) suggested that life on a planet would change the original atmospheric composition by several orders of magnitude. Moreover, such changes could be recognized even at astronomical distances.

To study what kind of biosignatures we should expect to find in extrasolar planets, we first must turn to Earth, as it is the only known planet which harbors life. By studying the Earth, one can see that the biosignatures can be divided into atmospheric composition and surface reflectivity features.

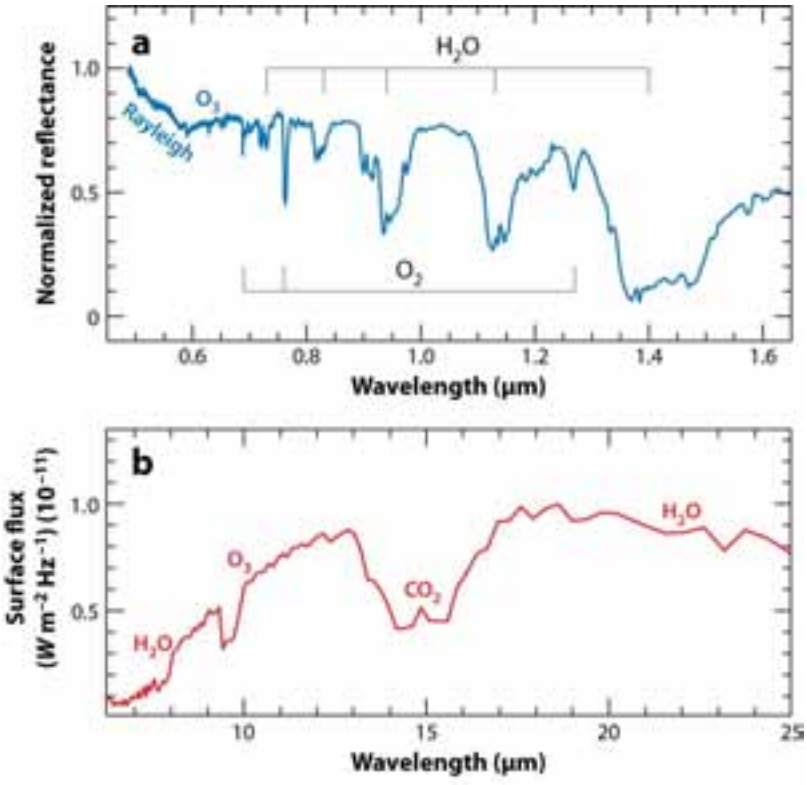

Figure 1.12: (a) Earth's visible and near-IR wavelength spectrum from Earthshine measurements (Turnbull et al. 2006). (b) Earth's mid-IR spectrum as observed by Mars Global Surveyor en route to Mars (Christensen & Pearl 1997). Major Earth's atmospheric biosignatures are noted. Adapted from Seager & Deming (2010).

An atmospheric biosignature is a chemical species in a planetary atmosphere that is out of equilibrium or is a byproduct of life processes. Taking the Earth as example, life produces oxygen as a metabolic byproduct, in this case a byproduct from photosynthesis, and can also produce methane. What is interesting about Earth is that oxygen co-exist with methane, while in normal conditions methane is rapidly consumed by oxygen. Thus the co-existence of high concentrations of a reducing gas with oxygen, or ozone, in planetary atmospheres can be used as a signature of life. In general, any combination of gasses out of equilibrium is considered a biosignature. Another atmospheric signature present in the Earth's atmosphere is ozone. Ozone is produced by the reaction of oxygen with sunlight in the upper atmosphere, and it has a strong signature in the Earth's spectrum. Therefore, we could use ozone as a proxy for the presence of oxygen in an atmosphere (Figure 1.12).

As well as looking at gases in the atmosphere, we could also look for surface features to detect life on the surface of a planet such as the "red-edge" of vegetation (see Figure 1.13). The red-edge is a sudden increase in the Earth's reflectance at approximately 700 nm due to the presence of photosynthetic vegetation, and it has been proposed as a possible biomarker in Earth-like planets (Montañés-Rodríguez et al. 2006; Tinetti et al. 2006c; Kiang et al. 2007a,b). This rise in reflectivity is typically of the order of 6 to 20 times the reflectivity at 500 nm, and depends on vegetation type. Although the red-edge is seen near 700 nm on the Earth's atmosphere, on other planets it could be located at different wavelengths, because of the different planetary atmospheres and host star spectral distribution (Wolstencroft & Raven 2002; Tinetti et al. 2006d).

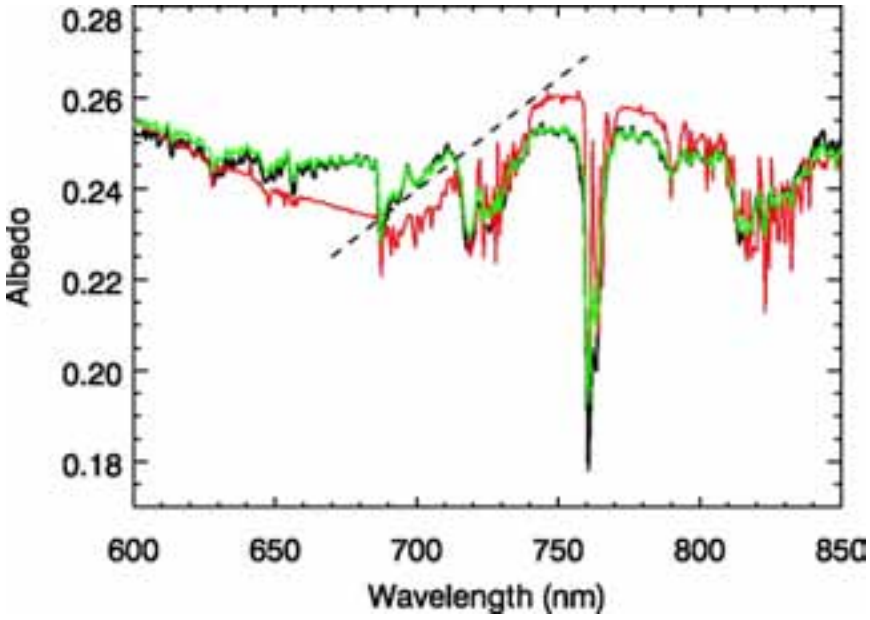

Figure 1.13: Example of the surface feature produced by vegetation (red-edge) on the Earth's spectrum. Black: Earthshine spectral albedo measured from Palomar Observatory. Green: Modeled spectral albedo for the same date as that of the black spectrum. Red: Modeled spectral albedo for a date when a strong vegetation red edge feature was visible due to the large relative percentage of cloud-free vegetated area in the Earth region contributing to the earthshine. Adapted from Montañés-Rodríguez et al. (2006).

It is also possible that we might one day find an inhabited planet but without any atmospheric signs or surface features related to life. Some possible reasons would be that life in such planet is in the subsurface (Cockell et al. 2009), or there is not enough life to produce an atmospheric signature detectable for us. In such cases we will never know that live exists in that planet.

1.6 The Earth as an exoplanet

As detection of exoplanets has increased rapidly in the last few years, one can confidently expect that true Earth analogues will be discovered in large numbers in the near future. Thus, it is clear that the exploration of our own Solar System and its planets is essential. This will allow us to test our theories and models, enabling more accurate determinations, and characterization of the exoplanets' atmospheres and surfaces. In particular, observation of our own planet, as the only example of habitable planet that we have, will be key for the search for life elsewhere. Habitable planets located beyond our Solar System are unlikely to look exactly like the Earth, however, they might share some key characteristics like the presence of an ocean, clouds or surface inhomogeneities.

The first attempt to remotely characterize Earth, as if it were seen by an extraterrestrial observer, was made by using spatially-resolved data obtained by the Galileo spacecraft (Sagan et al. 1993). The Galileo mission was launched on October 1989 and it was designed to study and orbit Jupiter, although, it carried out two flybys of Earth, one in December 1990, and the other in December 1992, which were used as gravitational assists to push the space craft out towards Jupiter's orbit. The data collected in these flybys included UV and NIR spectra, visible photometry at three separate sites on the planet, and radio signals. Sagan et al. 1993 found "evidence of abundant gaseous oxygen, a widely distributed surface pigment with a sharp absorption edge in the red part of the visible spectrum, and atmospheric methane in extreme thermodynamic disequilibrium", in other words, they found strong evidences of life on Earth. The least potentially ambiguous sign of life was the presence of modulated radio signals that were uniquely attributable to technology and therefore to intelligent life.

However, directly imaged exoplanets are unlikely to be spatially-resolved, i.e., we will have all planet's information collapsed in a single point of light (see Figure 1.14). Hence, disk-integrated views of Earth, at different viewing and phase angles, are the best way to understand what kind of information we could retrieve from such type of observations.

One observational approach to determine how Earth would look like to an extrasolar observer has been through earthshine observations. Earthshine is the sunlight which is reflected by Earth via the dark side of the Moon, and it provides a good approximation to a disk-averaged Earth since scattered light from the lunar surface results in a simultaneous sampling of many regions of Earth. Earthshine observations have allowed us to identify spectral features related with life in our own atmosphere, such as water vapor bands, spectral signatures of oxygen and ozone, carbon dioxide and methane.

The visible spectrum of the earthshine has been studied by several authors (Goode

Figure 1.14: The Pale Blue Dot: Earth 'portrait' taken by the Voyager 1 spacecraft at a distance of about 40 AU. Earth can be seen as a single blue dot on the right part of the image. Image credit NASA.

et al. 2001; Woolf et al. 2002; Qiu et al. 2003; Pallé et al. 2003, 2004), while more recent works have extended these studies to the near-infrared (Turnbull et al. 2006) and to the near-UV (Hamdani et al. 2006). More recently, Sterzik et al. 2012 have also studied the use of the linear polarization content of the earthshine to detect biosignatures, and were able to determine the fraction of clouds, oceans, and even vegetation. Several authors have also attempted to identify the presence of the vegetation red-edge (for more details about the red-edge see section 1.5.3) using earthshine observations (Arnold et al. 2002; Woolf et al. 2002; Seager et al. 2005; Montañés-Rodríguez et al. 2006; Hamdani et al. 2006), and also using simulations (Tinetti et al. 2006a,b; Montañés-Rodríguez et al. 2006 and see Figure 1.13).

Another approach has been to analyze Earth's observations from remote-sensing platforms (e.g., Christensen & Pearl 1997; Tinetti et al. 2006a; Cowan et al. 2009, 2011; Robinson et al. 2011). These observations are usually obtained by missions en route from Earth to other solar system targets. The first space mission to include dedicated observations of Earth was the NASA's EPOXI mission. EPOXI observed the disk-integrated Earth, and also the Moon, from distances of 0.18-0.34 AU from both equatorial and polar vantage points, and acquired spatially and temporally resolved visible photometric and near-IR spectroscopic observations (Livengood et al.

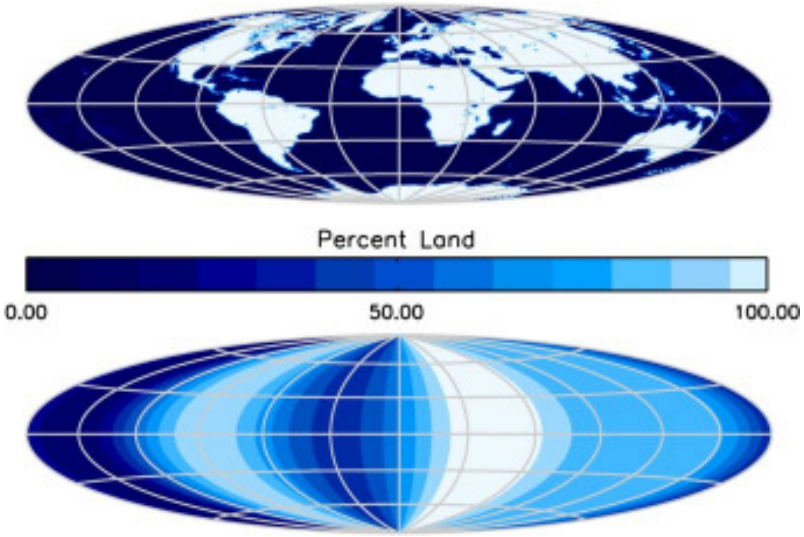

Figure 1.15: Bottom: reconstruction of Earth's continental distribution made by using the spectral and spatial distribution of eigencolors. Top: for comparison the real Earth's continental distribution. From Cowan et al. (2009).

2008). Cowan et al. 2009 were the first ones in analyzing the light curves of Earth obtained with the EPOXI mission. The aim of their work was to determine if it was possible to detect the presence of oceans and continents. Using a principal components analysis they found that 98% of the diurnal color changes of Earth are due to only two dominant eigencolors. The spectral and spatial distribution of the eigencolors correspond to cloud-free continents and oceans, enabling them the reconstruction of longitudinally averaged maps of Earth (Figure 1.15). This experiment demonstrated that it should be possible to retrieve spatial information from multiwavelength photometry of disk-integrated terrestrial planets. Also using EPOXI data, Kawahara & Fujii 2010, 2011 and Fujii & Kawahara 2012 proposed an inversion technique which enables to sketch a two-dimensional albedo maps from annual variations of the disk-averaged scattered light (Figure 1.16). Moreover EPOXI data allowed to empirically categorize Earth among the planets of our Solar System by using visible colors (Crow et al. 2011).

Several models of Earth have also been developed to better understand Earth's global characteristics, from vantage points, and at wavelengths, that may not be accessible to earthshine or spacecrafts. For example, Ford et al. (2001) presented a model that predicts features that are discernible in light curves obtained by low-precision photometry. For Earth-like planets they found daily flux variations of several percents, depending sensitively on ice and cloud cover. Moreover, Pallé et al. (2008) modeled Earth's photometric variability using three months of cloud data taken from satellite observations and determined that the light scattered by the Earth, as a function of time, contains sufficient information, even with the presence of clouds, to accurately measure Earth's rotation period. Furthermore Oakley & Cash

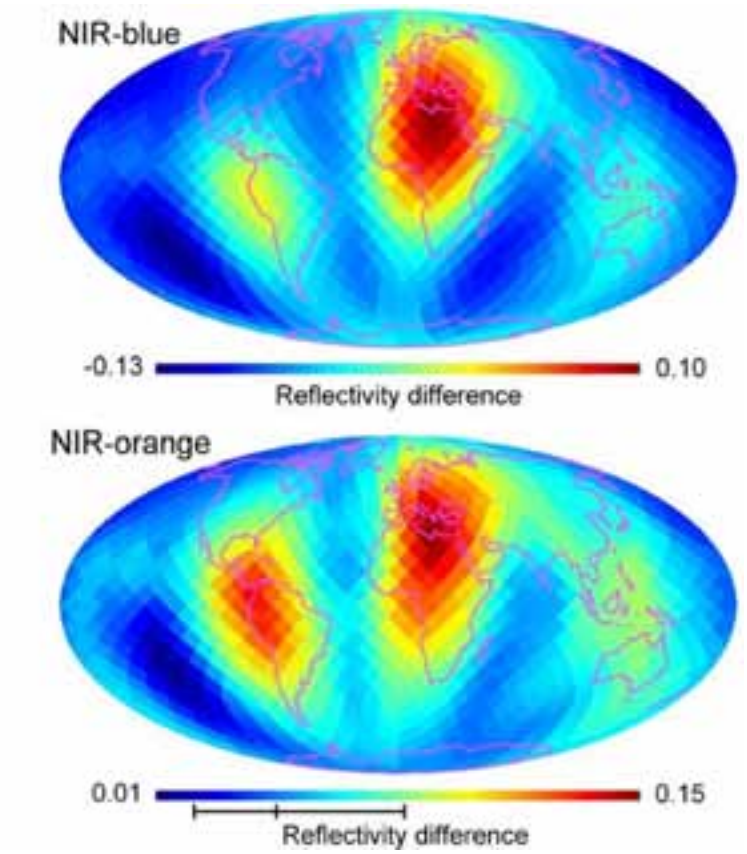

Figure 1.16: Two-dimensional maps of Earth calculated from NIR-Blue (top) and NIR-Orange (bottom) annual light curves by using the inversion technique. The contrast standing out in the NIR-blue map traces the approximate continental distribution of the Earth, while NIR-Orange traces the vegetation red-edge signature. Adapted from Kawahara & Fujii (2011).

(2009) constructed an empirically based code capable of simulating observations of the Earth from any orientation, at any time of year with continuously updated cloud and snow coverage. By simulating these observations, over a full orbital revolution, they determined that the detection of terrain change is possible and attempted to reproduce a longitudinal map of the Earth from these simulated photometric data by using the difference in reflectivity between land and oceans (Figure 1.17).

Other authors have studied the disk-integrated spectra of cryptic photosynthesis worlds: on Earth, photosynthetic organisms are responsible for the production of nearly all the oxygen in the atmosphere. However, in many regions of our planet, and particularly where surface conditions are extreme, photosynthetic organisms can be found in and under substrates where light is still sufficient for photosynthesis. Such a world would be an Earth analogue that show detectable atmospheric biosignatures like our own planet but do not exhibit a discernible biological surface feature in the disk-averaged spectrum (Cockell et al. 2009). Furthermore, Hegde & Kaltenegger (2013), using filter photometry in the visible, have also studied the color-color diagram

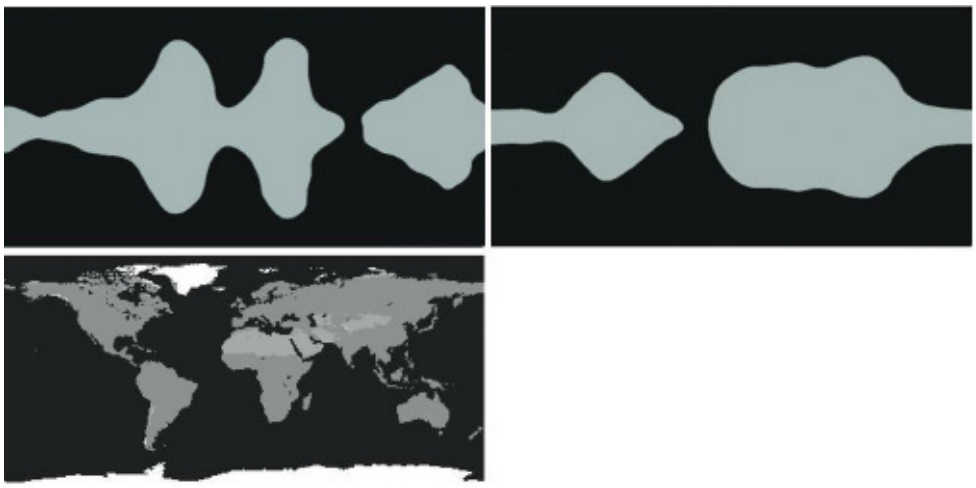

Figure 1.17: Top-left: reconstructed map of the Earth for a system inclined at 90°. Top-right: the same as top-left but for a system inclined 60°. These inversions map reasonably well the relative size of the land masses in their correct longitudinal location. Nevertheless, the shapes of these continents are not well matched. Bottom: map of Earth for comparison. Adapted from Oakley & Cash (2009).

of possible detectable surface signatures of extreme life forms by using the albedo of extremophiles as well as different surfaces where they reside in.

Kaltenegger et al. (2007) modeled the Earth's atmosphere and its biomarkers over geological timescales, both in the visible and in the near infrared. Their work shows that atmospheric features should have changed considerably over Earth evolution from a CO_2-rich to a CO_2/CH_4-rich atmosphere to the present-day atmosphere. Similar results were found by Meadows (2006) concluding that detection of the classic atmospheric biosignatures, the simultaneous presence of CH_4 and O_2, or its proxy O_3, may be easier in a Proterozoic type environment than for modern-day Earth. Thus, studying the Earth through time from the point of view of Earth as an exoplanet is extremely interesting.

1.7 The Earth through time

It is clear that, even if we were to find an Earth-twin, it would not necessarily be at an evolutionary stage similar to the Earth today. On the contrary, extrasolar planets are expected to exhibit a wide range of ages and evolutionary stages. The Earth's history provides a suite of environments different to the modern Earth, which serve as analogs for habitable exoplanets (Meadows 2006; Kaltenegger et al. 2007). Hence, it is of interest not only to use our own planet as it is today, as a template, but also at different epochs.

Earth is 4.500 million years old and during this time, it has undergone multiple changes that have affected its global properties as seem from an astronomical distance.

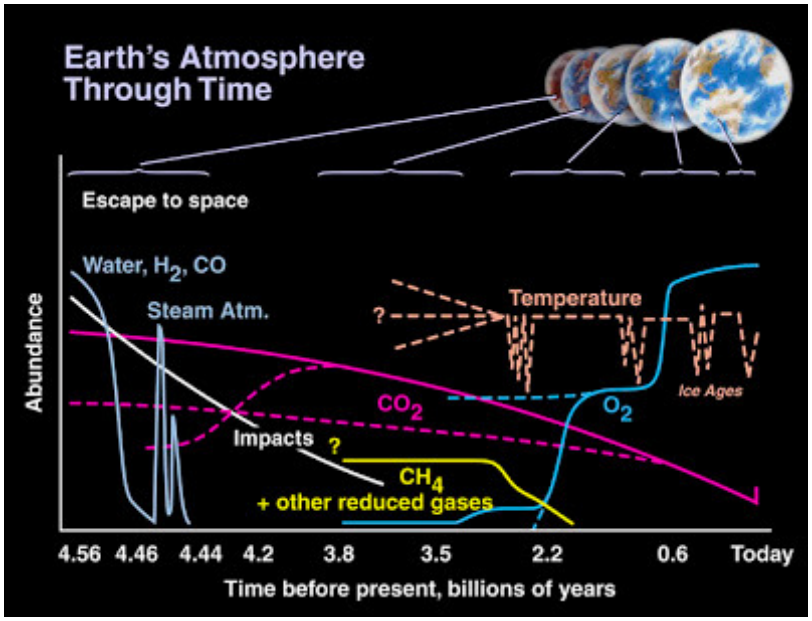

Figure 1.18: Evolution of the atmospheric composition and temperature of Earth. Image courtesy David Des Marais and Kevin Zahnle.

At long time scales, Earth's climate has been dominated by the increase of the solar luminosity and the changes in the greenhouse gases concentrations (Fig. 1.18).

The primitive atmosphere of Earth was likely dominated by CO_2, with N_2 being the most abundant gas, and trace amounts of methane, and ammonia, among others (Kasting & Siefert 2002). At that time, the Sun was about 70% dimmer than it is today, but the climate was generally warm enough to have oceans of liquid water at least since 4.4 Ga ago (Wilde et al. 2001), being this decreased luminosity probably compensated, at least in part, by a stronger greenhouse effect (Sagan & Mullen 1972; Owen et al. 1979; Walker et al. 1981). This primitive atmosphere was modified by two major processes: the reduction of CO_2 and the rise of O_2. A huge amount of CO_2 must have been removed from the atmosphere, most likely by the burial of carbon by reacting with silicates to form carbonate rocks (e.g., Sleep et al. 2001).

1.7.1 Plate tectonics

Plate tectonics characterizes the geodynamic behavior of the present-day Earth, and there are evidence suggesting that it was active since at least 3-3.5 Ga (Moyen et al. 2006; Chen et al. 2009) and probably more than 4 Ga (Hopkins et al. 2008). Although, other authors consider that plate tectonics may have started later, around 2.0 Ga (Thompson et al. 2010). This movement of plates has caused the formation and break up of continents over the Earth's history (Fig. 1.19), including the formation of supercontinents such as Rodinia (1.100-750 Ma ago), Pannotia (650-540 Ma ago) or Pangaea (300-180 Ma ago). The last supercontinent, Pangaea, was composed by

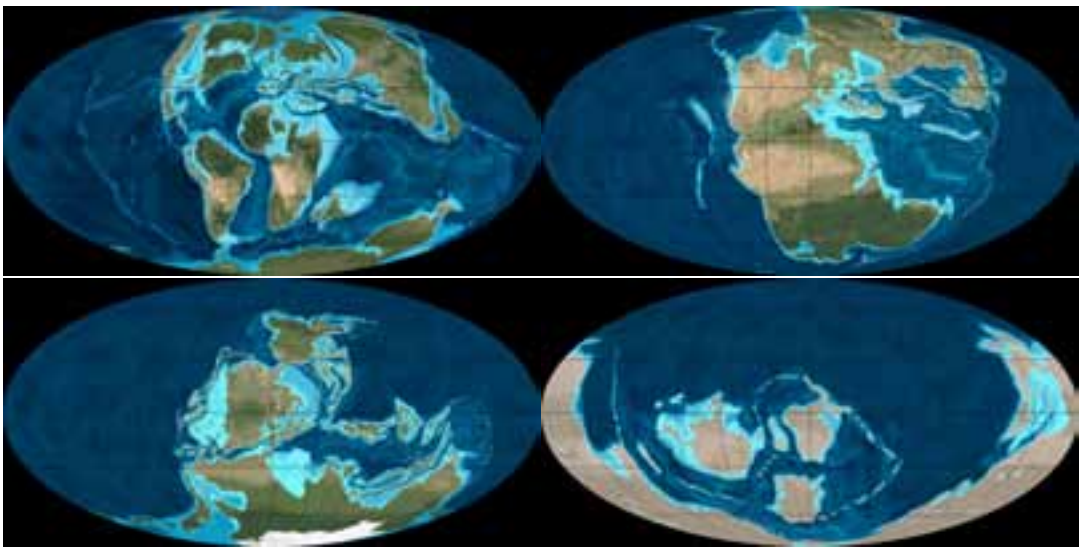

Figure 1.19: Paleogeographic views of Earth at the Late Cretaceous (90 Ma ago), Late Triassic (230 Ma ago), Mississippian (340 Ma ago), and Late Cambrian (500 Ma ago).

two subunits: Laurasia and Gondwana. With the final breakup of Laurasia (60 Ma ago), the continents acquired the current configuration (Vázquez et al. 2010).

Plate tectonics has been suggested to be important for the evolution of life (e.g., Parnell 2004; Lammer et al. 2009). On Earth, plate tectonics helps in the regulation of the atmospheric composition by recycling volatiles, including greenhouse gases such as CO_2, which is needed to stabilize the temperature and hence, the planet habitability. Plate tectonics is also involved in the generation of a magnetic field, which shields life on Earth from damaging radiation.

Although the mechanisms that drive plate tectonics are still far from being completely understood, there are indications that one of the requisites is water (e.g., Regenauer-Lieb et al. 2001; Solomatov 2004). Water acts as a lubricant that allows the plates of the crust to move and subduct. Without water in the mantle, the planetary tectonic engine would stop. Thus, worlds with plate tectonics are likely to have water, one of the main essential ingredients for the evolution of life.

1.7.2 The origin of life

It is though that life was establish on Earth at least 3.5 Ga ago, perhaps as early as 3.8 Ga ago (Mojzsis et al. 1996), although the precise timing remains uncertain (Nisbet & Sleep 2001; van Zuilen et al. 2002). This would suggest that life may have emerged during or shortly after the period called the Late Heavy Bombardment, a period of intense asteroid and comet impacts on the surface of the early Earth which

lasted several hundred million years (4.5-3.8 Ga ago, Strom et al. 2005).

The question about where life began is still open as we only have little knowledge about where the first prebiotic ingredients may have been synthetized. The potential places for the origin of life include submarine vents, primordial beaches (Bywater & Conde-Frieboesk Kilian 2005), and shallow pools and lagoons. An even more controversial aspect is whether the ingredients of life originated on Earth or were delivered to Earth from outerspace (Chyba & Sagan 1992).

The only direct evidence of early life on Earth is from fossil and chemical signatures preserved in the geological record. The earliest evidence of life on Earth comes from graphitic inclusions within >3.83 Gyr marine sediments from West Greenland (Mojzsis et al. 1996). However, one difficulty identifying the earliest evidence of life is that most of the rocks have been destroyed by erosion and plate tectonics. One of the main evidence of life on Earth that we have is ancient stromatolites. Stromatolites are dome - or column-like sedimentary rock structures that are formed today in shallow marine water, layer by layer, over long periods of geologic time, commonly of biological origin. This structures form the dominant part of Earth's early fossil record (Hofmann 2000) thus providing a potentially important source of information about early life. However, stromatolites are shaped by a complex interaction of physical, chemical, and biological processes, and identifying unambiguous signatures of life from the preserved morphology of the structures can be extremely difficult (Semikhatov et al. 1979; Grotzinger & Knoll 1999). The oldest stromatolite found is about 3.5 billion years old and was found in Western Australia.

There are also indirect ways to identify life and this is through chemical evidences. Carbon occurs in different varieties, for example ^{12}C and ^{13}C. When organisms ingest carbon, they preferentially use ^{12}C. Carbon with a high ratio of ^{12}C compared to ^{13}C is therefore an indicator of living processes.

Purple bacterias

Purple bacteria are likely among the first forms of life that colonized Earth. They are microorganisms that can inhabit both aquatic and terrestrial environments, and several species can live in extreme environments in temperature, pH, and salinity. These bacteria are photosynthetic and grow autotrophycally, with CO_2 being the carbon source. However, they are very metabolically flexible, allowing them to colonize a variety of niches. Unlike cyanobacteria, algae and plants, purple bacteria do not produce O_2 as a waste product of the photosynthesis. These bacteria contain bacteriochlorophyll a or b as a pigment along with carotenoids pigments that give them colors that range between red, brown and purple.

Microbial mats

Microbial mats are multilayered sheets of microorganisms generally composed of both Prokaryotes and Eukaryotes, being able to reach a thickness of a few centimeters. The time when microbial mats appeared on the Earth surface is still unclear, but prior to the evolution of algae and land plants on early Earth, photosynthetic microbial mats probably were among the major forms of life on our planet. Microbial mats are found in the fossil record as early as 3.5 billion years ago. Later, when advanced plants and animals evolved, extensive microbial mats became rarer, but they are still present in our planet in many ecosystems (Seckbach & Oren 2010). They persist in special environments such as thermal springs, high salinity environments, and sulfur springs.

Development of land plants

Land plants are believed to have appeared during the Ordovician period, 485-440 Ga ago, (e.g., Gray et al. 1985; Qiu et al. 2006) and are thought to have evolved from marine species, such as marine green algae (e.g., Kenrick & Crane 1997; Qiu et al. 2006; Finet et al. 2010). Green algae is one of the most diverse group of algae, with approximately 8000 different species (Guiry 2012). This transition from an aqueous to a gaseous medium must have required particular adaptations. Land plants were forced to develop both, structural and physiological characteristics for the new environmental conditions, such as the development of protection mechanisms against radiation and desiccation (Beraldi-Campesi 2013).

The appearance of land plants, and its later diversification, had dramatic effects on the atmospheric chemistry of our planet, by changing atmospheric CO_2 and O_2 concentrations. This evolution also changed the terrestrial and marine environments by accelerating rock weathering and increasing the release of mineral nutrient into oceans (e.g., Algeo et al. 2000; Berner 2004; Beerling & Berner 2005).

1.7.3 The faint young Sun problem

As the Sun was less bright when it was young, the Earth received during the Archean eon just about 75-80% of the energy that it receives today (e.g., Gough 1981; Bahcall et al. 2001). Hence, Earth would have been cold enough so that it could not support liquid water on its surface. However, life is known to exist during that epoch (see Subsection 1.7.2) and liquid water is believed to be essential for life (see Section 1.5). This contradiction is known as "the faint young Sun problem" and it was first pointed out by Sagan & Mullen (1972). Several possible solutions have been proposed since then but this problem is still under debate. The most common explanation is that the planet may have had larger concentrations of atmospheric greenhouse gases like carbon dioxide and methane (e.g., Kasting et al. 1984b; Kiehl & Dickinson 1987;

Haqq-Misra et al. 2008; Kienert et al. 2012). Other proposed explanations are related the smaller continental area that the Archean Earth may have had. For example, Rosing et al. (2010) stated that a lower reflectivity of the early Earth's surface could have led to environmental conditions above the freezing point.

1.7.4 The Great Oxidation Event

The Earth's atmosphere has undergone many changes since its formation, but one of the most interesting changes is the raise of oxygen to levels similar to that we are familiar with today. This period is the so called "Great Oxidation Event". Abundant levels of oxygen in the Earth's atmosphere distinguishes our planet from other in the Solar System. Moreover, it supports animals, fungi and multicellular plants, a fact that makes Earth's surface look quite different from that of our neighbors (Catling et al. 2005).

Over the last decades, new geochemical data suggest that there were two significant increases of oxygen in the Earth's atmosphere. The first rise of oxygen is thought to have taken place at the beginning of the Proterozoic era, around 2.45 Ga ago (Bekker et al. 2004). Oxygen might have risen up to about 5-18% PAL (present atmospheric level), although oxygen levels at this time are difficult to constraint (Canfield 2005). The second rise of oxygen is believe to have taken place within the Neoproterozoic era, about 1.0-0.6 Ga ago, to values $>$ 10% PAL (Canfield 1998, 2005).

Since organic compounds of dead organisms react with atmospheric oxygen, Karhu & Holland (1996) suggested that the oxidation event was probably driven by an increased input of oxygen to the atmosphere arising from an increased sedimentary burial of organic matter between 2.3 and 2.0 Gyr. Moreover, Kump & Barley (2007) also proposed that the rise of atmospheric oxygen was closely tied to Earth's tectonic evolution. An increase of subaerial volcanoes, with respect to the submarine ones, could have reduced an important oxygen sink leading to the rise of atmospheric oxygen.

As cyanobacteria can live both anaerobically and aerobically, several authors have also suggested that they might have been responsible for the initial rise of atmospheric oxygen (e.g., Kasting & Siefert 2002; Flannery & Walter 2012). Cyanobacteria, that appeared several hundred millions years ago on Earth, are microbes that conduct photosynthesis, they use sunlight, CO_2 and water producing oxygen as a waste product.

Therefore, how free oxygen became abundant in the early Earth's atmosphere is still an open question. What is clear is that these rise of oxygen has profound consequences for the Earth's environment. A rise in oxygen would lead to a reduction of methane and carbon dioxide, two powerful greenhouse gases, lowering the global temperature. In fact, it is thought that Earth's global glaciations might have been

related to the periods of rising atmospheric oxygen, since those correspond temporally with the two major glacial activity intervals (Pudritz et al. 2007). During this glacial periods, ice probably reached the equatorial regions, and the global mean temperature would have been about -50°C, as most of the Sun's radiation would have been reflected back to space by the icy surface. Furthermore, a rise in oxygen might have facilitated the rise of complex multicellular organisms.

1.8 Objectives

The aim of this thesis is to study the Earth as if it were an exoplanet, that is, to study the photometric and spectroscopic characteristics of the only known planet which harbors life, as if it was seen from an astronomical distance. As extrasolar planets are expected to be found at a wide range of different evolutionary stages, if we were to find an Earth analogue it is very unlikely that it were at a similar stage of evolution as the Earth is today. Hence, here we study our planet not only at its current stage of evolution but also at different epochs. In this work, we explore how different continental and cloud distributions, atmospheric compositions, and the evolution of different forms of life on our planet may have affected the way our planet looks from afar.

To this end, first of all we have attempted to understand the Earth's large-scale cloudiness behavior by using satellite-based cloud measurements. We have studied how clouds distribute themselves over the Earth's surface, based on surface types and latitude, with the final objective of applying this knowledge to try to reconstruct how the cloudiness of the Earth may have appeared along its history.

We have used a simple albedo model with the aim of studying the photometric variability of past epochs of Earth, when the planet showed a different continental layout, according to their different geographic and cloud distribution. Based on these results, and in order to complete this work, we have also modeled the visible, near-IR and IR disk-integrated radiation of the Earth, along different geological epochs, as a function of the planet's rotation. To do that, we have used a line-by-line radiative transfer model to generate a spectral library of more than 7500 spectra. This radiative transfer model makes use of atmospheric composition and temperature profiles, spectral albedos of surface types, and cloudiness and aerosol information as input data for the calculations. Since we are interested in obtaining disk-averaged views of our planet we created a code that allows to calculate disk-integrated Earth's spectrum for any viewing geometry, surface map and cloudiness distribution, by using the aforementioned spectral database.

Finally, by using the spectral library and the disk-integrated model we studied the influence that different forms of life have in the Earth spectra and if it could

be possible to detect such life forms taking into account different cloud covers, atmospheric composition, and continental scenarios.

2

Model Inputs

In this chapter, we give a detailed description of the data that have been developed and used as inputs in the photometric and spectroscopic simulations of Earth carried out in this thesis. These inputs are: atmospheric profiles of both the early and present-day Earth, geographical maps of continental distributions, cloudiness maps, aerosols properties, and spectral reflectances for a set of different surfaces.

2.1 Atmospheric profiles

Information about temperature and distribution of atmospheric gases for the present-day Earth and up to 500 Ma ago, were taken from FSCATM (Gallery et al. 1983). For these cases, we have considered five atmospheric profiles models: tropical, midlatitude summer, midlatitude winter, subartic summer, and subartic winter. These atmospheric profiles include mixing ratios of the most significant molecules in the Earth's atmosphere: H_2O, CO_2, O_3, N_2O, CO, CH_4, O_2 and N_2 (see Figure 2.1).

It is worth noting that over the past 500 Ma, on average, the Earth has maintained the same composition and mean averaged temperature (Hart 1978; Kasting & Siefert 2002). Something that is not true at longer time scales. Thus, in our simulations up to 500 Ma ago, we have used for our models the present-day temperature and composition profiles. We also used atmospheric and temperature profiles corresponding to the Earth 3.0 Ga ago. These profiles were calculated by R. Ramirez (private communication). A 1-D radiative-convective climate model, first developed by Kasting et al. 1984a and recently substantially updated by Kopparapu et al. 2013 and Ramirez et al. 2013, was used to calculate these atmospheric properties.

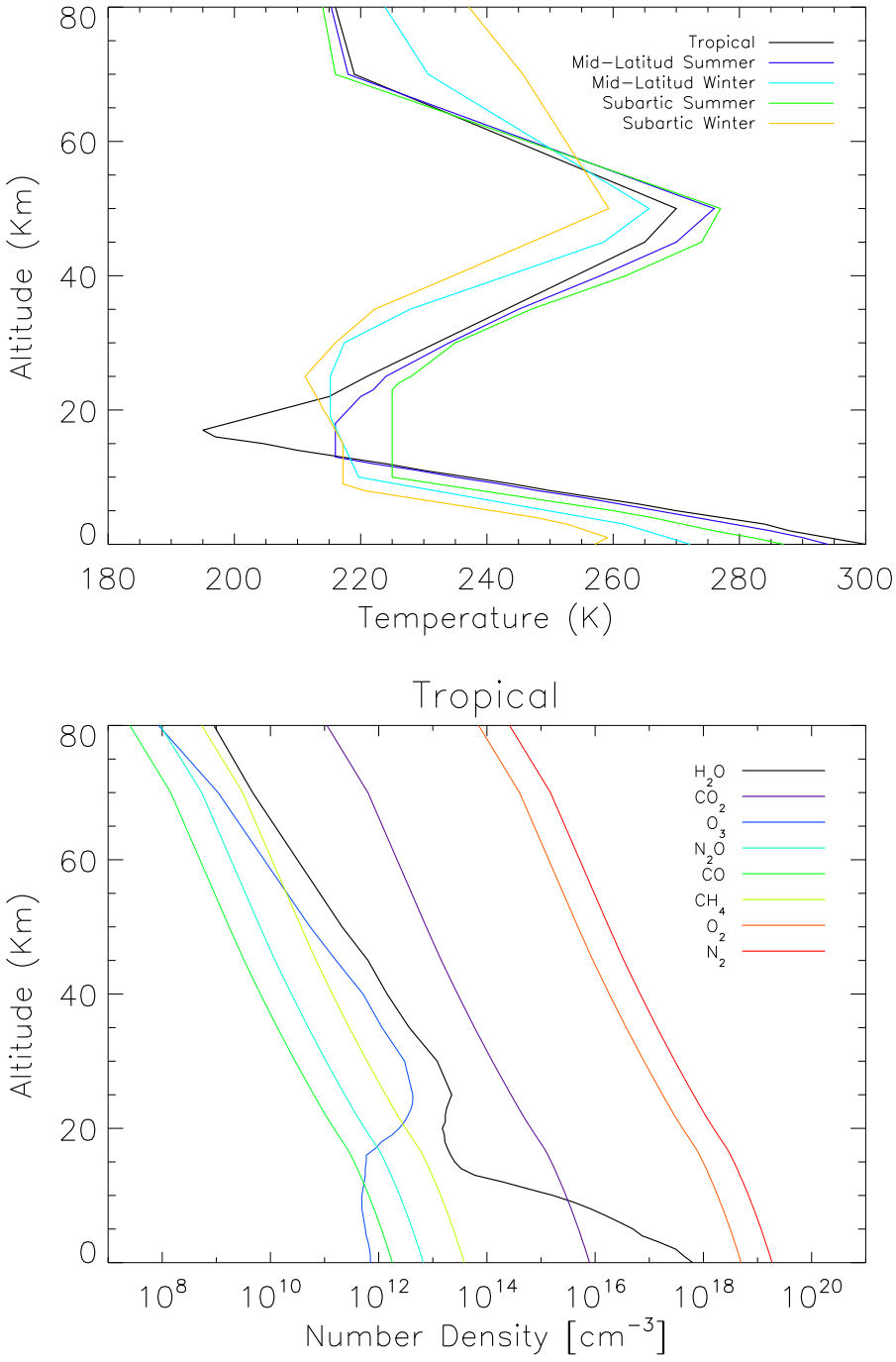

Figure 2.1: Atmospheric profiles of the Earth at present taken from FSCATM. Top Figure shows the temperature profiles as a function of altitude for each of the 5 atmospheric profiles chosen. Bottom Figure shows, for the tropical case, the number density profile as a function of altitude of each atmospheric species.

These profiles consist of 1% CO_2 and 0.2% CH_4, (according to Kaltenegger et al. 2007), being the remaining gas N_2. The temperature and mixing ratio profiles of these species are shown in Figure 2.2. A Manabe-Wetherald relative humidity profile was used (Manabe & Wetherald 1967). For the calculation of these profiles the Sun was assumed to have ∼79% of its present-day luminosity, as we aimed to simulate the Earth 3.0 Ga ago (Gough 1981; Bahcall et al. 2001).

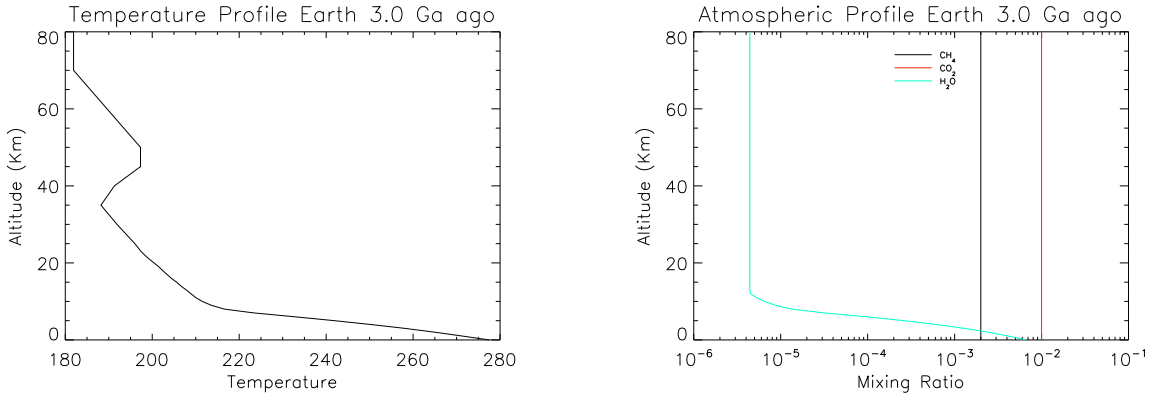

Figure 2.2: Temperature (left) and mixing ratio (right) profiles of the Earth 3.0 Ga ago as a function of altitude. For this epoch we have used 1% CO_2, 0.2% CH_4, and no O_2 or O_3 in the atmosphere.

These properties are prescribed into 33 uneven layers, spanning from 0 to 100 km height, being the spacing between layers of 1 km near the bottom of the atmosphere, and 5 km or more above 25 km height. As the original atmospheric profiles of the Earth 3.0 Ga ago were prescribed in layers up to 70 km, we assumed the same constant values between 70 and 100 km.

2.2 Earth's continental distribution along time.

In order to obtain detailed information on the varying distribution of oceans, continents, deserts, vegetation and ice at different epochs of the Earth's history, such as the Late Cretaceous (90 Ma ago), the Late Triassic (230 Ma ago), the Mississippian (340 Ma ago), or the Late Cambrian (500 Ma ago), we used RGB images of these epochs, which are available on Ron Blakey's Web page[1]. The choice of these epochs was made in order to cover a wide range of land distributions. These geological maps (see Figure 1.19) have been constructed using interpretations from a wealth of geologic literature and publications, available on the project's Web page (see, for

[1] http://jan.ucc.nau.edu

example, Frisch et al. 2011 and references therein).

A RGB image can be considered as a data array with $(n, m, 3)$ dimensions, where the first and second dimensions establish the size of the image and the third dimension defines the red, green and blue components of the image. Each point of each component has a value that ranges from 0 to 255. In this way, a pixel whose value is 0 will be shown in black, whereas another pixel with a value of 255 will be shown in white. As a result, we will have a gray scale image for each color component.

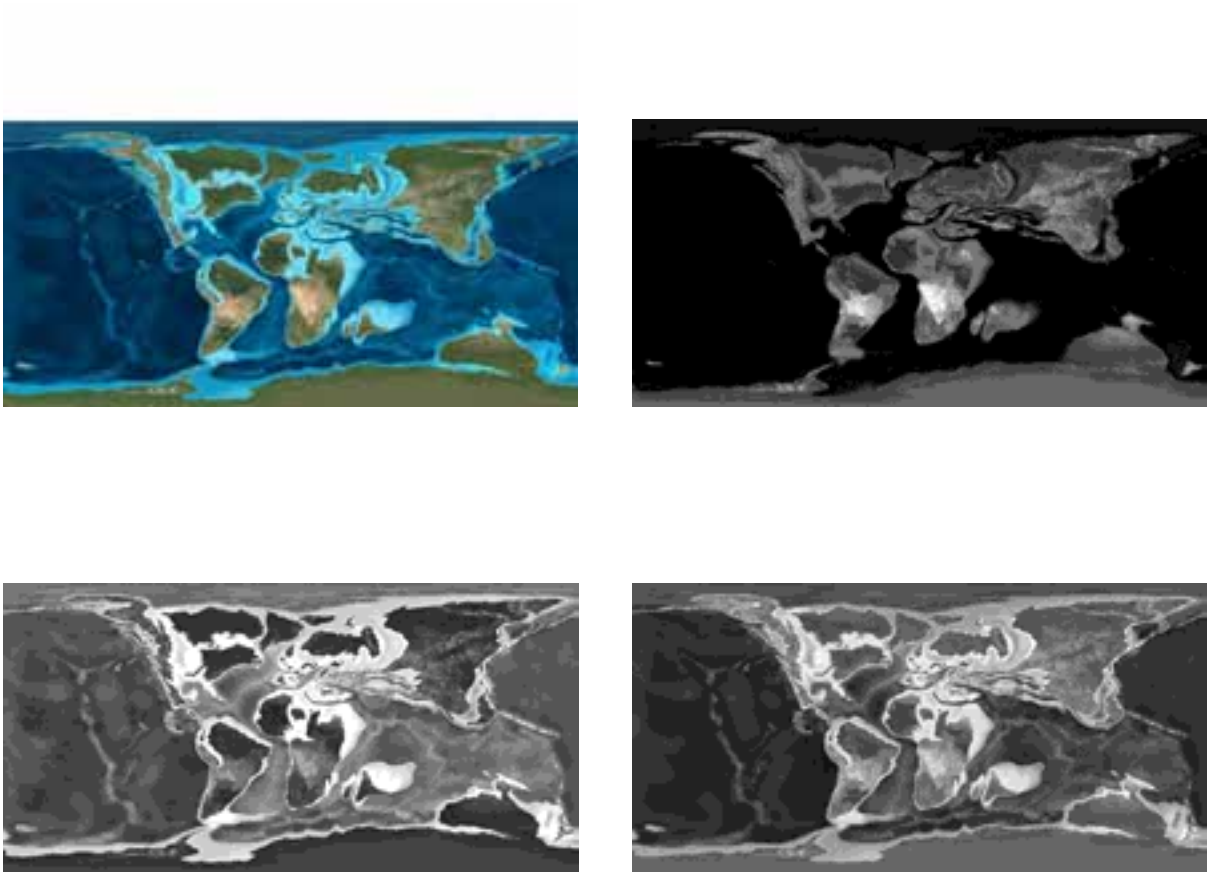

Figure 2.3: Appearance of Earth 90 Ma ago. The true color image is shown in the upper-left corner of the image. The red, blue, and green components are shown in the upper-right, bottom-left, and bottom-right corner, respectively.

A good technique for the segmentation of different parts of an image is the intensity thresholding method. This technique basically consists of the choice of a threshold. Then, image intensities greater than or equal to this threshold, are assigned to one class (which are then represented in white) and the remaining intensities are assigned to another class (represented in black). Taking into account that different areas in an image, in this case: oceans, deserts, vegetated areas, etc., have a different intensity in the same color component, to achieve the identification of these areas in our geological

Figure 2.4: Result obtained after applying the thresholding method to the image of Earth 90 Ma ago. The different zones are identified with different colors. Oceans are represented in black, vegetation in light gray and desserts in dark gray.

maps, we applied this thresholding method to each of the three color components.

To illustrate this method, consider the RGB image of the Earth 90 Ma ago (Figure 2.3 upper left corner). If one wants to separate, for example, oceans from vegetation and deserts, one just needs to perform a thresholding in the original image. By simple inspection of Figure 2.3 it is clear that oceans are going to be those areas in which pixels in the red component (Figure 2.3 upper right corner) are the darkest, intersected with those with the brightest pixels in the blue component (Figure 2.3 bottom right corner), whereas deserts will be found where pixels have the highest values in the red component. The remaining pixels will correspond to vegetation. As a result, we obtain an image with oceans, deserts and vegetation areas identified with a different intensity gray-scale color (see Figure 2.4). This image is then transformed into a grid, which our models read, containing information about surface types.

To carry out this project, we have considered five different land-masses configurations corresponding to: the Late Cambrian (500 Ma ago), the Mississippian (340 Ma ago), the Late Triassic (230 Ma ago), the Late Cretaceous (90 Ma ago), and the present-day Earth. We used the maps shown in Figure 1.19 and we applied them the thresholding method in order to identified each surface type. The original resolution of theses maps is 750(longitude)×375(latitude), however, this resolution was regridded to a lower resolution for the purposes of this thesis.

2.3 Cloud distribution and properties

2.3.1 A semiempirical model for Earth's clouds

One of the main difficulties when attempting to study the reflectance properties of Earth in the past, is the complete lack of reliable information about cloud distribution

at these timescales. One possibility is to use global climate models in order to model the expected cloud amount in past epochs. Nevertheless, this is not easy to do with accuracy, as in fact cloud amount and variability poses one of the most complicated puzzles for climate change today. Despite results of numerous general circulation models, it is still unclear how increasing atmospheric temperatures resulting from anthropogenic forcings may influence global cloud properties. Due to the large radiative influence exerted by cloud cover, a small change in cloud amount or distribution may potentially provide a strong feedback effect, significantly enhancing or mitigating the effects of global warming (Cess et al. 1996; Dessler 2010; Spencer & Braswell 2010). Here, we use a different approach to tackle this problem. We derived a semi-empirical model to map how clouds behave over the Earth's surface depending on latitude and surface types - such as ice, water, desert and vegetation - which then we applied to past epochs.

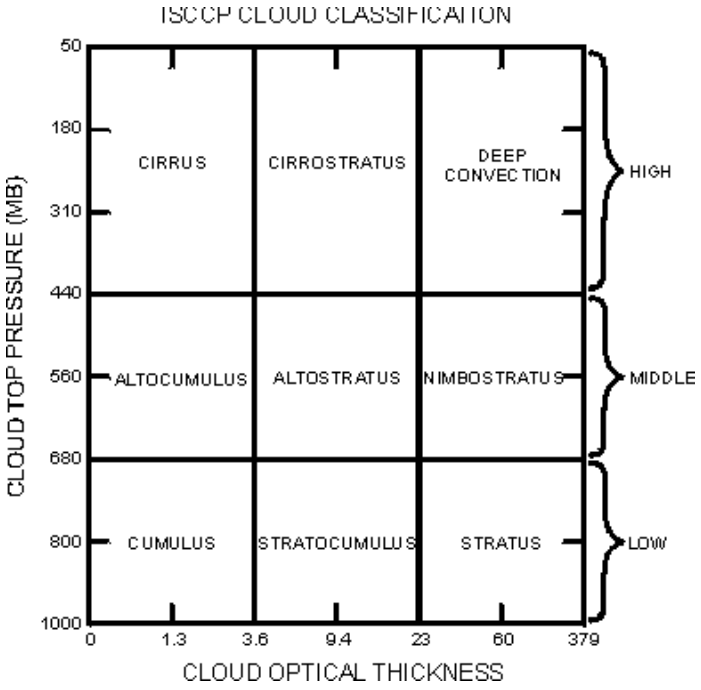

Figure 2.5: Cloud-type definition used in ISCCP dataset.

With this idea in mind, we have made use of cloudiness data from the International Satellite Cloud Climatology Project[2] (ISCCP). Since 1983, ISCCP have been collecting and analyzing satellite radiance measurements to infer the global distribution of clouds, their properties, and their diurnal, seasonal, and interannual variations. The resulting datasets and analysis products have been used to improve our understanding and modelling of the role of clouds in climate, with the primary focus being the elucidation of the effects of clouds on the radiation balance.

[2]http://isccp.giss.nasa.gov

To our purpose we used the monthly mean fractional cloud cover data (D2). These data are given for 280×280 km^2 cells, i.e., we have maps with a grid over the Earth's surface which has 144×72 cells in longitude and latitude, respectively. Each map's grid point has a value, between 0% and 100%, that represents the cloud cover fraction. This cloud fraction has been determined by dividing the number of cloudy pixels by the total number of pixels in each cell.

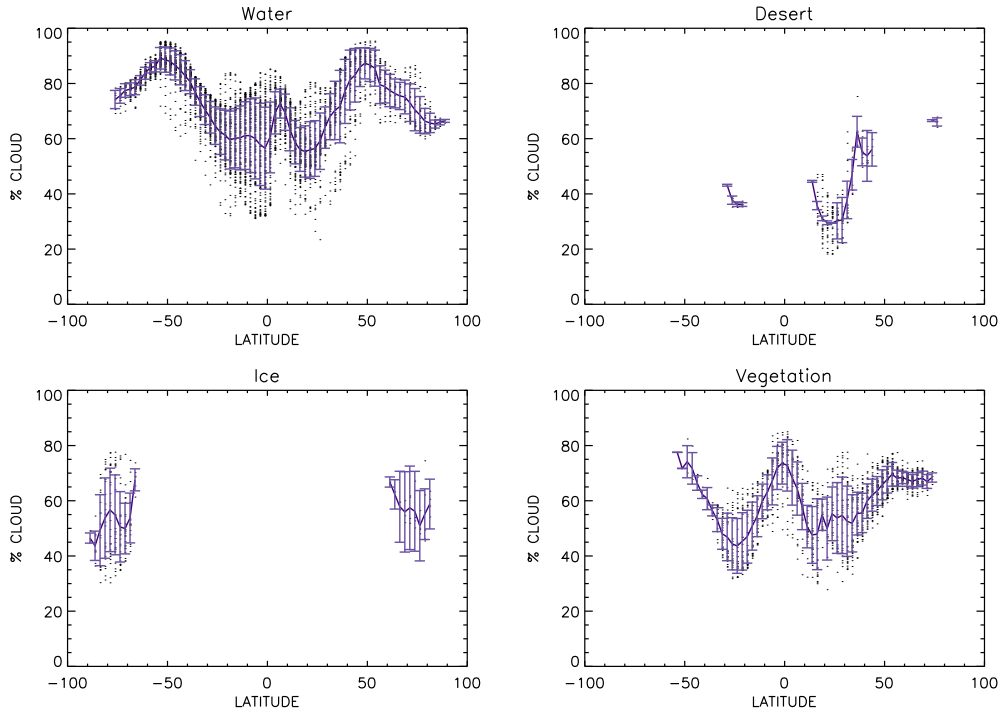

Figure 2.6: Annual mean total cloud amount (cloud fraction) as a function of latitude for each surface type: water (top left), desert (top right), ice (bottom left) and vegetation (bottom right). Dots correspond to the cloud amount at different longitudes along the same parallel. The solid lines represent the mean cloudiness along a terrestrial parallel and the bars represent the standard deviation of the mean. Mean cloudiness as a function of latitude keeps a well-defined pattern which is different for each surface type.

ISCCP's cloud dataset is classified into four cloud types: total cloud amount, low, mid, and high clouds. Total cloudiness is determined using both visible and infrared radiances, whereas the separation into low, mid and high level cloud types is determined using infrared radiance only. ISCCP's definition of cloud types is determined in terms of their cloud-top pressures and optical thicknesses as shown in Figure 2.5. For more details about ISCCP data see Rossow et al. 1996.

In order to obtain the cloud distribution at different epochs of the Earth's history, the first step was to calculate the 1984-2006 climatology of ISCCP cloudiness data.

With this climatology we performed a classification of cloud amount depending on surface types. That is, cloudiness were split up into four groups taking into account the surface type over which the cloud is located. To carry out this classification, we used geographical information about the different kinds of surfaces and vegetation types that are present in our planet according to the classification made by ISCCP. These surface types are: water, rain forest, deciduous forest, evergreen forest, grassland, tundra, shrub-land, desert, and ice. However, for our study we only distinguished between water, desert, ice, and vegetation, where the latest is defined as such zones where there are rain forest, deciduous forest, evergreen forest, grassland, tundra, or shrub-land. Although not shown here, separate analysis for these subgroups were performed giving very similar results.

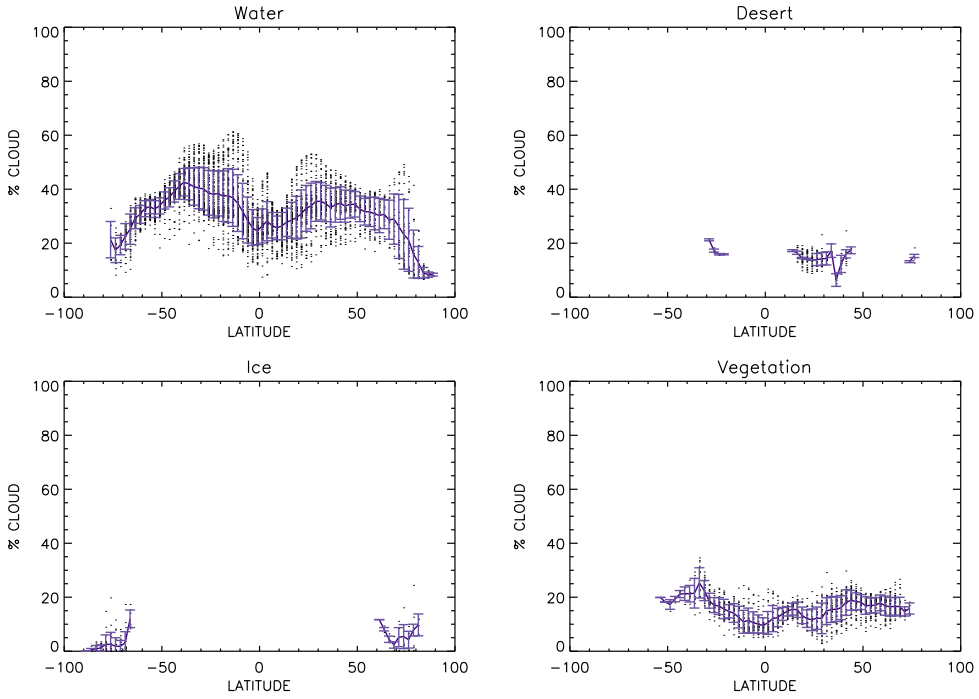

Figure 2.7: The same as the Figure 2.6 but here for low cloud amount.

Once we got the classification of cloud amount into these four groups, we represented the fraction of clouds as a function of latitude for each surface type. This scheme was used to calculate the mean cloudiness at each latitude point and its corresponding standard deviation, thus obtaining empirical relationships between cloud amount, surface type, and latitude (see Figure 2.6). These derived cloudiness functions have a particular shape which is different for each surface type, suggesting that global cloud distribution can be empirically traced according to latitude and the underlying surface type.

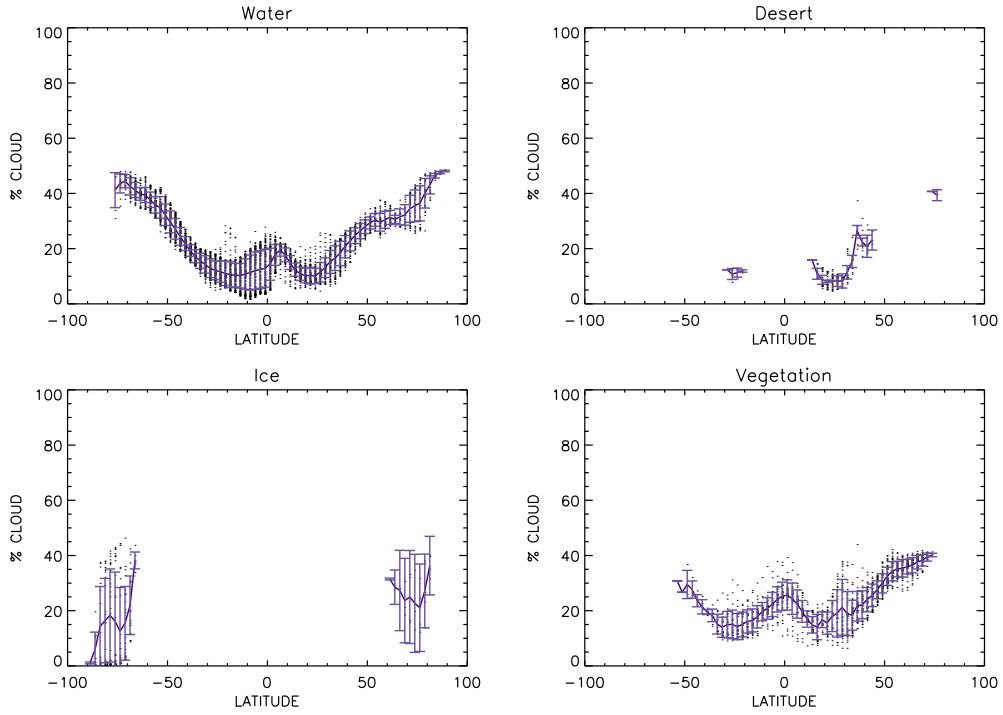

Figure 2.8: The same as the Figure 2.6 but here for mid cloud amount.

Mean cloudiness located over oceans as a function of latitude shows a relatively symmetrical shape in both hemispheres. This mean cloudiness varies between 30% and 95%, lying the maxima values in the middle-latitudes (between 30°- 60°) and in the tropics (0°- 15°). The subtropics (15°- 30°) are found to be regions of low cloudiness. Cloud cover in the Southern polar region tends to be higher than in the Northern polar region. Moreover, the major dispersion in cloudiness values are found at tropical and subtropical latitudes, whereas at higher latitudes the dispersion is lower.

As expected, cloud cover in desert zones tends to be lower than in the other surface types. Here, mean cloud amount varies from 20% to 70%, approximately. Regarding ice, the Northern polar region presents higher values of cloud cover than the Southern polar region. These measures of mean cloudiness over snow/ice present a huge dispersion. This is related to the fact that satellite-based cloudiness estimates over surfaces covered by snow or ice are somewhat uncertain.

Clouds located over surfaces covered by vegetation show a latitudinal distribution which varies from 30% to 85%, approximately. This distribution has a relative maximum in equator, and two minima at the tropics. In general, mid-latitude cloud cover values are generally lower over land than over oceans.

Differences in the cloud cover's behavior in each hemisphere are related to their differing land/ocean distribution/extension and to their opposite seasonal cycle. But not all cloud types follow the same patterns. This latitudinal distribution of clouds has a different behavior according to cloud types (see Figures 2.7, 2.8, and 2.9 for low, mid, and high clouds). In general, tropics are predominantly covered by both low and mid clouds, mid-latitudes are also mainly covered by low and mid clouds, and polar regions are covered by mid clouds.

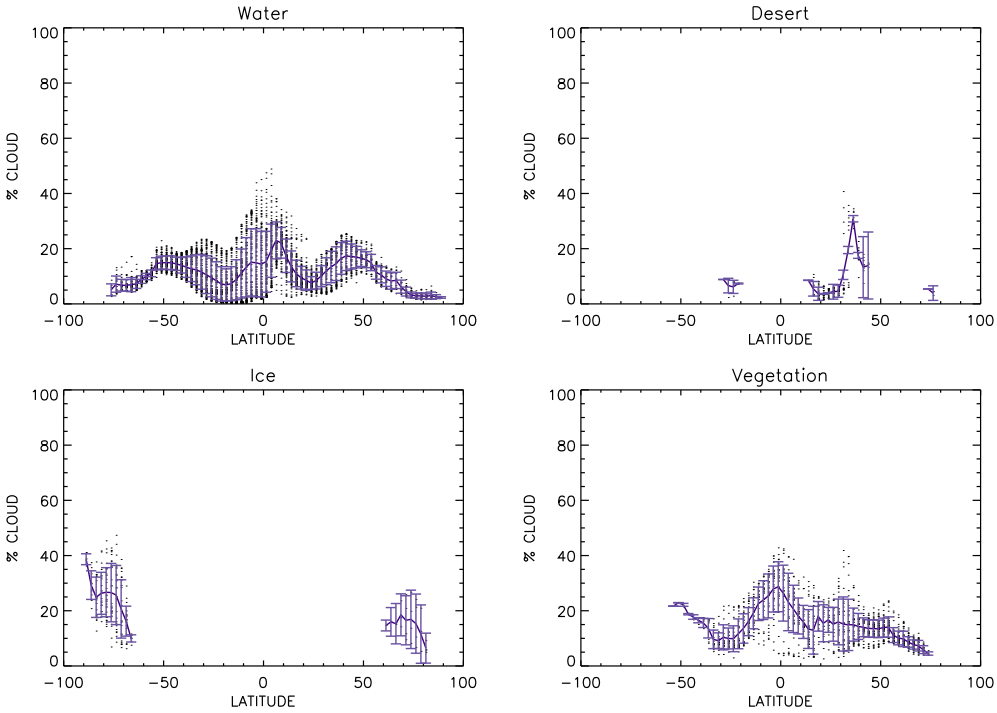

Figure 2.9: The same as the Figure 2.6 but here for high cloud amount.

The same procedure was applied to calculate monthly mean cloud amount instead of annual means. For clarity, the results obtained are shown in annex A. Figures A.1 - A.4, A.5 - A.8, A.9 - A.12, and A.13 - A.16 show the monthly mean cloud distribution for total, low, mid, and high cloud amount, respectively. In general, monthly mean cloud distribution resemble that of the annual mean. Figure A.1 shows that monthly mean cloud distribution over oceans is quite symmetrical in both the Northern and Southern hemispheres. The most noticeable changes month by month take place at the tropical and subtropical latitudes. At these latitudes, in wintertime (where the season refers to the Northern hemisphere) the minimum in cloudiness in the Northern hemisphere is lower than that in the Southern. But when summertime arrives, these

two minimums tend to show the same percentage of cloudiness, i.e., as months pass, the Northern minimum tends to be higher and the Southern minimum tends to be lower.

Results obtained for the vegetation surface type display a seasonal cloud cover variations. Whereas the behavior of cloud cover over vegetation calculated from annual mean data was symmetrical in both hemispheres, for monthly means, the behavior of cloud distribution is opposite in both hemispheres.

As can be seen in Figure A.4, this seasonal cloud cover variation in the tropic and subtropic latitudes is caused by a latitudinal shift of the maximum cloud cover. In wintertime, this maximum appear in the Southern hemisphere and it travels toward the Northern hemisphere until summertime, from that moment on it starts to move toward the Southern hemisphere again. All these differences in cloud distribution, depending on the hemisphere, season and surface type, show the big complexity of the global cloudiness behavior in our planet.

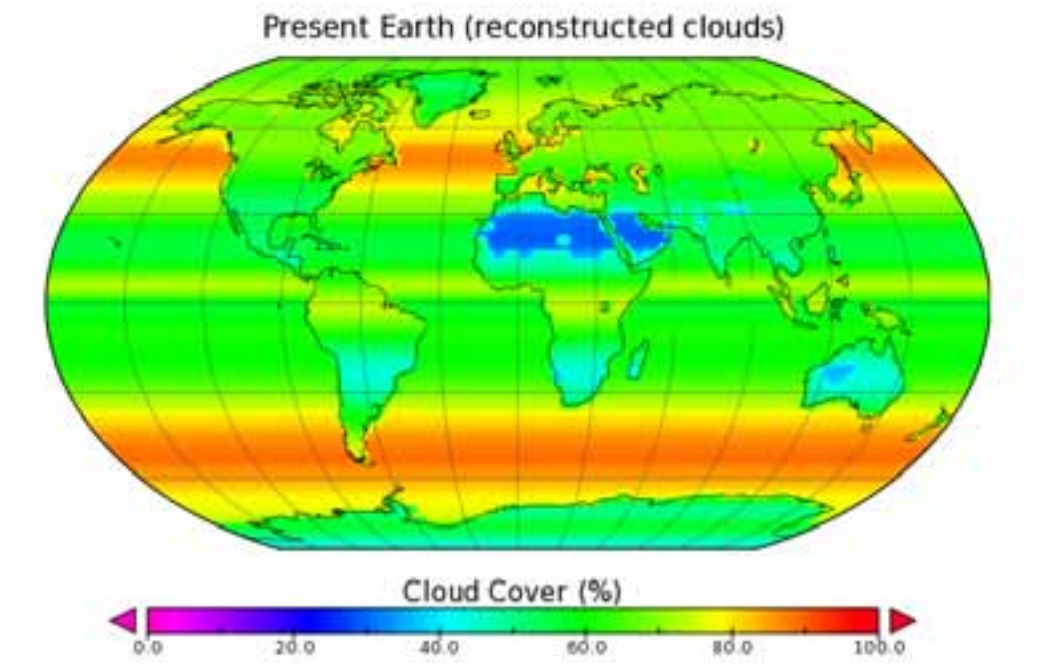

Figure 2.10: Earth global cloudiness distribution reconstructed as described in Section2.3.1. The color code of cloud cover is shown below the plot.

2.3.2 Cloud reconstruction

In the next step, we used these relationships with the aim of reconstructing the global mean cloudiness of present Earth and the possible cloud distribution of past epochs of

Earth's history. In order to do that, we start with a surface map, both for present and past epochs of the Earth (those calculated as described in Section 2.2), and assigned to each grid-point a cloudiness fraction by using the information of the previously derived cloudiness relationships, taking into account both latitude and surface type. This allowed us to reconstruct the global mean cloudiness of each historical epochs. Figure 2.10 shows an example of the reconstructed mean cloud distribution of present Earth.

Comparing the total cloud distribution reconstructed by using our simple model (Figure 2.10) with the real one (Figure 1.10), one can see that our semiempirical model for clouds reproduces well the general features of Earth's cloud distribution. In particular, the differences in cloud amount between land and water are considerably well reproduced, as well as the latitudinal range 40°-75°, both north and south. Nevertheless, there are some small-scale structures, principally over tropical oceanic areas, that our model can not reproduce. The major differences are found in the Pacific and in the Indian oceans, being these differences caused by oceanic effects such as ocean currents, surface temperature, trade winds, and regional meteorological phenomena such as "El Niño"/"La Niña", which can greatly influence cloud formation.

As can be seen in Figure 2.6, owing to the continental distribution of our own planet, we only have information about the cloud cover over vegetated areas in the latitudinal range from -60°to 80°. Thus, in order to reconstruct the cloud distribution of historical epochs of Earth which have vegetated areas out of that latitudinal range, we would have to extrapolate our functions to get the corresponding cloudiness. But, data obtained from extrapolation are subject to greater uncertainty. Thus, to avoid this problem, we decided to take the cloudiness value corresponding to the highest available latitude of the Northern hemisphere and assigned it as the fraction of clouds of the remaining Northern latitudes for which we had no information. Those latitudes in the Southern hemisphere for which we had the same problem, we assigned them the fraction of clouds corresponding to the same latitudes in the Northern hemisphere. This filling process will not affect substantially our results since the polar regions have a low contribution to both the total albedo and the disk-integrated spectrum.

We found a similar problem with clouds located over deserts (see Figure 2.6). As deserts in the present-day Earth are mainly located at low latitudes, and with the purpose of avoiding extrapolations, we chose to use only two cloud cover values, i.e., we calculated the mean cloudiness over deserts in [0°,30°] and [30°,90°] latitude ranges and assigned these mean values to those points which were located in these respective latitude ranges. These values are 33% for the former range and 55% for the last one. Note that this modification has been only used to reconstruct the cloud distribution of the Earth 500 Ma ago, since desert areas in other epochs are mainly located at low latitudes.

The same procedure was followed in order to reconstruct the low, mid, and high cloud distribution of present Earth and past epochs.

2.4 Optical properties of aerosols and clouds

For the generation of the synthetic spectral database (see Section 3.2) we classified clouds into three groups: low, mid, and high, and we placed them in the atmosphere at 2, 5 and 10 km, respectively (Rossow et al. 1996). We considered physical cloud thicknesses of 1 km for each cloud type and we assumed that the scattering phase function is described by the Henyey-Greenstein equation (Henyey & Greenstein 1941) inside clouds and by the Rayleigh scattering function outside them.

The optical properties of each cloud type and aerosols, wavelength-dependent scattering and absorption coefficients, and the asymmetry parameter, were obtained from the Optical Properties of Aerosols and Clouds (OPAC) database (Hess et al. 1998). OPAC datasets provide optical information of up to six water clouds, three ice clouds, and ten aerosol components. It also provides mixtures of different aerosols. These properties are calculated under the assumption of spherical particles in the case of aerosols and water clouds, and assuming hexagonal columns in the case of ice clouds. Data are prescribed in 61 wavelength points, between 0.25 and 40 μm, in the case of aerosols and water clouds and in 32 wavelengths in the case of ice cloud.

For the generation of the synthetic spectral database we took into account the optical properties of six types of clouds: stratus maritime, stratus continental, cumulus maritime, cumulus continental clean, cumulus continental polluted, and cirrus, and nine different mixtures of aerosols: continental clean, continental average, continental polluted, urban, desert, maritime clean, maritime polluted, maritime tropical, and arctic. For more detailed description about the different aerosols and cloud types available in the OPAC dataset see Hess et al. 1998.

Note that for the generation of the spectral database of the early Earth (about 3.0 Ga ago) we did not consider aerosols and we only took into account five types of clouds: stratus maritime, stratus continental, cumulus maritime, cumulus continental clean, and cirrus.

2.5 Spectral albedo

In order to take into account the effect that different surface types, and hence, their different albedos, can have on the reflectance spectrum, we have considered six different surface types: water, vegetation, desert, snow, purple bacteria, and microbial mats. The albedo curves of each surface type used for the simulations are shown in Figure 2.11. All these albedo spectra have been taken from the ASTER

Spectral Library[3] and the USGS Digital Spectral Library[4], except for that of purple bacteria (see Section 2.5.1).

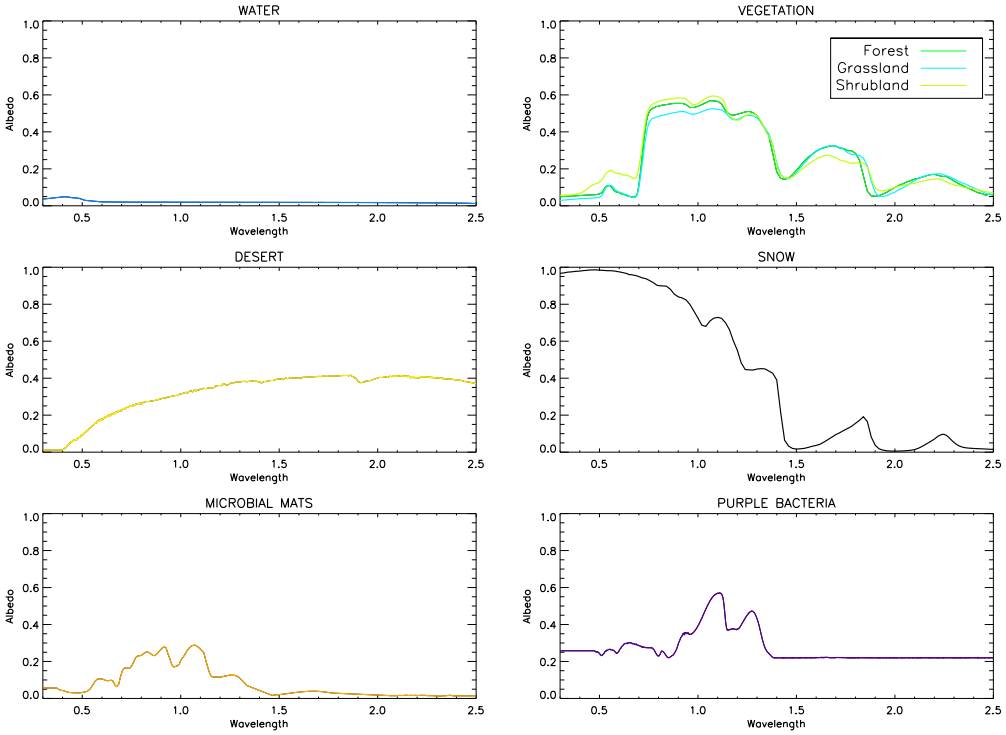

Figure 2.11: Wavelength-dependent albedos of water, vegetation, desert, snow, microbial mats, and purple bacteria, covering the 0.4-2.5μm spectral range, used for the construction of the synthetic spectral database.

As shown in Figure 2.11, the reflectance of water is quite plain. It is generally low and only has a small bump in the blue part of the spectrum. On the other hand, the reflectance of snow and ice is high in the near-UV and in the visible, and decreases rapidly towards the near-IR and stays low towards longer wavelengths.

Vegetation has a particular spectral signature which enables us to distinguish it readily from other surface types. The reflectance is low in the 0.4-0.5 μm and in the 0.6-0.7 μm ranges of the spectrum due to the absorption of the chlorophyll a and b. Between these two regions the reflectance increases, making plants appear green to our eyes. But around 0.70 μm the reflectance increases steeply. This rise in reflectance is called "the red-edge" (see Section 1.5.3) and is a defense mechanism to ensure the cooling of plants. In the near-IR, plants also present water absorption

[3]http://speclib.jpl.nasa.gov
[4]http://speclab.cr.usgs.gov/spectral-lib.html

bands at 1.4 and 1.9 μm.

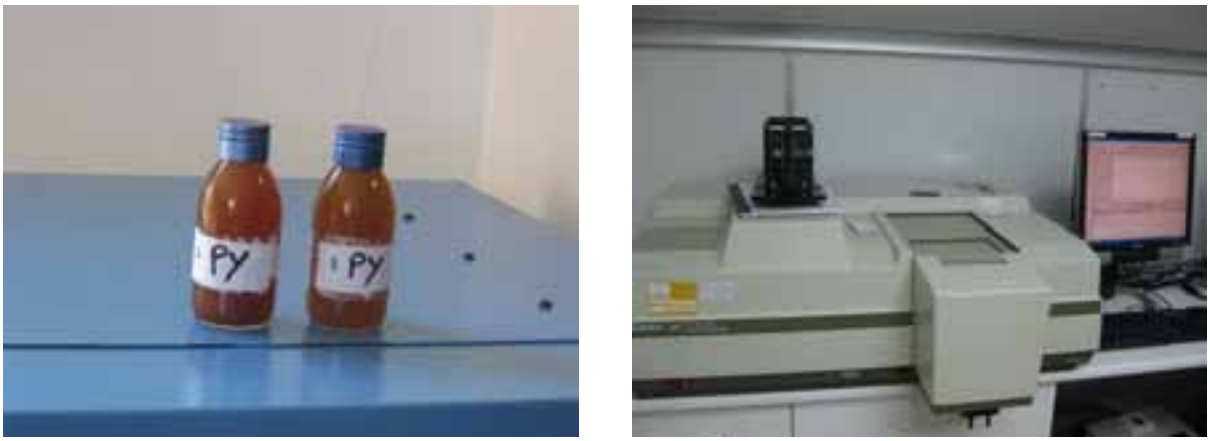

Figure 2.12: Purple bacteria liquid cultures (left) and the UV/VIS/NIR spectrophotometer (right) used to obtain the reflectance spectra of these bacteria.

Bare soil reflectivity depends on its composition. However, if one compares the reflectance of different samples of sand they all share a common shape: a low reflectance in the blue part of the spectrum, an increase in the reflectivity with increasing wavelength in the visible part, and a bumpy plateau at larger wavelengths.

The reflectance of microbial mats is low in the blue and shows an increase in the reflectivity up to 1.1 μm where it peaks to decrease redwards and stays low towards larger wavelengths. The microbial mat sample used for the measurement of the reflectance spectrum shown in Figure 2.11 was composed by two thermophilic species: thermophilic green gliding bacterium (*Chloroflexus aurantiacus*) and cyanobacterium (*Synechococcus lividus*), which are found at Octopus Springs in Yellowstone National Park, Wyoming, USA.

2.5.1 Purple bacteria spectral albedo

Along the history of Earth, not only the geology an the atmosphere have changed. Live has emerged and evolved together with the planet. In this thesis, we were also interested in studying how ancient forms of life that at some point were dominant in our planet affected the Earth spectra. Purple bacteria are thought to have been one of the first life forms that dominated our planet (Xiong et al. 2000; Olson 2006), however, information about the spectral albedo of such life forms were not available to us. Thus, in order to obtain the spectral reflectance of purple bacteria, we used cultures of *Rhodobacter* non-sulfur purple bacteria. Samples of these bacteria were

provided by Dr. Ángel Gutiérrez Navarro and were cultivated at Universidad de La Laguna. This type of photosynthetic bacteria exhibit diverse respiratory abilities, allowing them to survive in a wide range of environmental conditions. They can grow both aerobically, as a chemoheterotroph, and anaerobically by using photosynthetic electron transport or anaerobic respiration. Unlike other non-sulfur purple bacteria, they can grow in both the light and the dark.

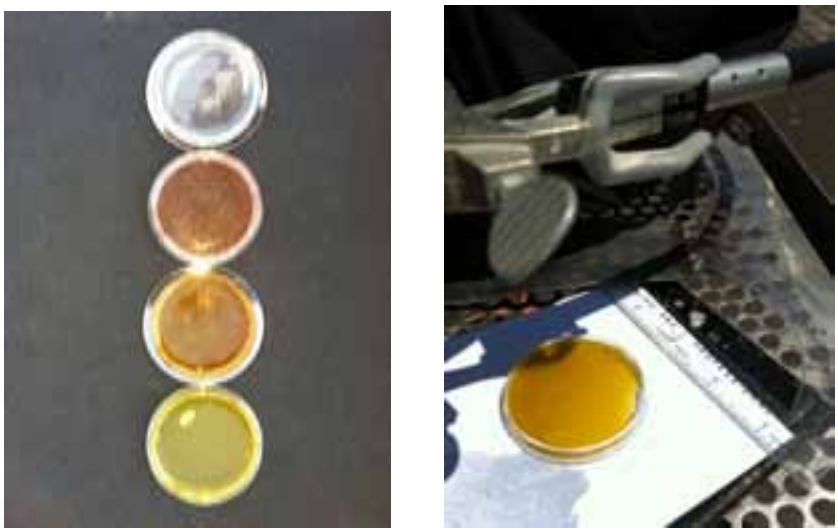

Figure 2.13: Purple bacteria (left, third petri dish) and the LiCor LI1800 spectroradiometer (right) used to obtain the reflectance spectra of these bacteria.

We made two different measurements to retrieve the reflectance spectrum of these bacteria. In the first one (E1), a liquid pure culture of purple bacteria were used to obtain their reflectance by using a UV/VIS/NIR spectrophotometer (VARIAN, CARY 5E). The measurements were taken from 0.3 to 2.5 μm. Both the purple bacteria cultures and the instrument used to obtain the reflectance are shown in Figure 2.12.

In the second experiment (E2), we used a LiCor LI1800 spectroradiometer with a remote cosine receptor that was positioned 5 cm above the culture. This culture of purple bacteria was in a petri dish sitting on top of a piece of white paper. In order to calculate the spectral albedo, spectral irradiance of the Sun was also measured. These measurements cover the 0.35-1.1 μm spectral range. The purple bacteria culture and the instrument used are shown in Figure 2.13

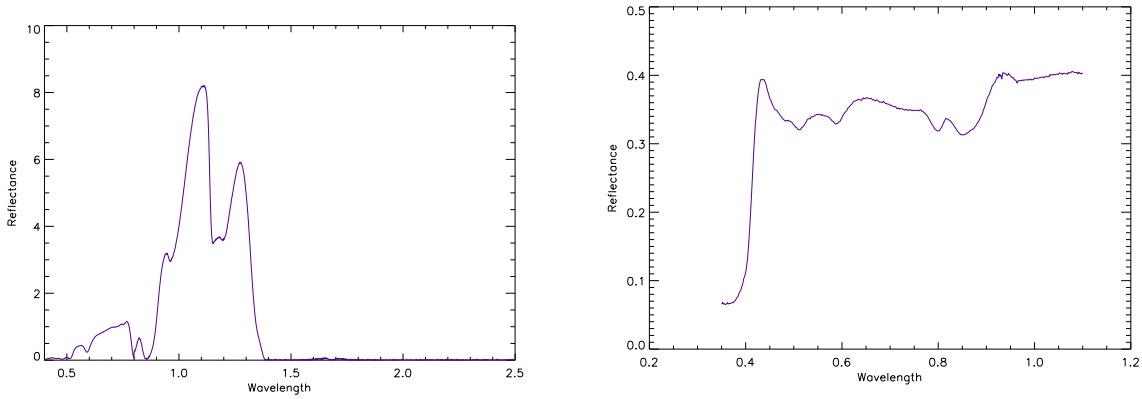

Figure 2.14: Relative reflectance of *Rhodobacter* non-sulfur bacteria obtained from the first experiment (left) and from the second experiment (right).

Figure 2.14 shows the relative reflectivity of the *Rhodobacter* non-sulfur purple bacteria obtained with the E1 experiment (left) and with the E2 experiment (right). Here, the reflectivity scale is arbitrary. Measurements taken in the E2 experiment have a better signal-to-noise ratio than those from E1. This is probably due to the fact that the lamps used in E1 were faint in order to get diffuse light measurements, while E2 measurements were taken by using direct sunlight. Thus, we selected E2 experiment measurements as our reference spectrum. However, as the reflectance from E2 only covers the visible range, we used E1 to extend the measurements to the near-IR.

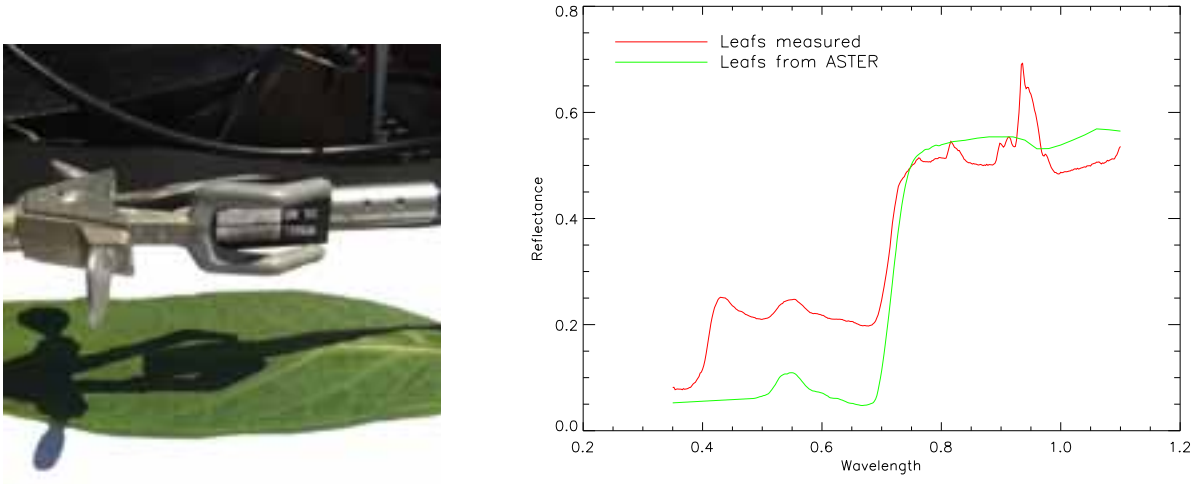

Figure 2.15: Left: set-up of the second experiment (E2) when taking the reflectance spectrum of a leaf. Right: measured albedo spectrum of a leaf (red line) and the one taken from the ASTER library (green line).

Notice that we did not use the information of the E2 reflectance spectrum from 0.45 μm short-wards due to the presence of artificial artifacts in the leaf reflectance spectrum (see next paragraph and Figure 2.15 right panel) in this part of the spectrum. Thus, we assumed the same constant value between 0.3 and 0.45 μm. We neither used the information of the E2 experiment from 0.9 μm red-wards for the same reason.

In order to absolutely calibrate the reflectance spectra of these bacteria, we also measured the reflectance spectra of a set of known tree leaves. Figure 2.15 shows the set-up of E2 when measuring the reflectance of a leaf (left) and the albedo spectrum obtained (right, red line). The comparison of our measured leave reflectance spectra with those tabulated in the ASTER library (Figure 2.15, green line) gave us a measure of our reflected flux, which we then applied to the reflectance spectra of the purple bacteria in order to calibrate the spectrum. This way we transformed the ratio scale into a reflectance scale.

Figure 2.11 (bottom-right) shows the reflectance spectrum of the non-sulfur *Rhodobacter* purple bacteria obtained. The most noticeable feature is the sharp increase in reflectivity from approximately 0.9 μm to 1.1 μm, and the equally strong decrease from 1.3 μm to 1.4 μm. The reflectance spectrum also shows several absorption features at 0.5, 0.6, 0.8, 0.87, and 1.2 μm. From 1.4 μm and redwards, the spectrum does not show any measurable variability.

3

Constructing a disk-integrated Earth spectrum model

In this chapter we describe the photometric and spectroscopic models that we have used and developed in order to perform simulations of the appearance of Earth along its history, as seen from an astronomical distance, i.e., as if it were an extrasolar planet. These of simulations could help us to determine what to expect when searching for life and habitability in exoplanets, and allow us to understand and interpret data from remote sensing platforms.

3.1 A simple reflectance model

To simulate the Earth's Bond albedo we used a simple Earth reflectance model. This model was previously published by Pallé et al. (2003) and was slightly modified to fit the purpose of this project. This model calculates the reflected visible light curves of our planet (output) for a given day and time by using ground scene models from the Earth Radiation Budget Experiment (Suttles et al. 1988), surface maps, and cloud and snow/ice cover data (inputs). With this information the model is able to determine the Bond albedo at each time of a day and in any direction.

This code first calculates the albedo of each element of area of the planet's surface taking into account the surface type, the cloud and snow/ice cover and the solar zenith angle. Once this local albedo is calculated, the program performs the calculations of the Bond albedo, taking into account the albedo of each element of area, by integrating as follows:

$$A = \frac{1}{\pi {R_E}^2} \int_{(\hat{R}\cdot\hat{S})\geq 0} a(\hat{R}\cdot\hat{S}) d^2R$$

where d^2R is an element of the planet's surface, $\hat{R}$ is a unit vector pointing toward

the local zenith, $\hat{S}$ is a unit vector pointing toward the Sun, and a is the albedo of each surface element. The integral is calculated over all portions of the globe which are illuminated by the Sun, i.e., where $\hat{R} \cdot \hat{S} \geq 0$ (see Figure 3.1).

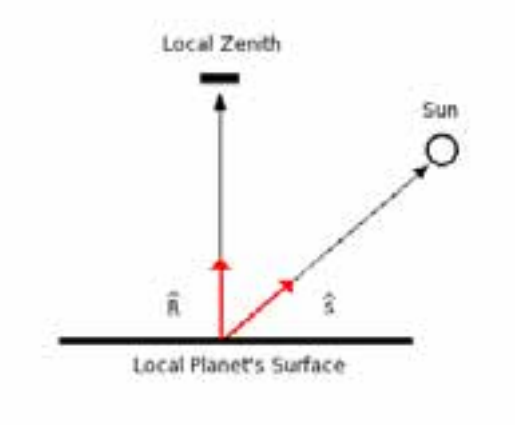

Figure 3.1: Geometry for computing the Bond albedo.

Nonetheless, this model can only be considered as a first-order approximation since it does not take into account any other climate parameters, apart from snow and ice, that might contribute to changes in Bond albedo. Moreover, the model just contemplates 12 different surface scenes and only 4 cloud cover levels (0%-5%,5%-50%,50%-95%, and 95%-100%).

3.1.1 Example model outputs: Test planets

Before we modeled the Earth's Bond albedo along its history, we modeled the photometric albedo of five simple "test planets". These planets were assumed to have the same characteristics as Earth does (star-planet distance, atmospheric composition, temperature, etc.) but with a different continental distribution (see Figure 3.2). The test planets are the following:

- An ocean world (planet totally covered by water)
- A planet totally covered by vegetation
- A planet with only one continental mass which goes from the North Pole to the South Pole and takes up half of the planet. This continent is completely covered by vegetation and the other half of the planet is covered by water.
- A planet with two continents completely covered by vegetation. Each continental mass takes up a quarter of the planet and they go from the North Pole to the South Pole. The other two quarters of the planet are covered by water.

- A planet divided by latitudinal bands of ice (at the poles), vegetation and deserts (at different latitudes), each one parallel to the equator.

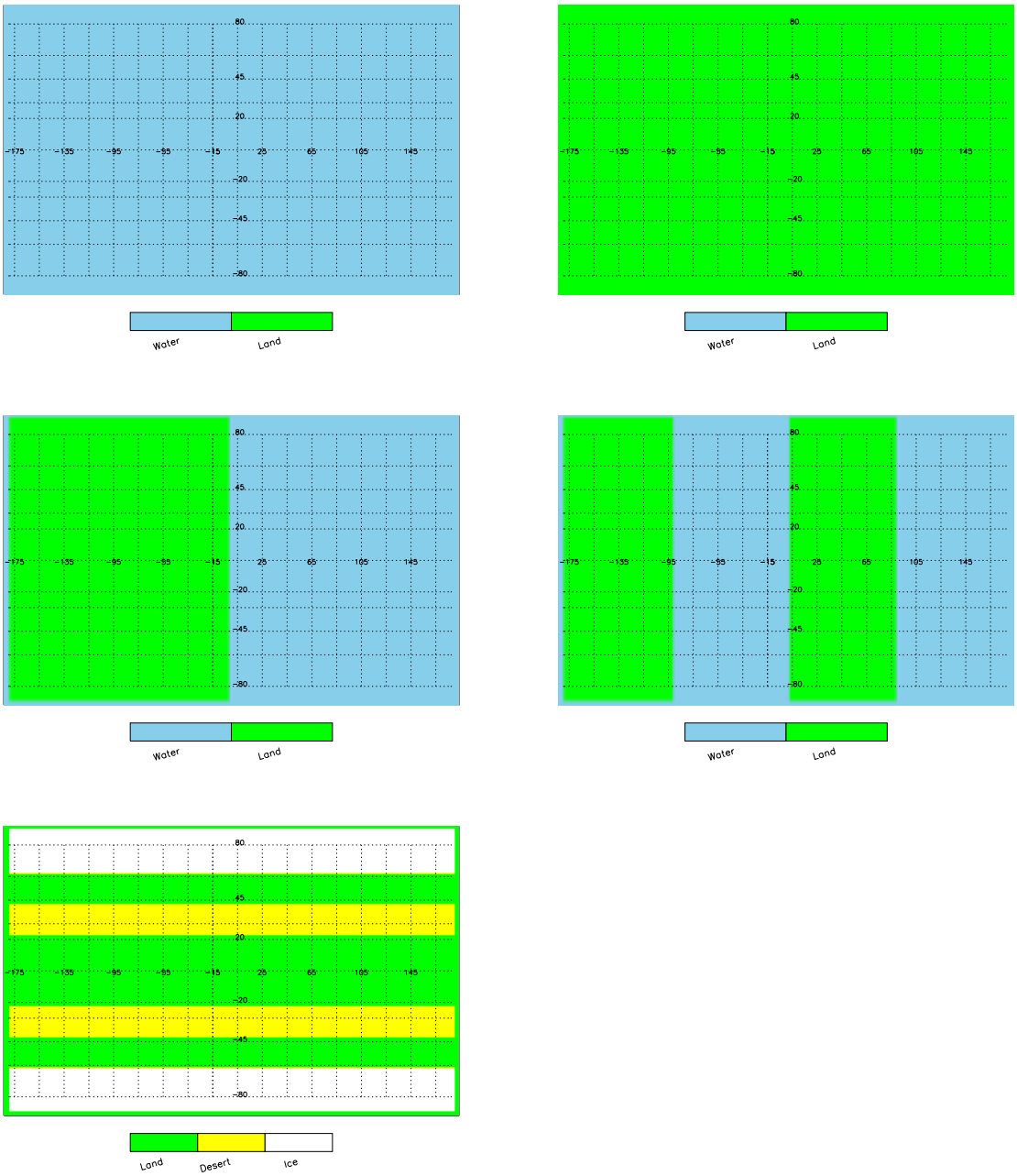

Figure 3.2: Different land-mass distributions of the "test planets" created for the albedo model. These planets are: an ocean world (top left), a planet totally covered by vegetation (top right), a planet with one continent covered by vegetation (mid left), a planet with two continental masses covered by vegetation (mid right) and a planet divided by bands of ice, deserts and vegetation (bottom left). Water is represented in blue, vegetation in green, deserts in yellow and ice in white.

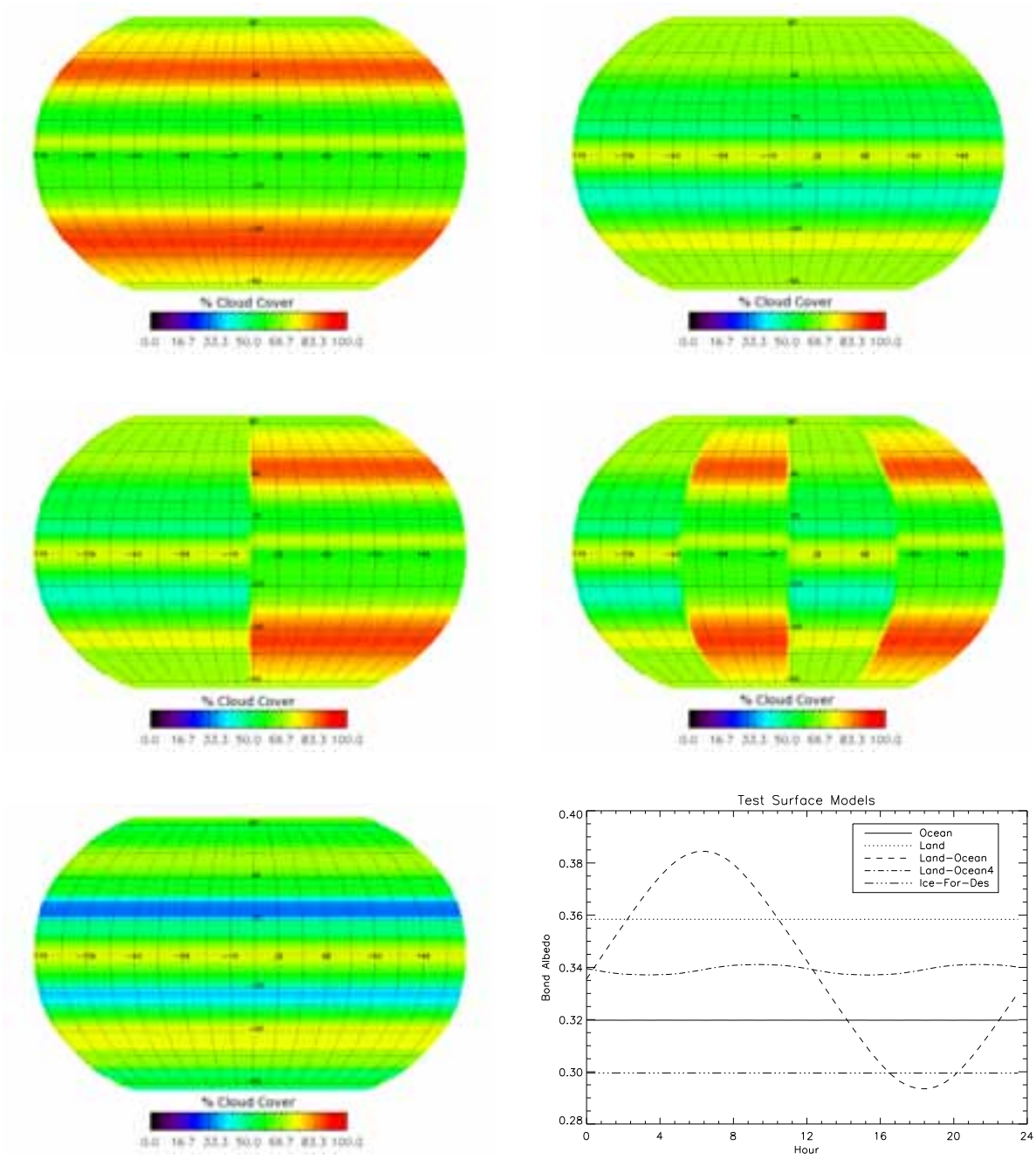

Figure 3.3: Cloudiness reconstruction of the test surface models: an ocean world (top left), a planet covered by vegetation (top right), a planet with one continent (mid left), a planet with two continental masses (mid right) and a planet divided in bands of ice, vegetation and deserts (bottom left). These cloud cover maps were calculated following the procedure described in Section 2.3.1. The color code is shown below each graphic. The bottom right panel shows the Bond albedo variability along a day calculated for each test planet. The different line styles represent the results obtained for the different cases as indicated in the legend.

To calculate the Bond albedo variability of these test planets along a day, we ran the albedo model for a fixed day once every half an hour, i.e., we have 48 measurements of the Bond albedo per day. Note that here we have assumed that these test planets have a rotational period similar to that of Earth. Figure 3.3 shows the reconstructed cloud distribution (see Section 2.3.1 for a description of how these cloud cover maps were constructed) of each test planet and their corresponding daily Bond albedo.

As can be seen in the bottom right panel of Figure 3.3, when the distribution of the surface type is longitudinally homogeneous, and hence so is the longitudinal distribution of clouds, the Bond albedo remains constant along the day, as expected. However, these mean values of Bond albedo are not the same for the different surface types considered. A planet totally covered by vegetation has a higher albedo value, $\sim$0.36, than the real Earth (0.30). For an ocean world this value is $\sim$0.32, while for a planet divided by latitudinal bands of different surface types, we obtained a Bond albedo value of around 0.30.

In contrast, when a planet has well differentiated continental masses, the Bond albedo undergoes daily variations. If the planet has only one continental mass, these Bond albedo's variations are far larger than in the case of a planet with two continental masses. These variations are $\sim$27% and $\sim$1%, respectively. Moreover, the number of maxima in the variability coincides with the number of continental masses.

Note that these values are due to clouds. If we do not consider clouds in the model, the mean albedo values for the ocean world, the planet covered by vegetation, and the planet divided by latitudinal bands of different surface types are: $\sim$0.11, $\sim$0.18 and $\sim$0.17, respectively. Moreover, the albedo variation owing to the presence of differentiate continental masses increases: $\sim$43% and $\sim$22% for one and two equally-sized continents, respectively.

3.2 Spectral Earth model

Much more information can be gained using spectroscopy instead of photometry to study extrasolar planets. For instance, spectroscopy allows us to identify signatures of individual molecules in exoplanet's atmospheres, providing us with information about its atmospheric composition. It also allows us to retrieve information about surface properties, identify possible biomarkers, and study their reflectance variability. Hence, in this Section we describe the spectral Earth models that have been developed for the Earth simulations presented in this thesis.

Many different processes of emission and absorption from atoms and particles take place within the atmosphere of a planet. The radiative transfer problem aims to determine how radiation changes when it passes through a medium. Hence, we use radiative transfer models to help in the interpretation of spectra of exoplanet atmospheres.

For many applications, in particular in cases of planetary atmosphere problems where vertical variations are much more rapid than horizontal ones, it is a good approximation to consider that the atmosphere is plane-parallel, i.e., the atmosphere is layered by several infinite parallel planes where each layer has homogeneous properties.

Radiative transfer models are basically based on the equation of radiative transfer. This equation under the assumption of plane-parallel atmosphere can be written as:

$$\mu \frac{dI_\lambda(\tau_\lambda, \mu, \phi)}{d\tau_\lambda} = I_\lambda(\tau_\lambda, \mu, \phi) - S_\lambda(\tau_\lambda, \mu, \phi)$$

where I_λ is the specific intensity in a solid angle at vertical optical depth τ_λ along the direction $\mu\phi$ (μ is the cosine of the polar angle and ϕ is the azimuthal angle), and S_λ is the source function.

3.2.1 Radiative transfer model

In order to simulate the disk-integrated spectrum of some epochs of the Earth's history, we generated a database of one-dimensional synthetic spectra. These spectra have been calculated for a variety of surface and cloud types, and for several viewing and illumination angles. This database have been generated by means of a line-by-line radiative transfer algorithm, based on DISORT[1] (Stammnes et al. 1988). This radiative transfer model (RTM) makes use of atmospheric composition and temperature profiles, spectral albedos of surface types, and cloudiness information as input data for the calculations. The Earth's atmosphere is considered plane-parallel, and its radiative properties are prescribed on a grid of contiguous spectral bins. This spectral grid is specially designed to solve the rapid variations in the radiative properties near molecular absorption lines. Moreover, each spectrum is calculated at very high spectral resolution, with no less than three points per Doppler width. Positions, intensities, and lineshape parameters for molecular absorption bands are taken from HITRAN2008 (Rothman et al. 2009). Eventually, for storage purposes, each spectrum is degraded to a lower resolution (R = 10,000). We ran this radiative code using input parameters covering a wide range of viewing and illumination angles, surface and cloud types, atmospheric profiles, and aerosol concentrations, leading to the generation of a database containing more than 7500 spectra.

[1] ftp://climate1.gsfc.nasa.gov

This RTM is an extension of the RTM for transits described in García Muñoz & Pallé (2011) and García Muñoz et al. (2012) to a viewing geometry for which the light reaching the observer has been reflected at the planet.

Validation of the radiative transfer model

In order to validate the radiative transfer model we used spectral measurements of the Moon. These spectra contains information about the local atmosphere, the Moon, and also the Sun spectrum. Observation were taken on 2009 August 4, from 21:21:19 to 21:42:07 UT, with the HERMES instrument which is installed in the Mercator Telescope located at the Roque de los Muchachos Observatory on La Palma Island, Spain. The spectra cover the 0.4-0.9 μm spectral range, have a resolution of R$\simeq$90000 and were taken at an altitude $\simeq$65°.

We ran our radiative transfer code taking into account only two atmospheric species: H_2O and O_2, for a variety of altitudes, and spectral resolutions. Then, we combined these synthetic spectra with the Sun spectrum and we used the AMOEBA IDL routine in order to fit the observations to the simulations. We found that the best fit was achieved for a synthetic spectra with a spectral resolution R=85000 and an altitude of 65°, with a good agreement in both lineshape and depth.

Table 3.1: Parameters used for the generation of the 1-D synthetic database.

Atm. profile	Surface type	Clouds	Aerosols	Incident and Observer angles (°)
Tropical	water	stratus continental	continental clean	0
Mid-latitude summer	forest	stratus maritime	continental average	15
Mid-latitude winter	grassland	cumulus continental clean	continental polluted	30
Subartic summer	shrubland	cumulus continental polluted	maritime clean	45
Subartic winter	tundra	cumulus maritime	maritime polluted	55
Early Earth	snow	cirrus	artic	65
	desert	clear	desert	70
	microbial mats		urban	75
	purple bacteria		clear	80
				85

Synthetic spectral database description

In order to simulate a wide range of possible geometries and scenarios, we generated a database of more than 7500 synthetic spectra. For the calculation of this 1-dimensional spectral database we considered 10 solar angles and 10 observer angles (85°, 80°, 75°, 70°, 65°, 55°, 45°, 30°, 15°, and 0° for both angles). Hence, radiance values for arbitrary solar and observer angles need to be interpolated from the calculated radiances. We also chose 9 different surface types (water, forest, grassland, shrubland, tundra, snow, desert, microbial mats, and purple bacteria), 3 cloud types (low, mid, and high clouds), and 6 atmospheric profiles. Five of these atmospheric profiles correspond to present-day atmospheric abundances, and

the other one corresponds to the atmospheric composition of the early Earth, about 3.0 Ga ago. See Chapter 2 for a more detailed description of these parameters. Table 3.1 summarizes all the parameters used for the generation of the spectral database.

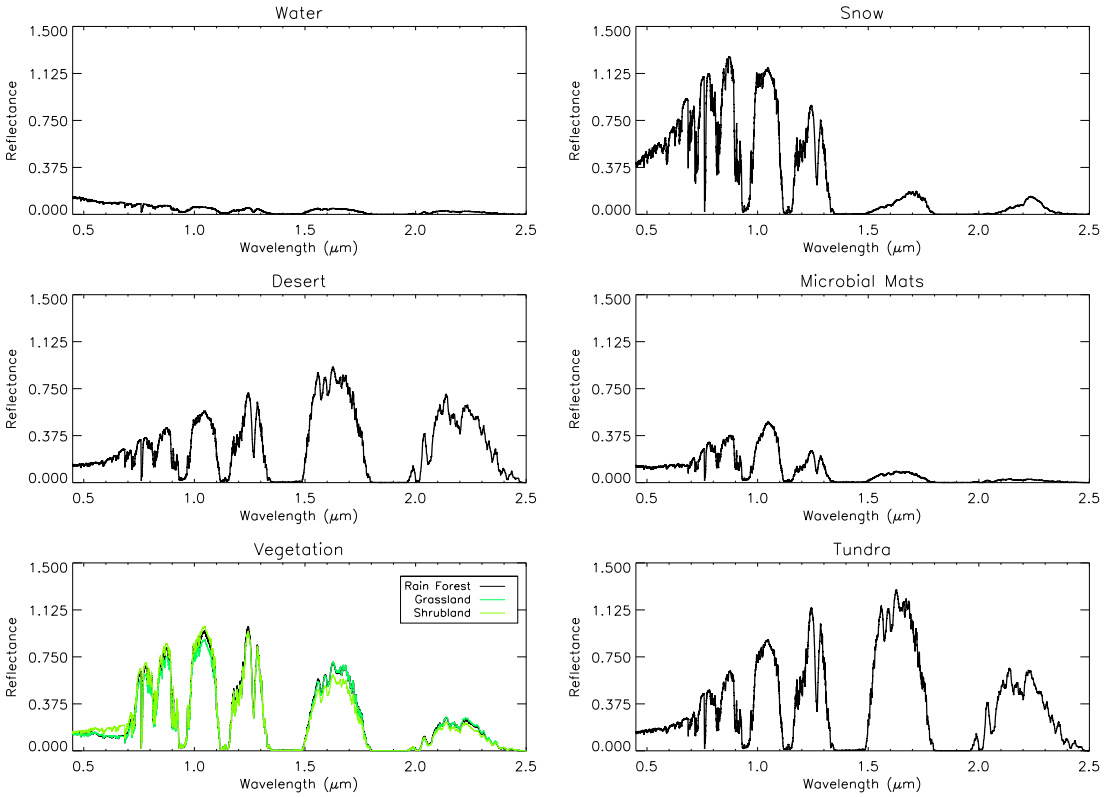

Figure 3.4: Sample of the one-dimensional synthetic spectral library. The different panels show the reflectance spectra of water, snow, desert, microbial mats, forest, grassland, shrubland, and tundra, in a cloud-free atmosphere. This reflectance is taken as 10^6 times the radiance divided by the solar flux, in the VIS-NIR, for a fixed viewing geometry and illumination. The atmospheric profile considered here is that of the current Earth, at a mid-latitude position during the summer. The spectra have been smoothed with a 100 point running mean for illustrative purposes.

The generation of each of these 1-dimensional spectrum takes about 48 hours (time calculated with a regular desktop PC equipped with an Intel(R) Core(TM) i5 with 4 cores and 8GB RAM). Hence, owing to the high computational cost of the generation of this synthetic spectral database, we had to make use of a high parallel computer: LaPalma supercomputer. LaPalma supercomputer is located at the La Palma Astrophysics Centre (CALP), in La Palma island, and is one of the seven nodes of the Spanish Supercomputing Network. It has 2 Terabytes of main memory, equivalent to the memory of approximately 200000 regular computers, and 512 processors, which enables it to make more than 4.5 billions of operations per second. We have also used the Condor distributed computing system, which is

available in the IAC. This system takes advantage of computers which are not being used by their users and allows you to run computational tasks on them. Currently, 656 processors are part of the Condor pool.

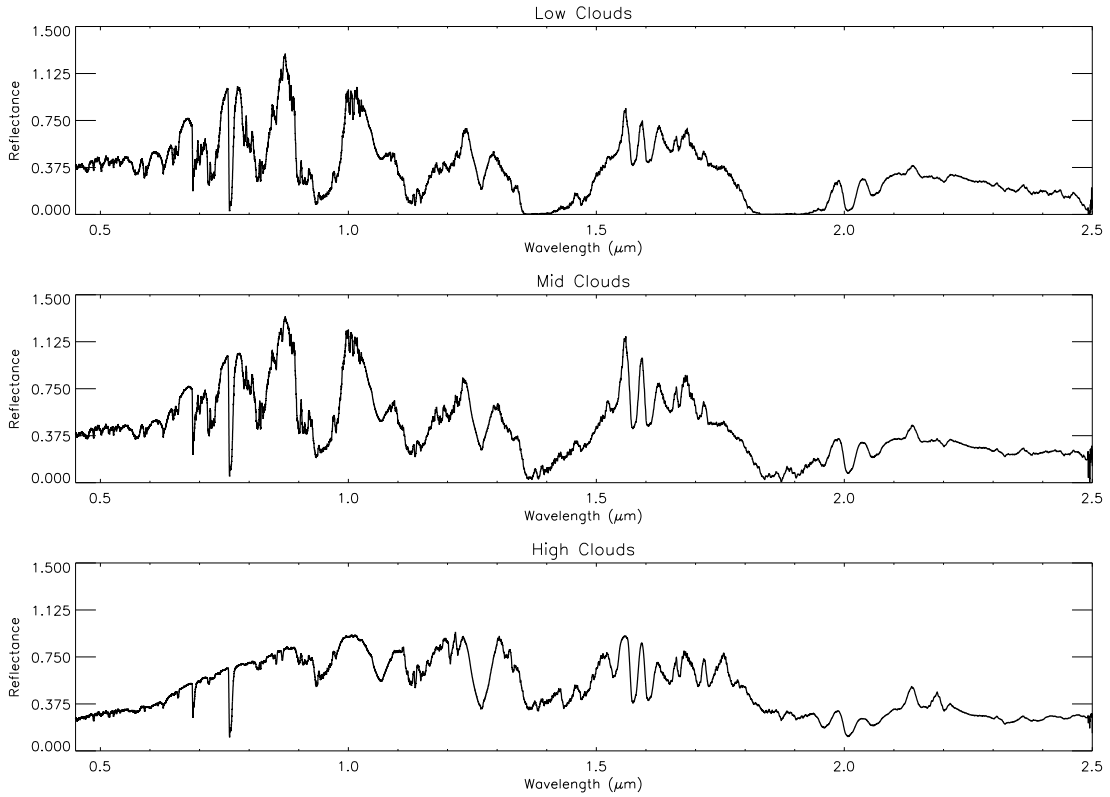

Figure 3.5: The same as Figure 3.4 but for low, mid, and high clouds. Note that the shape of the spectra is independent of the surface type since here we are considering surfaces totally covered by clouds.

Figures 3.4 and 3.5 show a sample of the calculated synthetic spectra database in the VIS-NIR. These spectra correspond to water, snow, desert, microbial mats, forest, grassland, shrubland, tundra, and low, mid and high clouds. The illumination and viewing geometry are the same for all plots, and the atmosphere profile used in these plots is the midlatitude summer (current Earth's atmospheric composition). These figures show the different effects that each surface and cloud type has on the VIS-NIR spectrum. Figure 3.4 shows that the spectra of the different surface types are quite diverse and resemble the albedo distribution of each surface (see Figure 1.9). In fact, it is possible to distinguish among the different surface types. For instance, water hardly shows any particular signature, whereas, in the spectrum of vegetation, one can easily identify at 0.7 μm the red-edge signal characteristic of leafy plants. Note that spectra shown in this Figure are calculated for a cloud-free sky.

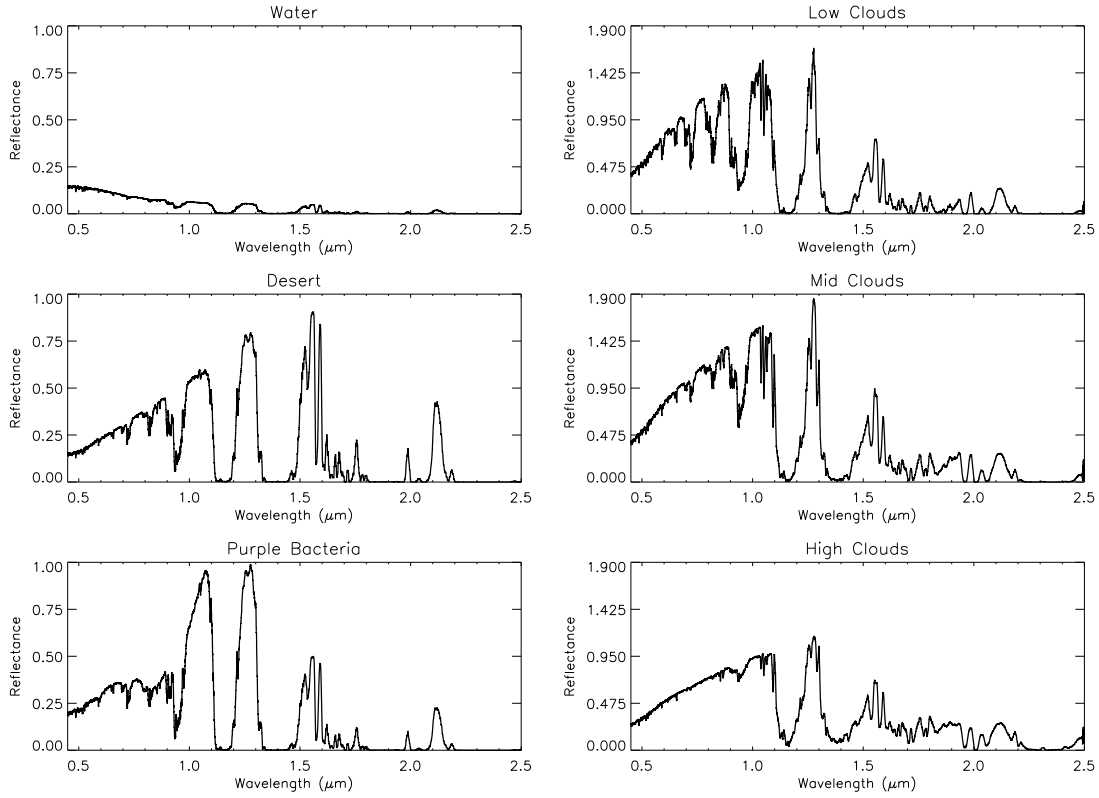

Figure 3.6: Some examples of the 1-D synthetic spectral library when the atmospheric profiles are those of early Earth. Plots show the reflectance spectra of water, desert, and purple bacteria, in a cloud-free atmosphere (left column). The contribution of clouds is shown in the right column. This reflectance is taken as 10^6 times the radiance divided by the solar flux in the VIS-NIR, for a fixed viewing geometry and illumination, for the atmospheric profiles corresponding to early Earth, 3.0 Ga ago, approximately. The spectra have been smoothed with a 100 point running mean for illustrative purposes.

Figure 3.5 shows the importance of considering clouds when modelling exoplanet spectra owing to their wavelength-dependent absorption and scattering properties. Note that here surfaces are totally covered by clouds. Hence, the shape of the spectra is independent from the surface type under clouds. We used two types of water clouds (low and mid clouds, located at 2 km and 5 km, respectively) and one type of ice cloud (high clouds, located at 10 Km). Clouds have a high reflection spectrum in the VIS-NIR, relatively flat with wavelength, and they block the access to those parts of the atmosphere below them, hiding the surface properties. In contrast to Figure 3.4, Figure 3.5 shows small differences among the three cloud types, being low and mid clouds almost indistinguishable.

Figure 3.6 shows the same as Figures 3.4 and 3.5 but when the atmospheric profiles is that of early Earth (3.0 Ga ago, approximately), when the Sun was 79% as bright as it is today, O_2 was absent in the Earth's atmosphere, and CO_2 and CH_4 were much

more abundant. The main differences between Figure 3.6 and Figures 3.4 and 3.5 are that the former lacks of the characteristic absorption lines of O_2 and O_3, that are clearly distinguishable in Figures 3.4 and 3.5, and the strong absorption in the NIR part of the spectra due to the higher concentrations in atmospheric CO_2 and CH_4.

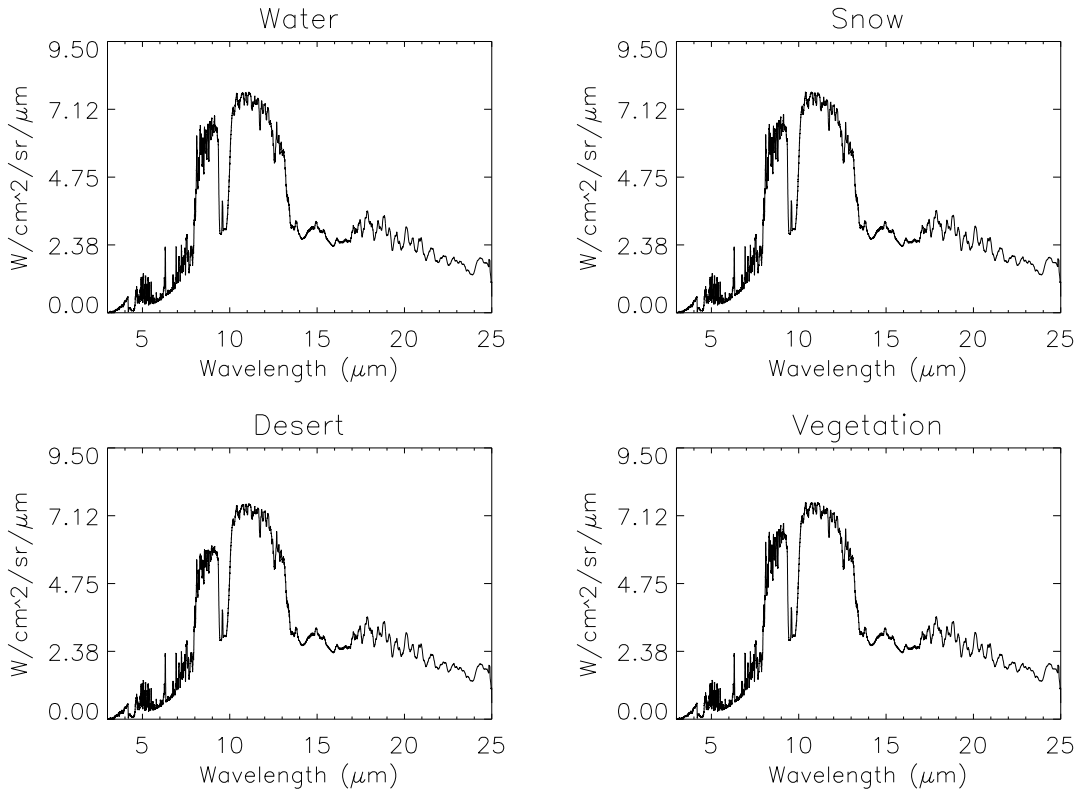

Figure 3.7: Examples of the 1-D synthetic spectral library in the IR spectral range for a fixed illumination-viewing geometry. The atmospheric composition is that of present-day Earth. Plots show the spectral radiance of water, snow, desert, and vegetation, in a cloud-free atmosphere. The spectra have been smoothed with a 100 point running mean for illustrative purposes.

We also calculated one-dimensional synthetic spectra in the IR spectral range (2.5-25 μm). Here we only ran our model for one atmospheric profile (subartic summer), and four surface types: water, snow, desert, and vegetation. As OPAC provides only information about optical properties of high clouds up to 10 μm we only used low and mid clouds for the generation of the IR database. Figure 3.7 shows the spectral radiance of water, ice, desert, and vegetation in the IR. In contrast to the spectra calculated in the VIS-NIR, by simple inspection of the IR spectra it is difficult to distinguish between the different surface types. This is related to the fact that the reflectance of these surfaces in this spectral range is low and does not vary appreciably.

Only desert surface reflectance shows a small bumpy plateau between 9 and 10 μm.

Figure 3.8 shows the contribution of clouds in the IR. In contrast to the spectra of clouds in the VIS-NIR, the two types of clouds have a different spectral shape that make it possible to distinguish between them.

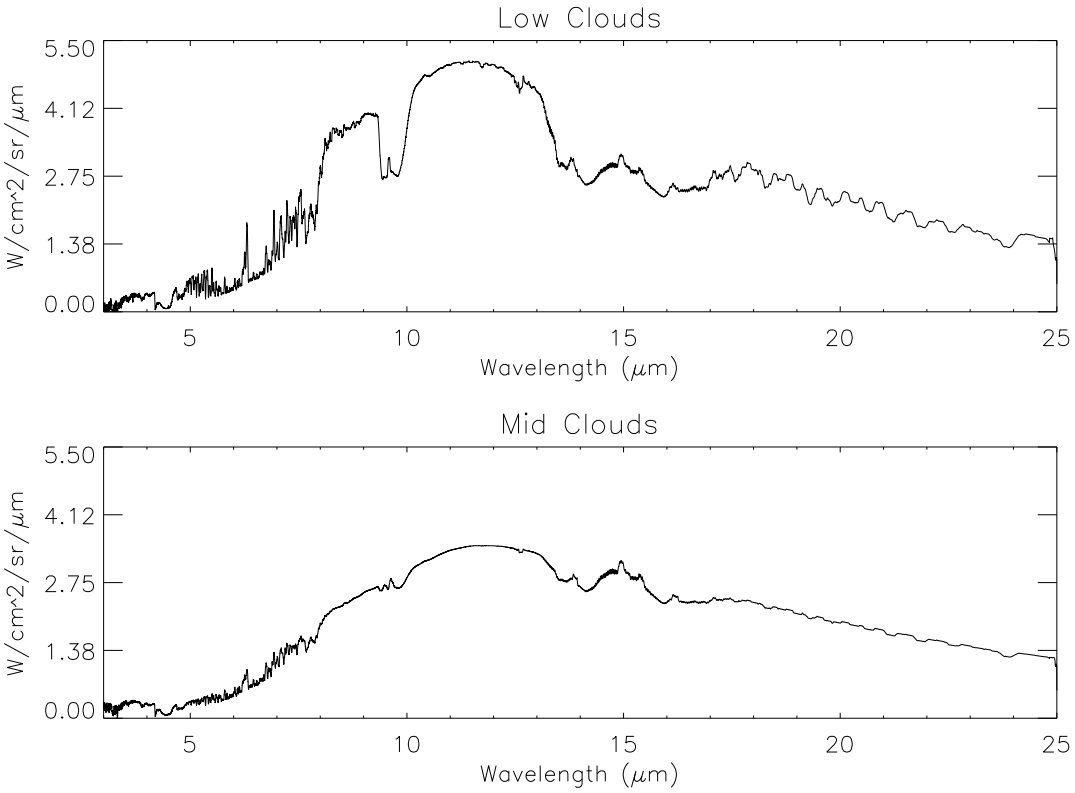

Figure 3.8: The same as Figure 3.7 but for low and mid clouds.

3.2.2 Disk-integrated spectrum of Earth

Once the spectral library was generated, we developed a computer code to calculate the disk-averaged irradiance of our planet. This code is able to calculate the disk-integrated spectrum of the Earth for a given observing geometry and resolution by using as inputs a surface map (related to the continental distribution of a specific epoch of the planet), a cloudiness map, and the spectral library. To get the disk-integrated spectra of our planet, this code divides the Earth in an equal-angle grid, taking into account the resolution given by the user. Then, cloudiness coverage, and atmospheric and surface properties, are mapped onto this grid. Finally, the

program selects the appropriate 1-D synthetic spectra for each grid point, $I_\lambda(\hat{n}_i, \hat{o}, \hat{s})$, taking into account the surface, cloud type, and cloud amount in that pixel, and integrates all over the Earth's globe to yield a disk-averaged radiance spectrum, $I_\lambda(\hat{o}, \hat{s})$:

The disk-integrated spectral irradiance F_λ of a planet of radius R at a distance D from the observer can be written as an integral over the solid angle of a hemisphere:

$$F_\lambda(\hat{o}, \hat{s}) = \frac{R^2}{D^2} \int_{2\pi} I_\lambda(\hat{n}, \hat{o}, \hat{s})(\hat{n} \cdot \hat{o}) d\omega \tag{3.1}$$

where $I_\lambda(\hat{n}, \hat{o}, \hat{s})$ is the intensity from a specific location on the sphere toward the observer, $d\omega$ is the element of solid angle on the globe, $\hat{n}$ is the normal unit vector corresponding to the solid angle, and $\hat{o}$ and $\hat{s}$ are unit vectors pointing to the observer and the Sun, respectively. The dot product at the end of the equation ensures that an element of area near the limb has a smaller weight than one with the same size near the sub-observer point.

To obtain the disk-integrated radiance I_λ from a source of radius R at a distance D from the observer, we have to divide the disk-integrated irradiance F_λ by the solid angle projected by the planet $\pi D^2/R^2$ yielding to:

$$I_\lambda = F_\lambda \frac{D^2}{\pi R^2} \tag{3.2}$$

Then, we can write Equation 3.1 as:

$$I_\lambda(\hat{o}, \hat{s}) = \frac{1}{\pi} \int_{2\pi} I_\lambda(\hat{n}, \hat{o}, \hat{s})(\hat{n}, \hat{o}) d\omega \tag{3.3}$$

As we divided the Earth in a grid of pixels, we can approximate the integral in Equation 3.3 by a finite sum:

$$I_\lambda(\hat{o}, \hat{s}) = \frac{1}{\pi} \sum_{i \in \Omega} I_\lambda(\hat{n}_i, \hat{o}, \hat{s})(\hat{n}_i, \hat{o}) \omega_i \tag{3.4}$$

where $\hat{n}_i$ is the normal unit vector of each pixel i, Ω is the set of indices of the observable pixels, i.e., $\Omega = \{ i \in \{0, 1, ..., n_{pixels}\} / \ \hat{n}_i \cdot \hat{o} > 0 \ \}$, and ω_i is the element of solid angle corresponding to each pixel i. Note that in the VIS-NIR part of the spectrum we only take into account pixels which are both illuminated by the Sun and visible by the observer.

Geographic resolution for the disk-integrated spectrum

In order to find an optimal balance between computational cost and accuracy, we calculated the disk-integrated spectrum of Earth using 4 different geographical resolutions. The planet was divided in: 16x8 (longitude by latitude), 32x16, 64x32, and 128x64 grid cells (see Figure 3.9). For these simulations both the observer and the Sun were located above the equator with the observer looking at a full-illuminated disk, and a cloud-free atmosphere was assumed.

Figure 3.9 shows that the spectra calculated with the two lowest resolutions present relatively large differences with the one with the highest resolution compared to the one calculated with a resolution of 64x32. Moreover, differences between the two highest resolution cases are quite small (relative error 0.85%). Hence, we decided to use a resolution of 64x32, as it shows slight differences with the spectrum calculated with a higher resolution and takes only half of the computational time.

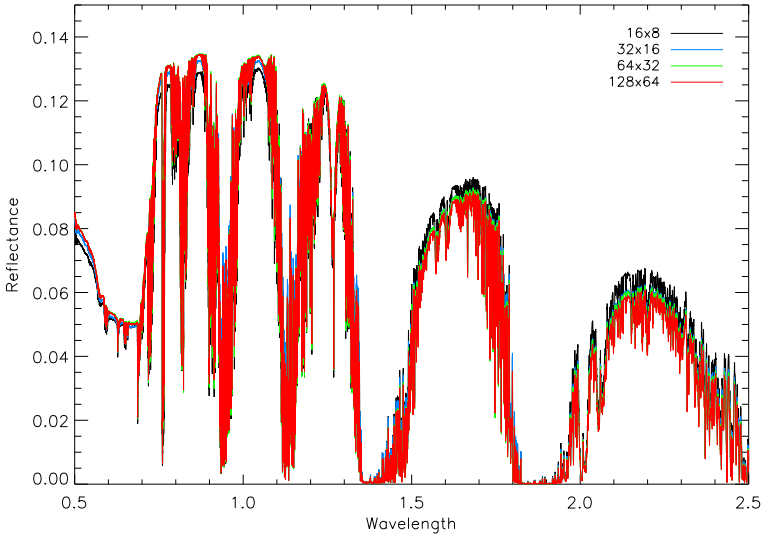

Figure 3.9: Disk-integrated spectra of Earth using four different grid resolutions: 16x8, 32x16, 64x32, and 128x64. These spectra were calculated considering that both the Sun and the observer were located at the equator at a phase angle of 0°.

Example model outputs: Earth's disk-integrated spectra

Before calculate the disk-integrated reflectance spectra of Earth, we simulated the disk-averaged spectra of hypothetical planets which were completely and homogeneously covered by only one surface type: water, desert, and vegetation (see Figure 3.10). To do this, we used the spectral database and the disk-integrated code

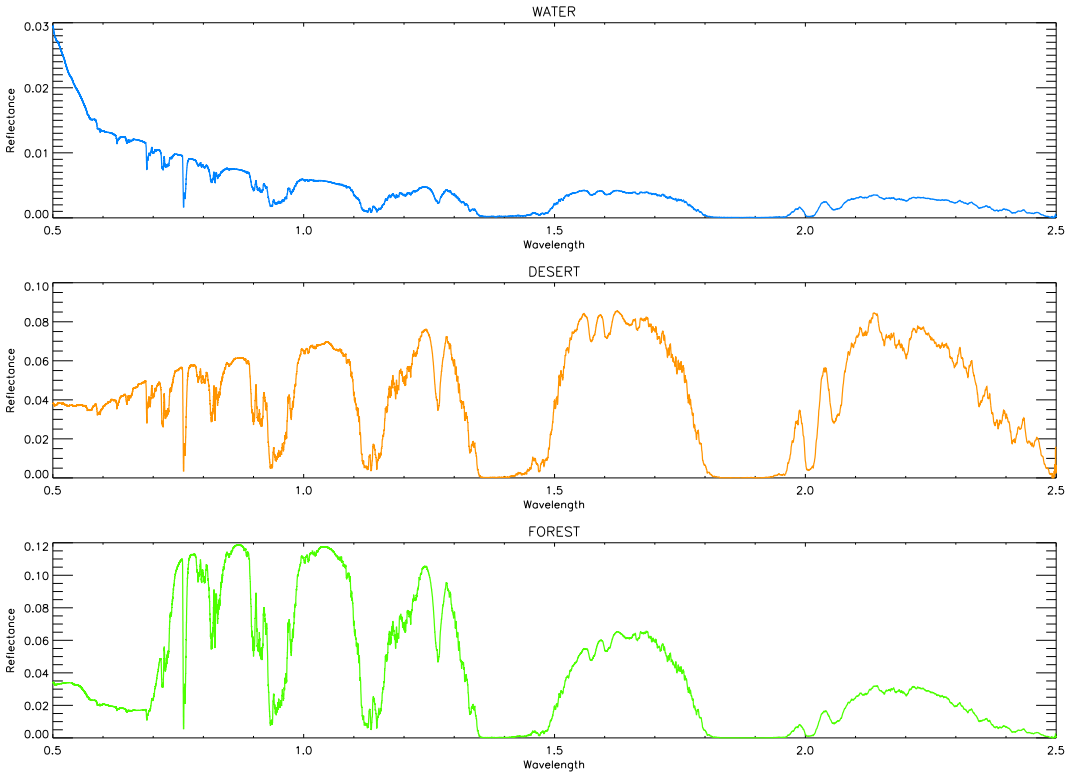

Figure 3.10: VIS-NIR disk-integrated reflectance spectrum of an ocean planet (top), a desert planet (mid), and a forest planet (low). Both the observer and the Sun are located over the equator and the phase angle is 90°. Spectra have been smoothed for illustration purposes.

described in Section 3.2. We assumed that both the Sun and the observer were located over the equator looking at a quarter-illuminated disk (phase angle 90°), the atmospheric composition was that of present-day Earth, and we considered a cloud-free atmosphere. In general, the spectra shown in Figure 3.10 resemble those shown in Figure 3.4. Among these three cases, the forest planet is the only one that shows a strong surface feature. We also calculate the disk-integrated reflectance spectra of theses hypothetical planets throughout a day. As it is expected, owing to their homogeneous surfaces they do not show any variation as the planets rotate.

The models described above were also used to calculate the present-day Earth's reflectance. Figure 3.11 shows synthetic disk-integrated spectra of Earth in the VIS-NIR, over the course of a day, considering both, clear-sky conditions (top) and a cloudy atmosphere (bottom). For these simulations we considered that the observer and the Sun were located over the equator with the observer looking at a quarter-illuminated planet. We used the atmospheric profiles described in Section 2.1, with present-day atmospheric abundances, and the 1984-2006 climatology of ISCCP cloudiness data for the cloud distribution.

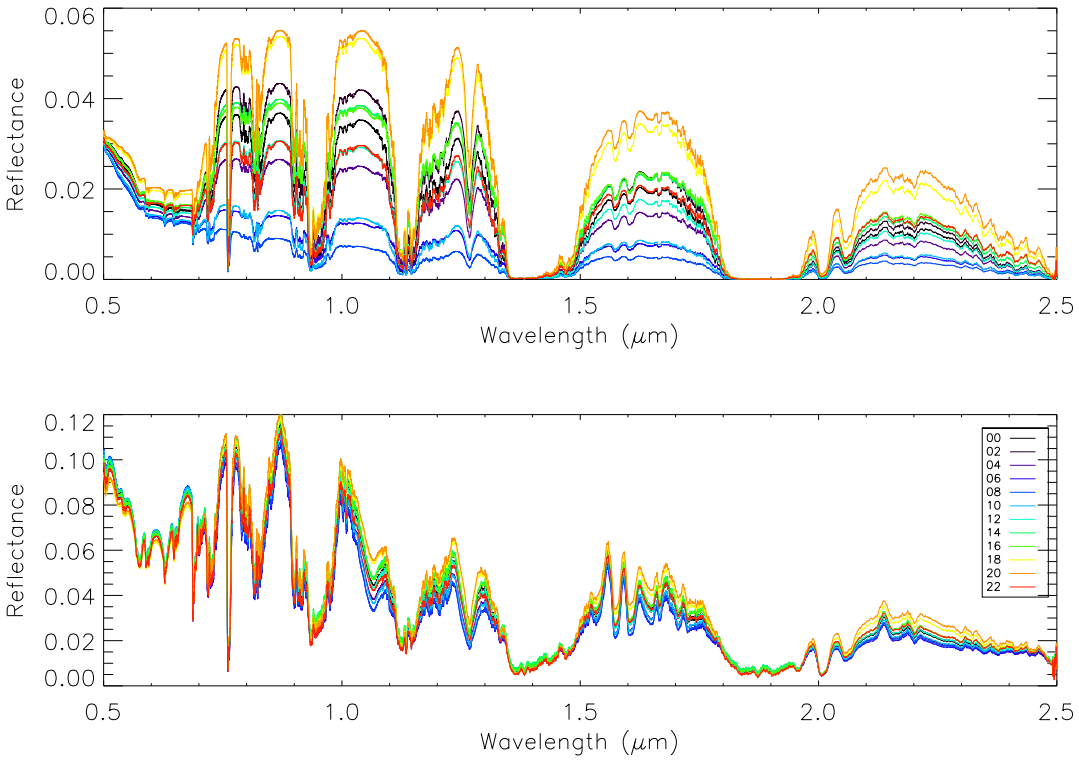

Figure 3.11: Earth's reflectance, taken as π times the disk-integrated radiance divided by the solar flux in the VIS-NIR along a day. Both the observer and the Sun are located over the equator. The spectra have been smoothed with a 100 point running mean for illustration purposes.

The dominant features of the present Earth's reflection spectrum can be distinguished in the modeled spectra shown in Figure 3.11. These features are: a slope in the continuum near 0.5 μm decreasing towards the red due to Rayleigh scattering, many strong absorption bands owing to water vapor increasing in strength from the middle of the visible toward the red, and several absorption features of O_2, O_3, CO_2 and CH_4.

In Figure 3.11 (top) one can also see that as continents come in and out of the field of view, the global Earth's spectrum changes dramatically throughout a day. These changes are much more significant when the percentage of land over ocean which is visible and illuminated at the same time is at maximum (18:00 UT) than when this ratio is lower (8:00 UT). The presence of vegetation over continents produce a strong signal which is easily detected by simple inspection of the spectra when the fraction of land compared to that of the oceans that is in the field of view is greater than $\sim$35%. However, when oceans dominate the view, the red-edge is undetectable. The addition of clouds to the model (Figure 3.11 bottom) results in an enhancement of

the light reflected back by the Earth, the decrease in the reflectance variability over the course of a day, and in a significant loss of information about the different surface types, making it much more difficult to distinguish between them.

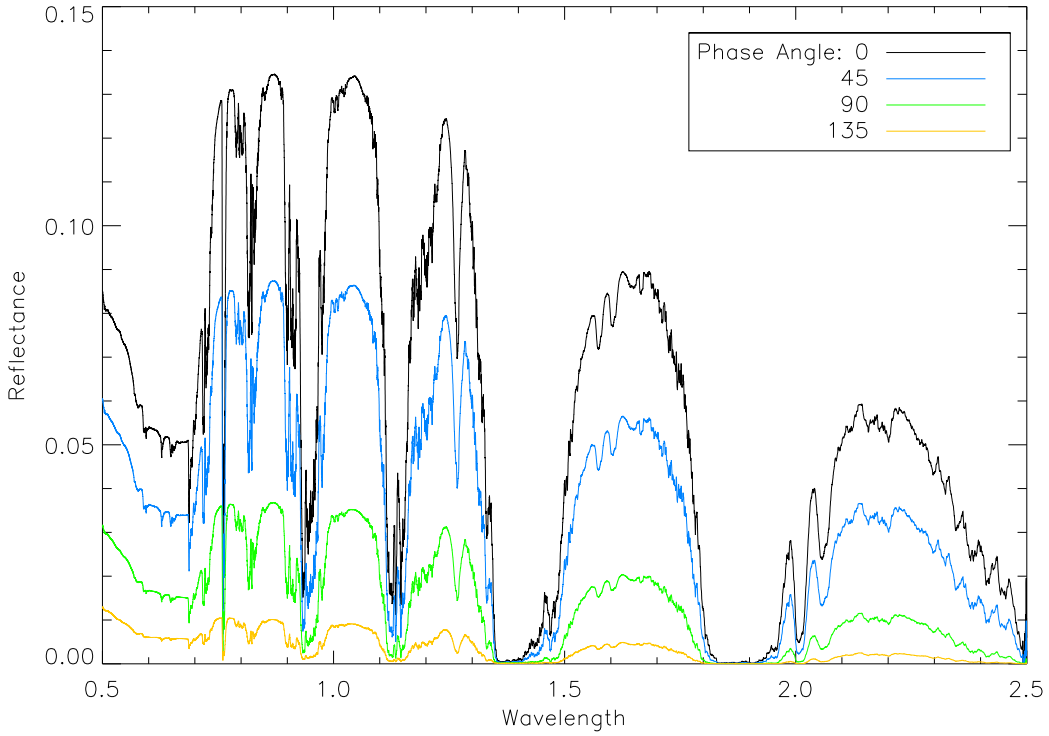

Figure 3.12: Disk-averaged reflectance spectra of Earth calculated at four different phase angles: 0°, 45°, 90°and, 135°, for a cloud-free atmosphere. The Sun and the observer are located over the equator.

We also performed experiments to explore the effect of considering different phase angles on the VIS-NIR disk-averaged spectra of Earth. Figure 3.12 shows the Earth's reflectance, for a cloud-free atmosphere, at different phase angles. Here, we have assumed that both the Sun and the observer are located over the equator at a phase angle 90°. It can be readily seen that both the amplitude and the spectral shape of the Earth's reflectance change considerably with the phase angle. These differences are related to the different path-lengths that light has to go through in each geometry. When the Earth's disk is completely illuminated (phase angle 0°) both the Sun and the observer are located at the same position and the disk-integrated spectra contain information of all the possible incident and emission angles. When the phase angle increases, the solar and viewing angles increase as well, resulting in a longer path to be covered by light. These differences are also due to the different scenarios that are in the field of view, i.e., if the field of view is dominated by water, vegetation, deserts,

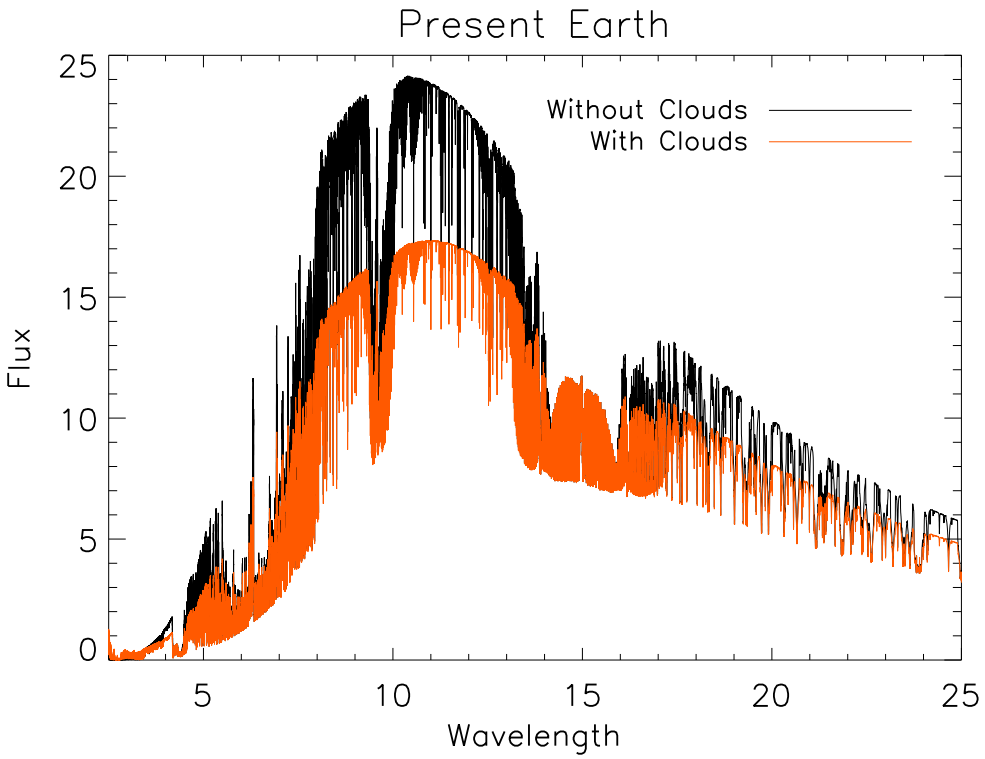

Figure 3.13: IR disk-integrated spectra of present-day Earth for a cloud-free atmosphere (black) and for a cloudy one (orange). The Sun and the observer are located over the equator looking at a half-illuminated disk.

etc., the shape of the spectrum is different (see Figure 3.4).

Figure 3.13 shows the disk-averaged thermal flux of present-day Earth with and without clouds. These spectra show strong absorption bands of CO_2 at 4.3 and 15 μm, O_3 at 9.6 μm, CH_4 at 7.7 μm, and several absorption features due to water vapor from 5 to 8 μm and from 15 μm longward. Opposite to the VIS-NIR Earth spectra, in the IR the inclusion of clouds in the model produces a decrease of the overall emitted flux of the planet, due to the fact that clouds radiate at lower temperatures. Although not shown here, we also calculated the daily variations of the disk-integrated flux of Earth, and we explored the effect of using different phase angles. However, all these spectra show small differences in the IR.

This spectroscopic model is a powerful tool and has many applications. For instance, this model not only allows to study the spectroscopic characteristics of Earth at present day, but also at different moments of its history. Hence, we also used the spectral library and the disk-integrated code to explore the VIS-NIR Earth's reflectance at different historical epochs: 90, 230, and 340 Ma ago (see Figure 3.14). To do that, we used the continental and cloudiness distribution maps described in Chapter 2 as input data. We assumed a present-day atmospheric composition, and

that both the Sun and the observer were located over the equator with a phase angle of 90°.

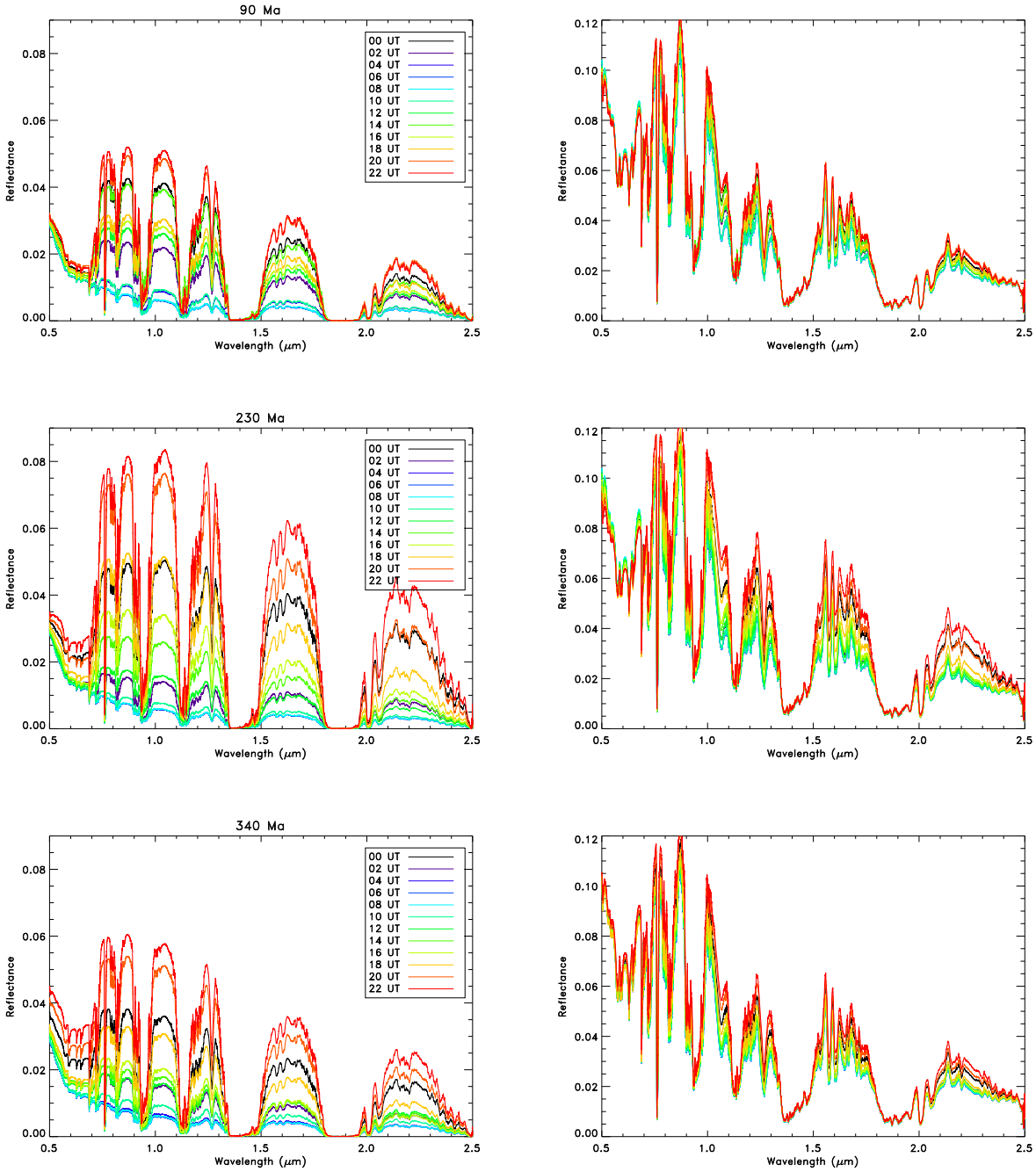

Figure 3.14: Disk-integrated spectra of Earth along its history (90, 230, and 340 Ma ago) for a cloud-free atmosphere (left panels) and for a cloudy one (right panels). The Sun and the observer are located over the equator looking at a half-illuminated disk. The atmospheric composition is assumed to be that of present-day Earth.

Figure 3.14 shows the effect that considering different continental distributions has on the disk-integrated spectra of Earth. Left panels (calculated without clouds) show that the shape of the spectra is very similar in these three cases, and is also similar to those of present-day Earth (see Figure 3.11). However, the amplitude of the spectra and their variations are distinct. This is related to the fact that each epoch has a different continental configuration, in which the distribution of oceans, deserts, and vegetation is different in each case. In contrast, when clouds are added to the model (right panel of Figure 3.14) these differences are diluted.

More applications of the Earth spectral model are presented in Chapters 5 and 6. In the former chapter, we used the spectral model to simulate disk-averaged views of Earth 500 Ma ago in order to explore how the evolution of life over land may have affected they way our planet looked from afar and if it could be possible to discriminate between a lifeless planet and a planet where microbial mats or land plants have colonized the planet's surface. In the latter chapter, we calculated disk-averaged spectra of the early Earth, taking into account different continental and cloudiness distribution, in order to explore if it would be possible to detect ancient life forms, such as purple bacteria, in these globally averaged views of our planet.

4

Reconstructing the Cloud Distribution and Light Curves of Earth Along its History

Clouds are one of the most important parameters in the global energy balance of our planet and have profound interactions with weather and climate. In the first part of this thesis we attempted to provide an understanding of the Earth's large-scale cloudiness behavior using satellite-based estimations. We studied how clouds distribute themselves over the Earth's surface, and classified them according to the underlying surface and the geographic latitude. This knowledge was then used in an attempt to reconstruct the possible cloud distribution of past historical epochs of Earth when the landmass distributions were very different from today's.

As Bond albedo is one of the parameters that control the Earth's temperature and hence its climate, one of the possible mechanism that have been proposed to explain how Earth was kept warm during the Archean, even though the Sun was 30% dimmer than it is today, is the development of continents and their distribution. Moreover, future detected Earth-like planets are expected to show any stage of evolution and any continental surface distribution would be possible. Hence, in the first part of this thesis we also explored the effect that considering different continental configurations has on the visible light reflected by Earth and the changes that these different distributions cause in its daily light curves. To do that, we used a simple albedo model and the reconstructed cloud distribution of the different continental distributions considered in this work.

This first part of the thesis was originally published in the paper entitled "Reconstructing the photometric light curves of Earth as a planet along its history" in the January 2012 edition of the Astrophysical Journal (Sanromá & Pallé 2012).

Abstract: By utilizing satellite-based estimations of the distribution of clouds, we have studied Earth's large-scale cloudiness behavior according to latitude and

surface types (ice, water, vegetation, and desert). These empirical relationships are used here to reconstruct the possible cloud distribution of historical epochs of Earth's history such as the Late Cretaceous (90 Ma ago), the Late Triassic (230 Ma ago), the Mississippian (340 Ma ago), and the Late Cambrian (500 Ma ago), when the landmass distributions were different from today's. With this information, we have been able to simulate the globally integrated photometric variability of the planet at these epochs. We find that our simple model reproduces well the observed cloud distribution and albedo variability of the modern Earth. Moreover, the model suggests that the photometric variability of the Earth was probably much larger in past epochs. This enhanced photometric variability could improve the chances for the difficult determination of the rotational period and the identification of continental landmasses for a distant planets.

The Astrophysical Journal, 744:188 (7pp), 2012 January 10 doi:10.1088/0004-637X/744/2/188

RECONSTRUCTING THE PHOTOMETRIC LIGHT CURVES OF EARTH AS A PLANET ALONG ITS HISTORY

E. Sanromá[1] and E. Pallé[1]
Instituto de Astrofísica de Canarias (IAC), Vía Láctea s/n 38200, La Laguna, Spain; mesr@iac.es
Received 2011 July 29; accepted 2011 September 29; published 2011 December 22

ABSTRACT

By utilizing satellite-based estimations of the distribution of clouds, we have studied Earth's large-scale cloudiness behavior according to latitude and surface types (ice, water, vegetation, and desert). These empirical relationships are used here to reconstruct the possible cloud distribution of historical epochs of Earth's history such as the Late Cretaceous (90 Ma ago), the Late Triassic (230 Ma ago), the Mississippian (340 Ma ago), and the Late Cambrian (500 Ma ago), when the landmass distributions were different from today's. With this information, we have been able to simulate the globally integrated photometric variability of the planet at these epochs. We find that our simple model reproduces well the observed cloud distribution and albedo variability of the modern Earth. Moreover, the model suggests that the photometric variability of the Earth was probably much larger in past epochs. This enhanced photometric variability could improve the chances for the difficult determination of the rotational period and the identification of continental landmasses for a distant planets.

Key words: astrobiology – atmospheric effects – Earth – planets and satellites: atmospheres – planets and satellites: general – planets and satellites: surfaces

1. INTRODUCTION

Since the discovery of the first extrasolar planet by Mayor & Queloz (1995), more than 500 planets orbiting stars other than the Sun have been detected using a variety of techniques (Beaulieu et al. 2006; Beuzit et al. 2007; Charbonneau et al. 2007; Udry et al. 2007). Most of them are gas giants, as larger planets are easier to detect than smaller, rocky planets. However, tens of planets in the super-Earth mass range have also been discovered (Beaulieu et al. 2006; Bennett et al. 2008; Charbonneau et al. 2009; Mayor et al. 2009; Queloz et al. 2009). Although we are not yet capable of detecting and exploring planets like our own (the smallest planet yet known has $R_P = 0.127 R_J$; Batalha et al. 2011), ambitious ground and space-based projects are already being planned for the next several years, suggesting that in the near future it is very likely that Earth-size planets can be discovered in large numbers (Lindensmith 2003; Schneider et al. 2006).

The atmospheric characterization of giant (Jupiter-like) planets has already started with promising results (Tinetti et al. 2010 and reference therein) and several atmospheric models are being developed to help us understand these observations. In this sense, it is clear that the exploration of our own solar system and its planets will provide a useful opportunity for method validation, enabling more accurate determinations and characterization of extrasolar planets. In particular, observations of the solar system rocky planets, including Earth, will be key to the search for life elsewhere.

In the last several years many studies, both observational and theoretical, have been performed to investigate how the Earth would look to an extrasolar observer. One of the observational approaches has been to observe the light reflected by Earth, referred to as Earthshine, via the dark side of the moon at visible (Pallé et al. 2003; Qiu et al. 2003) and near-IR wavelengths (Turnbull et al. 2006). Another approach has been the analysis of the earth light curves from remote sensing platforms (Cowan et al. 2011; Robinson et al. 2011). Several authors have also attempted to model the diurnal photometric variability on an Earth-like planet (Ford et al. 2001; Tinetti et al. 2006a, 2006b; Fujii et al. 2010), while other authors such as Woolf et al. (2002), Arnold et al. (2002, 2009), Seager et al. (2005), and Montañés-Rodríguez et al. (2005, 2006) have attempted to measure the characteristics of the reflected spectrum and the enhancement of Earth's reflectance at 700 nm due to vegetation. In addition, Pallé et al. (2008) determined that the light scattered by the Earth as a function of time contains sufficient information, even with the presence of clouds, to accurately measure Earth's rotation period. Even crude reconstruction of the continental distribution could be attempted given sufficient signal-to-noise observations (Cowan et al. 2009; Oakley & Cash 2009).

However, it is unlikely, even if we were to find an Earth-twin, that the planet will be at a similar stage of evolution as the Earth is today. On the contrary, extrasolar planets are expected to exhibit a wide range of ages and evolutionary stages. Because of that, it is of interest not only to use our own planet as it is today as an exemplar case, but also at different epochs.

In this paper, we have used information about the surface properties and continental distribution of the Earth with the aim of studying the behavior of the large-scale cloud patterns. We have obtained empirical relationships between the amount of cloudiness and their location on Earth's surface depending on latitude and underlying surface types. This relationships have been used to reconstruct the possible cloud distribution for different epochs of the Earth such as 90, 230, 340, and 500 Ma ago. With this information, we here attempt to reconstruct and understand the photometric variability of these epochs according to their different geographic and clouds distribution.

2. CLOUD AND CONTINENTAL DISTRIBUTION DATA

The International Satellite Cloud Climatology Project (ISCCP) was established in the early 1980s. One of its main goals has been to obtain more information about how clouds alter the radiation balance of the Earth. To this end ISCCP has been collecting and analyzing satellite radiance measurements

[1] Also at Departamento de Astrofísica, Universidad de La Laguna, La Laguna, Spain.

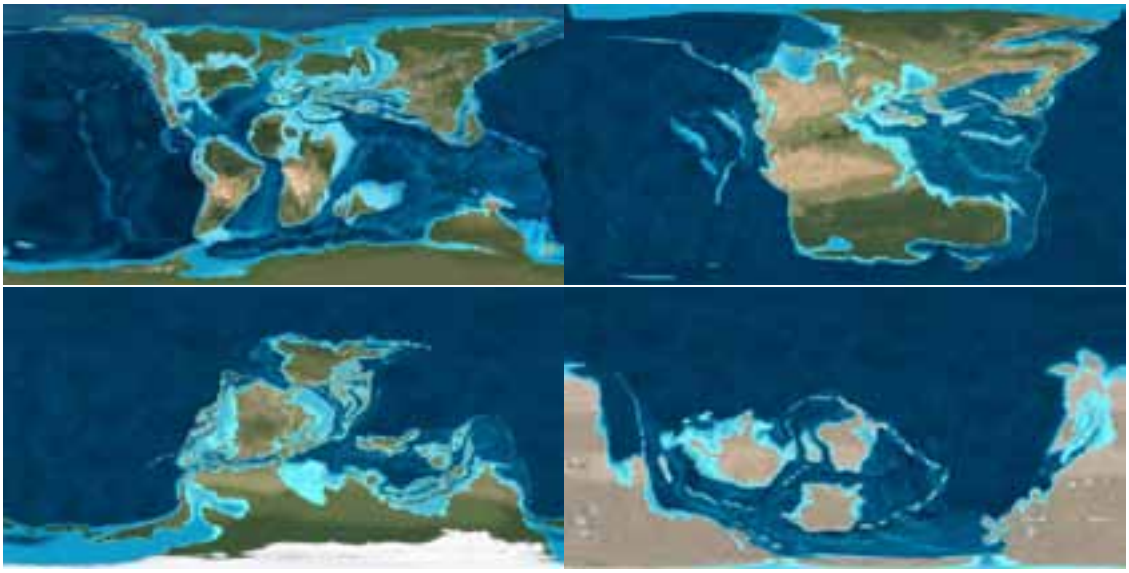

Figure 1. Global views of the Earth's continental distribution during the Late Cretaceous (90 Ma ago; top left), the Late Triassic (230 Ma ago; top right), the Mississippian (340 Ma ago; bottom left), and the Late Cambrian (500 Ma ago; bottom right). Courtesy: Ron Blakey, Colorado Plateau Geosystems Inc.

to infer the global distribution of clouds, their properties, and their diurnal, seasonal, and interannual variations.

In our analysis we have used the monthly mean (D2) fractional cloud cover, derived from a combination of both VIS and IR measurements, for the 23 year period of 1984–2006. The data are given for $2.^{\circ}5 \times 2.^{\circ}5$ grid cells in latitude and longitude. The ISCCP data set[2] provides information on several surface, atmospheric, and cloud parameters at each grid point. In particular total cloud amount and several cloud types are given at each grid point. For further details on the ISCCP data see Rossow et al. (1996).

Detailed information on the varying distribution of continents, deserts, vegetation, and ice in different epochs of Earth's history, is available at Ron Blakey's Web page[3] on paleoclimate reconstructions. These geological maps have been constructed by using interpretations from a wealth of geologic literature and publications, available on the project's Web page (see, for example, Frisch et al. 2011 and references therein).

In order to classify the correspondences between the land areas of these paleomaps and the ISCCP land-types classification scheme, we used an intensity thresholding method (Sonka et al. 1993). Next, the information was regridded to a geographical resolution of 144 (longitude) by 72 (latitude) cells, equal to the ISCCP cloud products, as input for our albedo models. Figure 1 shows the four historical periods that we have chosen to carry out our study. These epochs are 90, 230, 340, and 500 Ma ago. Note that we have assumed that the Earth 500 Ma ago was entirely desert as the development of advance plants is believed to have taken place in the Late Ordovician (450 Ma ago; Gray et al. 1985), although fungi, algae, and lichens might have greened many land areas some time before. Whether this is really the case for the Late Cambrian or not is not the real issue, as our supposition is meant to illustrate the albedo properties for a planet with a continental crust but not life in its surface, which was probably the case for Earth in many previous epochs and a plausible scenario for Earth-like extrasolar planets.

The selection of these four geological epochs corresponds to a period of time during which plate tectonics has radically changed the face of the planet. However, albeit with large temporal excursions, Earth's atmosphere can be considered similar to the present (Hart 1978; Kasting & Siefert 2002). On average the same atmospheric composition and mean averaged temperature have existed during this period. This is a necessary condition for our supposition of cloud distribution related to latitude and surface type to hold as a valid approximation.

3. A SEMIEMPIRICAL MODEL FOR CLOUDS

When attempting to study the reflectance properties of the Earth in the past, one of the major difficulties is the complete lack of reliable information on cloudiness at these timescales. One of the possibilities would be to model the expected cloud amount based on global climate models tuned to those past epochs. However, this is not easy to do with reliability, as in fact cloud amount and variability poses one of the most complicated puzzles for climate change today. For example, despite results of numerous general circulation models, it is unclear how increasing atmospheric temperatures resulting from anthropogenic forcings may influence global cloud properties (Cess et al. 1996), which is important because due to the large radiative influence exerted by cloud cover, a small change in cloud amount or distribution may potentially provide a strong feedback effect, significantly enhancing or mitigating the effects of global warming (Dessler 2010; Spencer & Braswell 2010). Here, we use a different approach to tackle this problem, by using a semiempirical model to map how clouds behave over Earth's surface depending on latitude and surface types—such as ice, water, desert, and vegetation—which then we apply to past epochs.

To reach this objective the first step has been to calculate the 1984–2006 climatology of ISSCP cloudiness data. With this climatology, we have performed a classification of the amount of clouds depending on surface types. That is, cloudiness data have been split up into four groups according to the surface type over which the cloud is located. To carry out this classification we have made use of real geographical

[2] http://isccp.giss.nasa.gov
[3] http://jan.ucc.nau.edu

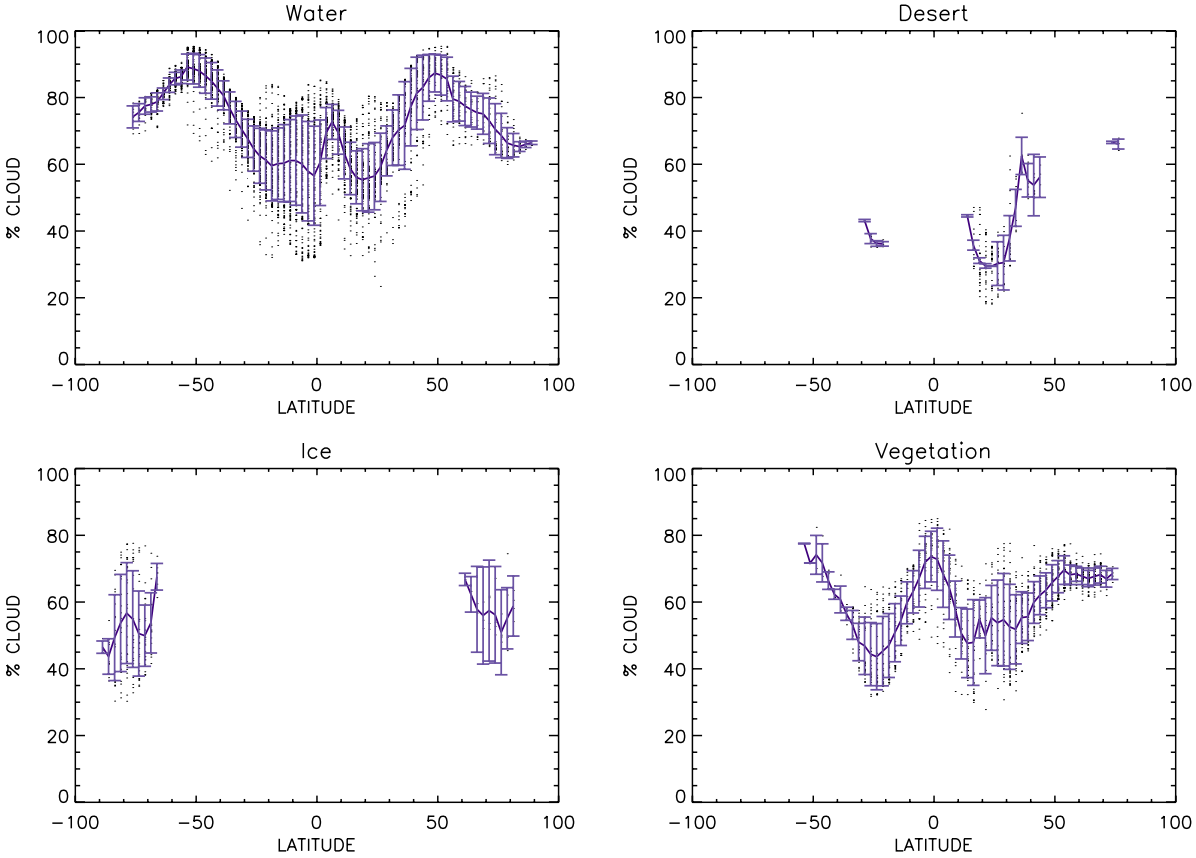

Figure 2. Empirical relationships between the amount of clouds, surface type, and latitude. These figures show the ISCCP 1984–2006 average climatology of cloudiness for each grid cell on Earth as a function of latitude (dots), for each surface type separately: water (top left), desert (top right), ice (bottom left), and vegetation (bottom right). Solid lines represent the mean cloudiness at each latitude and the error bars represent the standard deviation of the mean.

information about the different kinds of surfaces and vegetation in our planet. The ISCCP classifies the different surfaces as water, rain forest, deciduous forest, evergreen forest, grassland, tundra, shrub-land, desert, and ice, but for our study we have only distinguished between water, desert, ice, and vegetation, where the latest is defined as such zones where there were rain forest, deciduous forest, evergreen forest, grassland, tundra, or shrub-land (separate analysis for these subgroups gave very similar results).

Once we got the classification of the cloudiness into these four groups, we represented the fraction of clouds as a function of latitude for each surface type. We have used this scheme to calculate the mean cloudiness at each latitude point and its corresponding standard deviation, thus obtaining empirical relationships between the amount of clouds, surface type, and latitude. As can be seen in Figure 2, these derived cloudiness functions have a particular shape which is different for each surface type, suggesting that global cloudiness distribution can be empirically traced according to the latitude and the underlying surface type. We have repeated this analysis for separate years and in seasonal and monthly climatologies with very similar results, most of them not shown in this paper for space reasons.

In the next step, these relationships are used in an attempt to reconstruct the global mean cloudiness of the present Earth and the possible cloud distribution of past epochs of Earth's history. In order to do that, we have taken each surface map, both for present and past epochs of the Earth (those calculated in Section 2), and we have assigned to each gridpoint a cloudiness fraction by using the information of the previously derived cloudiness relationships, taking into account both surface type and latitude. In this way, we obtained global mean reconstruction of cloudiness for each surface map.

As can be seen in Figure 2, because of the continental distribution of our own planet, we only have information about the fraction of clouds located over vegetation in the latitude range [−60°, 80°]. Thus in order to reconstruct the cloudiness of historical epochs with vegetated areas out of this latitude range, we would have to extrapolate our functions to get the corresponding cloudiness. Since data obtained from extrapolation are subject to greater uncertainty, we decided to take the cloudiness value corresponding to the higher available latitude of the Northern Hemisphere and assigned it as the fraction of clouds of the remaining northern latitudes for which we had no information. For the Southern Hemisphere latitudes for which we had no information about cloudiness, we assigned to these the fraction of clouds corresponding to the same latitudes in the Northern Hemisphere. This filling process does not affect substantially our results because the polar regions have a low contribution to the total albedo.

A similar problem arises with clouds located over deserts (see Figure 2). As deserts on the present-day Earth are mainly located at low latitudes, in order to avoid extrapolations we have chosen to use only two cloudiness values. That is, we calculated the mean cloudiness over deserts in the latitude range [0°–30°] and in the range [30°–90°] and we assigned these mean values to those points which were located in the respective latitude range. These values are 33% for the former range and 55% for the

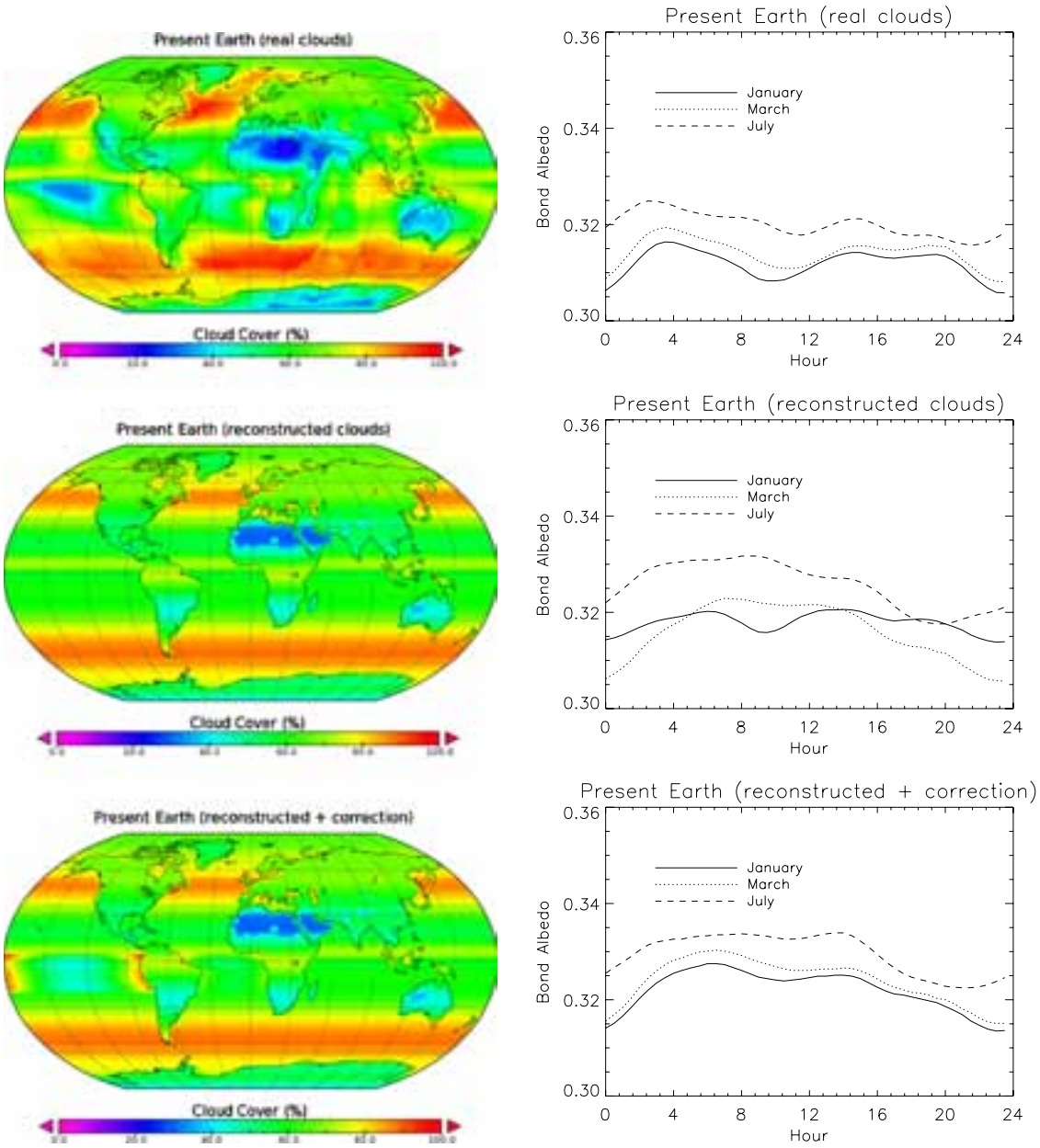

Figure 3. Cloud distribution and light curves of the present Earth. The left panels illustrate the global distribution of real (top) and reconstructed (middle and bottom) cloud cover. Colors represent a different fraction of cloudiness as the color code below each panel show. The difference between middle left and bottom left is that the latter is the same as the former but after applying the parabolic correction over oceans (see the main text). The right panels show the corresponding simulations of Bond albedo 24 hr variability. The different lines styles represent the results obtained for three different months as indicated in the legend.

last one. Note that we have only used this modification in our empirical cloud reconstruction for the Cambrian (500 Ma ago), since for the other epochs desert areas are located mainly at low latitudes.

In the top left panel of Figure 3, the real Earth cloud distribution is shown. In the middle left panel it is shown the global cloud distribution as reconstructed from our simple model. As can be seen in the figure, our semiempirical model for clouds reproduces well the general features of Earth's cloudiness distribution. The latitudinal range 40°–75°, both north and south, is quite well reproduced, as well as the differences in cloud amount between land and water at the same latitude. There are, however, some small-scale structures, mostly over tropical oceans, that our model does not reproduce, being the major differences located in the Pacific and in the Indian oceans. These differences are due to oceanic effects, such as surface temperature, trade winds, ocean currents, and regional meteorological phenomena such as "El niño"/"La niña," which can greatly influence the cloud formation. This is difficult to parameterize in a general model valid for any continental distribution.

However, with the aim of improving our result over the oceanic areas, we have tried to capture the longitudinal variations in cloud amount by introducing an oceanic longitudinal variation in our model. We observe that in all large ocean basins, although the effect is larger for the Pacific, clouds tend to accumulate over the eastern margin (cold currents) and have a minimum over the western margins (hot currents). Taking the

Pacific as the rule, we have selected the region where the major differences take place, i.e., the region between -20° and 0° latitude and between -70° and -180° longitude, approximately. We calculated the mean cloudiness over this box as a function of longitude and fit it with a two-degree polynomial curve (a parabola). We have applied this parabolic effect to all tropical ocean basins to make a second-order correction to our modeled cloud distributions. To do that, the parabola was normalized to the mean cloud amount and then the cloud amount in each ocean basin was multiplied by this normalized parabola. As mentioned previously, the same correction is applied to all ocean areas within -20° to 0°, although the effect is almost unnoticeable for small oceans.

Figure 3 bottom left shows the reconstructed cloud distribution of the Earth today after applying the longitudinal correction. As can be seen cloudiness at the Pacific area has a similar aspect to that shown in the same area in the real cloud map. In general, a differential map between the real cloud amount and our reconstructed cloudiness clearly indicates that this second-order correction greatly improves the prediction errors.

4. LIGHT CURVE RECONSTRUCTIONS

Once we have been able to reconstruct the cloud distribution for present and past epochs of the Earth, we want to transform this information into Bond albedo values to test the photometric variability of the Earth as seen from a distant observer. To this end, we have used a simple Earth reflectance model, which calculates the visible reflected light curves of our planet for a given day, by using as inputs ground scene models from the Earth Radiation Budget Experiment (Suttles et al. 1988), cloud and snow/ice cover maps, and surface maps as inputs (Pallé et al. 2003). With this information the model is able to determine the Bond albedo at each time of the day and in any particular direction. Nevertheless, the model can only be considered as a first-order approximation since it does not take into account any other climate parameters beyond snow and ice that might contribute to changes in Bond albedo. Furthermore, the model contemplates only 12 different surface scenes and 4 cloudiness levels (0%–5%, 5%–50%, 50%–95%, and 95%–100%).

Our model calculates first the albedo of each element of area of the planet's surface taking into account surface type, cloud amount, snow/ice cover, and solar zenith angle. Then the model performs the calculation of the Bond albedo in terms of the albedo of each element of area by integrating over all portions of the globe illuminated by the Sun. For more details see Pallé et al. (2003).

Obviously both cloudiness and surface type play a role in the albedo variability and deconvolving the effects of both components can be an impossible task for extrasolar planets. However, Pallé et al. (2008) demonstrated that if sufficient signal to noise can be obtained, it is possible to detect both the presence of continents and the clouds. In any case, our aim here is to characterize the photometric variability of both components combined.

4.1. Present Day Earth

As representative light curves, we have arbitrarily chosen the months of January, March, and July 2000 to carry out the Bond albedo simulations of the Earth at the present day, and at 90, 230, 340, and 500 Ma ago. In the right panels of Figure 3, we plot the modeled 24 hr Bond albedo variation for the whole Earth over one day.

Table 1
Percentage of the Daily Variability and Mean Albedo of the Light Curves for Each Epoch

Epoch	%	⟨Albedo⟩
Present Earth (real clouds)	3.29	0.315
Present Earth (reconstructed clouds)	4.16	0.325
Late Cretaceous (90 Ma ago)	4.27	0.331
Late Triassic (230 Ma ago)	5.02	0.327
Mississippian (340 Ma ago)	4.46	0.329
Late Cambrian (500 Ma ago)	12.2	0.351

Note. These quantities have been calculated by performing the mean of these results obtained for 2000 January, March, and July.

As can be seen in Figure 3, the agreement between the light curve obtained from reconstructed clouds (bottom right) and that calculated from real cloud cover (top right) is quite good. The general shape of the light curves are quite similar, with the local maximums/minimums located at the same hour of the day in both cases. But the result obtained from the reconstructed cloudiness tends to be higher than that obtained from real cloud cover (0.325 as opposed to 0.315). Furthermore, the amplitude of the light curve is similar to that obtained from real cloud data (4.16% and 3.29% for reconstructed and real cloudiness, respectively). These differences in the variability of the Bond albedo are owing to the fact that real cloud cover presents larger changes in the longitudinal direction in contrast to the low variability in such direction of the reconstructed clouds, affecting Bond albedo values.

In Figure 3, it can also be seen that the resulting light curve after applying the longitudinal correction, i.e., after applying the aforementioned parabolic smoothing technique applied over oceans, in the Pacific Ocean (bottom right) is more similar to that obtained with real cloud data than the light curve calculated before the correction (middle right), confirming that the Earth's cloudiness behavior is better reproduced by using this longitudinal correction.

4.2. Historical Epochs

In the right panels of Figure 4, the light curves for the different epochs (90, 230, 340, and 500 Ma ago) are shown. As can be seen, the light curves of the first three epochs are quite similar. This is related to the fact that these epochs have a similar ocean–land–vegetation distribution, having a nearly totally clustered continents located principally in one hemisphere and deserts located at low latitudes. These light curves have a soft shape with an enhancement in brightness produced by continental masses. This smooth behavior is also due to the longitudinal relative homogeneity of the reconstructed cloud maps.

The reflected light of the Earth at 500 Ma ago, however, presents much more variability in contrast to the light curves obtained for the other epochs. That is again related to the continental distribution. In this epoch, most of the continents were clustered in one hemisphere, but it also has several big islands that cause strong variability in the reflected light. Moreover, this epoch presents a significantly higher mean albedo value. That can be related to the fact that in this epoch continents were covered by deserts, thus involving a higher reflectivity.

The mean Bond albedo values and their variability obtained for the Earth at different epochs are summarized in Table 1. By comparing the results shown in Table 1 one can note that

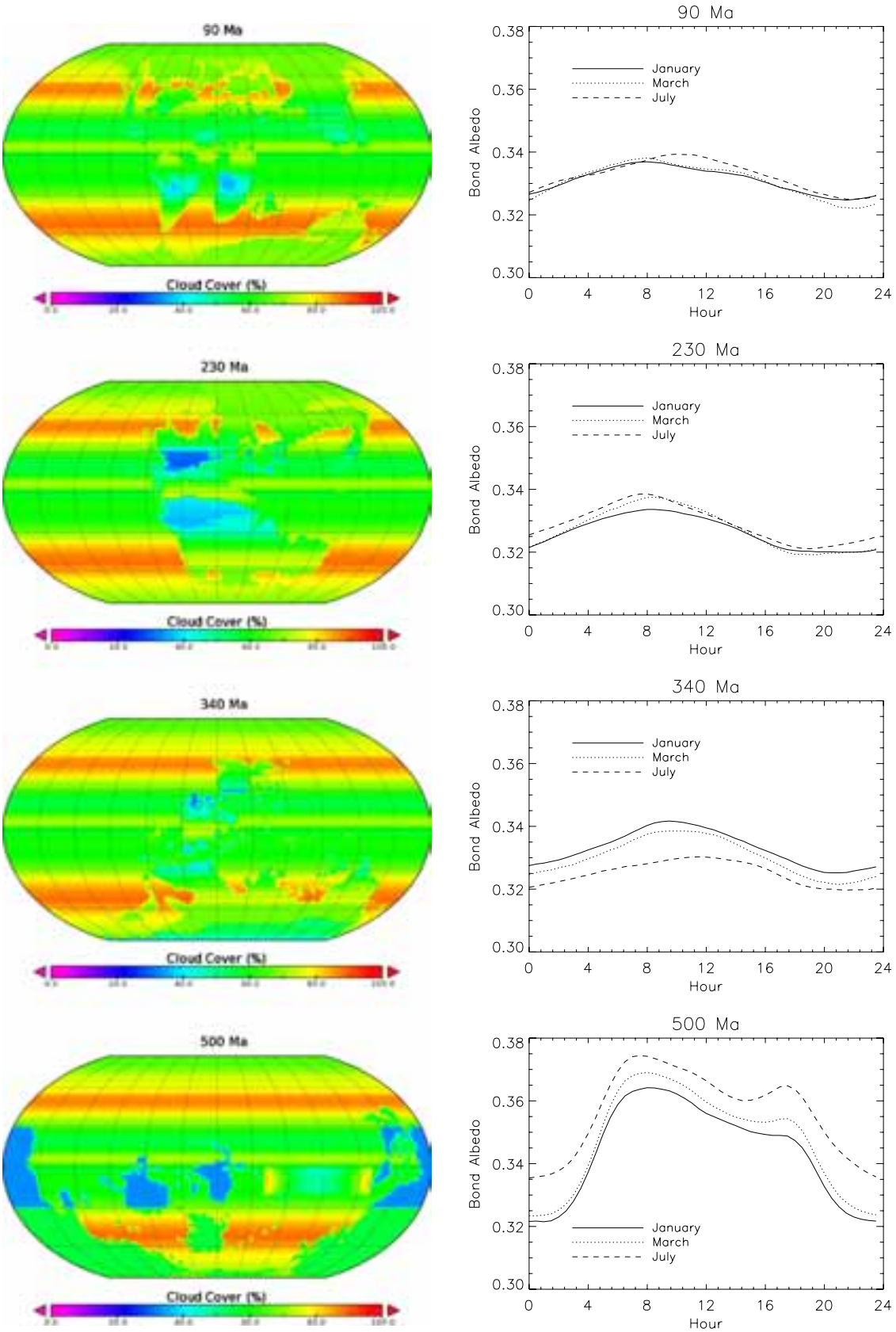

Figure 4. Same as Figure 3 but, from top to bottom, during the Late Cretaceous (90 Ma ago), the Late Triassic (230 Ma ago), the Mississippian (340 Ma ago), and the Late Cambrian (500 Ma ago).

daily variations were larger than present day's, for instance 500 Ma ago, when the variations were larger by a factor of three. Not only that, but also the mean albedo values were larger, which should have profound influences on the global climate by introducing a cooling effect, probably compensated by the increased greenhouse gas concentrations over that period, 16 times that of pre-industrial modern levels (Augustin et al. 2004).

5. CONCLUSIONS

In this paper, we have used information about the surface properties and continental distribution of the Earth with the aim of studying the behavior of the large-scale cloud patterns. We have obtained empirical relationships between the amount of cloudiness and their location on Earth's surface depending on latitude and underlying surface types. These relationships have been used to reconstruct the possible cloud distribution for different epochs of the Earth's history such as 90, 230, 340, and 500 Ma ago. With this information, and with the help of an albedo model we have attempted, for the first time, to reconstruct and understand the photometric variability of these past epochs according to their different geographic and cloudiness distribution.

We find that our model reproduces well the major features of the cloud distribution and the photometric light curve of the Earth at present. When applied to past epochs of the Earth, we find that both the mean albedo value and the diurnal light curve variability remain stable as long as desert area are confined to the tropical regions. When this condition is not met, as during the Late Cambrian about 500 Ma ago, both the mean albedo value and the photometric variability are greatly increased. This increased variability could help in the determination of the rotational period of the planet from an astronomical distance. Due to the large compositional and chemical changes of Earth's atmosphere, we have not attempted to reconstruct cloud cover maps for epochs prior to the Late Cambrian. However, it is likely that the conditions for this period, i.e., higher albedo values and photometric variability, hold for much of the previous epochs of the Earth, not considering possible albedo variations due to atmospheric changes coming from clouds, aerosols, and hazes.

Research by E.P. is supported by a Ramón y Cajal fellowship from the MICIIN.

REFERENCES

Arnold, L., Bréon, F.-M., & Brewer, S. 2009, Int. J. Astrobiol., 8, 81
Arnold, L., Gillet, S., Lardière, O., et al. 2002, A&A, 392, 231
Augustin, L., Barbante, C., Barnes, P. R. F., et al. 2004, Nature, 429, 623
Batalha, N. M., Borucki, W. J., Bryson, S. T., et al. 2011, ApJ, 729, 27
Beaulieu, J.-P., Bennett, D. P., Fouqué, P., et al. 2006, Nature, 439, 437
Bennett, D. P., Bond, I. A., Udalski, A., et al. 2008, ApJ, 684, 663
Beuzit, J.-L., Mouillet, D., Oppenheimer, B. R., & Monnier, J. D. 2007, in Protostars and Planets V, ed. B. Reipurth, D. Jewitt, & K. Keil (Tuscon: Univ. Arizona Press), 717
Cess, R. D., Zhang, M. H., Ingram, W. J., et al. 1996, J. Geophys. Res., 101, 12791
Charbonneau, D., Berta, Z. K., Irwin, J., et al. 2009, Nature, 462, 891
Charbonneau, D., Brown, T. M., Burrows, A., & Laughlin, G. 2007, in Protostars and Planets V, ed. B. Reipurth, D. Jewitt, & K. Keil (Tuscon: Univ. Arizona Press), 701
Cowan, N. B., Agol, E., Meadows, V. S., et al. 2009, ApJ, 700, 915
Cowan, N. B., Robinson, T. D., Livengood, T. A., et al. 2011, ApJ, 731, 76
Dessler, A. E. 2010, Science, 330, 1523
Ford, E. B., Seager, S., & Turner, E. L. 2001, Nature, 412, 885
Frisch, W., Meschede, M., & Blakey, R. 2011, Plate Tectonics: Continental Drift and Mountain Building (1st ed.; Berlin: Springer)
Fujii, Y., Kawahara, H., Suto, Y., et al. 2010, ApJ, 715, 866
Gray, J., Chaloner, W., & Westoll, T. 1985, Phil. Trans. R. Soc. B, 309, 167
Hart, M. H. 1978, Icarus, 33, 23
Kasting, J. F., & Siefert, J. L. 2002, Science, 296, 1066
Lindensmith, C. 2003, BAAS, 35, 947
Mayor, M., & Queloz, D. 1995, Nature, 378, 355
Mayor, M., Udry, S., Lovis, C., et al. 2009, A&A, 493, 639
Montañés-Rodríguez, P., Pallé, E., Goode, P. R., Hickey, J., & Koonin, S. E. 2005, ApJ, 629, 1175
Montañés-Rodríguez, P., Pallé, E., Goode, P. R., & Martín-Torres, F. J. 2006, ApJ, 651, 544
Oakley, P. H. H., & Cash, W. 2009, ApJ, 700, 1428
Pallé, E., Ford, E. B., Seager, S., Montañés-Rodríguez, P., & Vazquez, M. 2008, ApJ, 676, 1319
Pallé, E., Goode, P. R., Yurchyshyn, V., et al. 2003, J. Geophys. Res. (Atmos.), 108, 4710
Qiu, J., Goode, P. R., Pallé, E., et al. 2003, J. Geophys. Res. (Atmos.), 108, 4709
Queloz, D., Bouchy, F., Moutou, C., et al. 2009, A&A, 506, 303
Robinson, T. D., Meadows, V. S., Crisp, D., et al. 2011, Astrobiology, 11, 393
Rossow, W. B., Walker, A. W., Beuschel, D. E., & Roiter, M. D. 1996, World Climate Research Programme Report WMO/TD 737 (Geneva, Switzerland: World Meteorological Organization)
Schneider, J., Boccaletti, A., Mawet, D., et al. 2009, Exp. Astron., 23, 357
Seager, S., Turner, E. L., Schafer, J., & Ford, E. B. 2005, Astrobiology, 5, 372
Sonka, M., Hlavac, V., & Boyle, R. 1993, Image Processing. Analysis and Machine Vision (London: Chapman & Hall Computing)
Spencer, R. W., & Braswell, W. D. 2010, J. Geophys. Res. (Atmos.), 115, D16109
Suttles, J. T., Green, R. N., Minnis, P., et al. 1988, Angular Radiation Models for Earth-Atmosphere Systems. Vol. I, Shortwave Radiation (NASA RP-1184; Hampton, VA: NASA)
Tinetti, G., Meadows, V. S., Crisp, D., et al. 2006a, Astrobiology, 6, 34
Tinetti, G., Meadows, V. S., Crisp, D., et al. 2006b, Astrobiology, 6, 881
Tinetti, G., Waldmann, I., Griffith, C., et al. 2010, BAAS, 42, 1079
Turnbull, M. C., Traub, W. A., Jucks, K. W., et al. 2006, ApJ, 644, 551
Udry, S., Fischer, D., & Queloz, D. 2007, in Protostars and Planets V, ed. B. Reipurth, D. Jewitt, & K. Keil (Tuscon: Univ. Arizona Press), 685
Woolf, N. J., Smith, P. S., Traub, W. A., & Jucks, K. W. 2002, ApJ, 574, 430

5

On the Effects of the Evolution of Microbial Mats and Land Plants on Earth

In this chapter we extend the work presented in Chapter 4 by using spectrospy instead of photometry to study the radiation reflected by Earth as a function of the planet's rotation. Here, spectroscopy allow us to retrieve more information than photometry since the former allows us to identify surface signatures related to the presence of life in the spectrum of our planet. As we were interested in exploring the possible effects that the evolution of life over land might have had on the way our planet looked from afar, here we concentrated on the Earth 500 Ma ago, as this is approximately the time when advanced land-plants evolved. To study this effect on the VIS-NIR disk-integrated Earth spectra we explored several scenarios which go from bare surfaces, to continents covered by microbial mats, to continents inhabited by evolved plants.

We used a radiative transfer model to generate a 1-dimensional synthetic spectral library that covers a wide range of viewing and incident angles, surface and cloud types, and atmospheric composition, in order to be able to model a variety of planet scenarios. We also present a disk-integrated code that allows us to calculate disk-integrated spectra for any viewing geometry, surface map and cloudiness distribution, by using the aforementioned spectral database.

This part of the thesis was originally published in the paper entitled "On the effects of the evolution of microbial mats and land plants on the Earth as a planet. Photometric and spectroscopic light curves of paleo-Earths" in the April 2013 edition of the Astrophysical Journal (Sanromá et al. 2013).

Abstract: Understanding the spectral and photometric variability of the Earth and the rest of the solar system planets has become of utmost importance for the future characterization of rocky exoplanets. As this is not only interesting at present times

but also along the planetary evolution, we studied the effect that the evolution of microbial mats and plants over land has had on the way our planet looks from afar. As life evolved, continental surfaces changed gradually and non-uniformly from deserts through microbial mats to land plants, modifying the reflective properties of the ground and most likely the distribution of moisture and cloudiness. Here, we used a radiative transfer model of the Earth, together with geological paleo-records of the continental distribution and a reconstructed cloud distribution, to simulate the visible and near-IR radiation reflected by our planet as a function of Earth's rotation. We found that the evolution from deserts to microbial mats and to land plants produces detectable changes in the globally averaged Earth's reflectance. The variability of each surface type is located in different bands and can induce reflectance changes of up to 40% in period of hours. We conclude that by using photometric observations of an Earth-like planet at different photometric bands it would be possible to discriminate between different surface types. While recent literature proposes the red-edge feature of vegetation near 0.7 μ as a signature for land plants, observations in near-IR bands can be equally or even better suited for this purpose.

The Astrophysical Journal, 766:133 (8pp), 2013 April 1 doi:10.1088/0004-637X/766/2/133

ON THE EFFECTS OF THE EVOLUTION OF MICROBIAL MATS AND LAND PLANTS ON THE EARTH AS A PLANET. PHOTOMETRIC AND SPECTROSCOPIC LIGHT CURVES OF PALEO-EARTHS

E. Sanromá[1,2], E. Pallé[1,2], and A. García Muñoz[1,2]
[1] Instituto de Astrofísica de Canarias (IAC), Vía Láctea s/n, E-38200 La Laguna, Spain; mesr@iac.es
[2] Departamento de Astrofísica, Universidad de La Laguna, E-38206 La Laguna, Spain
Received 2012 December 4; accepted 2013 February 13; published 2013 March 15

ABSTRACT

Understanding the spectral and photometric variability of the Earth and the rest of the solar system planets has become of utmost importance for the future characterization of rocky exoplanets. As this is not only interesting at present times but also along the planetary evolution, we studied the effect that the evolution of microbial mats and plants over land has had on the way our planet looks from afar. As life evolved, continental surfaces changed gradually and non-uniformly from deserts through microbial mats to land plants, modifying the reflective properties of the ground and most likely the distribution of moisture and cloudiness. Here, we used a radiative transfer model of the Earth, together with geological paleo-records of the continental distribution and a reconstructed cloud distribution, to simulate the visible and near-IR radiation reflected by our planet as a function of Earth's rotation. We found that the evolution from deserts to microbial mats and to land plants produces detectable changes in the globally averaged Earth's reflectance. The variability of each surface type is located in different bands and can induce reflectance changes of up to 40% in period of hours. We conclude that by using photometric observations of an Earth-like planet at different photometric bands it would be possible to discriminate between different surface types. While recent literature proposes the red-edge feature of vegetation near 0.7 μm as a signature for land plants, observations in near-IR bands can be equally or even better suited for this purpose.

Key words: astrobiology – Earth – planets and satellites: atmospheres – planets and satellites: surfaces – radiative transfer

Online-only material: color figures

1. INTRODUCTION

In the past several decades, more than 850 exoplanets have been detected outside the solar system, while thousands of potential planet candidates from the *Kepler* mission are waiting for confirmation. Even though most of the discovered exoplanets are gas giants, as the larger planets are easier to detect than the smaller rocky ones, evolving observational capabilities have already allowed us to discover tens of planets in the super-Earth mass range (e.g., Udry et al. 2007; Charbonneau et al. 2009; Pepe et al. 2011; Borucki et al. 2012), some of which likely lie within the habitable zone of their stars (Borucki et al. 2012). Moreover, some Earth-sized, and even smaller, exoplanets have already been reported in the literature (Fressin et al. 2012; Muirhead et al. 2012). Indeed, early statistics indicate that about 62% of the Milky Way stars may host a super-Earth (Cassan et al. 2012). Thus, one can confidently expect that true Earth analogues will be discovered in large numbers in the near future.

To be prepared for the characterization of future exoearth detections, the exploration of our own solar system and its planets is essential. This will allow us to test our theories and models, enabling more accurate determinations, and characterization of the exoplanets' atmospheres and surfaces. In particular, observation of the solar system rocky planets, including Earth, will be key for the search for life elsewhere.

Over the past several years, a variety of studies, both observational and theoretical, to determine how the Earth would look like to an extrasolar observer have been carried out. One of the observational approaches has been to observe the Earthshine, i.e., the sunlight reflected by Earth via the dark side of the moon. The visible spectrum of the Earthshine has been studied by several authors (Goode et al. 2001; Woolf et al. 2002; Qiu et al. 2003; Pallé et al. 2003, 2004), while more recent studies have extended these observations to the near-infrared (Turnbull et al. 2006) and to the near-UV (Hamdani et al. 2006).

Several authors have also attempted to measure the characteristics of the reflected spectrum and the enhancement of Earth's reflectance at 700 nm due to the presence of vegetation, known as red edge, directly (Arnold et al. 2002; Woolf et al. 2002; Seager et al. 2005; Montañés-Rodríguez et al. 2006; Hamdani et al. 2006), and also by using simulations (Tinetti et al. 2006a, 2006b; Montañés-Rodríguez et al. 2006). The red edge has been proposed as a possible biomarker in Earth-like planets (Tinetti et al. 2006c; Kiang et al. 2007a, 2007b). Furthermore, Pallé et al. (2008) determined that the light scattered by the Earth as a function of time contains sufficient information, even with the presence of clouds, to accurately measure Earth's rotation period. More recently, Sterzik et al. (2012) have also studied the use of the linear polarization content of the Earthshine to detect biosignatures, and were able to determine the fraction of clouds, oceans, and even vegetation.

Another approach has been to analyze Earth's observations from remote-sensing platforms (e.g., Cowan et al. 2009, 2011; Robinson et al. 2011). These kinds of observations have also allowed the possibility to reconstruct the continental distribution of our own planet from scattered light curves. Cowan et al. (2009) performed principal components analysis in order to reconstruct surface features from the EPOXI data. Kawahara & Fujii (2010, 2011) and Fujii & Kawahara (2012) proposed an inversion technique that enables us to sketch a two-dimensional albedo map from annual variations of the disk-averaged scattered light. In addition, Oakley & Cash (2009) attempted to reproduce a longitudinal map of the Earth from simulated photometric data by using the difference in reflectivity between land

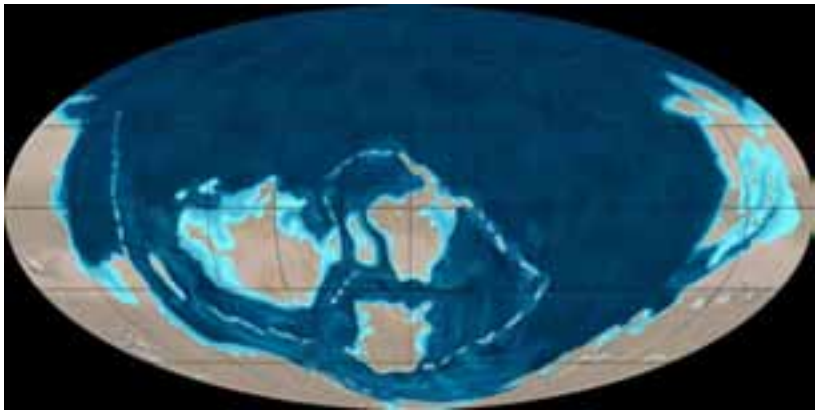

Figure 1. Geologic map of the Earth during the Late Cambrian (500 Ma ago). In our simulations the meridian line crossing the image center has been taken as longitude 0. Image credit: Ron Blakey.

(A color version of this figure is available in the online journal.)

and oceans. Other authors have also studied what the color of an extreme Earth-like planet might be by utilizing filter photometry (Hegde & Kaltenegger 2013), while others have studied the disk-averaged spectra of cryptic photosynthesis worlds (Cockell et al. 2009).

However, it is unlikely, even if we were to find an Earth-twin, that the planet will be at an evolutionary stage similar to the Earth today. On the contrary, extrasolar planets are expected to exhibit a wide range of ages and evolutionary stages. Because of this, it is of interest not only to use our own planet as it is today as an exemplar case, but also at different epochs (Kaltenegger et al. 2007).

The development of advanced plants is believed to have taken place on Earth during the Late Ordovician, about 450 Ma ago, albeit fungi, algae, and lichens may have greened many land areas before then (Gray et al. 1985). Microbial mats are multilayered sheets of microorganisms generally composed of both Prokaryotes and Eukaryotes, being able to reach a thickness of a few centimeters. The time when microbial mats appeared on the Earth's surface is still not clear, but prior to the evolution of algae and land plants on early Earth, photosynthetic microbial mats were probably among the major forms of life on our planet. Microbial mats are found in the fossil record as early as 3.5 billion years ago. Later, when advanced plants and animals evolved, extensive microbial mats became rarer, but they are still presented in our planet in many ecosystems (Seckbach & Oren 2010). Even today, they still persist in special environments such as thermal springs, high-salinity environments, and sulfur springs.

In this paper, we aimed to discern the effect that the evolution of life over land might have had on the way our planet would look like to a remote extraterrestrial observer. To this end, we have simulated both visible and near-IR disk-integrated spectra of our planet, considering a scenario of such simulations the Earth during the Late Cambrian (Figure 1), the period during which the development of the first plants is believed to have taken place. Thus, it is clear that as life evolved over land, Earth's continental masses must have changed gradually going through different states that go from deserts, to microbial mats, to evolved plants.

2. MODEL DESCRIPTION

With the aim of deriving disk-averaged spectra of the Earth 500 Ma ago, at any viewing and illumination geometry, and for several surface types covering the continental crust, we have generated a database of one-dimensional synthetic radiance of the Earth, i.e., we have calculated synthetic spectra for a variety of surface and cloud types, and for several viewing and illumination angles. To do that, we have used a line-by-line radiative transfer algorithm, based on the DISORT[3] (Discrete Ordinates Radiative Transfer Program for a Multi-Layered Plane-Parallel Medium) code (Stammnes et al. 1988).

Our radiative transfer model (RTM) uses profiles of temperature and atmospheric composition, spectral albedos of each surface type, and cloudiness information as input data for the calculations (see subsequent subsections for a detailed description of inputs). The code considers Earth's atmosphere as plane parallel, and its radiative properties are prescribed on a grid of contiguous spectral bins. This spectral grid is unevenly spaced, and designed to resolve the rapid variations in the radiative properties near molecular absorption lines. Each spectrum is calculated at very high spectral resolution, with no less than three points per Doppler width. Positions, intensities, and line shape parameters for molecular absorption bands are taken from HITRAN2008 (Rothman et al. 2009). Only a single angle of incidence and 10 angles of reflection can be used for each model run. Finally, each spectrum is degraded to a lower resolution for storage purposes ($R = 10{,}000$). We have run this radiative code using input parameters covering a broad range of viewing and illumination angles, surface and cloud types, atmospheric profiles, and aerosol concentrations, leading to the generation of a database containing about 7000 spectra. The RTM is essentially an extension of the RTM for transits described in García Muñoz & Pallé (2011) and García Muñoz et al. (2012) to a viewing geometry for which the light reaching the observer has been reflected at the planet. The RTM is also capable of modeling the planet's emission of thermal radiation, although that possibility is not explored here.

Once the spectral library was generated, we developed a computer code to calculate the disk-integrated irradiance of our planet for given sub-solar and sub-observer points, a surface map, and a cloudiness distribution. At any given date the code calculates both the fraction of the planet visible to the observer and the illuminated fraction of the Earth from the location of the observer. The planets is subdivided in a 64×32 pixel (longitude by latitude) grid. This grid resolution offers the best balance

[3] ftp://climate1.gsfc.nasa.gov

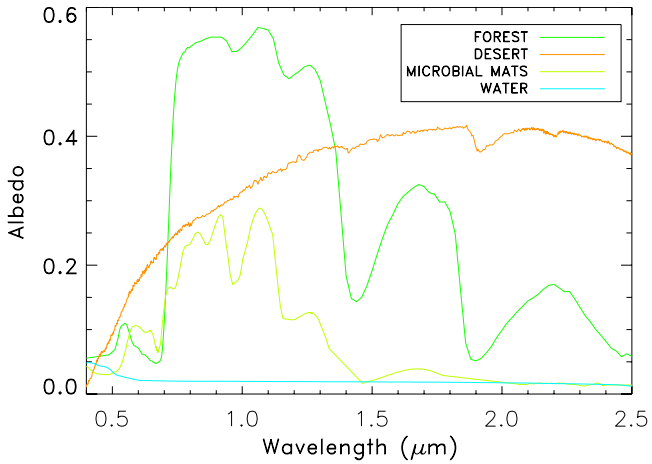

Figure 2. Spectral reflectance of the four surface types used in our model for the Earth 500 Ma ago: forest (green), desert (orange), microbial mats (light green), and water (blue).

(A color version of this figure is available in the online journal.)

between computational cost and accuracy. For each grid a radiance spectrum from the aforementioned database is assigned to each detectable and illuminated surface's pixel taking into account the surface type, and the percentage cloud type and amount of such pixel. Note that the full spectral database was generated only for 10 solar angles and for 10 observer angles (85°, 80°, 75°, 70°, 65°, 55°, 45°, 30°, 15°, and 0° for both angles). Thus, radiance values for arbitrary solar and observer angles were interpolated into the angles from the calculated radiances.

Finally, to get the disk-averaged spectrum of the ancient Earth, we have weighted each pixel's spectrum by their solid angle and we have integrated over the whole Earth.

2.1. Atmospheric Properties

Information about temperature and distribution of atmospheric gases were taken from FSCATM (Gallery et al. 1983). We have considered five atmospheric profiles models: tropical, midlatitud summer, midlatitud winter, subartic summer, and subartic winter. These atmospheric profiles include mixing ratios of the most significant molecules in Earth's atmosphere: H_2O, CO_2, O_3, CH_4, O_2, and N_2. These properties are prescribed into 33 uneven layers, which go from 0 to 100 km height, being the spacing between layers of 1 km near the bottom of the atmosphere, and 5 km or more above 25 km height.

Note that Earth's atmosphere 500 Ma ago can be considered similar to the present one, since, on average, the same atmospheric composition and mean averaged temperature have existed during this period (Hart 1978; Kasting & Siefert 2002). This is a necessary condition for our simulations to hold as a valid approximation.

2.2. Surface Distribution and Albedos

To carry out our goal of finding out how the appearance of life over land could affect Earth's reflectance properties, we have considered four different continental land types: water, desert, microbial mats, and forest. Figure 2 shows the wavelength-dependent albedos of each surface type according to the ASTER Spectral Library[4] and the USGS Digital Spectral Library.[5]

The continental distribution during the Late Cambrian has been taken from Ron Blakey's Web site.[6] Surface maps of our planet in that epoch are available online. The Earth geologic information has been regridded into the 64 × 32 pixel grid used by our model.

2.3. Cloud Distribution and Optical Properties

In our model, the spatial distribution of clouds was taken from the International Satellite Cloud Climatology Project (ISCCP; Rossow et al. 1996) cloud climatology. With the aim of getting information about the global distribution of clouds over different surface types, and in order to reconstruct the possible cloud distribution of the Late Cambrian (500 Ma ago), we have proceeded in the same way as in Sanromá & Pallé (2012) but here, instead of using only the total cloud amount information, we have used information on three separate cloud layers: low (1000–680 Mb), mid (680–440 Mb), and high cloud (440–30 Mb) data.

The optical properties of each cloud type, wavelength-dependent scattering and absorption coefficients, and the asymmetry parameter, were obtained from the Optical Properties of Aerosols and Clouds (OPAC) data base (Hess et al. 1998). We have considered physical cloud thicknesses of 1 km, and we have assumed that the scattering phase function is described by the Henyey–Greenstein equation inside clouds, and by the Rayleigh scattering function outside them.

We calculated the spatial distribution of these three cloud types according to the surface type lying beneath. To perform this classification, we used real geographical information about the different types of surfaces and vegetation in the present Earth, available from the ISCCP Web site.[7] Although the ISCCP classifies the surfaces as water, rain forest, deciduous forest, evergreen forest, grassland, tundra, shrub-land, desert, and ice, we have only distinguished between four surface types: water, desert, ice, and vegetation, where the latest is defined as the sum of rain forest, deciduous forest, evergreen forest, grassland, tundra, or shrub-land. We then computed the mean cloudiness at each latitude point, obtaining the empirical relationships between the amount of clouds, surface type, and latitude for low, mid, and high clouds (see Sanromá & Pallé 2012 for details on the method). These relationships allow us to reconstruct the possible cloudiness distribution of the Earth 500 Ma ago.

It is worth noting that we do not have any empirical information about how clouds behave over extended microbial mat surfaces. Thus, in our calculation we have used both the cloudiness information corresponding to deserts and vegetation. The answer is likely somewhere in between, as microbial mats will increase transpiration and moisture compared to bare land. However, we will show how the choice of cloud amounts does not substantially affect the results.

3. SPECTRA AND LIGHT CURVES OF EARTH 500 Ma ago

3.1. Spectral Models

The development of advanced land plants is believed to have taken place during the Late Ordovician, about 450 Ma ago, albeit fungi, algae, and lichens may have greened many land areas long before (Gray et al. 1985). Thus, to determine the impact that such changes could cause in the appearance of the ancient Earth's spectrum, we have run our model for four separate

[4] http://speclib.jpl.nasa.gov
[5] http://speclab.cr.usgs.gov/spectral-lib.html
[6] http://jan.ucc.nau.edu
[7] http://isccp.giss.nasa.gov

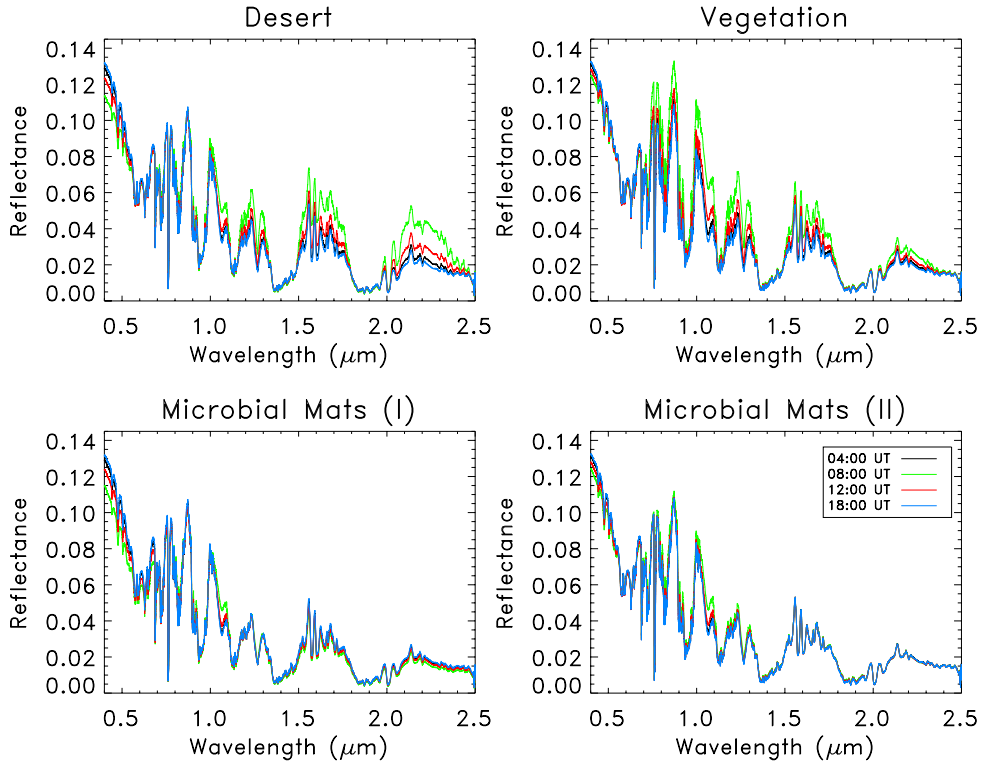

Figure 3. Earth's reflectance 500 Ma ago, taken as π times the disk-averaged radiance divided by the solar flux, in the VIS-NIR, for our four cases in which the continents are covered by deserts, vegetation, microbial mats with the cloudiness information corresponding to desert (I), and microbial mats with the cloudiness information corresponding to vegetation (II). The Earth is viewed at a phase angle of 90° and the different spectra follow their diurnal rotation. Both the observer and the Sun are located over the equator. The spectra have been smoothed with a 100 point running mean for illustration purposes.

(A color version of this figure is available in the online journal.)

scenarios. First of all, to illustrate the spectrum properties of a planet without life on its surface, we have considered that the continental crust of the Earth 500 Ma ago was entirely desert. While this might not be entirely true, it certainly was true at some point earlier in Earth's history, with an unknown continental distribution. Here, we chose to keep the Late Cambrian continental structure in order to isolate the spectral changes due to land scenery changes from those introduced by changing continental distribution (Sanromá & Pallé 2012). Then, we have regarded a case where continents were covered by microbial mats. Here, two separate simulations were run, with the cloud type's distribution over land corresponding to desert and to vegetated areas. We have also considered the case where the continental crust during the Late Cambrian was entirely covered by evolved plants, like those that dominate the continental surface today. Finally, in Section 3.2 we have also considered more realistic cases with 50% mixtures between different surface types. In all cases ocean areas remained the same, and a three-layer cloud distribution over the whole planet is applied.

Figure 3 shows synthetic disk-integrated spectra of the Earth 500 Ma ago covering the spectral ranges between 0.4 and 2.5 μm, at different times of the day, for each of our four cases where continents are totally covered by (1) deserts, (2) vegetation, (3) microbial mats with the cloudiness information corresponding to deserts, and (4) microbial mats with the clouds corresponding to vegetation. In all cases throughout this paper, the observer and the Sun are both located over the planet's equator in such a way that the observer is looking at a quarter-illuminated planet (phase angle 90°). For an extrasolar planet, the maximum angular separation from the parent star along the orbit occurs at phase 90°, as defined from the observer's position. Thus, this is the more relevant geometry for future exoplanet studies.

Table 1
The Diurnal Variability of the Vegetation's Red Edge Strength for the Earth 500 Ma Ago

Surface Type	2 UT	8 UT	12 UT	18 UT
Desert	1.14	1.35	1.16	1.03
Forest	1.03	1.05	1.03	1.01
Microbial mats (I)	1.05	1.12	1.05	1.02
Microbial mats (II)	1.04	1.10	1.05	1.02

Notes. Ratio between the intensity in the 0.740–0.750 μm and 0.678–0.682 μm range.

One can note that as continents come in and out of the field of view, the global Earth's spectra change. At 8:00 UT, when the continental presence is at maximum, the changes are more dramatic, in contrast to the spectra at 18:00 UT where differences between the four scenarios cannot be appreciated. That is related with the percentage of land that were illuminated and visible at each time. These percentages are approximately 24%, 46%, 36%, and 6% for 4:00, 8:00, 12:00, and 18:00 UT, respectively.

In order to show such intensity changes in terms of the strength of the vegetation's red edge, we have calculated the ratio between the 0.740–0.750 μm and the 0.678–0.682 μm spectral ranges (Table 1). The choice of these spectral regions was made according to Montañés-Rodríguez et al. (2006).

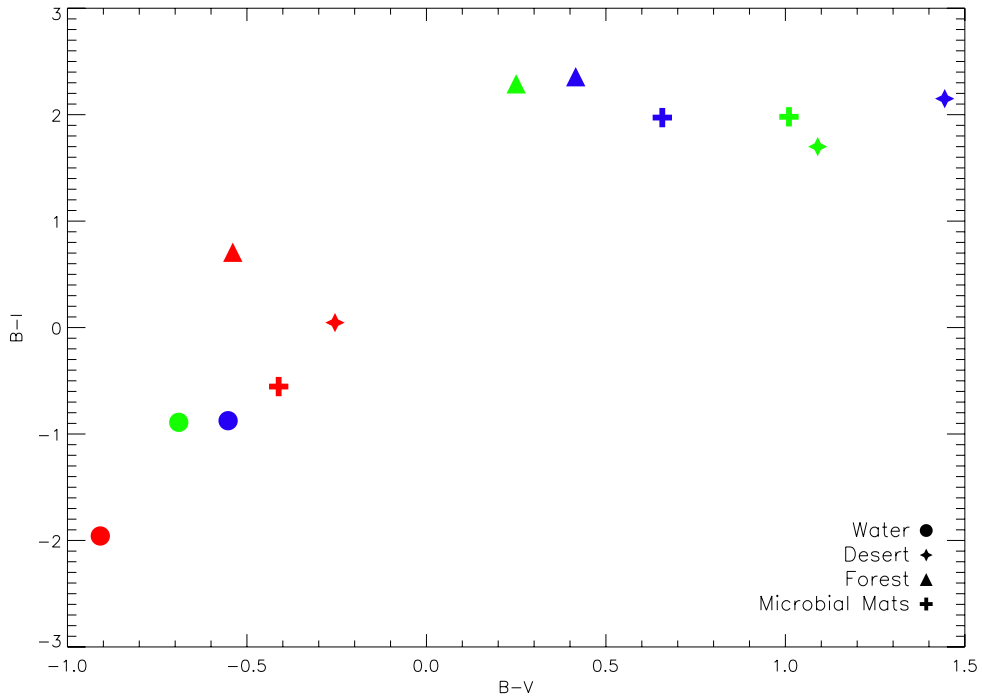

Figure 4. Color–color diagram of homogeneous test planets. Symbols denote planets whose surface is totally covered by water (circles), deserts (stars), vegetation (triangles), and microbial mats (crosses). The values are shown for planets without atmosphere (this work in blue and Hegde & Kaltenegger 2013 in green), and for planets with an Earth-like atmosphere (red). Note that adding an atmosphere to the model reduces considerably the variability of the colors of the different planets.
(A color version of this figure is available in the online journal.)

As expected, at 18:00 UT (6% of land) this rate is almost the same in our four cases, while at 08:00 UT (46% of land) the maximum is reached in the vegetation case where the red edge is more pronounced.

For a planet covered by bare dirt, Figure 3 illustrates some diurnal temporal variability, which is small in the visible range, but increases toward redder wavelengths. Gómez-Leal et al. (2012) studied the mid-IR emission of the planet in order to derive the rotational period. They found that the signature of the emission from the Sahara desert, among others, can be seen from space and determines a clear maximum in emission. Thus, it is probable that this variability would be even larger in the mid-IR.

In the case of a planet with continents covered by microbial mats, the spectra do not seem to vary much along the planet rotation, despite the fact of having a large and well-differentiated land mass. The impact of using two different clouds layers in the model (desert or vegetation) is almost negligible, the former being just a little bit more variable.

On the contrary, the spectrum of a planet covered entirely by plants varies significantly along the day, with the maximum variance occurring in the visible and near-IR. In particular, the variability along the red-edge feature (at 700 nm) is large, and it extends all the way into the near-IR.

3.2. Photometric Light Curves

Observing a detailed reflectance spectrum of an exoplanet would no doubt be a major advantage toward characterizing its atmospheric composition and surface features. However, given the low signal-to-noise ratio scenarios that are expected for such observations, spectral information might be difficult to retrieve, especially at high enough temporal resolution to allow sampling of the planet's rotation. Broadband photometric observations are perhaps a more realistic scenario. In order to simulate such photometric observations, we have convolved our modeled spectra with standard visible and near-infrared photometric filters, namely, B, V, R, I, z, J, H, and K.

Figure 4 shows the $B-V$ versus $B-I$ color–color diagram of test planets fully covered by one specific surface type, i.e., planets totally covered by water, desert, vegetation, and microbial mats, with and without atmosphere (blue and red symbols, respectively). As can be seen, the addition of an atmosphere in our models moves the position of the planets in the color–color diagram significantly, reducing the color spread of the different surface types along the diagram.

Figure 5 shows the photometric time-dependent variations in the disk-integrated reflected light along one day. The rotational light curves are plotted for our four scenarios, and for each photometric filter. For the Johnson visible system filters, these light curves show a relatively smooth shape, with the four scenarios being quite similar one to another, and with albedo changes lower than 6% in general. The only noticeable signature is the enhancement in brightness, about 20%, in the I filter, for the vegetated case (green line) between 6 and 12 UT. This is again related to the vegetation's signature, the red edge, since the main continental mass is in full view (and illuminated by the Sun) at this time.

More interesting results are obtained when one moves redward (bottom part of Figure 5). The diurnal light curves of a planet with bare desert surfaces (black line) in J, H, and K filters show a considerable increase in brightness between 6 and 12 UT of about 20%, 30%, and 40%, respectively, making immediately obvious the existence of a continent. The same is found in the vegetation case (green line), being these variability of around 30%, 20%, and 15% for J, H, and K, respectively.

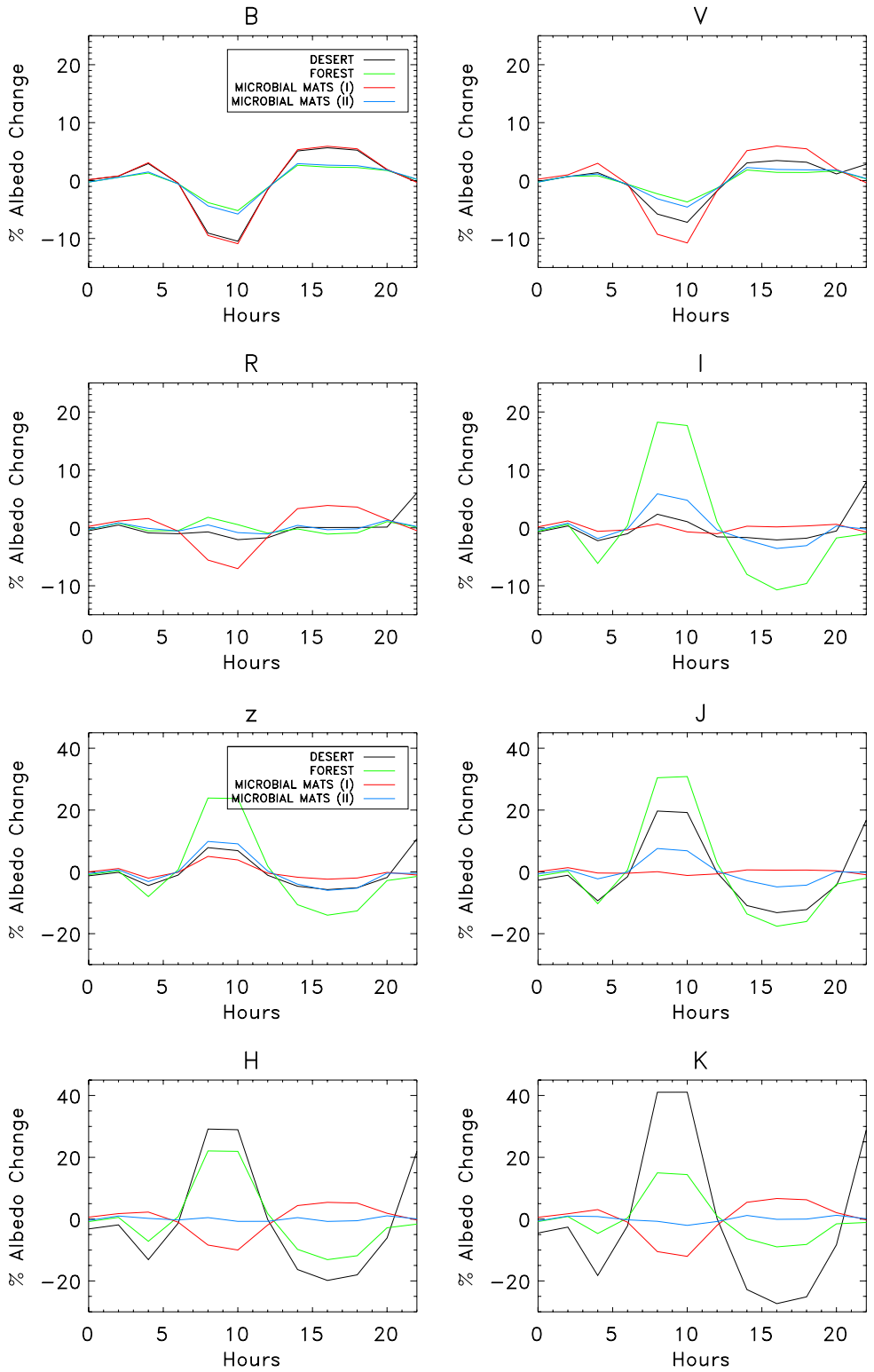

Figure 5. Diurnal light curves of the Earth for the four scenarios contemplated in this paper. The *y*-scale is the same for all standard photometric filters. The light curves represent the percentage of the albedo change along a day for the four scenarios.
(A color version of this figure is available in the online journal.)

The light curve for a planet with continents covered with microbial mats with cloudiness distribution corresponding to vegetation (blue line) is very muted, with little variability in either the visible or the near-IR spectral ranges. In contrast, light curves of the microbial mats case with cloudiness distribution corresponding to desert (red line) show a decrease in the albedo of around 10% in the *H* and *K* filters, when the main continental mass is facing the observer. In the *J* filter, these light curves do not exhibit any variation, making it impossible to even discern the presence of continental masses.

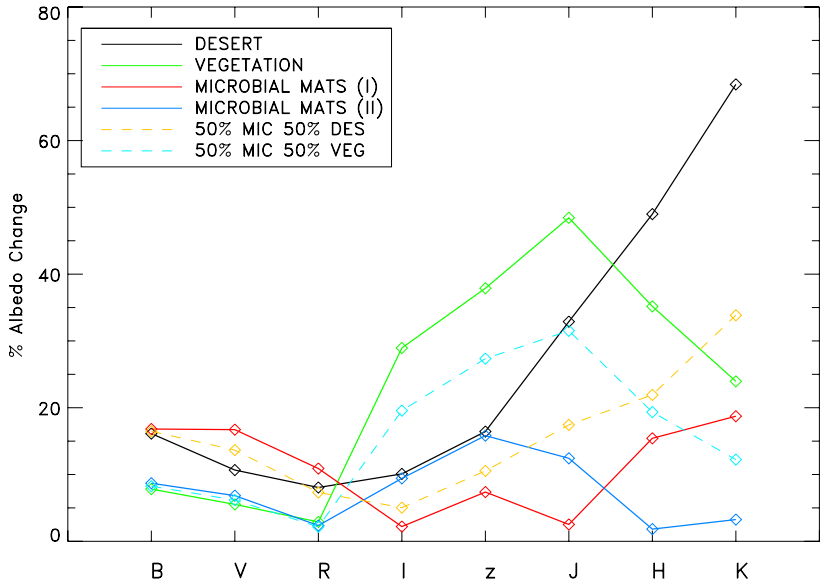

Figure 6. Amplitude of the albedo variability as a function of the standard photometric filters. Colors represent the different cases studied here: the Earth 500 Ma ago with continents completely covered by deserts (black solid line), vegetation (green solid line), microbial mats (red and blue solid lines), and a mixture of surface types: 50% microbial mats—50% deserts (yellow dashed line) and 50% microbial mats—50% vegetation (blue dashed line).

(A color version of this figure is available in the online journal.)

Figure 6 shows the amplitude of albedo variability of each of the studied cases as a function of the different photometric filters. As considering continents completely covered by just only one surface type might not be very realistic, we have also analyzed cases where continents were covered by patchy microbial mats, desert, and vegetation. As an example, in Figure 6 we present the results obtained for (1) continental masses irregularly covered by 50% deserts and 50% microbial mats, and (2) for continents unevenly covered by 50% vegetation and 50% microbial mats.

The curves in Figure 6 show a distinctive shape depending on surface type. When continents are completely covered by deserts (black line), the amplitude of albedo change increases rapidly when one moves from z filter redward, while the variability is nearly constant in the visible. When continents are totally covered by vegetation (green line), that albedo variability increases nearly monotonously from R filter to J filter, where it peaks, and then decreases redward. In contrast to these two cases, when continents are covered by microbial mats (blue and red lines), the amplitude of albedo change is not strongly dependent on the filter selected and is much more muted. Moreover, when we considered that the Earth 500 Ma ago had continents covered by a mixture of microbial mats and deserts/vegetation (yellow and light-blue lines), the shape of these amplitude variability curves resembles the typical shape of the desert/vegetated cases, but with muted variability.

At the light of these results we conclude that it should be a priori possible to determine the type of continental surface on a rocky Earth-like planet based on color photometry and given a high enough signal-to-noise ratio. A planet covered by bare desert areas will have a large diurnal variability in the J, H, and K bands. While this is also the case for vegetated continents, in this case an additional bump in the I band is to be expected, which would be missing in a desert planet. Furthermore, the hypothesis of deserted continents could be further tested/confirmed by observations in the mid-IR photometric bands (Gómez-Leal et al. 2012).

In the case of a planet with extended microbial mats, its nature would be determined by the detection of the presence of continents by using the light curves in B and V bands, and then finding a lower than expected percentage variability in the J, H, and K bands, with the reflection peak characteristics of plants and deserts missing.

Although not shown in this work, we also studied the same scenarios but with cloud-free atmospheres. As expected, we find that the omission of clouds decreases the amount of reflected light in comparison to the respective non-clear sky condition. Nevertheless, daily variations in the disk-integrated spectra become more dramatic in the cloud-free case than in the cloudy one. These cases, however, are highly unrealistic.

4. CONCLUSIONS

In this paper we have used a radiative transfer code to simulate the globally integrated spectral variability of the Earth 500 Ma ago, using four possible scenarios regarding the continental surface properties. Our simulations also include realistic distributions of clouds over the whole planet at three altitude layers. We find that as the continental surface changes from desert ground to microbial mats and to land plants, it produces detectable changes in the globally averaged Earth's reflectance that vary substantially as the Earth rotates. By binning the data into standard astronomical photometric band we see that the variability of each surface type is located in different bands and can induce reflectance changes of up to 40% in periods of hours. We conclude that using photometric observations of an Earth-like planet at different photometric bands, it would be possible to discriminate between bare continental surfaces, large microbial mats extensions, or plant-covered continents. While in the recent literature the red-edge feature of vegetation at visible wavelengths has been proposed as a signature for land plants, observations in near-IR bands can be equally suited for this purpose.

The authors thankfully acknowledge the technical expertise and assistance provided by the Spanish Supercomputing Network (Red Española de Supercomputación), as well as the

computer resources used: the La Palma Supercomputer, located at the Instituto de Astrofísica de Canarias. The authors also acknowledge support from the Spanish MICIIN, grant CGL2009-10641 and AYA2010-18080.

REFERENCES

Arnold, L., Gillet, S., Lardière, O., Riaud, P., & Schneider, J. 2002, A&A, 392, 231
Borucki, W. J., Koch, D. G., Batalha, N., et al. 2012, ApJ, 745, 120
Cassan, A., Kubas, D., Beaulieu, J.-P., et al. 2012, Natur, 481, 167
Charbonneau, D., Berta, Z. K., Irwin, J., et al. 2009, Natur, 462, 891
Cockell, C. S., Kaltenegger, L., & Raven, J. A. 2009, AsBio, 9, 623
Cowan, N. B., Agol, E., Meadows, V. S., et al. 2009, ApJ, 700, 915
Cowan, N. B., Robinson, T., Livengood, T. A., et al. 2011, ApJ, 731, 76
Fressin, F., Torres, G., Rowe, J. F., et al. 2012, Natur, 482, 195
Fujii, Y., & Kawahara, H. 2012, ApJ, 755, 101
Fujii, Y., Kawahara, H., Suto, Y., et al. 2011, ApJ, 738, 184
Gallery, W. O., Kneizys, F. X., & Clough, S. A. 1983, Air Mass Computer Program for Atmospheric Transmittance/Radiance Calculations: FSCATM, Environmental Research Paper ERP-828/AFGL-TR-83-0065
García Muñoz, A., & Pallé, E. 2011, JQSRT, 112, 1609
García Muñoz, A., Zapatero Osorio, M. R., Barrena, R., et al. 2012, ApJ, 755, 103
Gómez-Leal, I., Pallé, E., & Selsis, F. 2012, ApJ, 752, 28
Goode, P. R., Qiu, J., Yurchyshyn, V., et al. 2001, GeoRL, 28, 1671
Gray, J., Chaloner, W., & Westoll, T. 1985, RSPTB, 309, 167
Hamdani, S., Arnold, L., Foellmi, C., et al. 2006, A&A, 460, 617
Hart, M. H. 1978, Icar, 33, 23
Hegde, S., & Kaltenegger, L. 2013, AsBio, 13, 47
Hess, M., Koepke, P., & Schult, I. 1998, BAMS, 79, 831
Kaltenegger, L., Traub, W. A., & Jucks, K. W. 2007, ApJ, 658, 598
Kasting, J. F., & Siefert, J. L. 2002, Sci, 296, 1066
Kawahara, H., & Fujii, Y. 2010, ApJ, 720, 1333
Kawahara, H., & Fujii, Y. 2011, ApJL, 739, L62
Kiang, N. Y., Segura, A., Tinetti, G., et al. 2007a, AsBio, 7, 252
Kiang, N. Y., Siefert, J., Govindjee, & Blankenship, R. E. 2007b, AsBio, 7, 222
Montañés-Rodríguez, P., Pallé, E., Goode, P. R., & Martín-Torres, F. J. 2006, ApJ, 651, 544
Muirhead, P. S., Johnson, J. A., Apps, K., et al. 2012, ApJ, 747, 144
Oakley, P. H. H., & Cash, W. 2009, ApJ, 700, 1428
Pallé, E., Ford, E. B., Seager, S., Montañés-Rodríguez, P., & Vazquez, M. 2008, ApJ, 676, 1319
Pallé, E., Goode, P. R., Montañés-Rodríguez, P., & Koonin, S. E. 2004, Sci, 304, 1299
Pallé, E., Goode, P. R., Yurchyshyn, V., et al. 2003, JGRD, 108, 4710
Pepe, F., Lovis, C., Ségransan, D., et al. 2011, A&A, 534, A58
Qiu, J., Goode, P. R., Pallé, E., et al. 2003, JGRD, 108, 4709
Robinson, T. D., Meadows, V. S., Crisp, D., et al. 2011, AsBio, 11, 393
Rossow, W. B., Walker, A. W., Beuschel, D. E., & Roiter, M. D. 1996, World Climate Research Programme Report WMO/TD 737 (Geneva: World Meteorological Organization)
Rothman, L. S., Gordon, I. E., Barbe, A., et al. 2009, JQSRT, 110, 533
Sanromá, E., & Pallé, E. 2012, ApJ, 744, 188
Seager, S., Turner, E. L., Schafer, J., & Ford, E. B. 2005, AsBio, 5, 372
Seckbach, J., & Oren, A. 2010, Microbial Mats: Modern and Ancient Microorganisms in Stratified Systems (Dordrecht: Springer)
Stammnes, K., Tsay, S. C., Wiscombre, W., & Jayaweera, K. 1988, ApOpt, 27, 2502
Sterzik, M. F., Bagnulo, S., & Palle, E. 2012, Natur, 483, 64
Tinetti, G., Meadows, V. S., Crisp, D., et al. 2006a, AsBio, 6, 34
Tinetti, G., Meadows, V. S., Crisp, D., et al. 2006b, AsBio, 6, 881
Tinetti, G., Rashby, S., & Yung, Y. L. 2006c, ApJL, 644, L129
Turnbull, M. C., Traub, W. A., Jucks, K. W., et al. 2006, ApJ, 644, 551
Udry, S., Fischer, D., & Queloz, D. 2007, in Protostars and Planets V, ed. B. Reipurth, D. Jewitt, & K. Keil (Tucson, AZ: Univ. Arizona Press), 685
Woolf, N. J., Smith, P. S., Traub, W. A., & Jucks, K. W. 2002, ApJ, 574, 430

6

Characterizing the Purple Earth

In the last part of this thesis we extended the work presented in the previous chapter by exploring the effect of considering a different atmospheric composition. As our planet seems to have been inhabited for at least ∼85% of its history, here instead of using the present-day atmosphere of Earth for the simulations of the globally-averaged views of our planet, as a study case, we focus on the Earth 3.0 Ga ago. At that time, oxygen was negligible in the atmosphere and CO_2 and CH_4 were much more abundant. This particular period in history is also interesting due to the presence of purple bacteria as the dominant form of life over the Earth's surface.

Thus, here we also studied the possibility of detecting primitive life forms, such as purple bacteria, on the disk-integrated spectra of Earth, taking into account different levels of cloud cover, continental distributions, and different scenarios where purple bacteria could be found. These type of bacteria are photosynthetic microorganisms that convert sunlight into chemical energy through anoxygenic photosynthesis and are among the first forms of life on Earth, they are thought to have appeared 3.8 Ga ago. To conduct this study we had to take measurements of the reflectance spectrum of such bacteria in the laboratory. To do that, we used cultures of *Rhodobacter* non-sulfur bacteria grown as a suspension of cells in a liquid media.

This part of the thesis was originally published in the paper entitled "Characterizing the purple Earth: Modelling the globally-integrated spectral variability of the Archean Earth" in the January 2014 edition of the Astrophysical Journal (Sanromá et al. 2014).

This part of the thesis will be published in the paper entitled "Characterizing the purple Earth: Modelling the globally-integrated spectral variability of the Archean Earth" in the Astrophysical Journal (Sanromá et al., 2013, ApJ in press).

Abstract: The ongoing searches for exoplanetary systems have revealed a wealth of

planets with diverse physical properties. Planets even smaller than the Earth have already been detected, and the efforts of future missions is placed on the discovery, and perhaps characterization, of small rocky exoplanets within the habitable zone of their stars. Clearly what we know about our own planet will be our guideline for the characterization of such planets. But the Earth has been inhabited for at least 3.8 Ga, and its appearance has changed with time. Here, we have studied the Earth during the Archean eon, 3.0 Ga ago. At that time one of the more widespread life forms on the planet were purple bacteria. These bacteria are photosynthetic microorganisms and can inhabit both aquatic and terrestrial environments, with several species able to live in extreme environments. Here, we used a radiative transfer model of Earth to simulate the visible and near-IR radiation reflected by our planet, taking into account several scenarios regarding the possible distribution of purple bacteria over continents and oceans. We find that purple bacteria have a reflectance spectrum which has a strong reflectivity increase, similar to the red-edge of leafy plants, although shifted redwards. This feature produces a detectable signal in the disk-averaged spectra of our planet, depending on cloud amount and on purple bacteria concentration/distribution. We concluded that by using multi-color photometric observations, it is possible to distinguish between an Archean Earth in which purple bacteria inhabit vast extensions of the planet, and a present-day Earth with continents covered by deserts, vegetation or microbial mats.

The Astrophysical Journal, 780:52 (11pp), 2014 January 1 doi:10.1088/0004-637X/780/1/52

CHARACTERIZING THE PURPLE EARTH: MODELING THE GLOBALLY INTEGRATED SPECTRAL VARIABILITY OF THE ARCHEAN EARTH

E. Sanromá[1,2], E. Pallé[1,2], M. N. Parenteau[3,4], N. Y. Kiang[5], A. M. Gutiérrez-Navarro[6], R. López[1,2], and P. Montañés-Rodríguez[1,2]
[1] Instituto de Astrofísica de Canarias (IAC), Vía Láctea s/n E-38200, La Laguna, Spain; mesr@iac.es
[2] Departamento de Astrofísica, Universidad de La Laguna, E-38206 La Laguna, Spain
[3] NASA Ames Research Center, Exobiology Branch, Mountain View, CA 94035, USA
[4] SETI Institute, Mountain View, CA 94035, USA
[5] NASA Goddard Institute for Space Studies, New York, NY 10025, USA
[6] Department of Microbiology, Faculty of Biology, University of La Laguna, ES-38206 La Laguna, Spain
Received 2013 September 5; accepted 2013 November 4; published 2013 December 11

ABSTRACT

Ongoing searches for exoplanetary systems have revealed a wealth of planets with diverse physical properties. Planets even smaller than the Earth have already been detected and the efforts of future missions are aimed at the discovery, and perhaps characterization, of small rocky exoplanets within the habitable zone of their stars. Clearly, what we know about our planet will be our guideline for the characterization of such planets. However, the Earth has been inhabited for at least 3.8 Gyr and its appearance has changed with time. Here, we have studied the Earth during the Archean eon, 3.0 Gyr ago. At that time, one of the more widespread life forms on the planet was purple bacteria. These bacteria are photosynthetic microorganisms and can inhabit both aquatic and terrestrial environments. Here, we use a radiative transfer model to simulate the visible and near-infrared radiation reflected by our planet, taking into account several scenarios regarding the possible distribution of purple bacteria over continents and oceans. We find that purple bacteria have a reflectance spectrum that has a strong reflectivity increase, similar to the red edge of leafy plants, although shifted redward. This feature produces a detectable signal in the disk-averaged spectra of our planet, depending on cloud amount and purple bacteria concentration/distribution. We conclude that by using multi-color photometric observations, it is possible to distinguish between an Archean Earth in which purple bacteria inhabit vast extensions of the planet and a present-day Earth with continents covered by deserts, vegetation, or microbial mats.

Key words: astrobiology – Earth – planets and satellites: atmospheres – planets and satellites: surfaces – radiative transfer

Online-only material: color figures

1. INTRODUCTION

Since the discovery of the first exoplanet orbiting a main sequence star in 1995 (Mayor & Queloz 1995), nearly 950 extrasolar planets have been detected and more than 2000 potential planet candidates from NASAs Kepler mission are waiting to be confirmed (Batalha et al. 2013). In the last few years, we have been able to discover several planets in the super-Earth mass range (e.g., Udry et al. 2007; Charbonneau et al. 2009; Pepe et al. 2011; Borucki et al. 2012), some of them lying within, or close to, the habitable zone of their stars (e.g., Borucki et al. 2012; Barclay et al. 2013; Anglada-Escudé et al. 2013). Even some Earth- and Moon-sized planets have been recently announced (Fressin et al. 2012; Muirhead et al. 2012; Gilliland et al. 2013; Borucki et al. 2013) and this number is expected to increase in the future. In fact, early statistics have pointed out that around 62% of the Milky Way's stars might host a super-Earth (Cassan et al. 2012), while studies from the Kepler mission indicate that about 16.5% of stars have at least one Earth-size planet with orbital periods up to 85 days (Fressin et al. 2013). To be prepared for the characterization of future discovered exoearths, first we must take a look at our own solar system and its planets.

Without a doubt, the possibility of finding life will drive the characterization of rocky exoplanets over the coming decades. Earth is the only planet where life is known to exist; observations of our planet will be a key instrument for the characterization and search for life elsewhere. However, even if we discovered a second Earth, it is very unlikely that it would present a stage of evolution similar to the present-day Earth. The Earth has been far from static since its formation about 4.5 Gyr ago. On the contrary, during this time, it has undergone multiple changes in its atmospheric composition, its temperature structure, its continental distribution, and even changes in the forms of life that inhabit it. All these changes have affected the global properties of Earth as seen from an astronomical distance. Thus, it is of interest not only to characterize the observables of the Earth as it is today, but also at different epochs (Kaltenegger et al. 2007; Sanromá & Pallé 2012).

Aiming at determining how Earth would look to a hypothetical distant observer, several studies have been carried out over the last few years. Earthshine observations have been one of the observational approaches used for this purpose, providing a tool to study the spectrum of Earth in the visible (e.g., Goode et al. 2001; Woolf et al. 2002; Qiu et al. 2003; Pallé et al. 2003, 2004), in the near-infrared (NIR; Turnbull et al. 2006; Pallé et al. 2009), and in the near-ultraviolet (Hamdani et al. 2006). Sterzik et al. (2012) studied the use of the linear polarization content of the earthshine to detect clouds and biosignatures.

Another possible approach is through analysis of Earth's observations obtained from remote-sensing platforms (e.g., Tinetti et al. 2006a; Cowan et al. 2011; Robinson et al. 2011; Fujii et al. 2013). Cowan et al. (2009) performed Principal Components Analysis in order to determine if it was possible to identify surface features such as oceans and continents from EPOXI data. They were able to reconstruct a longitudinally

averaged map of the Earth's surface. Crow et al. (2011) were able to categorize Earth among the planets of the solar system by using visible colors.

Also using EPOXI data, Kawahara & Fujii (2010, 2011) and Fujii & Kawahara (2012) proposed an inversion technique that allowed them to sketch two-dimensional planetary albedo maps from annual variations of the disk-integrated scattered light.

Some authors have attempted to detect the vegetation red edge through earthshine measurements (Arnold et al. 2002; Woolf et al. 2002; Seager et al. 2005; Montañés-Rodríguez et al. 2006; Hamdani et al. 2006) and also using simulations (Tinetti et al. 2006a, 2006b; Montañés-Rodríguez et al. 2006). The red edge is characterized by strong absorption in the visible part of the spectrum due to the presence of chlorophyll, which contrasts with a sharp increase in reflectance in the NIR due to scattering from the refractive index difference between cell walls and the surrounding media. This particular signature of vegetation has been proposed as a possible biomarker in Earth-like planets (e.g., Seager et al. 2005; Montañés-Rodríguez et al. 2006; Kiang et al. 2007a). The possibility of detecting hypothetical alien vegetation on terrestrial planets has also been studied. Tinetti et al. 2006c explored the detectability of exovegetation in a planet orbiting an M star, on which vegetation with photosynthetic pigments might show a shifted red edge signature. Kiang et al. (2007b) conjectured further about rules for pigment adaptations to other stellar types.

In this paper, we concentrate on the Archean eon (3.8–2.5 Gyr ago), particularly on the Earth at 3.0 Gyr ago when the Sun was about 80% as bright as it is today (Gough 1981; Bahcall et al. 2001) and the atmospheric composition of our planet was completely different from that of the present day. At this time, the Earth's atmosphere was likely dominated by N_2, CO_2, and water vapor (e.g., Walker 1977; Pinto et al. 1980; Kasting 1993; Kasting & Brown 1998), with little or no free oxygen. Methane might have also been present as well, helping to compensate for the reduced solar luminosity (e.g., Kiehl & Dickinson 1987; Pavlov et al. 2000; Haqq-Misra et al. 2008).

While controversial, the first evidence of life is at 3.8 Gyr in isotopically light graphite inclusions in apatite from Greenland (Mojzsis et al. 1996). Most likely, the life was non-photosynthetic, although this is still a subject of debate. The earliest photosynthetic life was probably anoxygenic bacteria like purple bacteria (Xiong et al. 2000; Olson 2006), utilizing reductants such as H_2 or H_2S instead of water. The Archean biosphere has been proposed to be a mix of anoxygenic phototrophs and chemotrophs such as sulfate-reducing bacteria, methanogens, and other anaerobes (Kharecha et al. 2005). The former perform photosynthesis requiring a band gap energy smaller than that needed to split water, such that the photosynthetically active radiation relevant for anoxygenic photosynthetic bacteria can extend into the NIR to as long as ∼1025 nm (Scheer 2003). Thus, their color is distinctly different from that of the land plants that dominate the Earth today.

Because directly imaged extrasolar planets are unlikely to be spatially resolved, we will have all the planet's information collapsed in a single point of light. Thus, disk-averaged views of Earth are one of the best ways to understand what kind of information one can expect from such type of observations of an Earth analog. In this paper, we present disk-integrated spectra of the ancient Earth, with the aim of discerning the effect that a different composition of the atmosphere and the presence of purple bacteria in different land/ocean configurations might have had in the way our planet looked from afar.

2. MODEL DESCRIPTION

For our calculations, we make use of a line-by-line radiative transfer algorithm, based on theDiscrete Ordinates Radiative Transfer Program for a Multi-Layered Plane-Parallel Medium[7] code (Stammnes et al. 1988), in order to derive disk-integrated spectra of the early Earth. This radiative transfer model (RTM) utilizes spectral albedo of different surface types, profiles of atmospheric composition and temperature, cloudiness information, and viewing and illumination angles as input data for the calculations. Only a single angle of incidence and 10 angles of reflection can be used for each model run. The RTM used here is basically an extension of the RTM for transits described in García Muñoz & Pallé (2011) and García Muñoz et al. (2012) to a viewing geometry for which the light reaching the observer has been reflected at the planet. With this RTM, we have generated a database of about 160 one-dimensional synthetic spectra that cover a wide range of illumination and viewing angles and different surface and cloud types. Each spectrum has been calculated at very high spectral resolution, with at least three points per Doppler width, although we have degraded them to a lower resolution ($R = 10,000$) for storage purposes. Once the one-dimensional spectral library was constructed, we calculated the disk-averaged irradiance of the early Earth given a particular viewing/illumination geometry and a map of surface properties, as described in Section 2 of Sanromá et al. (2013).

It is worth noting that unlike in Sanromá et al. (2013) where clouds are prescribed through a semi-empirical model, for the Archean there is a complete lack of reliable information on cloudiness behavior. Thus, we have assumed that the same cloud frequency occurs at each grid point, with this cloud amount an input parameter in our model.

2.1. Atmospheric Properties

Temperature and atmospheric composition profiles for the Archean were calculated by R. Ramirez (2013, private communication). A one-dimensional radiative-convective climate model, first developed by Kasting et al. (1984) and recently substantially updated by Kopparapu et al. (2013) and Ramirez et al. (2013), was used to calculate the atmospheric properties.

These atmospheric profiles consist of 1% CO_2 and 0.2% CH_4, according to Kaltenegger et al. (2007), where the remaining gas is N_2. For the relative humidity, a Manabe–Wetherald profile was used (Manabe & Wetherald 1967). For the calculation of these profiles, the Sun was assumed to have ∼79% of its present-day luminosity, as we aimed to simulate the Earth 3.0 Gyr ago. The temperature and mixing ratios profiles of these species are shown in Figure 1.

In our model, we divided the atmosphere into 33 uneven layers, which go from the boundary layer to 100 km in height, with a 1 km spacing between layers near the bottom of the atmosphere and a spacing of 5 km or more above 25 km in height. As the original atmospheric profiles were prescribed in layers up to 70 km, we assumed the same constant values between 70 and 100 km.

2.2. Surface Properties

To perform the disk-averaged spectra of the ancient Earth, we have considered four different planetary surfaces: water, desert, water with purple bacteria in suspension, and purple

[7] ftp://climate1.gsfc.nasa.gov

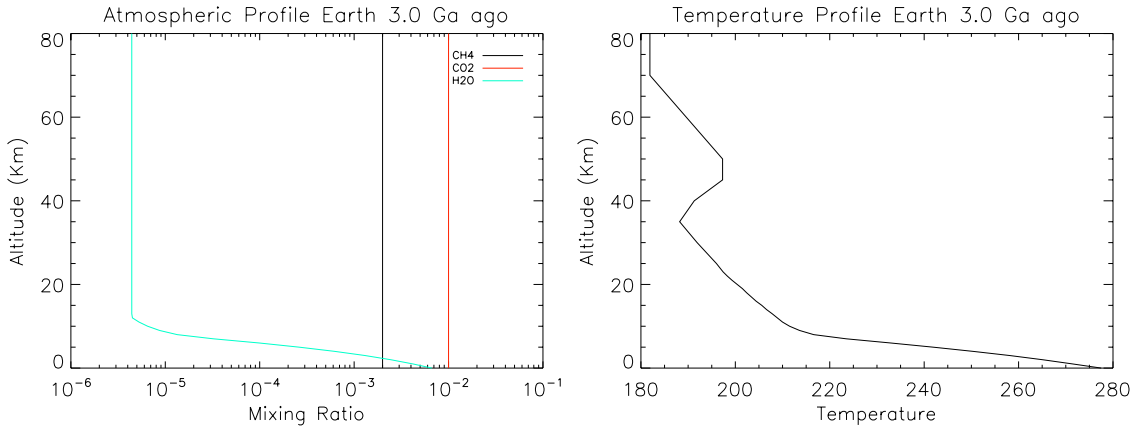

Figure 1. Atmospheric composition and temperature profiles of the Earth 3.0 Gyr ago.
(A color version of this figure is available in the online journal.)

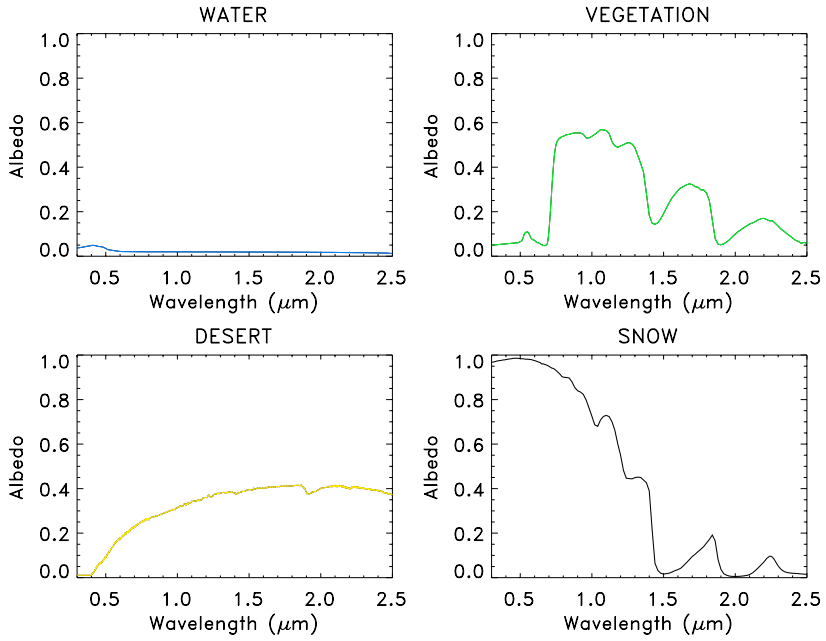

Figure 2. Spectral reflectance of water, vegetation, desert, and snow. The data are taken from the ASTER Spectral Library and the USGS Digital Spectral Library.
(A color version of this figure is available in the online journal.)

bacteria in microbial mats. There is some discussion in the literature whether purple non-sulfur bacteria could have colonized extended areas of soil and whether such a signal would be remotely detectable. Here, we have assumed that these microbial mats are located in marine intertidal environments as the most likely scenario. The wavelength-dependent surface reflectivity of the two first surface types were derived from the ASTER Spectral Library[8] and the USGS Digital Spectral Library.[9] Figure 2 shows the spectral albedo of these surface types. The wavelength-dependent albedo of surfaces involving purple bacteria were obtained as described in Section 2.4 (Figure 3).

2.3. Surface Distribution

The movement of Earth's tectonic plates has caused the formation and the break up of continents over Earth's history, including the formation of supercontinents. The orientation of Earth's earliest continents is still unknown, although it is believed that the fraction of the surface covered by continents during the Archean was smaller than at the present day (e.g., Goodwin 1981; Belousova et al. 2010; Dhuime et al. 2012). Earth might have been almost entirely covered by water with some small continents. Hence, due to the complete lack of information about the continental distribution of the Earth 3.0 Gyr ago, we decided to use that of the Earth during the Late Cambrian (500 Myr ago; see Figure 4) and at the present day as two possible characteristic examples. The continental distribution of these two epochs has been taken from Ron Blakey's Web site,[10] where these surface maps are available online. The Earth's geological information has been regridded into the 64 × 32 pixel grid used by our model.

We have also defined the coastal areas of these maps. These coastal zones were determined as those land grid cells that have adjacent ocean grid cells and those ocean cells that have adjacent land grid cells.

[8] http://speclib.jpl.nasa.gov
[9] http://speclab.cr.usgs.gov/spectral-lib.html
[10] http://jan.ucc.nau.edu

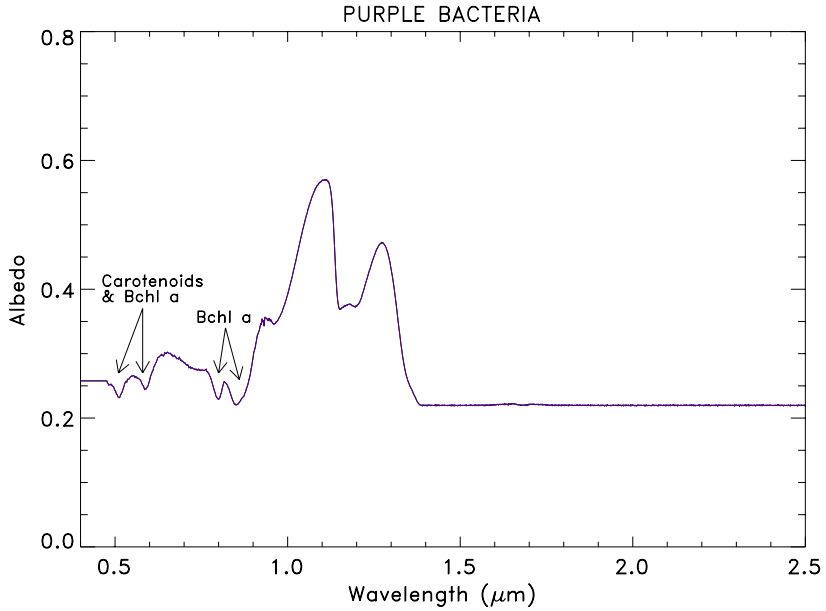

Figure 3. Wavelength-dependent albedo obtained for purple bacteria in the visible–NIR spectral range where major absorption features of carotenoids and *bacteriochlorophyll a* are labeled.

(A color version of this figure is available in the online journal.)

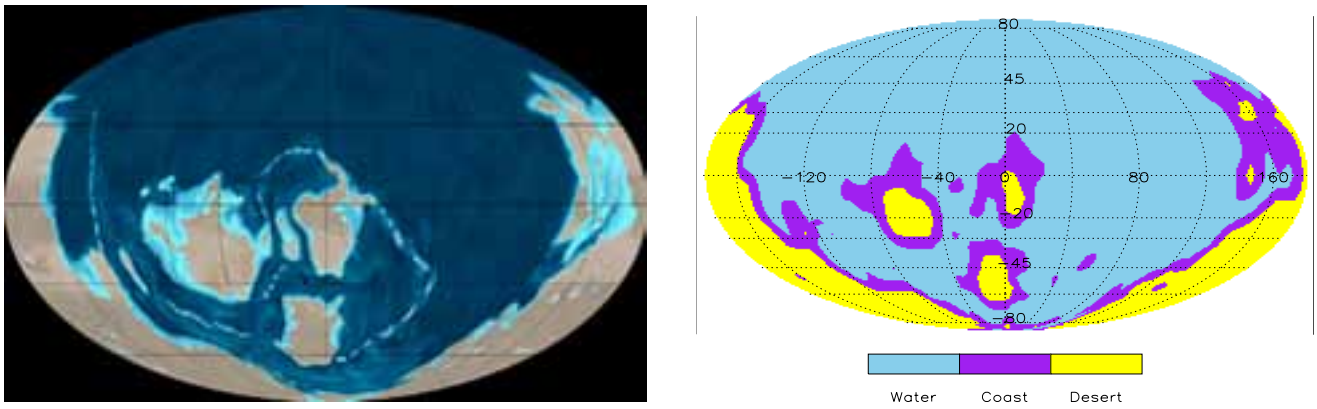

Figure 4. Left: a map of the Earth's continental distribution during the Late Cambrian (500 Myr ago). Image credit: Ron Blakey. Right: same as in left panel but here oceans, continents, and coastal zones are indicated in blue, yellow, and purple, respectively. The data are plotted with a geographical resolution of 64 × 32 grid cells (longitude by latitude), the same that our models use. Coastal areas constitute 14% of the total grid cells when using this continental distribution and geographic resolution. In our simulations, 00:00 UT corresponds to the subsolar point crossing the image center.

(A color version of this figure is available in the online journal.)

2.4. Cloud Optical Properties

For these simulations, we have taken into account three different cloud layers: low (1000–680 mb), mid (680–440 mb), and high cloud (440–30 mb). The optical properties of each cloud type, wavelength-dependent scattering and absorption coefficients, and the asymmetry parameter were taken from the Optical Properties of Aerosols and Clouds database (Hess et al. 1998). We have considered physical cloud thicknesses of 1 km and we have assumed that the scattering phase function is described by the Henyey–Greenstein equation inside clouds and by the Rayleigh scattering function outside them.

The atmospheric composition of our planet has not changed drastically in the last 500 Myr. On average, the same atmospheric composition and mean averaged temperature have existed during this period (Hart 1978; Kasting & Siefert 2002). Hence, in Sanromá et al. (2013), we used a semi-empirical model of clouds in order to reconstruct the possible cloud distribution of the Earth in the past, up to 500 Myr ago. However, this does not hold true for a longer period of time and such a cloudiness reconstruction is not a valid approximation for the Archean. Thus, we prescribe the mean cloud frequency of the Archean as an input parameter and explore how different levels of cloudiness may have affected the way our planet looked from afar, and in particular, the effect that could have had on the possible detection of biomarkers. Note that detailed cloud structures, tied to ocean currents or continents, are missing in or simulations. However, for globally integrated spectra like the ones investigated here, this limitation is minimal.

To obtain the reflectance spectra of purple bacteria, we used pure cultures of *Rhodobacter sphaeroides* ATCC 49419, a purple non-sulfur bacterium growing as a suspension of cells in liquid media. This type of phototroph exhibits diverse metabolic abilities, allowing survival in a wide range of dynamic environmental conditions. Purple non-sulfurs can grow aerobically in the dark as a chemoheterotroph and anaerobically in the light

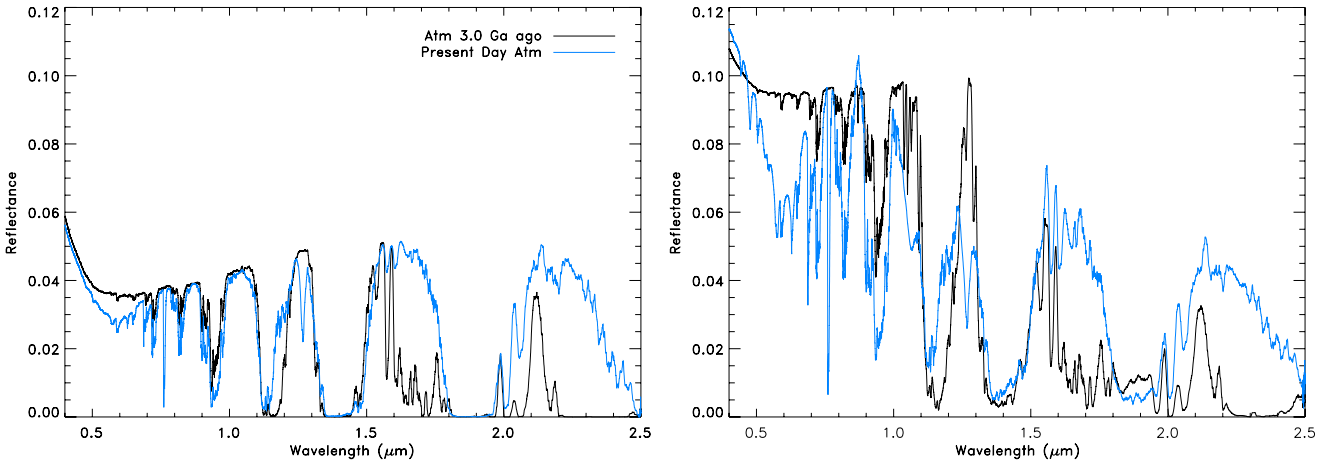

Figure 5. Visible and NIR disk-averaged spectra of a planet with a continental distribution of the Earth 500 Myr ago, with an atmospheric composition similar to that of the Earth 3.0 Gyr ago (black) and with a present-day composition (blue). Here, continents are totally deserts and we have considered both a cloud-free atmosphere (left) and a cloudy atmosphere (right). We have assumed that clouds cover 50% of the surface. The spectra have been smoothed with a 100 point running mean for display purposes.

(A color version of this figure is available in the online journal.)

using hydrogen and organic compounds as electron donors for photosynthesis.

We made two different measurements to retrieve the reflectance spectrum of these bacteria. In the first one, the reflectance of a liquid pure culture of purple bacteria was measured using an ultraviolet/visual/NIR spectrophotometer (VARIAN, CARY 5E). The measurements were taken from 0.3–2.5 μm.

In the second experiment, we used an LiCor LI1800 spectroradiometer with a remote cosine receptor that was positioned 5 cm above the culture. These measurements cover the 0.35–1.1 μm spectral range. This culture of purple bacteria was in a petri dish sitting on top of a piece of white paper. In order to calculate the spectral albedo, the spectral irradiance of the Sun was also measured.

Both sets of retrieved reflectances spectra were merged into one, covering from the visible to the NIR (Figure 3), using as a reference the second experiment, which had a higher signal-to-noise ratio (S/N). In order to absolutely calibrate the reflectance spectra of the bacteria, we also measured the reflectance spectra of a set of known leaves. The comparison of our measured leaf reflectance spectra with those tabulated in the ASTER library gave us a measure of our reflected flux, which we then applied to the reflectance spectra of the purple bacteria. This way, we transformed the ratio scale into a reflectance scale.

Figure 3 shows the reflectance spectrum of the purple non-sulfur bacterium *Rhodobacter sphaeroides*. The photosynthetic pigments of these bacteria are *bacteriochlorophyll a* esterified with phytol and carotenoids of the spirilloxanthin series. Due to the combination of these two pigments, living cells of this species show absorption features at 375, 468, 493, 520–545, 589, 802, and 860–875 nm (Imhoff 2005). Some of these features can be detected, and are marked, in Figure 3. Moreover, as the purple non-sulfur bacteria cultures used were red, the reflectance increase between ∼600–700 nm is due to the reddish light reflected back from the cultures' cells. The most noticeable feature of this spectrum is the sharp increase in reflectivity from approximately 0.9–1.1 μm and the equally strong decrease from 1.3–1.4 μm. Information about the physical nature of the absorption features at $\lambda > 1$ μm is not found in the literature. Starting at 1.4 μm and redward, the spectrum does not show any measurable features and the overall albedo value is probably that of water, made slightly more reflective due to the presence of bacteria in suspension that lower its transmissivity. The overly featureless variability is probably due to the low sensitivity of the instrument used at these wavelengths.

The bacteria concentration in our sample culture was very high ($\sim 10^9$ cells ml^{-1}), probably much more than the typical concentrations that would be found in seawater. Thus, when we modeled purple bacteria in open oceans, we used a combination of pure seawater and our bacteria (+water) spectra, weighted in varying percentages, to simulate different bacteria concentrations. Throughout the rest of the paper, we refer to the percentage dissolution (for example, a dissolution of 10% means nine parts of seawater and one part of our culture, equivalent to concentrations of the order of $\sim 10^8$ cells ml^{-1}). Note that as we used liquid cultures to measure the reflectance of purple bacteria, the effect of the transmittance of water is already included in the spectrum.

3. THE SPECTRA OF THE EARLY EARTH

In order to determine if it would be possible to discern the presence of life forms such as purple bacteria in the spectra of an extrasolar planet, we have simulated the disk-integrated spectra of the ancient Earth, taking into account different continental distributions, cloud coverage, and several abundance scenarios that extend from a planet where purple bacteria have colonized both oceans and continents to a planet where purple bacteria are only found in oceanic coastal areas in low concentrations.

In all the cases studied in this paper, both the observer and the Sun are located over the planet's equator in such a way that the observer is looking at a half-illuminated planetary disk, i.e., at a phase angle of 90°. This is the most relevant geometry for studying exoplanets, since the maximum angular separation of an extrasolar planet from its parent star along its orbit takes place at phase 90°, as defined from the observer's position.

In order to see the effect of considering different atmospheric compositions in the disk-averaged spectra of a lifeless planet, Figure 5 compares the spectrum of a planet with a CO_2–CH_4 rich atmosphere and no oxygen (black) with the spectrum of a planet with Earth's current atmospheric composition (blue). In both cases, the continental distribution is that of the Earth 500 Myr

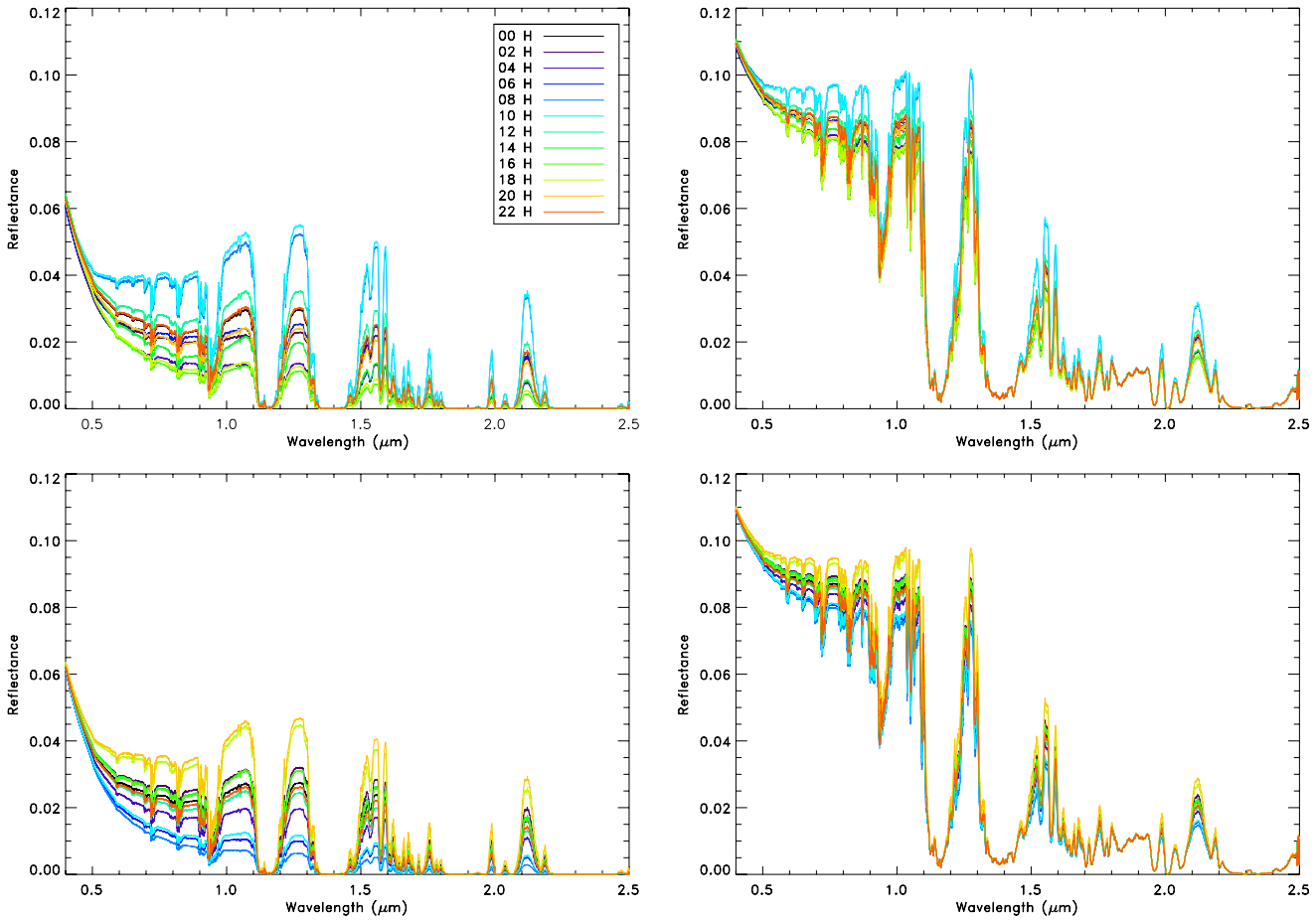

Figure 6. Visible and NIR Earth reflectance spectra 3.0 Gyr ago, taken as π times the disk-integrated radiance divided by the solar flux, over the course of a day. Continents are totally deserts and the coastal points that are closest to continent are totally populated by purple bacteria. Coastal points that are closest to oceans are a mixture of purple bacteria (10%) and water (90%). The left panels show a cloud-free atmosphere and the right panels show a cloudy atmosphere. We have assumed that clouds cover 50% of the surface and that the continental distribution corresponds to that of the Earth 500 Myr ago (top panels) and that of the present Earth (bottom panels). The spectra have been smoothed with a 100 point running mean for display purposes.

(A color version of this figure is available in the online journal.)

ago and continents are assumed to be completely covered by deserts. The black lines in Figure 5 show strong absorption in the NIR part of the spectrum due to the increased levels of CO_2 and CH_4, while in the visible region the most noticeable difference from Earth's current atmosphere is the lack of the absorption features typical of O_2 and O_3.

3.1. The Effects of Clouds

The visibility of surface inhomogeneities, such as continents or surface types, on a planet is naturally very dependent on the frequency of cloud formation. The top panels of Figure 6 shows synthetic disk-averaged spectra of the ancient Earth over a course of a day, one spectrum every two hours, covering the spectral range between 0.4–2.5 μm, for both a cloud-free (left) and a cloudy atmosphere (right). Cloud cover is assumed to be 50%. In the top panels, the continental distribution corresponds to that of Earth 500 Myr ago and continents are dry lands (deserts), while the coastal points closest to land are completely covered by purple bacteria and the coastal points closest to the ocean are a mixture of 10% purple bacteria and 90% water. We have chosen this particular scenario since bacteria are expected to be found where nutrients are more abundant, like in shallow waters or coastal zones.

It is expected that as continents come in and out of the field of view, the light reflected back by the Earth changes, with these changes being more drastic for the cloud-free cases. The reflectance is higher when continents occupy most of the observable half-disk (at 8:00–10:00 UT, when the percentage of the continental surface in the sunlit area of the planet visible from our observer's location is ∼50%) than when oceans dominate the field of view (at 16:00–18:00 UT, when the percentage of continental surface is ∼95%).

The addition of clouds to the model results in an overall enhancement of the light reflected back by the planet and a strong decrease in the reflectance variability over a diurnal cycle. This results in a significant loss of information about the surface types lying under clouds. It is worth noting that changing cloud cover or even varying cloudiness distributions can significantly change the overall shape of these disk-averaged spectra.

3.2. The Effects of Continental Distribution

The land-mass distribution of the Earth 500 Myr ago consisted of a large continental mass, mostly located in the southern hemisphere. There was also an additional group of three large islands in the southern hemisphere. On the other hand, the present-day Earth has two major continental land masses spread over the

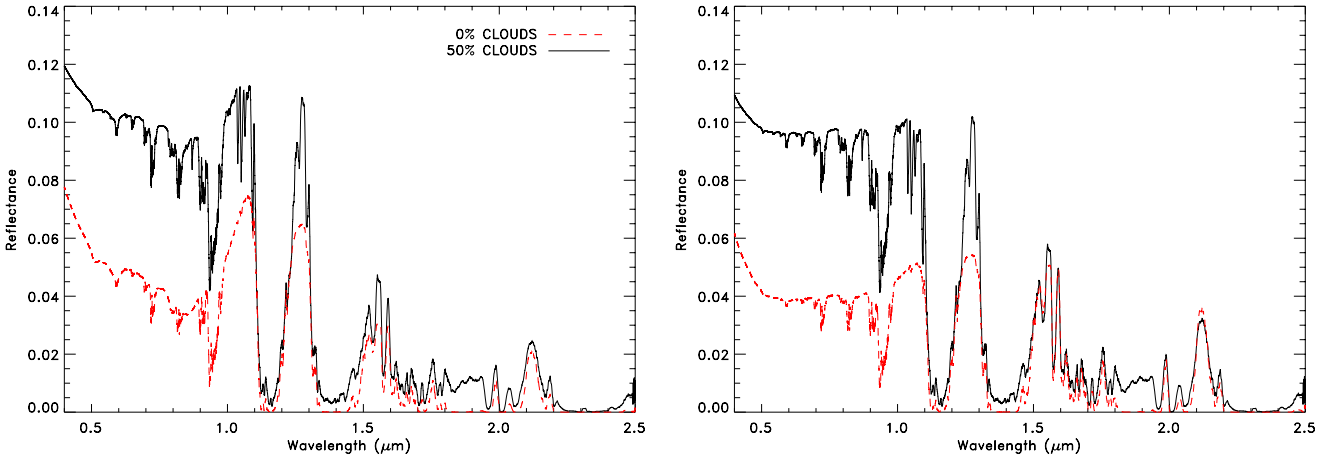

Figure 7. Visible and NIR disk-integrated spectra of the early Earth for a cloud-free atmosphere (red dashed lines) and a 50% cloudy atmosphere (black solid lines). In the left panel, continents are totally covered by mats of purple bacteria and oceans are a mixture of water and purple bacteria (90% and 10%, respectively). The same is shown in the right panel but here continents are bare deserts.

(A color version of this figure is available in the online journal.)

northern and southern hemispheres. In order to estimate the effect of considering different land-mass distributions, the bottom panels of Figure 6 show the same spectra as the top panels, but here the input continental distribution corresponds to that of the present-day Earth. Although these two continental distributions are considerably different, the disk-integrated spectra of both cases are quite similar. The rotational variability is also similar in both cases, with a comparable amplitude, only slightly smaller for the present-day Earth when clouds are considered.

3.3. Abundances and Detectability

Figure 7 (left) shows disk-integrated spectra obtained for the early Earth where continents are completely covered by purple bacterial mats and oceans are a mixture of water and bacteria, 90% and 10%, respectively. Both a cloud-free (red) and a 50% cloudy case (black) are shown. The continental distribution used here is that of the Earth 500 Myr ago.

Whether or not purple bacteria would have been able to colonize the continental surfaces during the Achean is still unknown. Due to the lack of O_2 in the early Earth's atmosphere and therefore the lack of an ozone layer, harmful radiation probably did reach the Earth's surface and purple bacteria might have suffered from DNA damage. Studies of modern microbes, however, suggest that their photoprotective pigments that absorb in the blue and ultraviolet (e.g., carotenoids) are sufficient to have allowed for their survival in terrestrial and shallow water environments on the early Earth (Cockell 1998). Moreover, some purple bacteria have been shown to use reduced iron (Fe(II)) for photosynthesis and Pierson et al. (1993) pointed out that the oxidized iron products of this type of photosynthesis could have provided substantial protection from ultraviolet radiation for surface-dwelling phototrophs prior to the development of an ozone shield. Thus, the presence of bacterial mats in continental areas, while not being our most likely scenario, cannot be ruled out.

In Figure 7 (left), we only show the spectra at the time when the continental presence is at maximum, i.e., at 08:00 UT, when the percentage of land over ocean that is illuminated and visible at the same time is about 50%. The same is shown in the right panel of this figure, but here considering that purple bacteria do not exist over continents and are only found in the oceans. For comparison, the black lines of Figure 5 show the spectra of a planet without bacteria in either the water or the land.

Table 1
Strength of the Purple Bacteria Signal as a Function of Bacterial Percentage in Oceans

Bact. in Water (%)	No Clouds	With Clouds
10	0.0295	0.0088
20	0.0400	0.0140
30	0.0505	0.0193
40	0.0610	0.0245
50	0.0715	0.0298

Notes. Slope between the intensity in the 0.745–0.770 μm and the 1.010–1.034 μm range.

When the amount of purple bacteria is high, 100% over continents and 10% diluted in the water, the presence of purple bacteria on the early Earth produces a strong feature, a steep increase in the reflectance around 1.0 μm in the disk-integrated spectrum (Figure 7, left). When clouds are included in the model, this signature is naturally significantly diluted. However, it is still easily detectable by simple inspection of the disk-average spectra.

When considering a more realistic case where purple bacteria are only found in coastal areas (Figure 6), the increase in reflectivity around 1.0 μm due to these bacteria is readily seen in the cloud-free case and is still detectable in the cloudy case.

For a planet with marine bacterial life only and bare continental surfaces, this spectral feature produced by purple bacteria becomes harder to discriminate in the spectra (Figure 7, right) and is practically undetectable in the cloudy case. Here, we have considered a mixture of 10% bacteria and 90% water. In fact, if one compares the cloudy spectrum of this case with a case where there are no bacteria, either over continents or in the water (Figure 5, black lines), it is impossible to distinguish between these cases by simple exploration of the spectra. Thus, to estimate the marine-only purple bacteria detectability, we have considered several bacteria concentrations in oceans: 20%, 30%, 40%, and 50%. Table 1 shows the slope of the straight line that connects the averaged planetary radiance in the 0.745–0.770 μm and 1.010–1.034 μm spectral intervals. The data are given as a function of the bacterial concentration in water for both a cloud-free and a cloudy atmosphere. The slope between these

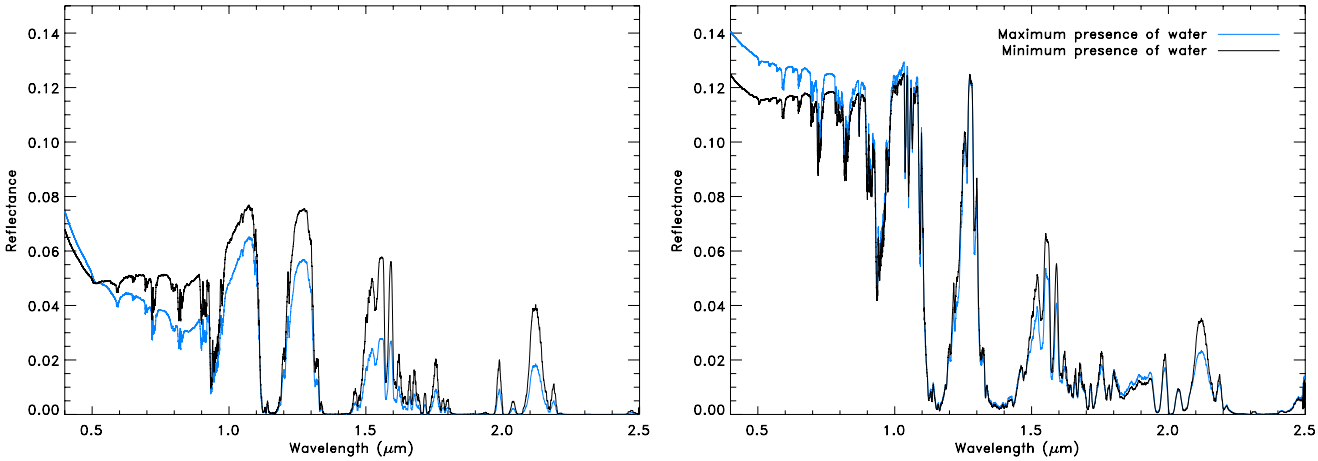

Figure 8. Disk-averaged spectra of Earth for a cloud-free (left) and a cloudy atmosphere (right). Here, the continental and cloud distribution is that of the present-day Earth and the atmospheric composition corresponds to that of the early Earth (3.0 Gyr ago). Continents are assumed to be deserts, coastal zones are completely populated with purple bacteria, and oceans are a mixture of water and purple bacteria according to the present-day chlorophyll a distribution. The blue lines represent when oceans dominate the field of view and the black lines represent when continents dominate the field of view.

(A color version of this figure is available in the online journal.)

two spectral regions, free of atmospheric absorption features, is mainly influenced by the contribution of purple bacteria to the globally integrated spectrum of the Earth. Thus, this slope can be used as a measure of the strength of the purple bacteria signal, similar to what has been previously done to quantify the red edge of vegetation (Montañés-Rodríguez et al. 2006). Table 1 shows how increasing the bacterial concentration in water from 10% to 50% monotically increases this slope. Although not shown here, the identification of the presence of purple bacteria by simple inspection of these spectra in the cloudy atmosphere case is almost impossible for bacterial concentrations in oceans lower than 30%.

Finally, although it is a very improbable scenario, we have run a comparison test to estimate the purple bacteria detectability. Figure 8 shows disk-averaged spectra of Earth considering the present-day continental and cloud distribution and the early Earth atmosphere. The cloud distribution was taken to be the 1984–2006 climatology of ISCCP[11] cloudiness data. Here, we have assumed that continents are completely deserts and we have used the 2012 annual mean ocean chlorophyll a content map from the SeaWiFS project[12] as a proxy for the distribution of purple bacteria. Thus, we have considered that the ocean latitudinal range (90°—35°, both north and south) and the -10°—10°latitudinal range are a mixture of 90% bacteria and 10% water. Coastal zones are also populated with purple bacteria and the rest of the ocean is a mixture of 10% bacteria and 90% water. The figure shows the spectra at 8:00 UT (when oceans dominate the field of view; blue lines) and at 18:00 UT (when continents dominate the field of view; black lines). As in previous cases in a cloud-free atmosphere, purple bacteria are readily detectable. For a present-day cloud amount (roughly 60%), the detectability is not so obvious and high S/N spectra of the planet would be needed.

4. PHOTOMETRIC LIGHT CURVES

In the case of a terrestrial planet in the habitable zone of a G, F, or K star, obtaining even a low-resolution spectrum in the near future might be a difficult task (e.g., Pallé et al. 2011; Rugheimer et al. 2013; Hedelt et al. 2013). Photometric observations in a few filters might actually be a more realistic possibility, even if the data are obtained via spectroscopic observations, as is the case of *Hubble Space Telescope and Spitzer Space Telescope* observations nowadays (e.g., Tinetti et al. 2007; Swain et al. 2008; Désert et al. 2011; Pont et al. 2013). The fact that a planet shows photometric variability over one rotational period already speaks about the presence of inhomogeneities on its surface or in its atmosphere (Ford et al. 2001). With a sufficiently accurate time series, it might be possible to distinguish the presence of cloudiness and continents based on this variability (Pallé et al. 2008). Moreover, the rotational photometric variability as a function of wavelength can reveal information about the major wide-spread composition of continental surfaces.

Thus, following Sanromá et al. (2013), we have convolved our modeled disk-integrated spectra with standard astronomical filters, both visible and NIR, namely *B*, *V*, *R*, *I*, *z*, *J*, *H*, and *K*. Figure 9 shows the photometric daily variations in each photometric filter of the disk-averaged reflected light, for a cloud-free atmosphere (red) and for a cloudy atmosphere (black).

For these simulations, we have used a conservative scenario: the continental distribution assumed is that of the Earth 500 Myr ago: continents are bare desert, coastal land areas are covered by purple bacteria mats, oceanic coastal areas are a mixture of 10% purple bacteria and 90% water, and open ocean areas are only water.

The light curves shown in Figure 9 all have a similar shape; the peak in brightness takes place in each of the photometric filters when continents dominate the field of view, between 8:00 and 10:00 UT, while minimum values of reflectance occur when oceans occupy most of the view, approximately at 4:00 and at 16:00 UT.

The cloud-free case shows a larger variability in the diurnal light curves in each filter and a considerable rise in brightness that increases monotically redward. A similar result is found when clouds are added to the model, although the model shows much less variability owing to the effect of clouds on the spectra.

Figure 10 (top) shows the amplitude of albedo variations of the two scenarios shown in Figure 9 as a function of the different

[11] http://isccp.giss.nasa.gov
[12] http://oceancolor.gsfc.nasa.gov/

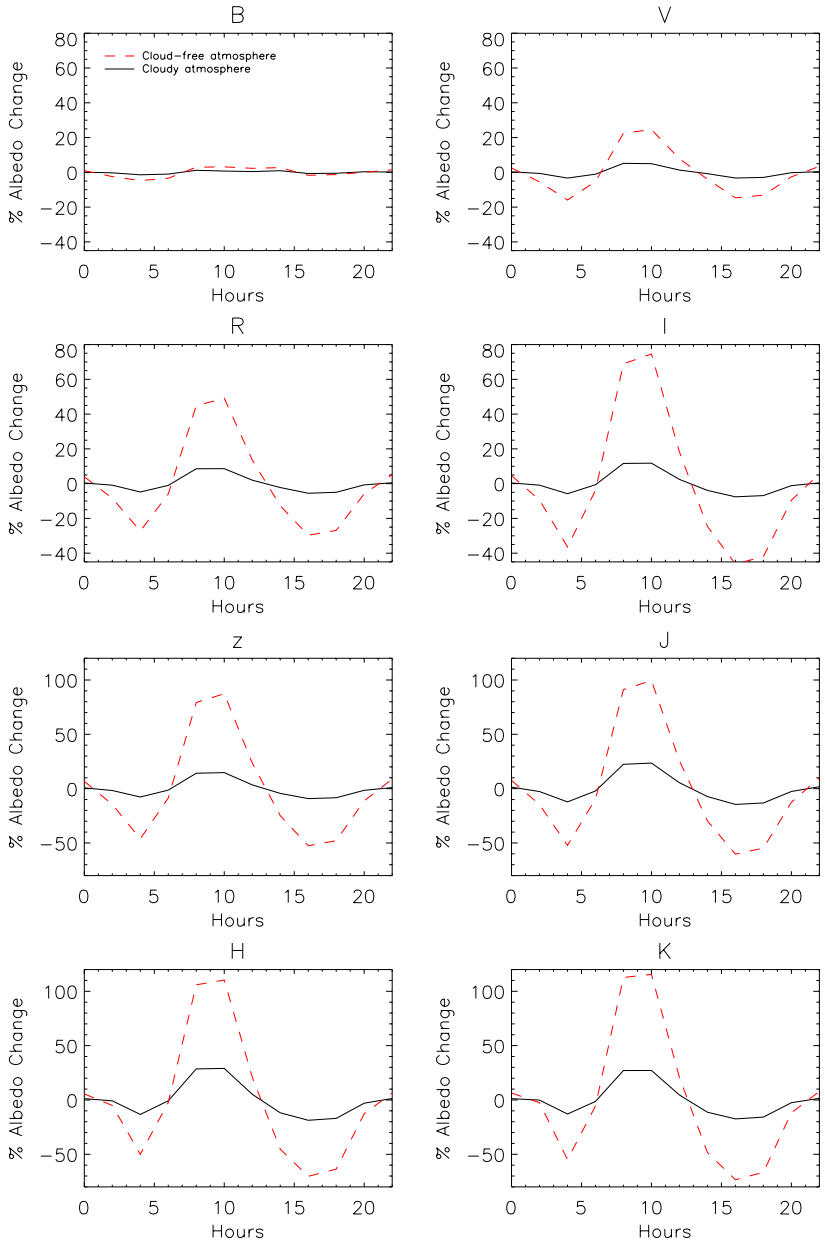

Figure 9. Daily variations of the light reflected by the early Earth for a cloud-free (red lines) and for a cloudy atmosphere (black lines). The cloud cover is assumed to be 50%. The continental distribution is that of the Earth 500 Myr ago. Continents are completely covered by deserts, coastal land areas are covered by purple bacteria mats, and oceanic coastal areas are a mixture of 10% bacteria and 90% water.

(A color version of this figure is available in the online journal.)

photometric filters. As found before, the variability of the light reflected back by the planet in both the cloud-free and cloudy cases increases toward the red, with this increase being much more dramatic in the cloud-free case than in the cloudy one. The amplitude of these variations range from a few percent to around 180% and 50% for a cloud-free and a cloudy atmosphere, respectively.

Figure 10 (bottom) shows the expected photometric variability for a modern Earth with different surface compositions (data from Sanromá et al. 2013), together with the Archean Earth results for the cloudy case (from the top panel). The different colored lines show the amplitude of the albedo variability for a cloudy atmosphere with an atmospheric composition similar to that of the present Earth, for a planet that is totally a desert (black line), for a planet completely covered by vegetation (green line), for a planet completely covered by microbial mats (red and dark blue lines), and for a planet where the continents are a mixture of microbial mats and deserts (yellow line) and microbial mats and vegetation (cyan line). In all cases, the atmospheric composition in the models used to generate the data is that of the modern Earth. The purple line shows the albedo variability of a cloudy planet with an atmospheric composition similar to that of the early Earth (3.0 Gyr ago), where continents are covered by deserts and coasts are a mixture of purple bacteria and water.

In Sanromá et al. (2013), we concluded that it would be possible to discriminate among vegetated continents, large extension of microbial mats, and bare continental surfaces by comparing the amplitude of the albedo change, along the course

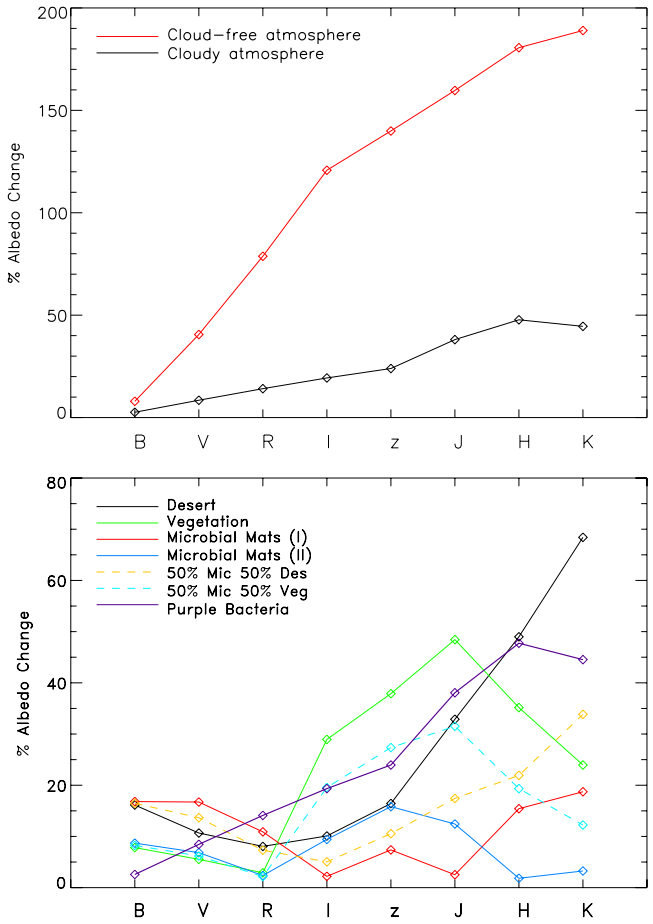

Figure 10. Top: amplitude of the albedo variability of the early Earth as a function of standard photometric filters. Continents are covered by deserts and coasts are a mixture of purple bacteria and water. Black represents a cloudy atmosphere and red represents a cloud-free atmosphere. Bottom: Figure 6 published in Sanromá et al. (2013), including the amplitude variability of the cloudy case shown in the top of this figure.

(A color version of this figure is available in the online journal.)

of a day, taken in different photometric filters. Here, the purple curve suggests that it would also be possible to discriminate between a purple Archean-like planet and the other scenarios studied in Sanromá et al. (2013). In contrast with the other scenarios, in the visible portion of the spectrum, the amplitude of the albedo change of the Archean Earth increases monotically from the *B* filter to the *z* filter, an effect due to the combination of the lack of oxygen in the atmosphere and the reflectance spectra of the purple bacteria. When one moves toward the red part of the spectrum, this increase is sharper and the curve peaks at the *H* filter to decrease redward in the *K* filter. However, if one only takes into account the NIR filters, it would be difficult to discriminate between a desert planet and the purple scenario.

5. CONCLUSIONS

In this paper, we have presented disk-integrated spectra of the Earth during the Archean eon with the aim of studying how a different atmospheric composition and the presence of early life forms, such as purple bacteria, may have affected the way our planet looked from afar.

As one of the inputs of our models is the reflectance spectrum of different surface types, we carried out two different experiments in order to retrieve the spectral albedo of these bacteria in the spectral rage 0.3–2.5 μm. We found that purple bacteria show a reflectance spectrum with a sharp increase in reflectivity similar to the red edge of leafy plants, but shifted redward.

In order to determine if it would be possible to detect such a biomarker, we have considered three different scenarios: one where purple bacteria have colonized the whole planet, both water and continents, another where purple bacteria are only found in oceans, and finally a scenario where these bacteria are found only in coastal regions. We have taken into account the effect of clouds in our models, finding that the inclusion of clouds results in an increase in the reflectivity of the planet, reduces drastically the albedo variability over the course of a day, and makes it more difficult to identify surface types under clouds. Changing the continental distribution does not seem to have a large impact on the globally averaged spectral variations.

We find that when the amount of purple bacteria is high, they can be readily detected in disk-averaged spectra, both in cloud-free and in cloudy atmosphere. On the other hand, if purple bacteria are only found in oceans, their spectral features become nearly undetectable in the cloudy case. When considering a more realistic scenario where purple bacteria are found on coasts, their presence can be detectable in the cloud-free case and even in the cloudy case, although the signal is lower.

Finally, by convolving these simulated spectra against standard astronomical filters, we conclude that using photometric observations in different filters might allow us to discriminate between a present-day Earth with continental surface covered by deserts, vegetation, or microbial mats and an Archean Earth where purple bacteria have colonized a large extent of the planet.

We thank Antígona Segura and Ramses Ramirez for kindly providing us with the atmospheric profiles of the early Earth. We thank Sebastián Hidalgo for assistance in the use of Condor. We thank the anonymous referee for the comments provided, which have improved the paper and the presentation of the results. We also thankfully acknowledge the technical expertise and assistance provided by the Spanish Supercomputing Network (Red Española de Supercomputación), as well as the computer resources used: the La Palma Supercomputer, located at the Instituto de Astrofísica de Canarias. This research was supported in part by the Spanish MICIIN grant CGL2009-10641, and MINECO grant AYA2012-39612-C03-02.

REFERENCES

Anglada-Escudé, G., Tuomi, M., Gerlach, E., et al. 2013, A&A, 556, A126
Arnold, L., Gillet, S., Lardière, O., Riaud, P., & Schneider, J. 2002, A&A, 392, 231
Bahcall, J. N., Pinsonneault, M. H., & Basu, S. 2001, ApJ, 555, 990
Barclay, T., Burke, C. J., Howell, S. B., et al. 2013, ApJ, 768, 101
Batalha, N. M., Rowe, J. F., Bryson, S. T., et al. 2013, ApJS, 204, 24
Belousova, E. A., Kostitsyn, Y. A., Griffin, W. L., et al. 2010, Litho, 119, 457
Borucki, W. J., Agol, E., Fressin, F., et al. 2013, Sci, 340, 587
Borucki, W. J., Koch, D. G., Batalha, N., et al. 2012, ApJ, 745, 120
Cassan, A., Kubas, D., Beaulieu, J.-P., et al. 2012, Natur, 481, 167
Charbonneau, D., Berta, Z. K., Irwin, J., et al. 2009, Natur, 462, 891
Cockell, C. S. 1998, J. Theor. Biol., 193, 717
Cowan, N. B., Agol, E., Meadows, V. S., et al. 2009, ApJ, 700, 915
Cowan, N. B., Robinson, T., Livengood, T. A., et al. 2011, ApJ, 731, 76
Crow, C. A., McFadden, L. A., Robinson, T., et al. 2011, ApJ, 729, 130
Désert, J.-M., Bean, J., Miller-Ricci Kempton, E., et al. 2011, ApJL, 731, L40
Dhuime, B., Hawkesworth, C. J., Cawood, P. A., & Storey, C. D. 2012, Sci, 335, 1334
Ford, E. B., Seager, S., & Turner, E. L. 2001, Natur, 412, 885
Fressin, F., Torres, G., Charbonneau, D., et al. 2013, ApJ, 766, 81

Fressin, F., Torres, G., Rowe, J. F., et al. 2012, Natur, 482, 195
Fujii, Y., & Kawahara, H. 2012, ApJ, 755, 101
Fujii, Y., Turner, E. L., & Suto, Y. 2013, ApJ, 765, 76
García Muñoz, A., & Pallé, E. 2011, JQSRT, 112, 1609
García Muñoz, A., Zapatero Osorio, M. R., Barrena, R., et al. 2012, ApJ, 755, 103
Gilliland, R. L., Marcy, G. W., Rowe, J. F., et al. 2013, ApJ, 766, 40
Goode, P. R., Qiu, J., Yurchyshyn, V., et al. 2001, GeoRL, 28, 1671
Goodwin, A. M. 1981, Sci, 213, 55
Gough, D. O. 1981, SoPh, 74, 21
Hamdani, S., Arnold, L., Foellmi, C., et al. 2006, A&A, 460, 617
Haqq-Misra, J. D., Domagal-Goldman, S. D., Kasting, P. J., & Kasting, J. F. 2008, Asbio, 8, 1127
Hart, M. H. 1978, Icar, 33, 23
Hedelt, P., von Paris, P., Godolt, M., et al. 2013, A&A, 553, A9
Hess, M., Koepke, P., & Schult, I. 1998, BAMS, 79, 831
Imhoff, J. 2005, in Bergey's Manual of Systematic Bacteriology, Vol. 2, ed. D. J. Brenner, N. R. Krieg, & J. T. Staley (2nd Ed.; New York: Springer)
Kaltenegger, L., Traub, W. A., & Jucks, K. W. 2007, ApJ, 658, 598
Kasting, J. F. 1993, Sci, 259, 920
Kasting, J. F., & Brown, L. L. 1998, in The Molecular Origin of Life (Cambridge: Cambridge Univ. Press)
Kasting, J. F., Pollack, J. B., & Ackerman, T. P. 1984, Icar, 57, 335
Kasting, J. F., & Siefert, J. L. 2002, Sci, 296, 1066
Kawahara, H., & Fujii, Y. 2010, ApJ, 720, 1333
Kawahara, H., & Fujii, Y. 2011, ApJL, 739, L62
Kharecha, P. J. K., & Siefert, J. 2005, Geobiology, 3, 53
Kiang, N. Y., Segura, A., Tinetti, G., et al. 2007a, Asbio, 7, 252
Kiang, N. Y., Siefert, J., Govindjee, & Blankenship, R. E. 2007b, Asbio, 7, 222
Kiehl, J. T., & Dickinson, R. E. 1987, JGR, 92, 2991
Kopparapu, R. K., Ramirez, R., Kasting, J. F., et al. 2013, ApJ, 765, 131
Manabe, S., & Wetherald, R. T. 1967, JAtS, 24, 241
Mayor, M., & Queloz, D. 1995, Natur, 378, 355
Mojzsis, S. J., Arrhenius, G., McKeegan, K. D., et al. 1996, Natur, 384, 55
Montañés-Rodríguez, P., Pallé, E., Goode, P. R., & Martín-Torres, F. J. 2006, ApJ, 651, 544
Muirhead, P. S., Johnson, J. A., Apps, K., et al. 2012, ApJ, 747, 144
Olson, J. 2006, Photosynth. Res., 88, 109
Pallé, E., Ford, E. B., Seager, S., Montañés-Rodríguez, P., & Vazquez, M. 2008, ApJ, 676, 1319
Pallé, E., Goode, P. R., Montañés-Rodríguez, P., & Koonin, S. E. 2004, Sci, 304, 1299
Pallé, E., Goode, P. R., Yurchyshyn, V., et al. 2003, JGRD, 108, 4710
Pallé, E., Zapatero Osorio, M. R., Barrena, R., Montañés-Rodríguez, P., & Martín, E. L. 2009, Natur, 459, 814
Pallé, E., Zapatero Osorio, M. R., & García Muñoz, A. 2011, ApJ, 728, 19
Pavlov, A. A., Kasting, J. F., Brown, L. L., Rages, K. A., & Freedman, R. 2000, JGR, 105, 11981
Pepe, F., Lovis, C., Ségransan, D., et al. 2011, A&A, 534, A58
Pierson, B. K., Mitchell, H. K., & Ruff-Roberts, A. L. 1993, OLEB, 23, 243
Pinto, J. P., Gladstone, G. R., & Yung, Y. L. 1980, Sci, 210, 183
Pont, F., Sing, D. K., Gibson, N. P., et al. 2013, MNRAS, 432, 2917
Qiu, J., Goode, P. R., Pallé, E., et al. 2003, JGRD, 108, 4709
Ramirez, R., Kopparapu, R., Zugger, M. E., et al. 2013, NatGe, in press
Robinson, T. D., Meadows, V. S., Crisp, D., et al. 2011, Asbio, 11, 393
Rugheimer, S., Kaltenegger, L., Zsom, A., Segura, A., & Sasselov, D. 2013, Asbio, 13, 251
Sanromá, E., & Pallé, E. 2012, ApJ, 744, 188
Sanromá, E., Pallé, E., & García Munõz, A. 2013, ApJ, 766, 133
Scheer, H. 2003, in Advances in Photosynthesis and Respiration, Vol. 13: Light-Harvesting Antennas in Photosynthesis, ed. B.R. Green & W.W. Parson (Dordrecht, The Netherlands: Kluwer), 29
Seager, S., Turner, E. L., Schafer, J., & Ford, E. B. 2005, Asbio, 5, 372
Stammnes, K., Tsay, S. C., Wiscombre, W., & Jayaweera, K. 1988, ApOpt, 27, 2502
Sterzik, M. F., Bagnulo, S., & Palle, E. 2012, Natur, 483, 64
Swain, M. R., Vasisht, G., & Tinetti, G. 2008, Natur, 452, 329
Tinetti, G., Meadows, V. S., Crisp, D., et al. 2006a, Asbio, 6, 34
Tinetti, G., Meadows, V. S., Crisp, D., et al. 2006b, Asbio, 6, 881
Tinetti, G., Rashby, S., & Yung, Y. L. 2006c, ApJL, 644, L129
Tinetti, G., Vidal-Madjar, A., Liang, M.-C., et al. 2007, Natur, 448, 169
Turnbull, M. C., Traub, W. A., Jucks, K. W., et al. 2006, ApJ, 644, 551
Udry, S., Bonfils, X., Delfosse, X., et al. 2007, A&A, 469, L43
Walker, J. C. G. 1977, Evolution of the Atmosphere (New York: Macmillan)
Woolf, N. J., Smith, P. S., Traub, W. A., & Jucks, K. W. 2002, ApJ, 574, 430
Xiong, J., Fischer, W., Inoue, K., Nakahara, M., & Bauer, C. 2000, Sci, 289, 1724

7

Results and Conclusions

In this thesis we have presented a comprehensive study about the Earth, the only planet known to support life, at present and over its geological evolution. Here, we have explored both the photometric and spectroscopic characteristics of our own planet as if it were seen from an astronomical distance with the aim of being prepared for the characterization of future detected Earth-like exoplanets. We have studied how different atmospheric composition, continental and cloud distribution, and the evolution of different life forms might have affected the way our planet looked from afar. In this Chapter we briefly summarize the main results and conclusions resulting from this work.

Models

- We used a simple albedo model in order to study the photometric variability of Earth at different epochs according to the different cloud and geographic distribution that Earth has shown along its history. This model calculates the visible reflected light curves of our planet for a given day, using as input data cloud and snow/ice cover maps, and surface maps. With this information the model is able to determine the Bond albedo at each time of the day and in any direction.
- A radiative transfer code was used to generate a 1-dimensional synthetic spectral library with the aim of being able to simulate the Earth's reflectance spectra for a wide range of scenarios and geometries. We produced more than 7500 synthetic spectra that cover a range of insolation and reflection angles, nine surface types, three cloud types, and seven atmospheric profiles, six of them corresponding to the composition of the present-day atmosphere and the other one corresponding to that of early Earth. These spectra cover both the VIS-NIR and the IR.
- We also developed an IDL code which calculates the disk-integrated spectrum of our planet for a given viewing geometry and resolution. This code uses as input data surface and cloudiness maps, and the spectral library discussed above.

Cloud Reconstruction

- We used satellite-based estimations of the distribution of clouds taken from the ISCCP as well as information about the surface properties and continental distribution of Earth in order to study the large-scale cloudiness behavior of our planet. By using these measurements we obtained empirical relationships between cloud cover and its location over Earth's surface depending on latitude and the underlying surface types.
- We found that our cloud model reproduces well the general features of Earth at present. Especially the differences in cloud cover between land and water at the same latitude, and the latitudinal range 40°- 75°, both North and South. However, there are some small-structures mainly over oceans that our models is not able to reproduce. These differences are due to oceanic effects, such us sea surface temperature, trade winds, ocean currents, and regional meteorological phenomena such as "El niño"/"La niña", which can influence cloud formation considerably.
- The empirical relations between cloud cover, longitude, and surface type were also used in order to reconstruct the possible cloud distribution of past epochs of Earth such as 90, 230, 340, and 500 Ma ago, when plate tectonics has changed the appearance of our planet.

Daily Light Curves

- We modeled the 24-hour Bond albedo variations of present Earth over the course of a day for both modeled and measured cloud cover, using the aforementioned albedo model. We found a good agreement between the shape of the light curve obtained from reconstructed clouds and that calculated from measured cloud cover. However, the mean value of the light curve obtained from the reconstructed cloudiness tends to be higher than the one obtained from real cloud cover. These discrepancies in the Albedo variability are owing to the fact that reconstructed cloud cover presents much less changes in the longitudinal direction than the real one, affecting the Bond albedo values.
- We also studied the 24-hour albedo variations of the past epochs of Earth: 90, 230, 340, and 500 Ma ago. The first three epochs presented similar daily variations, with a smooth enhancement in reflectivity due to the presence of continental masses. These similarities are related to the fact that these epochs have a similar ocean-land-vegetation distribution, where continents are almost totally clustered and located mainly in the Northern hemisphere. Whereas, the light curve of Earth 500 Ma ago presented more variability than that of the other epochs. This is again related to the continental distribution. In this case, continents were clustered in one hemisphere but it also had some big islands that caused strong variability in the light reflected by the planet. Moreover, this epoch showed a higher mean albedo which is due to the fact that continents were completely desert.

- We concluded that the mean albedo value of Earth has remained approximately constant along its recent history, around 0.3. However, daily variations in the past may have been larger than present day's. In particular, daily variation of Earth 500 Ma ago were three times larger than present's day. This increased variability could help in the determination of the rotational period of the planet seen from an astronomical distance. Moreover, these higher mean albedo values should have had profound influences on the global climate by introducing strong radiative effects, probably compensated by the increased greenhouse gas concentrations of past epochs.

Laboratory Measurements

- As one of the inputs of the radiative transfer model is the reflectance albedo of the different surface types, two different experiments were carried out in order to get the albedo spectrum of purple bacteria. These measurements were taken in the spectral range 0.3-2.5 μm. We found that purple bacteria have a reflectance spectrum which has a strong reflectivity increase similar to that of leafy plants, the red-edge, although shifted redwards.

Spectroscopy

- By using both the disk-integrated code and the spectral library, we simulated the VIS-NIR disk-averaged spectra of our planet at different historical epochs such as 90, 230, and 340 Ma ago, for a cloud-free atmosphere and for a cloudy one, and assuming that the atmospheric composition was the same as that of present-day Earth. We found that, in the case of considering the clear sky condition, the shape of the spectra is very similar for these three cases. However, the amplitude of the daily variations is different. The addition of clouds into the model results in the increase of the reflectivity of the planet and reduces dramatically the albedo variability over the course of a day. Hence, these differences between the albedo of different epochs are almost diluted, being very difficult to distinguish among them. We concluded that changing the continental distribution does not have a high impact in the globally-averaged spectral variations.

- The VIS-NIR globally-integrated spectral variability of Earth 500 Ma ago was also modeled. Aiming at exploring the effect that the evolution of life over land might have had on the spectra of our planet, we considered five different scenarios regarding the continental surface properties: bare continents (deserts), vegetated continents, continents covered by microbial mats, and continents covered by a mixture of microbial mats and deserts/vegetation. We also included the contribution of clouds in our simulations.

- We found that the evolution from bare surfaces, to the colonization of microbial mats over land, to the evolution of high plants over continents, produces detectable changes in the disk-integrated reflected light of Earth 500 Ma ago, that vary substantially as Earth rotates.

- We convolved the simulated spectra of Earth 500 Ma ago against standard astronomical filters. We concluded that using photometric observations of an Earth-like planet in different filters may allow us to discriminate between a planet whose continents are covered by deserts, vegetation or large extensions of microbial mats.
- The VIS-NIR spectra of Earth during the Archean (3.0 Ga ago) was also modeled. During this time the Sun was just ∼79% as bright as it is today, CO_2 and CH_4 were abundant in the atmosphere, and O_2 was negligible. We explored how a different atmospheric composition and early forms of life, such as purple bacteria, could have affected the spectra of our planet. We calculated these spectra taking into account three different scenarios: one where purple bacteria have colonized the whole planet (both continents and water), another where purple bacteria are found only in oceans, and finally a third one were purple bacteria are located over coastal regions.
- We found that the presence of purple bacteria could be detected in the disk-integrated spectra depending on how spread they are over the planet. If purple bacteria are found in oceans and over continents, its spectral feature is detectable in both cloud-free and cloudy scenarios. Whereas if purple bacteria are located only over oceans they are almost undetectable in the cloudy cases. When considering a more realistic case where purple bacteria are found only in coastal zones, purple bacteria's signature can be detected in both cloud-free and cloudy atmospheres, although the signal is smaller in the last case.
- Finally, by convolving the reflectance spectra of Earth 3.0 Ga ago against standard astronomical filters and comparing this result with that of Earth 500 Ma ago, we concluded that using photometric observations in different filters may allow us to distinguish between a present-day Earth whose continents are covered by deserts, vegetation or microbial mats, from an Archean Earth where purple bacteria have colonized the planet.

A

Annex A

In this annex we present the monthly mean cloud amount as a function of latitude for the different surface types (water, desert, ice, and vegetation) and for the four cloud types used (total cloud amount and low, mid, and high clouds). These plots have been calculated following the procedures explained in Chapter 2.

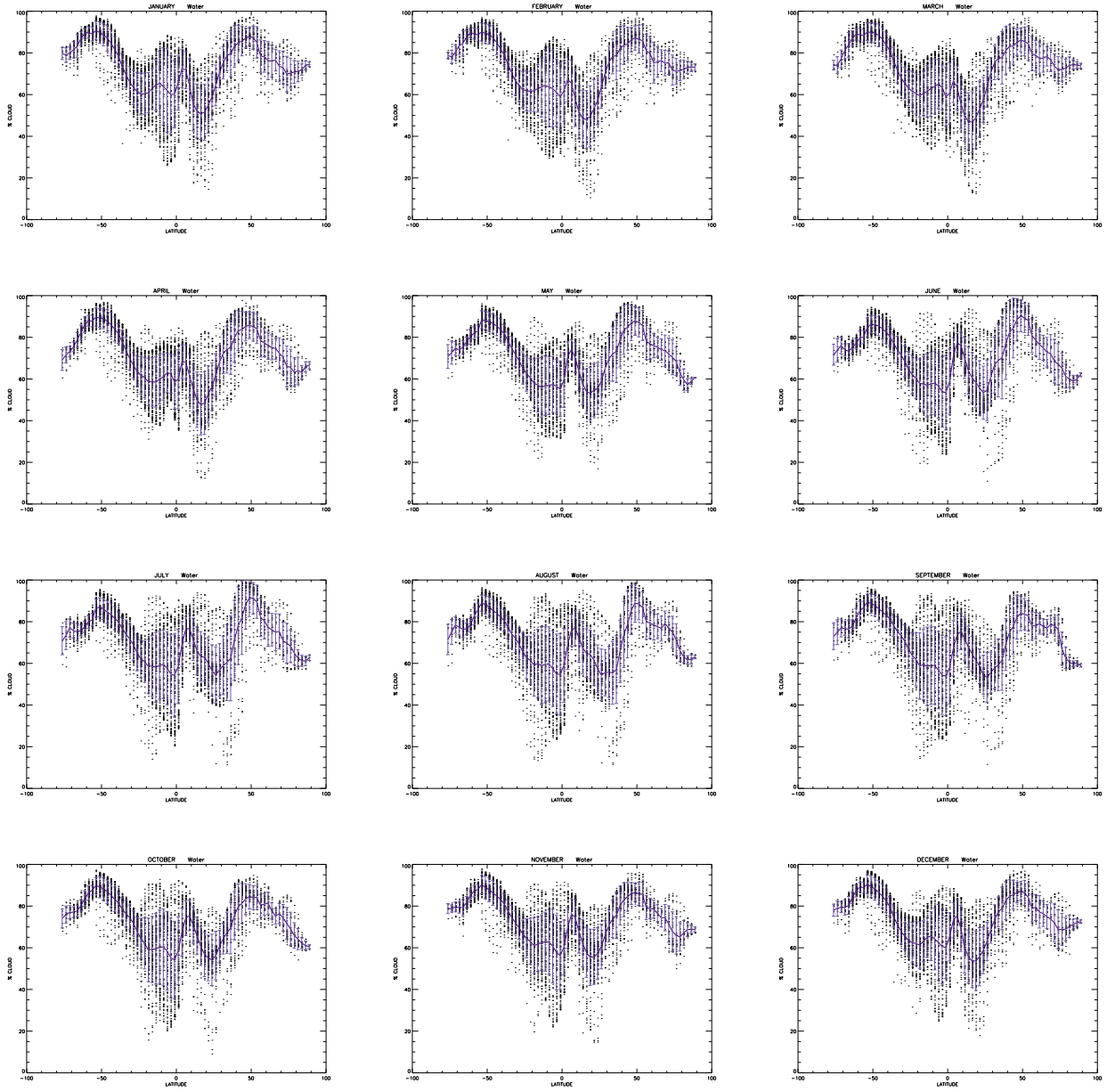

Figure A.1: Monthly mean total cloud amount (cloud fraction) as a function of latitude for clouds which are above the surface type "water". Dots correspond to the cloud amount at different longitudes along the same parallel. The solid line represents the mean cloudiness along a terrestrial parallel (zonal cloud cover) and the bars represent the standard deviation of the mean.

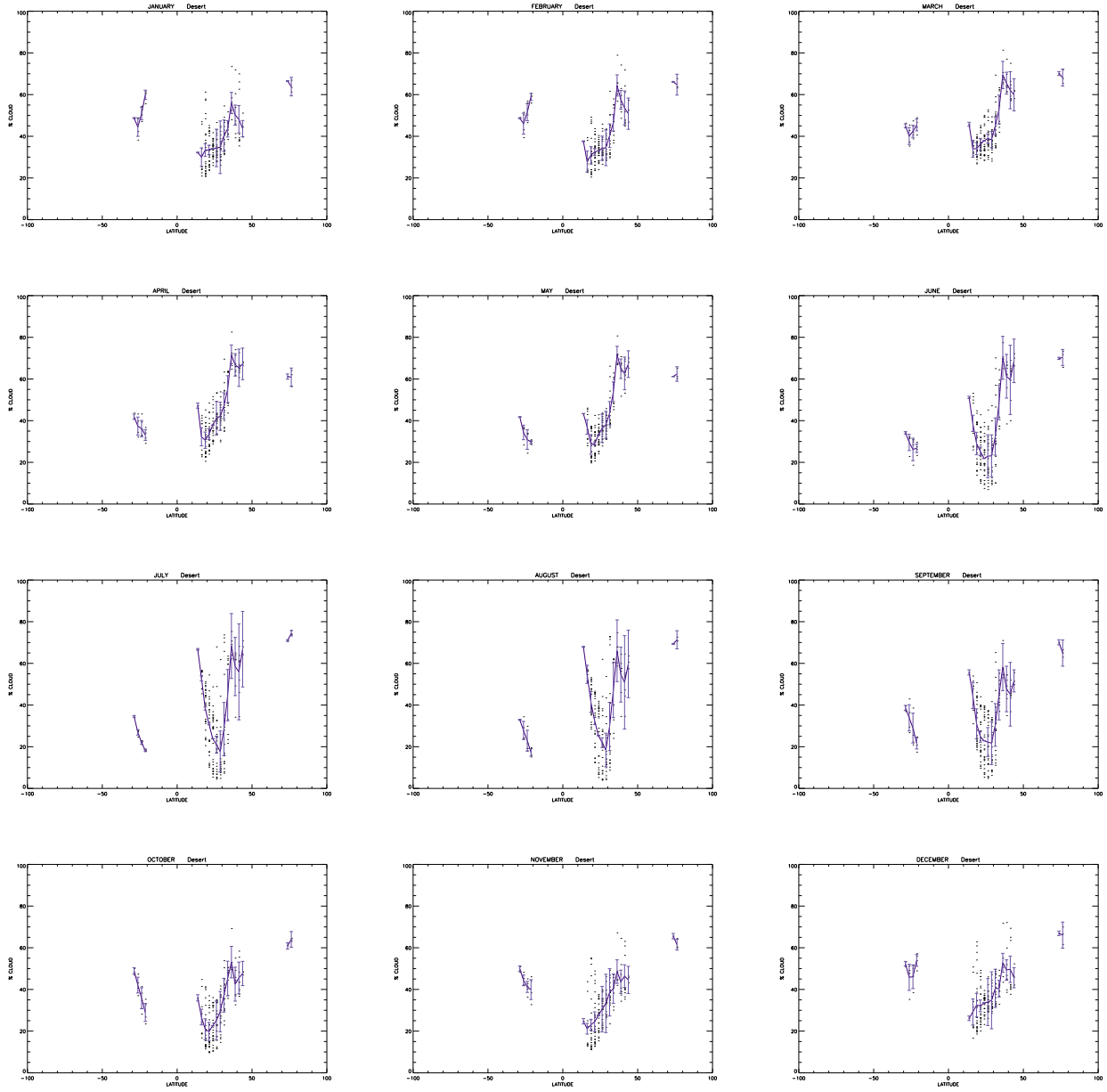

Figure A.2: Monthly mean total cloud amount (cloud fraction) as a function of latitude for clouds which are above the surface type "desert". Dots correspond to the cloud amount at different longitudes along the same parallel. The solid line represents the mean cloudiness along a terrestrial parallel (zonal cloud cover) and the bars represent the standard deviation of the mean.

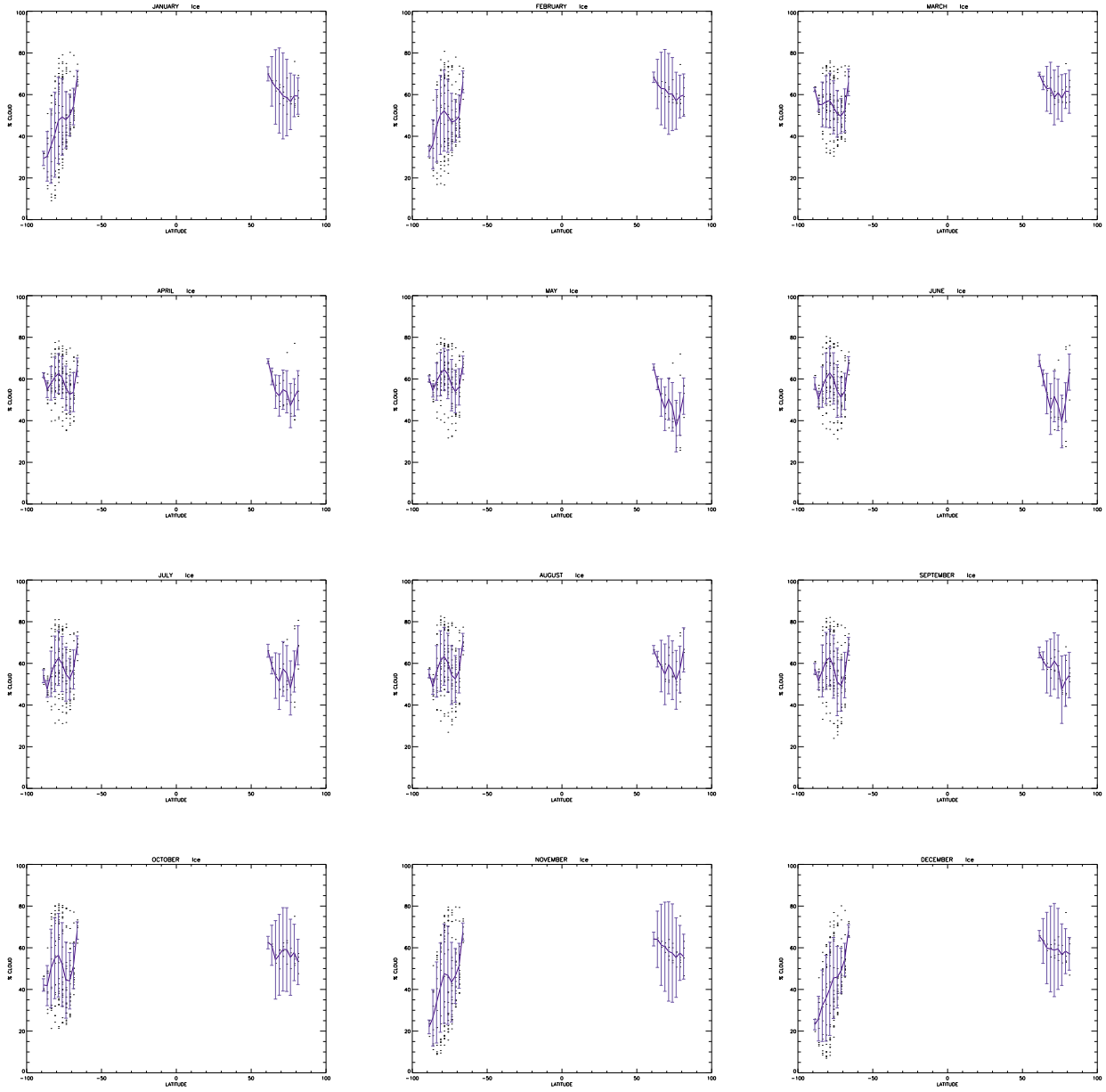

Figure A.3: Monthly mean total cloud amount (cloud fraction) as a function of latitude for clouds which are above the surface type "ice". Dots correspond to the cloud amount at different longitudes along the same parallel. The solid line represents the mean cloudiness along a terrestrial parallel (zonal cloud cover) and the bars represent the standard deviation of the mean.

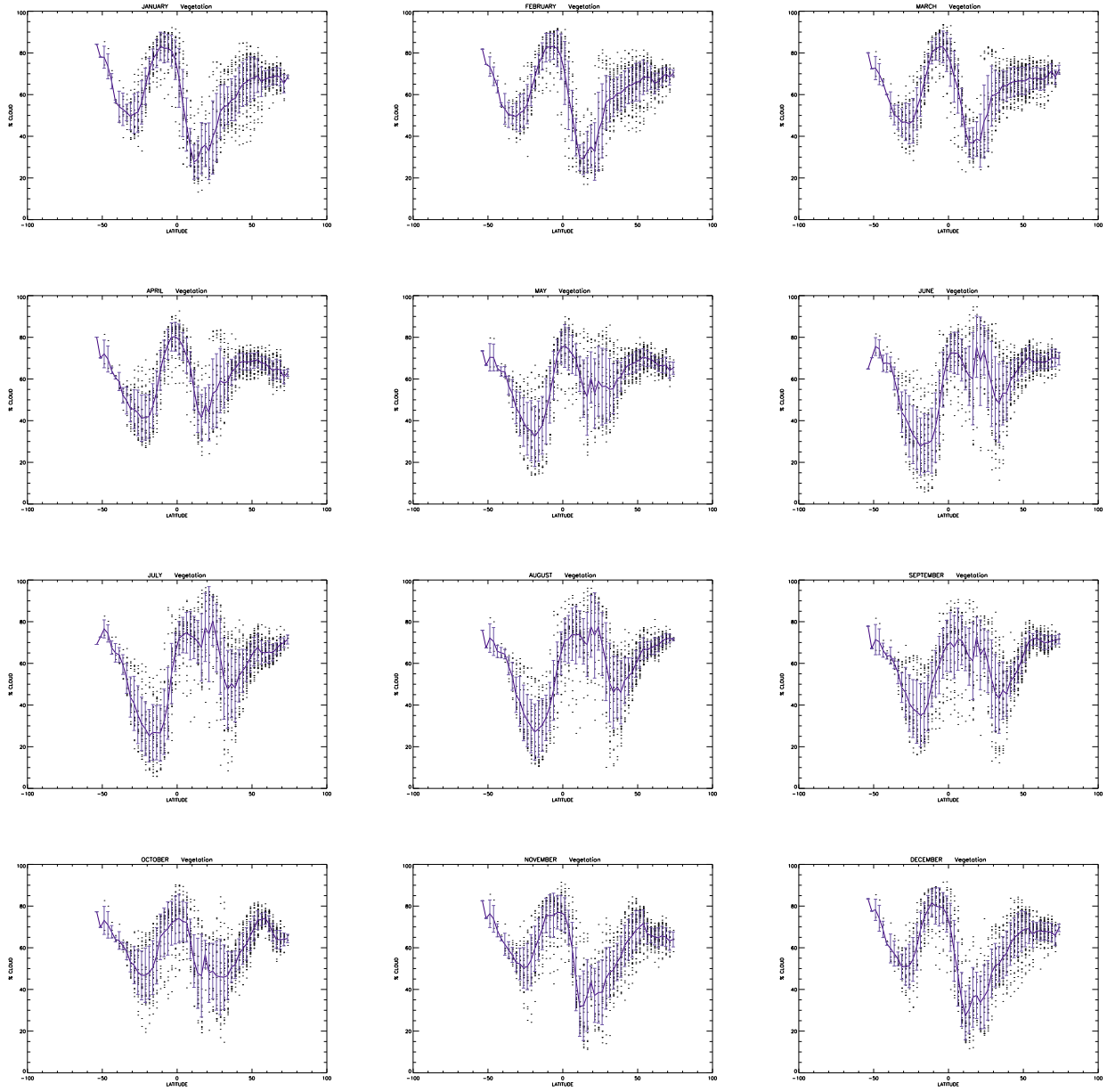

Figure A.4: Monthly mean total cloud amount (cloud fraction) as a function of latitude for clouds which are above the surface type "vegetation". Dots correspond to the cloud amount at different longitudes along the same parallel. The solid line represents the mean cloudiness along a terrestrial parallel (zonal cloud cover) and the bars represent the standard deviation of the mean.

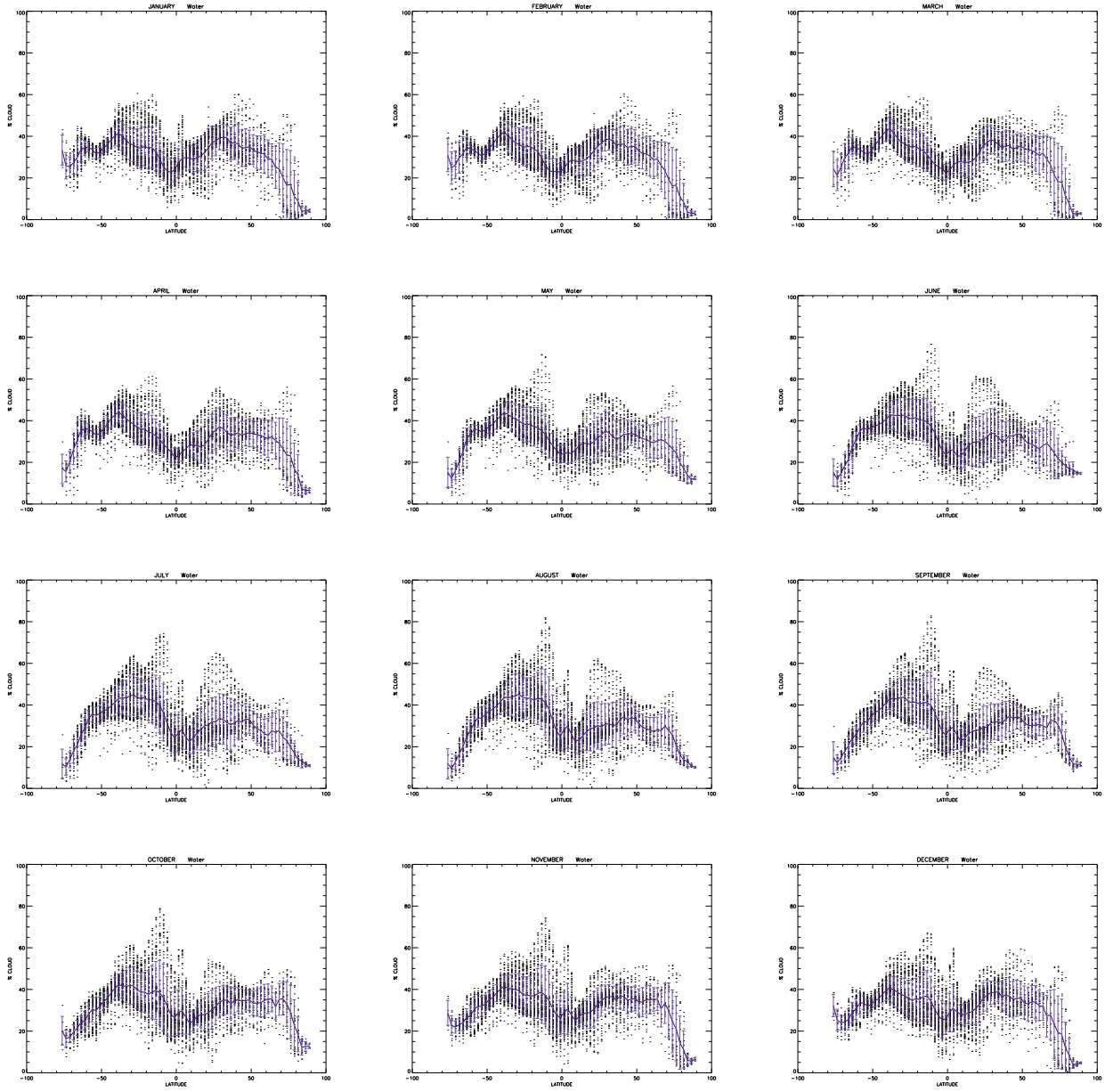

Figure A.5: The same as the figure A.1 but for low clouds.

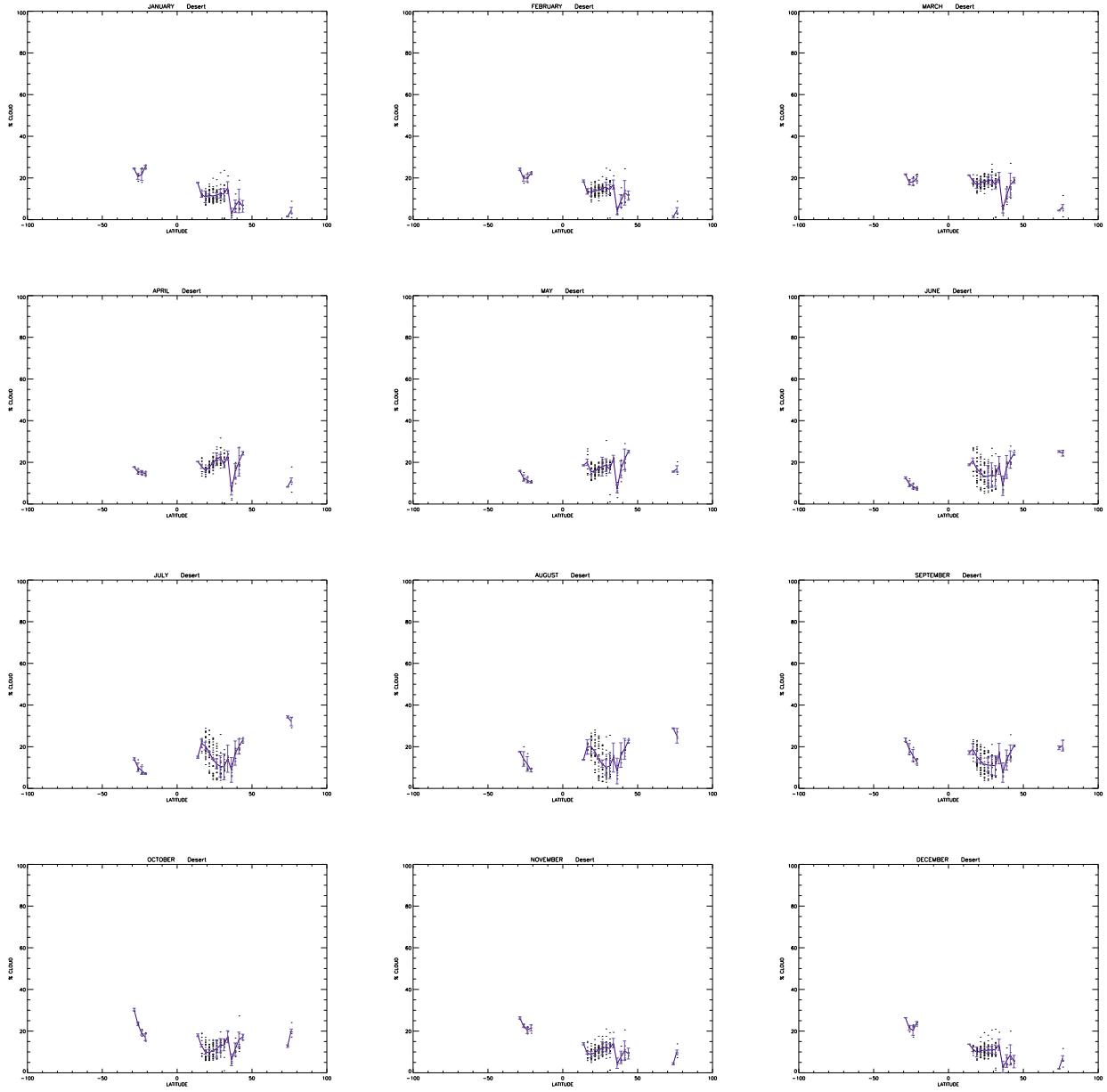

Figure A.6: The same as the figure A.2 but for low clouds.

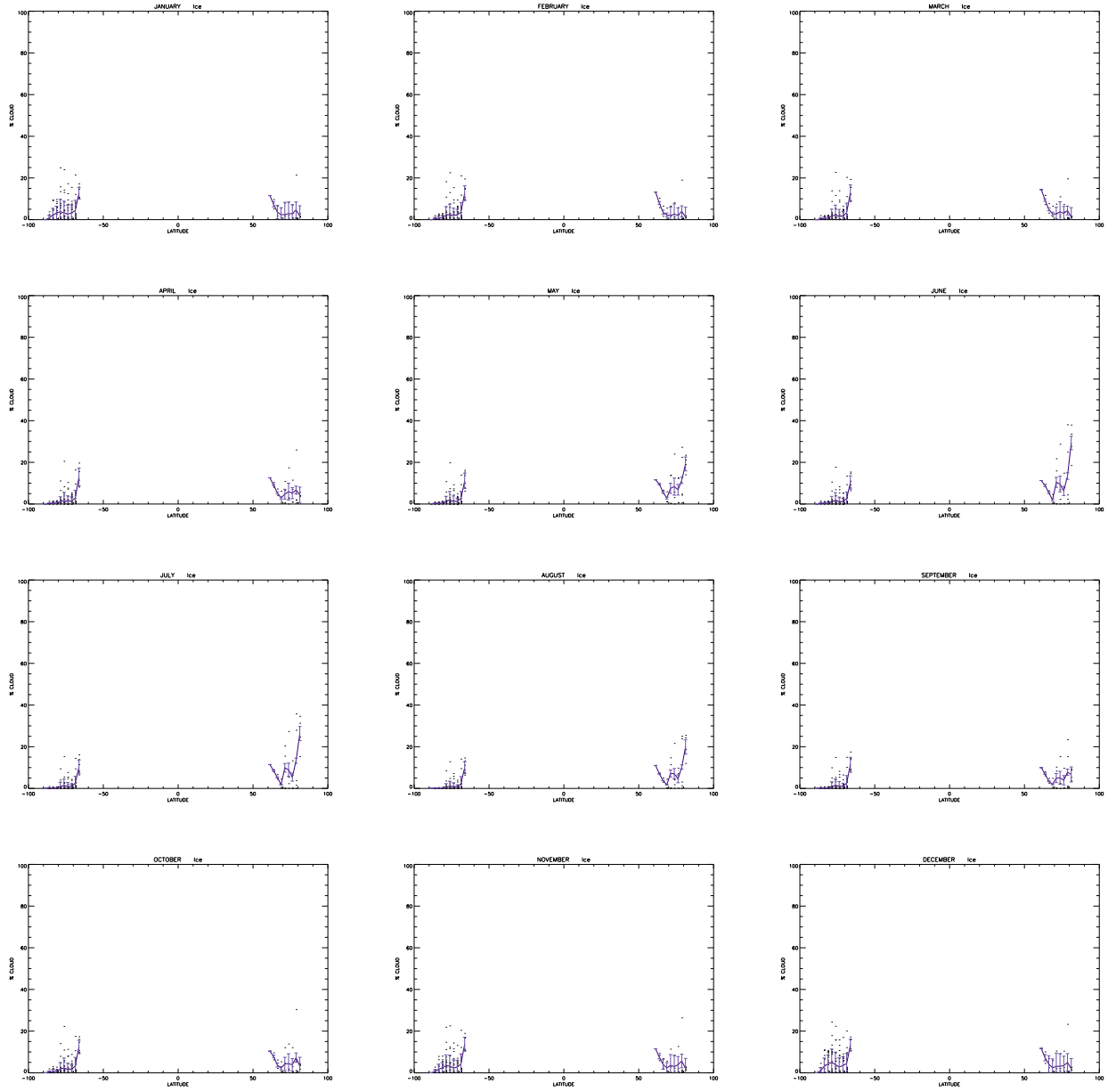

Figure A.7: The same as the figure A.3 but for low clouds.

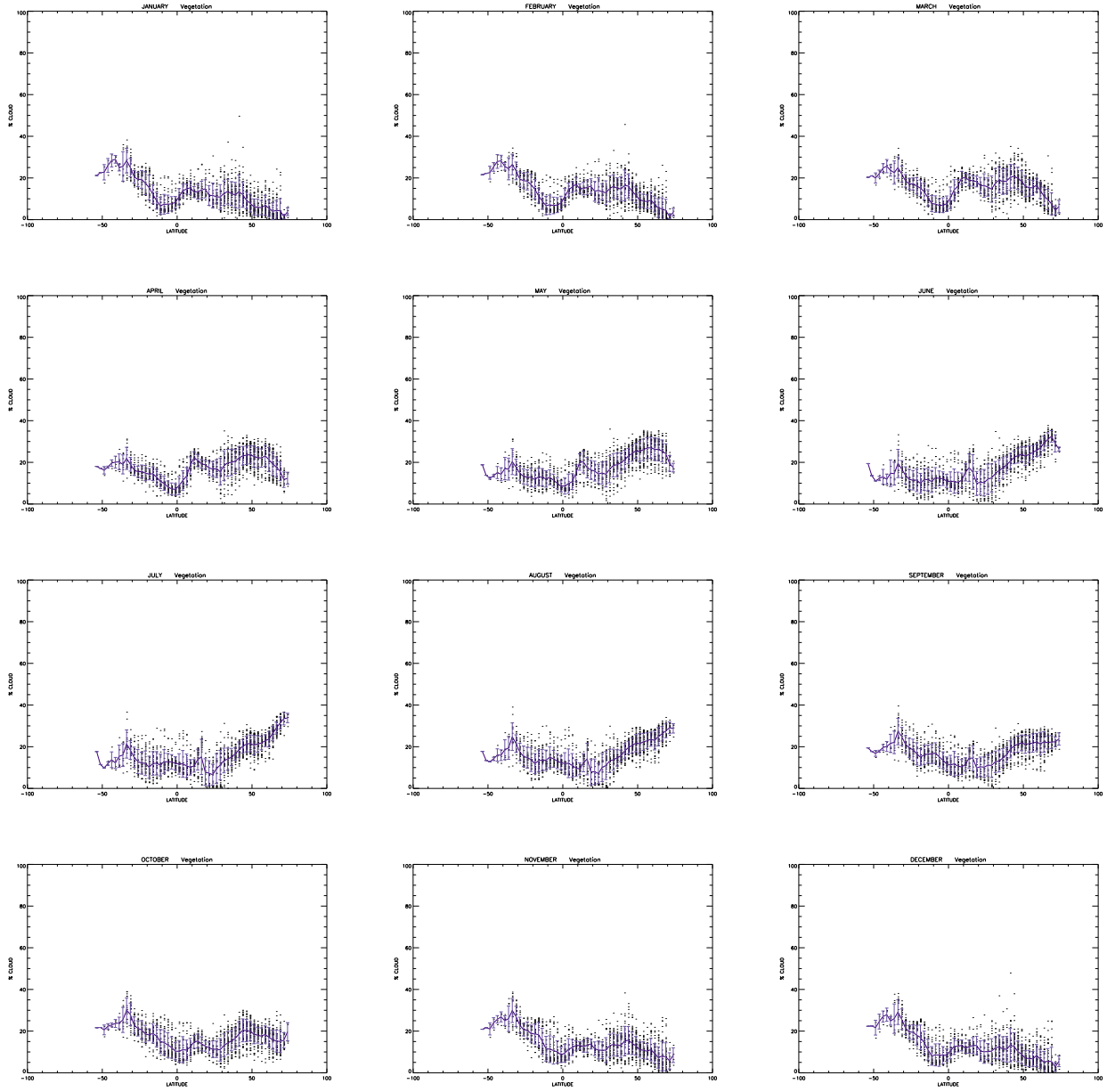

Figure A.8: The same as the figure A.4 but for low clouds.

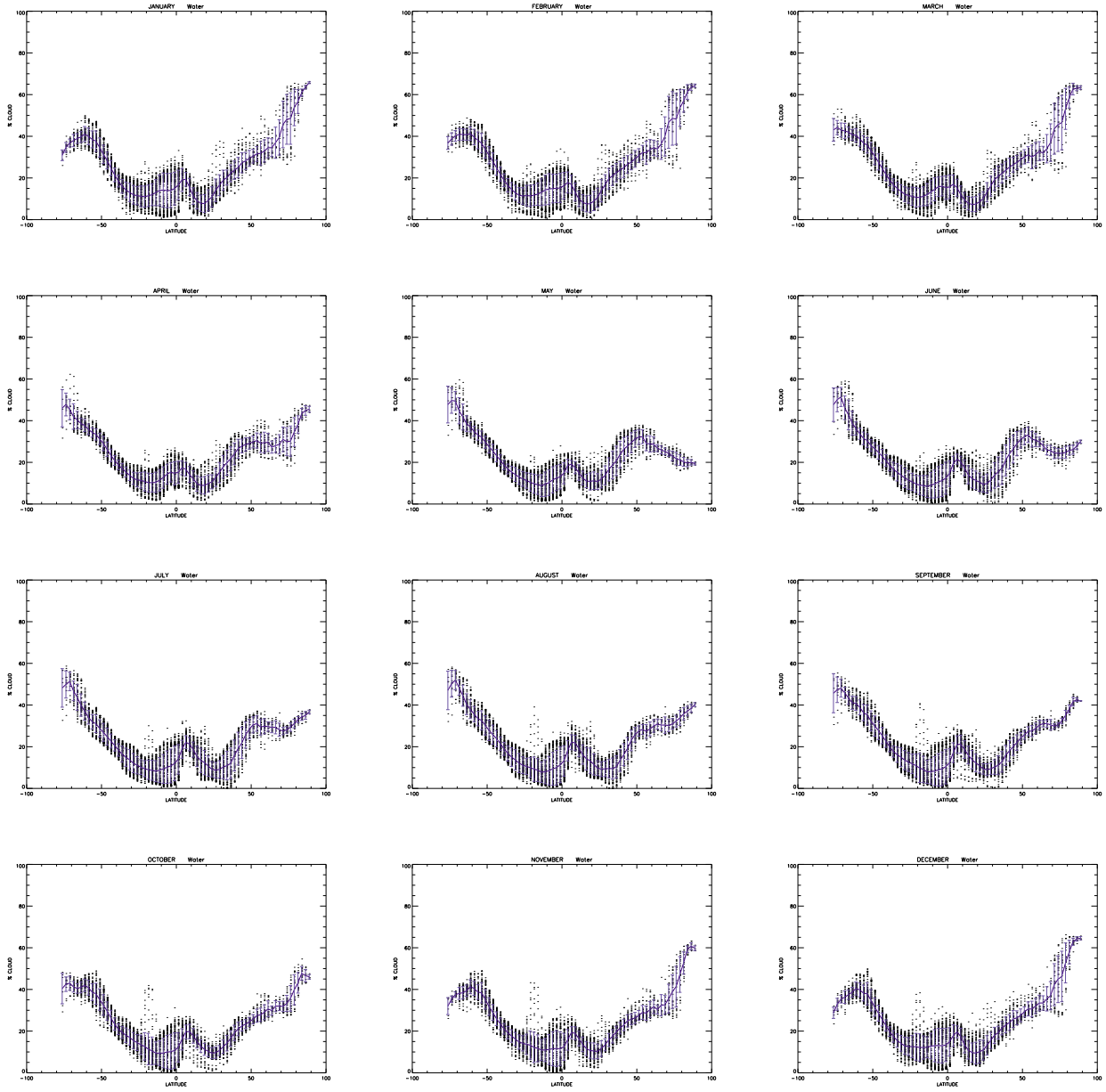

Figure A.9: The same as the figure A.1 but for mid clouds.

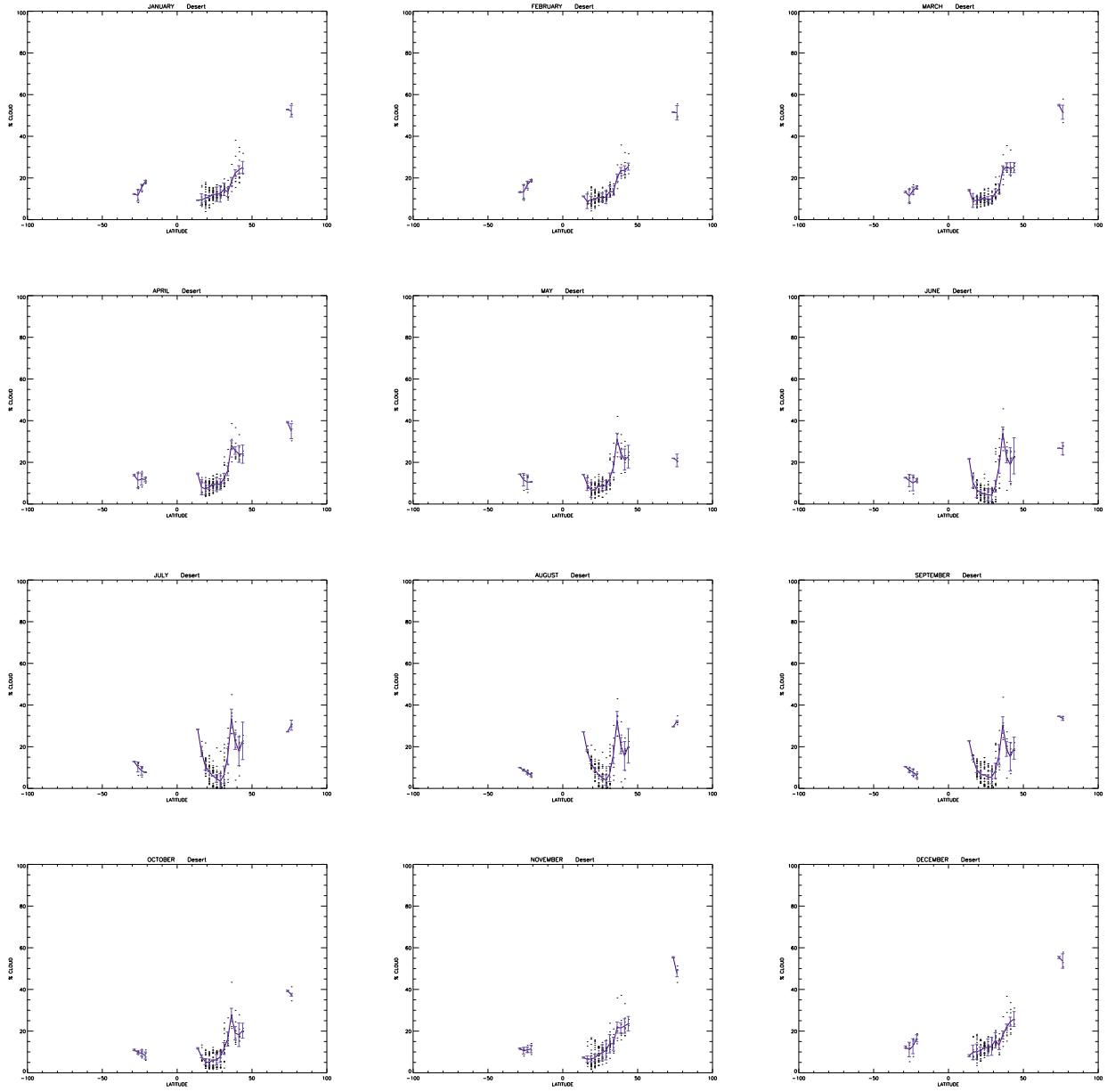

Figure A.10: The same as the figure A.2 but for mid clouds.

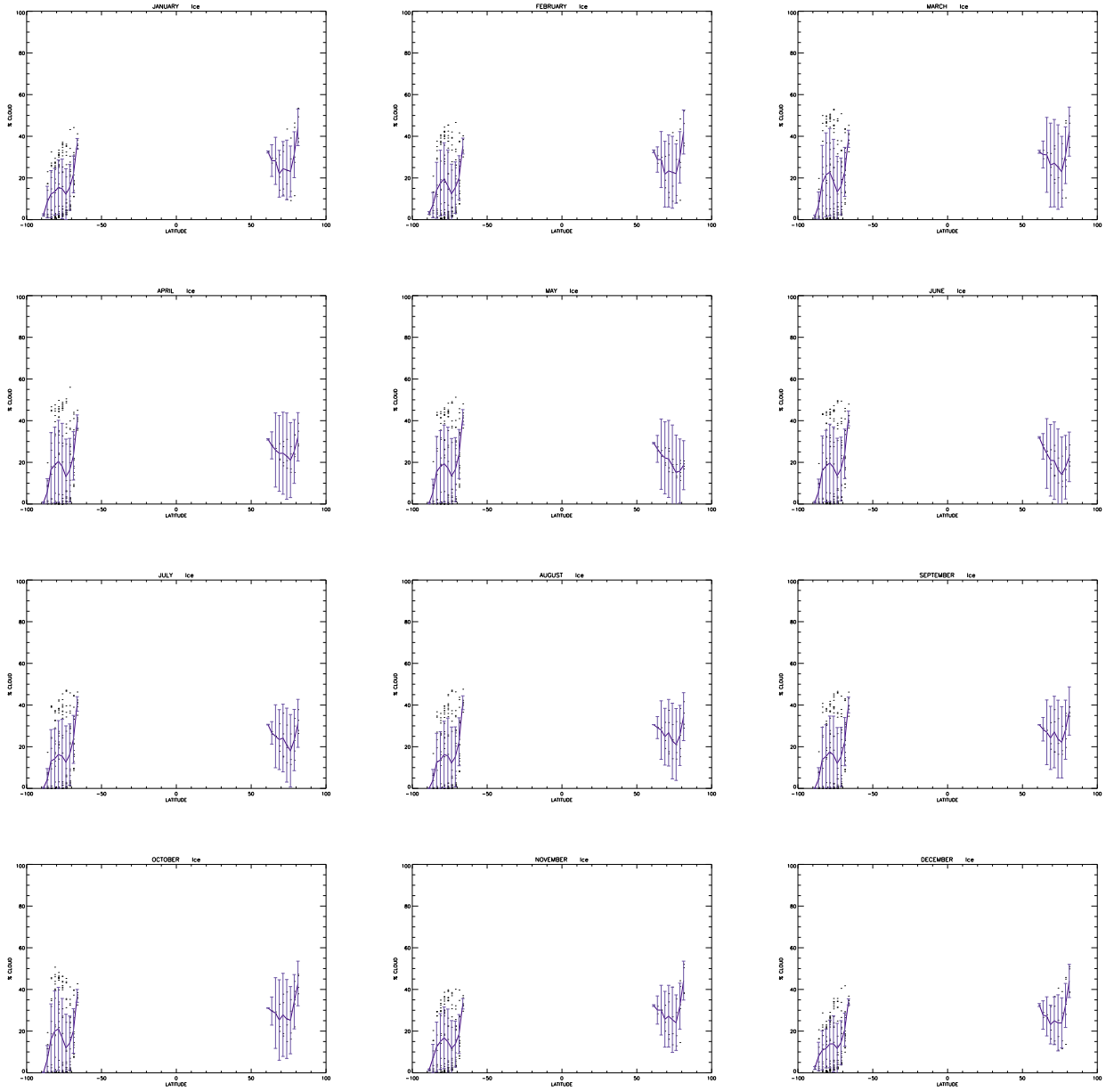

Figure A.11: The same as the figure A.3 but for mid clouds.

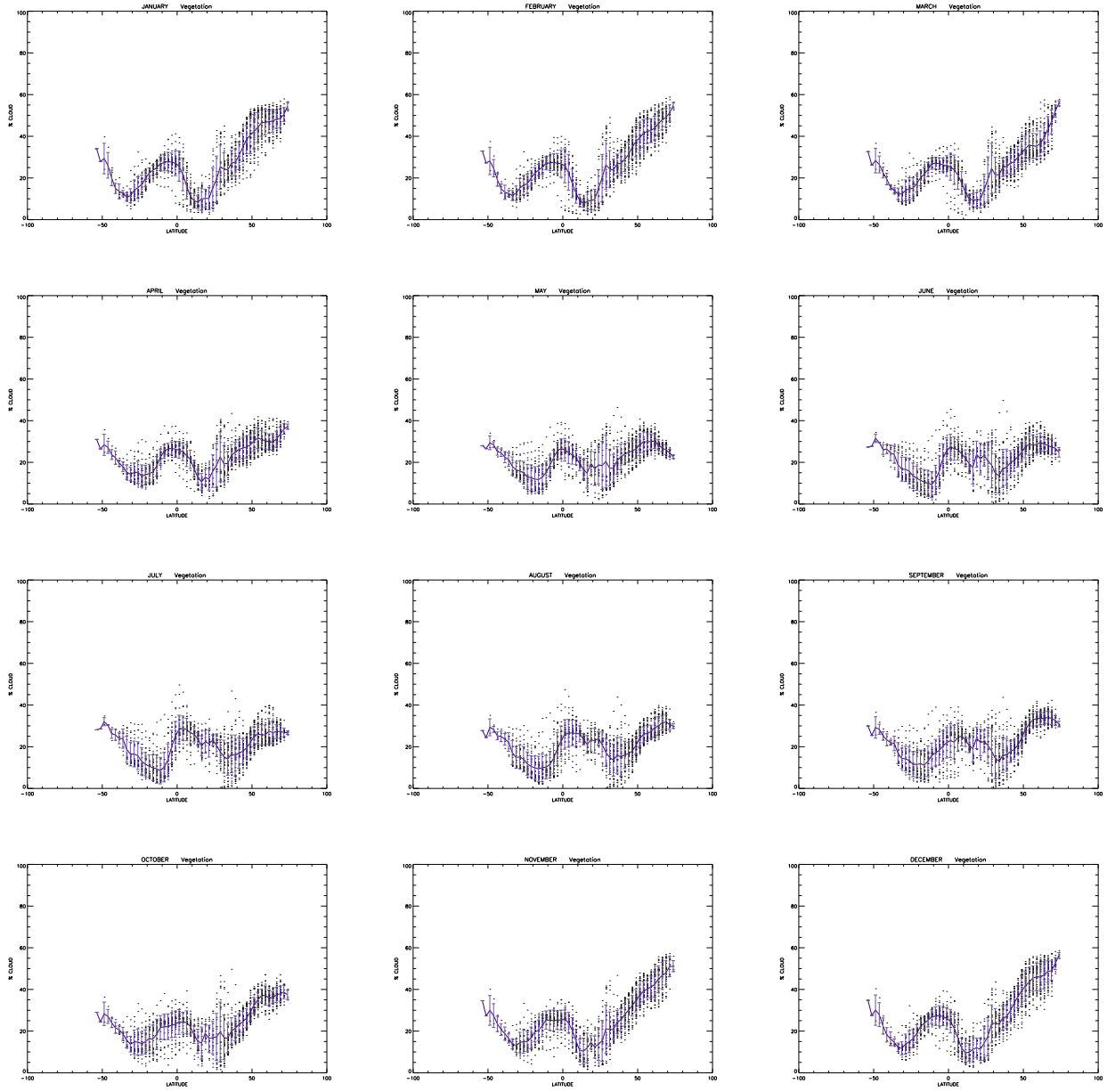

Figure A.12: The same as the figure A.4 but for mid clouds.

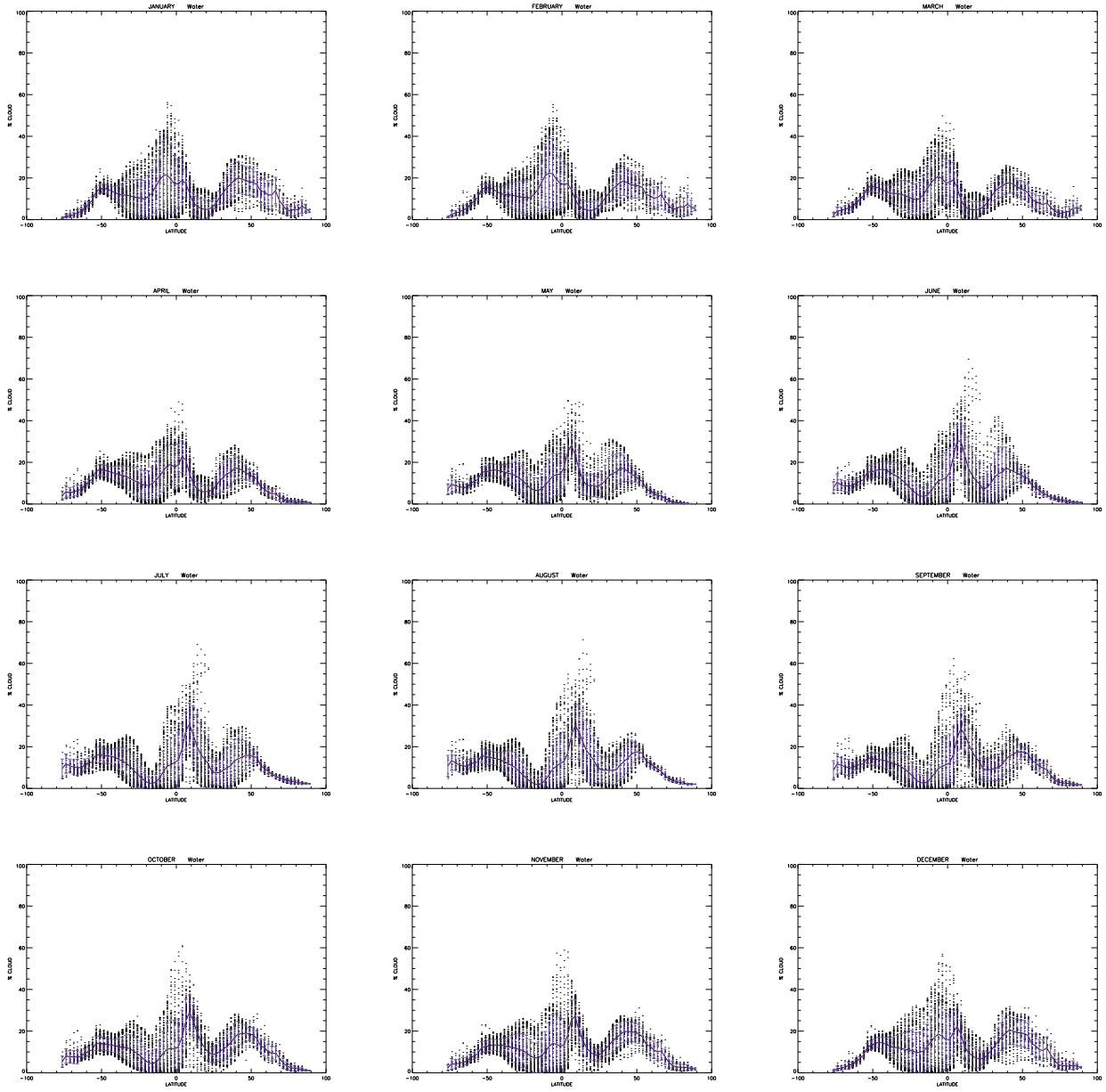

Figure A.13: The same as the figure A.1 but for high clouds.

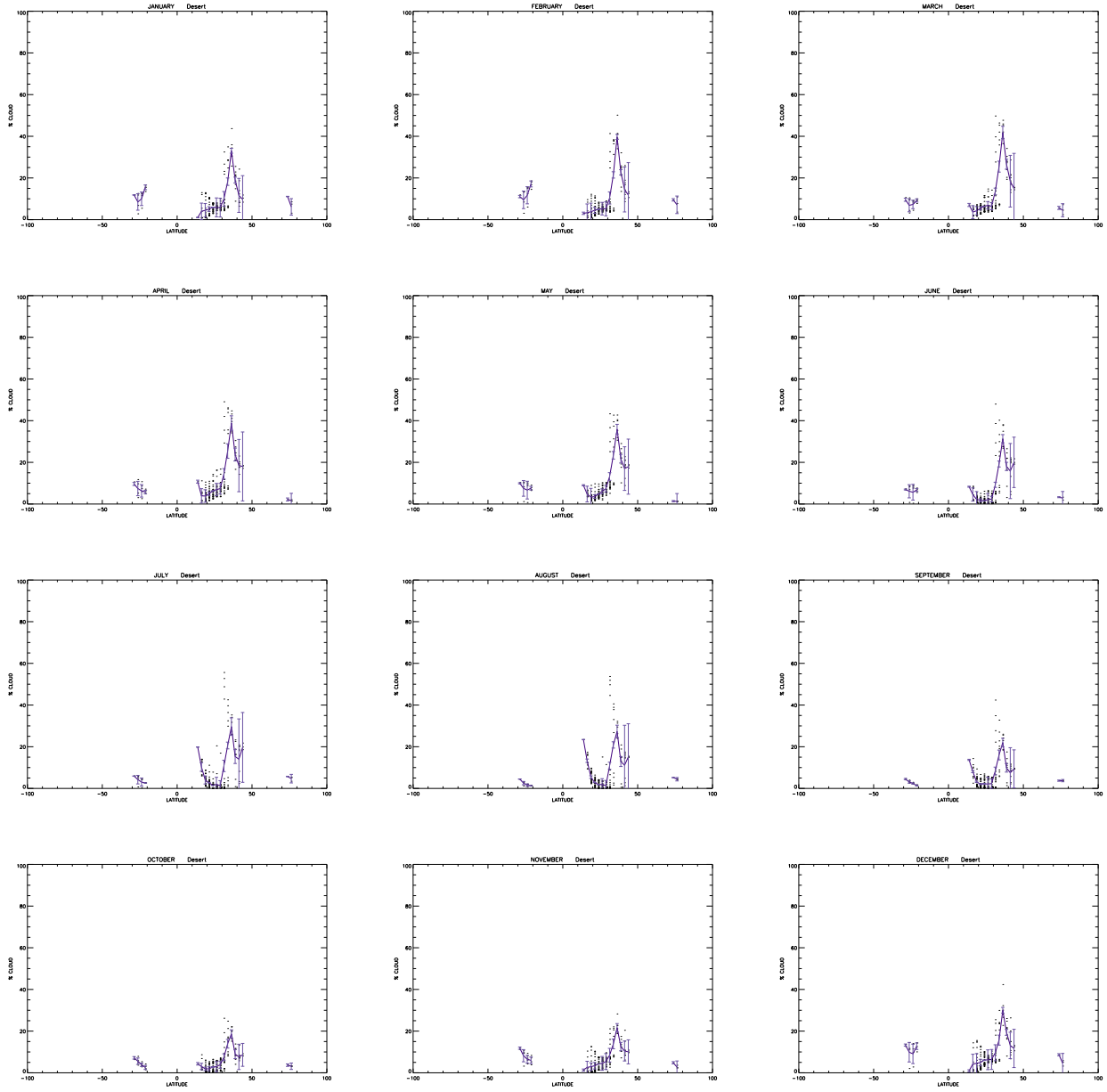

Figure A.14: The same as the figure A.2 but for high clouds.

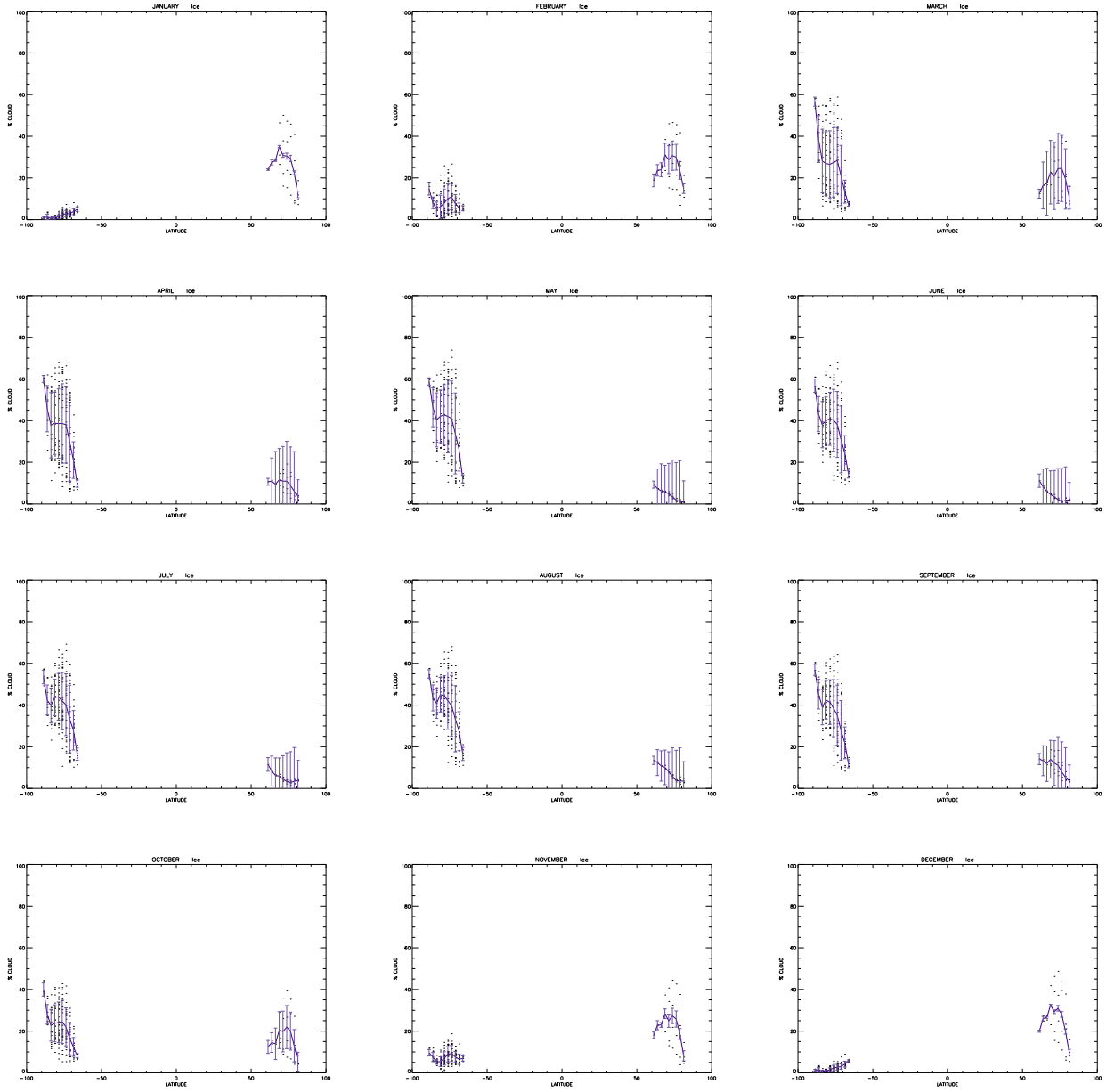

Figure A.15: The same as the figure A.3 but for high clouds.

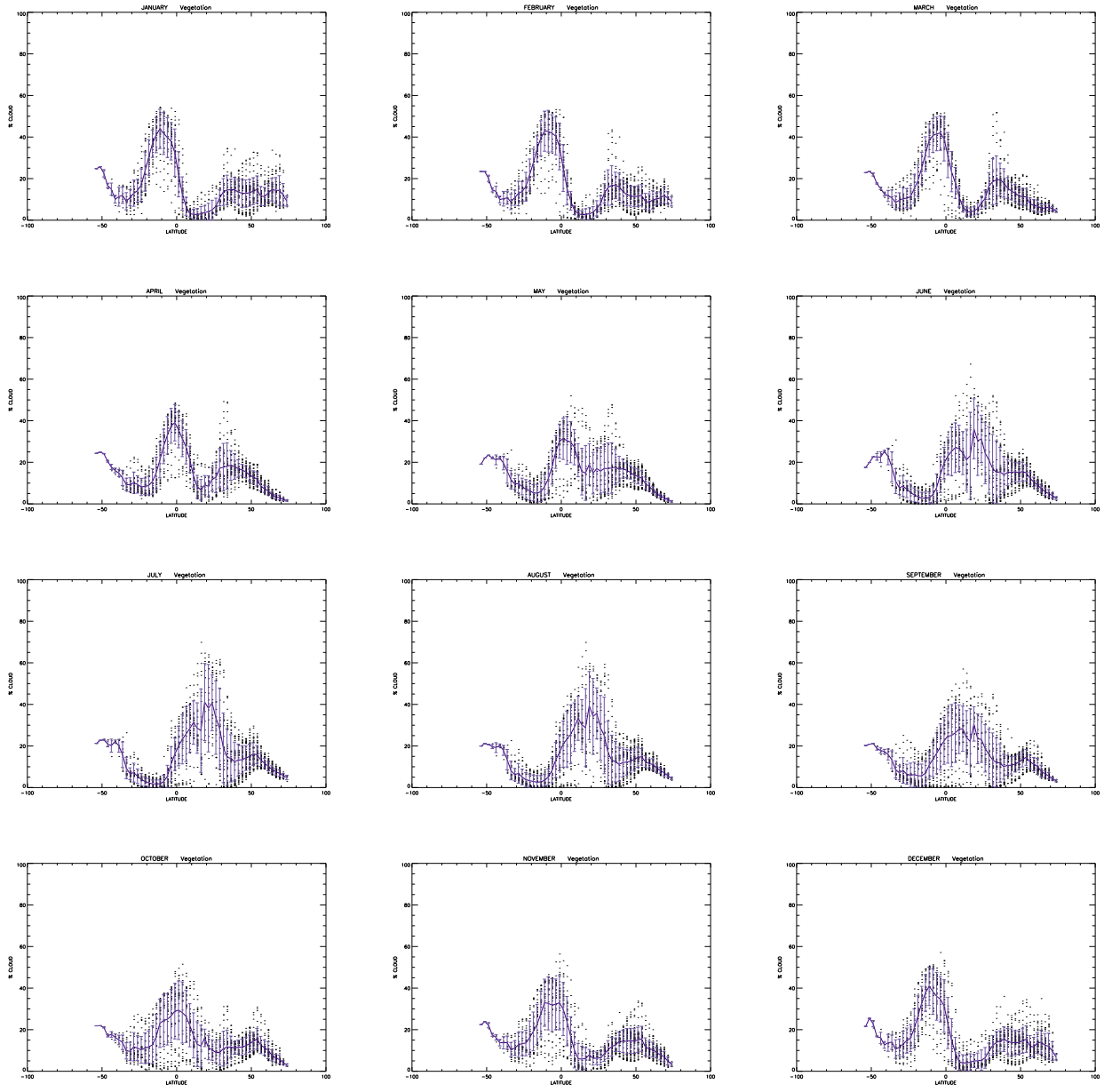

Figure A.16: The same as the figure A.4 but for high clouds.

References

Algeo, T., Scheckler, S., & Maynard, J. B. 2000, In: P.G. Gensel and D. Edwards (eds.). 2001 Plants Invade the Land: Evolutionary and Environmental Approaches. Columbia Univ. Press: New York., 213

Anderson, J. D., Schubert, G., Jacobson, R. A., et al. 1998, Science, 281, 2019

Anglada-Escudé, G., Arriagada, P., Vogt, S. S., et al. 2012, ApJ, 751, L16

Anglada-Escudé, G., Tuomi, M., Gerlach, E., et al. 2013, A&A, 556, A126

Arnold, L., Gillet, S., Lardière, O., Riaud, P., & Schneider, J. 2002, A&A, 392, 231

Bahcall, J. N., Pinsonneault, M. H., & Basu, S. 2001, ApJ, 555, 990

Bains, W. 2004, Astrobiology, 4, 137

Ballard, S., Charbonneau, D., Fressin, F., et al. 2013, ApJ, 773, 98

Barclay, T., Burke, C. J., Howell, S. B., et al. 2013, ApJ, 768, 101

Baross, J., Benner, S., Cody, G., Copley, S., & Pace, N. 2007, The Limits of Organic Life in Planetary Systems. Committee on the Limits of Organic Life in Planetary Systems, Committee on the Origins and Evolution of Life, National Research Council (The National Academies Press)

Beerling, D. J. & Berner, R. A. 2005, Proc Natl Acad Sci U S A, 102, 1302

Bekker, A., Holland, H. D., Wang, P.-L., et al. 2004, Nature, 427, 117

Beraldi-Campesi, H. 2013, Ecological Processes, 2, 1

Berner, R. A. 2004, The Phanerozoic Carbon Cycle: CO2 and O2 (New York, NY: Oxford Univ. Press)

Betts, R. A. 2000, Nature, 408, 187

Borucki, W. J., Agol, E., Fressin, F., et al. 2013, Science, 340, 587

Borucki, W. J., Koch, D., Basri, G., et al. 2010, Science, 327, 977

Borucki, W. J., Koch, D. G., Batalha, N., et al. 2012, ApJ, 745, 120

Bouchy, F., Pont, F., Santos, N. C., et al. 2004, A&A, 421, L13

Bouchy, F., Udry, S., Mayor, M., et al. 2005, A&A, 444, L15

Bowler, B. P., Liu, M. C., Dupuy, T. J., & Cushing, M. C. 2010, ApJ, 723, 850

Brogi, M., Snellen, I. A. G., de Kok, R. J., et al. 2012, Nature, 486, 502

Burke, C. J., Bryson, S., Christiansen, J., et al. 2013, in American Astronomical Society Meeting Abstracts, Vol. 221, American Astronomical Society Meeting Abstracts, 216.02

Butler, R. P., Marcy, G. W., Williams, E., et al. 1996, PASP, 108, 500

Bywater, R. P. & Conde-Frieboesk Kilian. 2005, Astrobiology, 5, 568

Campbell, B. & Walker, G. A. H. 1979, PASP, 91, 540

Campbell, B., Walker, G. A. H., & Yang, S. 1988, ApJ, 331, 902

Canfield, D. E. 1998, Nature, 396, 450

Canfield, D. E. 2005, Annual Review of Earth and Planetary Sciences, 33, 1

Cassan, A., Kubas, D., Beaulieu, J.-P., et al. 2012, Nature, 481, 167

Catling, D. C., Glein, C. R., Zahnle, K. J., & McKay, C. P. 2005, Astrobiology, 5, 415

Cess, R. D., Zhang, M. H., Ingram, W. J., et al. 1996, J. Geophys. Res., 101, 12791

Charbonneau, D., Berta, Z. K., Irwin, J., et al. 2009, Nature, 462, 891

Charbonneau, D., Brown, T. M., Latham, D. W., & Mayor, M. 2000, ApJ, 529, L45

Charbonneau, D., Brown, T. M., Noyes, R. W., & Gilliland, R. L. 2002, ApJ, 568, 377

Charlson, R. J., Schwartz, S. E., Hales, J. M., et al. 1992, Science, 255, 423

Chauvin, G., Lagrange, A.-M., Dumas, C., et al. 2004, A&A, 425, L29

Chen, C. W., Rondenay, S., Evans, R. L., & Snyder, D. B. 2009, Science, 326, 1089

Christensen, P. R. & Pearl, J. C. 1997, J. Geophys. Res., 102, 10875

Chyba, C. & Sagan, C. 1992, Nature, 355, 125

Cockell, C. S. 1999, Planet. Space Sci., 47, 1487

Cockell, C. S., Kaltenegger, L., & Raven, J. A. 2009, Astrobiology, 9, 623

Cowan, N. B., Agol, E., Meadows, V. S., et al. 2009, ApJ, 700, 915

Cowan, N. B., Robinson, T., Livengood, T. A., et al. 2011, ApJ, 731, 76

Crow, C. A., McFadden, L. A., Robinson, T., et al. 2011, ApJ, 729, 130

de Kok, R. J., Brogi, M., Snellen, I. A. G., et al. 2013, A&A, 554, A82

Delfosse, X., Bonfils, X., Forveille, T., et al. 2013, A&A, 553, A8

Dessler, A. E. 2010, Science, 330, 1523

Ehrenreich, D., Tinetti, G., Lecavelier Des Etangs, A., Vidal-Madjar, A., & Selsis, F. 2006, A&A, 448, 379

Finet, C., Timme, R. E., Delwiche, C. F., & Marleta, F. 2010, CURRENT BIOLOGY, 20, 2217

Flannery, D. T. & Walter, M. R. 2012, Australian Journal of Earth Sciences, 59, 1

Ford, E. B., Seager, S., & Turner, E. L. 2001, Nature, 412, 885

Fressin, F., Torres, G., Charbonneau, D., et al. 2013, ApJ, 766, 81

Fressin, F., Torres, G., Rowe, J. F., et al. 2012, Nature, 482, 195

Frisch, W., Meschede, M., & Blakey, R. 2011, Plate tectonics. Continental drift and mountain building (Springer)

Fujii, Y. & Kawahara, H. 2012, ApJ, 755, 101

Gallery, W. O., Kneizys, F. X., & Clough, S. A. 1983, AFGL-TR-0208 Environemental Research papers, 83, 0065

García Muñoz, A. & Pallé, E. 2011, J. Quant. Spec. Radiat. Transf., 112, 1609

García Muñoz, A., Zapatero Osorio, M. R., Barrena, R., et al. 2012, ApJ, 755, 103

Gargaud, M., Martin, H., López-García, P., Montmerle, T., & Pascal, R. 2012, Young Sun, Early Earth and the Origins of Life (Springer-Verlag, Berlin)

Gilliland, R. L., Marcy, G. W., Rowe, J. F., et al. 2013, ApJ, 766, 40

Goode, P. R., Qiu, J., Yurchyshyn, V., et al. 2001, Geophys. Res. Lett., 28, 1671

Gough, D. O. 1981, Sol. Phys., 74, 21

Gray, J., Chaloner, W., & Westoll, T. 1985, Phil. Trans. R. Soc., 309, 167

Grotzinger, J. P. & Knoll, A. H. 1999, Annual Review of Earth and Planetary Sciences, 27, 313

Guiry, M. D. 2012, Journal of Phycology, 48, 1057

Hamdani, S., Arnold, L., Foellmi, C., et al. 2006, A&A, 460, 617

Haqq-Misra, J. D., Domagal-Goldman, S. D., Kasting, P. J., & Kasting, J. F. 2008, Astrobiology, 8, 1127

Hart, M. H. 1978, icarus, 33, 23

Hatzes, A. P., Cochran, W. D., Endl, M., et al. 2003, ApJ, 599, 1383

Hegde, S. & Kaltenegger, L. 2013, Astrobiology, 13, 47

Hellier, C., Anderson, D. R., Collier Cameron, A., et al. 2009, Nature, 460, 1098

Henry, G. W., Marcy, G., Butler, R. P., & Vogt, S. S. 1999, IAU Circ., 7307, 1

Henry, G. W., Marcy, G. W., Butler, R. P., & Vogt, S. S. 2000, ApJ, 529, L41

Henyey, L. G. & Greenstein, J. L. 1941, ApJ, 93, 70

Hess, M., Koepke, P., & Schult, I. 1998, Bull. Am. Met. Soc., 79, 831

Hofmann, H. 2000, Microbial Sediments, Eds Riding R., Awramik S. (Springer, Berlin), pp. 315-327

Holman, M. J., Fabrycky, D. C., Ragozzine, D., et al. 2010, Science, 330, 51

Hopkins, M., Harrison, T. M., & Manning, C. E. 2008, Nature, 456, 493

Howard, A. W., Marcy, G. W., Johnson, J. A., et al. 2010, Science, 330, 653

Javaux, E. J. & Dehant, V. 2010, A&A Rev., 18, 383

Kaltenegger, L., Traub, W. A., & Jucks, K. W. 2007, ApJ, 658, 598

Karhu, J. A. & Holland, H. D. 1996, Geology, 24, 867

Kasting, J. F., Pollack, J. B., & Ackerman, T. P. 1984a, Icarus, 57, 335

Kasting, J. F., Pollack, J. B., & Crisp, D. 1984b, Journal of Atmospheric Chemistry, 1, 403

Kasting, J. F. & Siefert, J. L. 2002, Science, 296, 1066

Kasting, J. F., Whitmire, D. P., & Reynolds, R. T. 1993, Icarus, 101, 108

Kawahara, H. & Fujii, Y. 2010, ApJ, 720, 1333

Kawahara, H. & Fujii, Y. 2011, ApJ, 739, L62

Kenrick, P. & Crane, P. R. 1997, Nature, 389, 33

Kiang, N. Y., Segura, A., Tinetti, G., et al. 2007a, Astrobiology, 7, 252

Kiang, N. Y., Siefert, J., Govindjee, & Blankenship, R. E. 2007b, Astrobiology, 7, 222

Kiehl, J. T. & Dickinson, R. E. 1987, J. Geophys. Res., 92, 2991

Kienert, H., Feulner, G., & Petoukhov, V. 2012, Geophys. Res. Lett., 39, 23710

Kitzmann, D., Patzer, A. B. C., von Paris, P., Godolt, M., & Rauer, H. 2011a, A&A, 531, A62

Kitzmann, D., Patzer, A. B. C., von Paris, P., Godolt, M., & Rauer, H. 2011b, A&A, 534, A63

Kivelson, M. G., Khurana, K. K., & Volwerk, M. 2002, Icarus, 157, 507

Kopparapu, R. K., Ramirez, R., Kasting, J. F., et al. 2013, ApJ, 765, 131

Kump, L. R. & Barley, M. E. 2007, Nature, 448, 1033

Lammer, H., Bredehöft, J. H., Coustenis, A., et al. 2009, A&A Rev., 17, 181

Latham, D. W., Stefanik, R. P., Mazeh, T., Mayor, M., & Burki, G. 1989, Nature, 339, 38

Lindegren, L. & Perryman, M. A. C. 1996, A&AS, 116, 579

Lissauer, J. J., Fabrycky, D. C., Ford, E. B., et al. 2011, Nature, 470, 53

Livengood, T. A., A'Hearn, M. F., Deming, D., et al. 2008, in Bulletin of the American Astronomical Society, Vol. 40, AAS/Division for Planetary Sciences Meeting Abstracts #40, 385

Lovelock, J. E. 1965, Nature, 207, 568

Madhusudhan, N., Burrows, A., & Currie, T. 2011, ApJ, 737, 34

Manabe, S. & Wetherald, R. T. 1967, Journal of Atmospheric Sciences, 24, 241

Marcy, G., Butler, R. P., Fischer, D., et al. 2005, Progress of Theoretical Physics Supplement, 158, 24

Marcy, G. W. & Butler, R. P. 1996, ApJ, 464, L147

Marley, M. S., Saumon, D., Cushing, M., et al. 2012, ApJ, 754, 135

Mayor, M., Pepe, F., Queloz, D., et al. 2003, The Messenger, 114, 20

Mayor, M. & Queloz, D. 1995, Nature, 378, 355

McKay, C. P. & Smith, H. D. 2005, Icarus, 178, 274

Meadows, V. S. 2006, in IAU Colloq. 200: Direct Imaging of Exoplanets: Science and Techniques (Cambridge University Press), ed. C. Aime & F. Vakili, 25–34

Mojzsis, S. J., Arrhenius, G., McKeegan, K. D., et al. 1996, Nature, 384, 55

Montañés-Rodríguez, P., Pallé, E., Goode, P. R., & Martín-Torres, F. J. 2006, ApJ, 651, 544

Morowitz, H. 1967, Nature, 215, 1259

Moyen, J. F., Stevens, G., & Kisters, A. 2006, Nature, 442, 559

Muirhead, P. S., Johnson, J. A., Apps, K., et al. 2012, ApJ, 747, 144

Muterspaugh, M. W., Lane, B. F., Kulkarni, S. R., et al. 2010, AJ, 140, 1657

Nisbet, E. G. & Sleep, N. H. 2001, Nature, 409, 1083

Oakley, P. H. H. & Cash, W. 2009, ApJ, 700, 1428

Olson, J. 2006, Photosynth Res, 88, 109

Owen, T., Cess, R. D., & Ramanathan, V. 1979, Nature, 277, 640

Pallé, E., Ford, E. B., Seager, S., Montañés-Rodríguez, P., & Vazquez, M. 2008, ApJ, 676, 1319

Pallé, E., Goode, P. R., Montañés-Rodríguez, P., & Koonin, S. E. 2004, Science, 304, 1299

Pallé, E., Goode, P. R., Yurchyshyn, V., et al. 2003, J. Geophys. Res. (Atmos.), 108, 4710

Parkinson, C. D., Liang, M.-C., Yung, Y. L., & Kirschivnk, J. L. 2008, Origins of Life and Evolution of the Biosphere, 38, 355

Parnell, J. 2004, International Journal of Astrobiology, 3, 131

Pepe, F., Lovis, C., Ségransan, D., et al. 2011, A&A, 534, A58

Perryman, M. 2012, Astrobiology, 12, 928

Pudritz, R., Higgs, P., & Stone, J. 2007, Planetary Systems and the Origins of Life (Cambridge University Press)

Qiu, J., Goode, P. R., Pallé, E., et al. 2003, J. Geophys. Res. (Atmos.), 108, 4709

Qiu, Y., Li, L., Wang, B., et al. 2006, Proceedings of the National Academy of Sciences of the United States of America, 103, 15511

Quirrenbach, A., Amado, P. J., Mandel, H., et al. 2010, in Society of Photo-Optical Instrumentation Engineers (SPIE) Conference Series, Vol. 7735, Society of Photo-Optical Instrumentation Engineers (SPIE) Conference Series

Ramanathan, V., Cess, R. D., Harrison, E. F., et al. 1989, Science, 243, 57

Ramirez, R., Kopparapu, R., Zugger, M. E., et al. 2013, Nat.Geosc. (in review)

Randall, D. A., Cess, R. D., Blanchet, J. P., et al. 1994, J. Geophys. Res., 99, 20757

Raval, A. & Ramanathan, V. 1989, Nature, 342, 758

Regenauer-Lieb, K., Yuen, D. A., & Branlund, J. 2001, Science, 294, 578

Robinson, T. D., Meadows, V. S., Crisp, D., et al. 2011, Astrobiology, 11, 393

Rodler, F., Lopez-Morales, M., & Ribas, I. 2012, ApJ, 753, L25

Rosing, M. T., Bird, D. K., Sleep, N. H., & Bjerrum, C. J. 2010, Nature, 464, 744

Rossow, W. B., Walker, A. W., Beuschel, D. E., & Roiter, M. D. 1996, World Climate Research Programme Report WMO/TD 737 (Geneva, Switzerland: World Meteorological Organization)

Rothman, L. S., Gordon, I. E., Barbe, A., et al. 2009, J. Quant. Spec. Radiat. Transf., 110, 533

Rothschild, L. J. & Mancinelli, R. L. 2001, Nature, 409, 1092

Rugheimer, S., Kaltenegger, L., Zsom, A., Segura, A., & Sasselov, D. 2013, Astrobiology, 13, 251

Sagan, C. & Mullen, G. 1972, Science, 177, 52

Sagan, C., Thompson, W. R., Carlson, R., Gurnett, D., & Hord, C. 1993, Nature, 365, 715

Sanromá, E. & Pallé, E. 2012, ApJ, 744, 188

Sanromá, E., Pallé, E., & García Munõz, A. 2013, ApJ, 766, 133

Sanromá, E., Pallé, E., Parenteau, M. N., et al. 2014, ApJ, 780, 52

Schulze-Makuch, D., Grinspoon, D. H., Abbas, O., Irwin, L. N., & Bullock, M. A. 2004, Astrobiology, 4, 11

Seager, S. 2011, Exoplanets

Seager, S. & Deming, D. 2010, ARA&A, 48, 631

Seager, S., Turner, E. L., Schafer, J., & Ford, E. B. 2005, Astrobiology, 5, 372

Seckbach, J. & Libby, W. F. 1970, Space Life Sciences, 2, 121

Seckbach, J. & Oren, A. 2010, Microbial Mats: Modern and Ancient Microorganisms in Stratified Systems, Cellular Origin, Life in Extreme Habitats and Astrobiology (Springer London, Limited)

Selsis, F., Kasting, J. F., Levrard, B., et al. 2007, A&A, 476, 1373

Semikhatov, M. A., Gebelein, C. D., Cloud, P., Awramik, S. M., & Benmore, W. C. 1979, Canadian Journal of Earth Sciences, 16, 992

Sengupta, S. 2008, ApJ, 683, L195

Sertorio, L. & Tinetti, G. 2001, Nuovo Cimento C Geophysics Space Physics C, 24, 421

Sleep, N. H., Zahnle, K., & Neuhoff, P. S. 2001, Proceedings of the National Academy of Science, 98, 3666

Solomatov, V. S. 2004, Journal of Geophysical Research (Solid Earth), 109, 1412

Spencer, R. W. & Braswell, W. D. 2010, Journal of Geophysical Research (Atmospheres), 115, 16109

Spohn, T. & Schubert, G. 2003, Icarus, 161, 456

Stammnes, K., Tsay, S. C., Wiscombre, W., & Jayaweera, K. 1988, Appl. Opt., 27, 2502

Sterken, V. J., Altobelli, N., Kempf, S., et al. 2012, Planet. Space Sci., 71, 142

Sterzik, M. F., Bagnulo, S., & Palle, E. 2012, Nature, 483, 64

Street, R. A., Simpson, E., Barros, S. C. C., et al. 2010, ApJ, 720, 337

Strom, R. G., Malhotra, R., Ito, T., Yoshida, F., & Kring, D. A. 2005, Science, 309, 1847

Suttles, J. T., Green, R. N., & Minnis, P. e. a. 1988, Angular radiation models for earth-atmosphere system. Volume I, Shortwave radiation (NASA RP-1184; Hampton, VA: NASA), 1 v.

Swain, M. R., Tinetti, G., Vasisht, G., et al. 2009a, ApJ, 704, 1616

Swain, M. R., Vasisht, G., Tinetti, G., et al. 2009b, ApJ, 690, L114

Thompson, D. A., Bastow, I. D., Helffrich, G., et al. 2010, Earth and Planetary Science Letters, 297, 655

Tinetti, G., Meadows, V. S., Crisp, D., et al. 2006a, Astrobiology, 6, 34

Tinetti, G., Meadows, V. S., Crisp, D., et al. 2006b, Astrobiology, 6, 881

Tinetti, G., Rashby, S., & Yung, Y. L. 2006c, ApJ, 644, L129

Tinetti, G., Rashby, S., & Yung, Y. L. 2006d, ApJ, 644, L129

Tinetti, G., Vidal-Madjar, A., Liang, M.-C., et al. 2007, Nature, 448, 169

Turnbull, M. C., Traub, W. A., Jucks, K. W., et al. 2006, ApJ, 644, 551

Udry, S., Bonfils, X., Delfosse, X., et al. 2007a, A&A, 469, L43

Udry, S., Fischer, D., & Queloz, D. 2007b, Protostars and Planets V, 685

van Zuilen, M. A., Lepland, A., & Arrhenius, G. 2002, Nature, 418, 627

Vázquez, M., Pallé, E., & Rodríguez, P. M. 2010, The Earth as a Distant Planet: A Rosetta Stone for the Search of Earth-Like Worlds, Astronomy and Astrophysics Library. ISBN 978-1-4419-1683-9. Springer-Verlag New York, 2010

Walker, J. C. G., Hays, P. B., & Kasting, J. F. 1981, J. Geophys. Res., 86, 9776

Wilde, S. A., Valley, J. W., Peck, W. H., & Graham, C. M. 2001, Nature, 409, 175

Wolstencroft, R. D. & Raven, J. A. 2002, Icarus, 157, 535

Wolszczan, A. & Frail, D. A. 1992, Nature, 355, 145

Woolf, N. J., Smith, P. S., Traub, W. A., & Jucks, K. W. 2002, ApJ, 574, 430

Xiong, J., Fischer, W., Inoue, K., Nakahara, M., & Bauer, C. 2000, Science, 289, 1724

Zimmer, C., Khurana, K. K., & Kivelson, M. G. 2000, Icarus, 147, 329